MOLECULAR AND CELLULAR EVALUATION OF NOVEL DNA SEQUENCE SELECTIVE POLYAMIDES

BY

SHICAI LIN

Cancer Research UK Drug-DNA Interactions Research Group,
Cancer Institute, University College London, London, WC1E 6BT

DOCTOR OF PHILOSOPHY

Submitted to University College London (UCL) for PhD examination
2013

I, [SHICAI LIN] confirm that the work presented in this thesis is my own. Where information has been derived from other sources, I confirm that this has been indicated in the thesis

ABSTRACT

Pyrrole (P)-Imidazole (I) containing polyamides are small synthetic molecules which can target predetermined DNA sequences with high affinity and modulate gene expression by interfering with the binding of transcription factors to DNA. Hairpin and H-pin analogues show enhanced DNA binding affinity and selectivity compared to monomers, but are associated with poor cellular uptake. To address this problem, a new class of unlinked polyamide precursors containing appropriately designed pendant reactive and biocompatible functional groups is presented in this thesis. The ability of these agents to interact in situ and potentially form either H-pin or Hairpin conjugates was tested with DNase I footprinting analysis. The effects of modification on the formamido-imidazole-pyrrole-imidazole (f-IPI) polyamide and related analogues, by the addition of an amino group, on DNA binding affinity and sequence selectivity were also evaluated.

Dbf4 is the regulatory subunit of Cdc7 kinase, which is essential for the initiation of DNA replication. Human Cdc7/Dbf4 (HuCdc7/Dbf4) kinase activity is critical for cell proliferation and high expression levels occur in multiple solid human malignancies. F-IPI can target the *MIu*I Cell cycle Box (MCB) sequence 5'-ACGCGT-3'which is the critical site for transcription factor binding and activation of expression of the HuCdc7/Dbf4 core gene in mammalian cells. DNA sequence selective binding of f-IPI to the MCB sequence was shown in DNase I footrpinting experiments. A f-IPI-induced, dose-dependent inhibition of protein binding to the MCB was demonstrated in an Electrophoretic Mobility Shift Assay (EMSA). RT-PCR and immunoblotting analysis confirmed the inhibitory effects of f-IPI on HuDbf4 in MDA-MB231 cells. Small

interfering RNA-mediated depletion of HuDbf4 decreased cell survival and proliferation, and induced G_1 arrest in MDA-MB231 cells. F-IPI treatments also showed a dose-dependent reduction of cell survival and proliferation and induced G_1 arrest. Although the f-IPI H-pin analogue exhibited better DNA binding affinity and protein inhibition, no marked effects at mRNA and protein levels were detected in cells, likely attributed to its large size.

The unlinked f-IPI analogues containing reactive groups [i.e f-IP(C_3NH_2)I and f-IP(C_3Cl)I] able to interact *in situ* and form H-pin were tested in the Dbf4 promoter model system. f-IP(C_3NH_2)I presented the same DNA binding affinity and protein inhibition to the MCB as the combination of f-IP(C_3NH_2)I and f-IP(C_3Cl)I (potential hybrid) but it produced much higher effects than f-IP(C_3Cl)I. RT-PCR and immunoblotting analysis showed that the potential hybrid produced greater reduction of HuDbf4 mRNA and protein levels than either f-IP(C_3NH_2)I or f-IP(C_3Cl)I. In addition, the potential hybrid demonstrated greater G_1 arrest than each polyamide alone.

Finally, a series of fluorescent f-IPI analogues are presented, providing an intrinsic probe for monitoring the cellular uptake of polyamides. Aza-Hx-PI was shown to target the same sequence as f-IPI (DNase I footprinting), inhibit protein binding (EMSA) and reduce the levels of HuDbf4 in cells. Time and dose-dependent nuclear localisation was detected by confocal microscopy.

Overall the data presented in this thesis highlight the potential of small molecule polyamides as modulators of gene expression.

INDEX

INDEX OF THE FIGURES

LIST OF TABLES

ABBREVIATIONS

A	Adenine
ATP	Adenine triphosphate
APS	Ammonium persulfate
BrdU	5-Bromo-2’-deoxyuridine
C	Cytosine
CD	Circular dichrosim
cps	Counts per second
CDK	Cyclin-dependent kinases
Cdc7	Cell division cycle 7
Chk1	Checkpoint kinase 1
DAPI	4',6-diamidino-2-phenylindole
DSB	Double-strand break
DMSO	Dimethyl sulfoxide
DMEM	Dulbecco's Modified Eagle Medium
DNA	Deoxynucleoside acid
DNase I	Deoxyribonuclease I
Dbf4/ASK	Activator of S phase kinase
dNTP	Deoxynucleoside triphosphate
DTT	Dithiothreitol
EDTA	Ethylenediamine tetraacetic acid
FBS	Fetal bovine serum
G	Guanine
g	Gram

HIV-1	Human immunodeficiency virus
HRP	Horseradish peroxidase
Im	Imidazole
Ka	Equilibrium association constant
kb	Kilobase
M	Molar
µM	Micromolar
µl	Microlitre
mRNA	Messenger ribonucleic acid
Mcm	Minichromosome maintenance complex
MCB	*M1uI* cell cycle Box
MBF	MCB binding factor
NMR	Nuclear magnetic resonance
ORC	Origin recognition complex
pmol	Picomoles
PCR	Polymerase chain reaction
Py	Pyrrole
PI	Propidium iodide
PBS	Phosphate buffer saline
Pre-RC	Pre-replicative complex
RNA	Ribonucleic acid
RNase	Ribonuclease
SDS	Sodium dodecyl sulfate
SiRNA	Small interfering RNA

SPR	Surface plasmon resonance
T	Thymine
TAE	Tris-acetic acid EDTA buffer
TBE	Tris-boric acid EDTA buffer
TEMED	*N, N, N, N*-Teramethyl-ethylenediamine
Topo	Topoisomerase
TF	Transcription factor
UV	Ultraviolet

ACKNOWLEDGEMENTS

This thesis would not have been possible without the help of so many people in so many ways. I would like to take this opportunity to thank Professor John Hartley for his supervision and all supports, Professor Moses Lee for his help and advice regarding the chemistry and Dr Kostantinos Kiakos for his invaluable help and guidance from the beginning to the end of my research.

It has been a long journey and I cannot accomplish the PhD study without my family. In this memorable moment, I also would like to express my deeply thanks to my beloved parents, Huisheng Lin and Yingjun Zhou for their love, encouragement, and supports both financially and mentally. My final and special thanks are addressed to my beloved wife, Cui Liu, for her endless love and encouragement.

CHAPTER 1

INTRODUCTION

1.1 The aetiology of cancer

Cancer is characterized by an "uncontrolled growth" of cells caused by multiple changes in gene expression. This uncontrolled cell proliferation can ultimately evolve into a population of cells which can invade tissues ("invasion") and metastasize to distant sites ("metastasis"), causing significant morbidity and, if untreated, death of the host. These three malignant properties of cancers differentiate them from benign tumors, which are self-limited, and do not invade or metastasize. Cancer can be viewed as a disease of abnormal gene expression. There are a number of mechanisms by which this altered gene expression occurs, for example via a direct modification of DNA, such as a gene mutation, translocation, amplification, deletion, loss of heterozygosity, or via mechanisms resulting from abnormal gene transcription or translation. The outcome is an imbalance of cell replication and cell death in the tumor cell population which can lead to an expansion of tumor tissue, in contrast to normal tissues where cell proliferation and cell loss are in a state of equilibrium.

A large number of aetiological agents have been recognized that cause genetic damage and lead to neoplastic transformation. They fall into three general categories 1) Chemical Carcinogens. The role of chemicals in tumour development is widespread and was recognized because of links to occupational exposure. For example, inhalation of hardwood dusts has been associated with adenocarcinoma of the nasal sinuses, first described in workers in the furniture factories of High Wycombe (Hounam and Williams, 1974). Cigarette smoke contains over 4,000 chemical compounds and these

include over 70 that have been found to cause cancer (Cancer Research UK, 2012). 2) Radiation. Radiant energy, whether as ultraviolet rays or ionizing radiation, will transform cells *in vitro* and induce tumours *in vivo* in both humans and animals. As with most chemical carcinogens, radiation is mutagenic and thought to cause malignant transformation by DNA damage. There are usually many years between exposure to the initiating dose of radiation and the appearance of malignancy. 3) Tumour viruses cause transformation as a consequence of their ability to integrate their genome into the host cell DNA. Usually the virus is responsible for the production of a transforming protein, coded for by an oncogene, which maintains the transformed state within the cell (Butel, 2000).

1.2 Hallmarks of cancer

In 2011, Hanahan and Weinberg reviewed their original definition of the hallmarks of cancer, which are composed of six distinctive and complementary cellular capabilities during the course of multistep tumorigenesis (Hanahan and Weinberg, 2011). Briefly, the six hallmarks are identified by the following characteristics (Figure 1.1):

- Sustaining proliferation signaling

One of the most fundamental characteristics of cancer cells is to sustain chronic proliferation. Normal tissues regulate the production and release of growth-promoting signals that are associated with the cell growth-and-division cycle, hence balancing cell number and further maintaining normal tissue architecture and function. Cancer cells evade the regulation of these signals leading to uncontrolled cell proliferation.

- Evading growth suppressors

Cancer cells interrupt powerful programs that negatively regulate cell growth and proliferation in various ways. Tumour suppressor genes play a key role in many of these programs. For example, one of the prototypical tumor suppressors encodes the RB (retinoblastoma-associated) protein, which controls whether or not a cell should proceed through its growth-and-division cycle in response to a variety of extracellular and intracellular signals (Deshpande et al., 2005; Burkhart and Sage, 2008). However, cancer cells have evolved a dysfunction of the RB pathway, a critical gatekeeper of cell-cycle progression, allowing persistent cell proliferation.

- Resisting cell death

Tumor cells have developed various ways to constrain or circumvent apoptosis. Most common is the loss of the TP53 tumor suppressor function that triggers apoptosis in response to substantial levels of DNA breaks and other chromosomal abnormalities and, alternatively, insufficient survival factor signaling or hyperactive signaling. Alternatively, tumors may achieve a similar outcome by increasing expression of antiapoptotic regulators (Bcl-2, Bcl-W) or of survival signals (lgf1/2), by downregulating proapoptotic factors (Bax), or by short-circuiting the extrinsic ligand-induced death pathway.

- Enabling replicative immortality

Tumor cells formed from the eventual immortalization of rare variant cells can maintain telomeric DNA at lengths sufficient to circumvent senescence or apoptosis, achieved most commonly by increasing telomerase levels or, less frequently, via an alternative recombination-based telomere maintenance mechanism. Alternatively, the tumor-

associated neovasculature, generated by the process of angiogenesis, proceeds to the immortalization of rare variant cells, which become tumors cells.

- Activating invasion and metastasis

The best-characterized alterations associated with cancer cells in terms of their shape and attachment to other cells and to the extracellular matrix (ECM), involves the loss of E-cadherin, a key cell-to-cell adhesion molecule which helps assemble epithelial cell sheets and maintains the quiescence of the cells within these sheets. The capability of invasion and metastasis has been frequently observed and associated with the downregulation and occasional mutational quiescence of E-cadherin in human carcinomas.

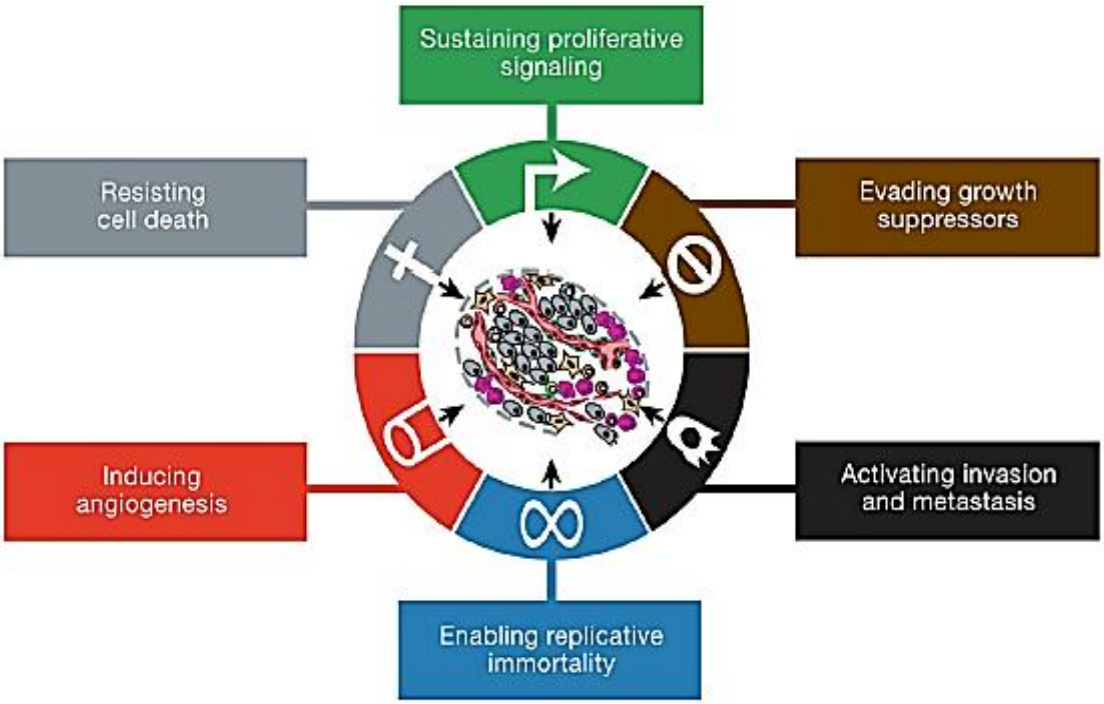

Figure 1.1 The hallmarks of cancer taken from Hanahan and Weinberg, 2011

More recently, two emerging hallmarks have been proposed to be important for the development of cancer and involve the reprogramming of the energy metabolism and the evasion of immune destruction (Figure 1.2).

- Reprogramming Energy Metabolism

The corresponding adjustment of energy metabolism is essential for fueling cell growth and division. Cancer cells can reprogram their glucose metabolism, and thus their energy production, by limiting their energy metabolism largely to glycolysis, given the relatively poor efficiency of generating ATP by glycolysis compared to the more efficient mitochondrial oxidative phosphorylation. However, a functional rationale for the glycolytic switch in cancer cells has been unclear. The altered energy metabolism is proving to be as widespread in cancer cells as many of the other cancer-associated traits that have been accepted as hallmarks of cancers.

- Evading immune destruction

The immune system plays an important role in resisting or eradicating formation and progression of incipient neoplasias, late-stage tumors, and micrometastases. Solid tumors manage to avoid detection by the immune system or constrain the extent of immunological killing, thus evading eradication.

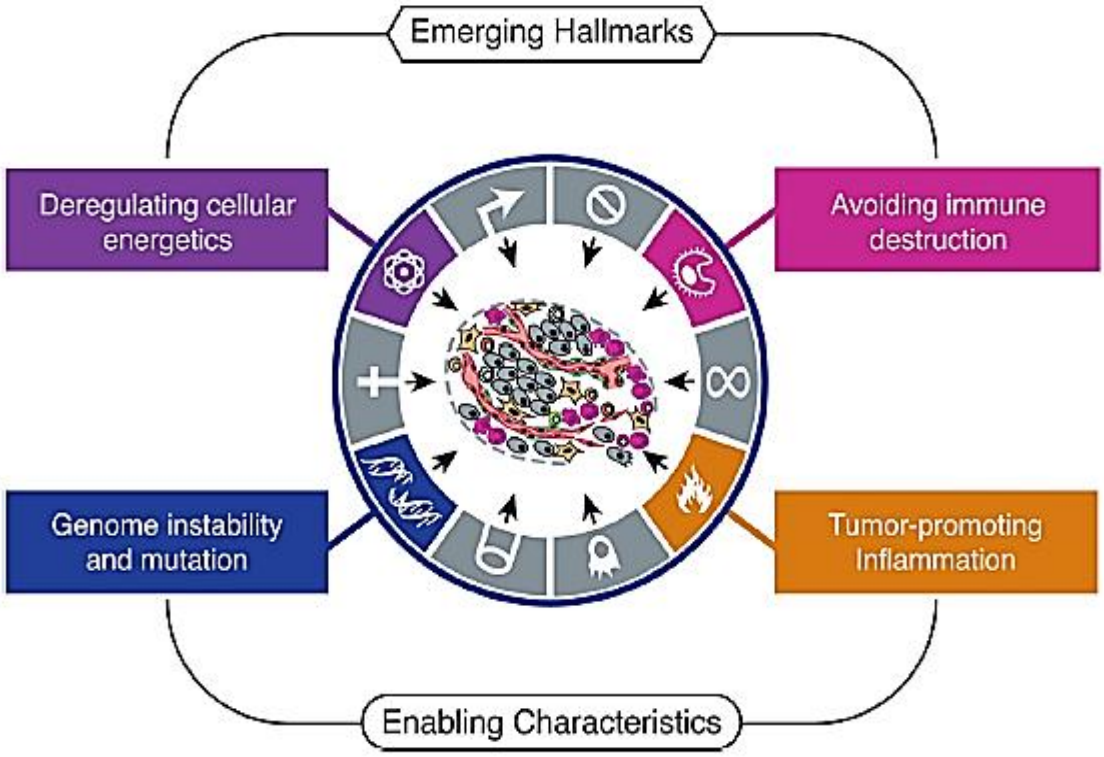

Figure 1.2 Emerging hallmarks and enabling characteristics taken from Hanahan and Weinberg, 2011

1.3 The epidemiology of cancer

Cancer is a leading cause of death worldwide. In the United Kingdom, cancer has now become the first cause of death exceeding cardiovascular disease. There are around 298,000 new cases of cancer (excluding non-melanoma skin cancer) diagnosed in the UK every year, and more than one in three people will develop some form of cancer during their lifetime. The overall incidence rates for cancer in Great Britain increased by 25%, with a 14% increase in men and a 32% increase in women, between 1978 and 2007. However, in the last decade incidence rates have remained fairly constant. There are more than 200 different types of cancer, but four of them - breast, lung, bowel and prostate together account for almost half (47%) of all cancer deaths. More than one in

five (22%) of all cancer deaths result from lung cancer, largely due to smoking. Colorectal cancer is the second most common cause of cancer death (10%) and despite being extremely rare in men, breast cancer is the third most common cause of cancer death (8%) (Cancer Research UK website).

1.4 Cancer treatment

The success of cancer treatment is variable and depends on several factors including the type and the specific characteristics of the cancer; the health status of the patient; and whether the objective of the treatment is to eradicate the patients' cancer, prevent metastasis or relieve symptoms. Often different types of treatment are used in combination, either simultaneously or sequentially. Generally, the three levels of decision-making used when formulating a treatment policy for an individual are: 1) the decision to treat or not to treat; 2) treatment intent, whether radical (aiming to long-term control or cure for the patient) or palliative (to improve the quality of life for a patient with no impact upon their survival), and; 3) specific aspects of treatment policy regarding local, systemic and supportive therapy (Figure 1.3) (Spence and Johnston, 2001). However, the practice of clinical cancer management demands more than the simple application of these instructions.

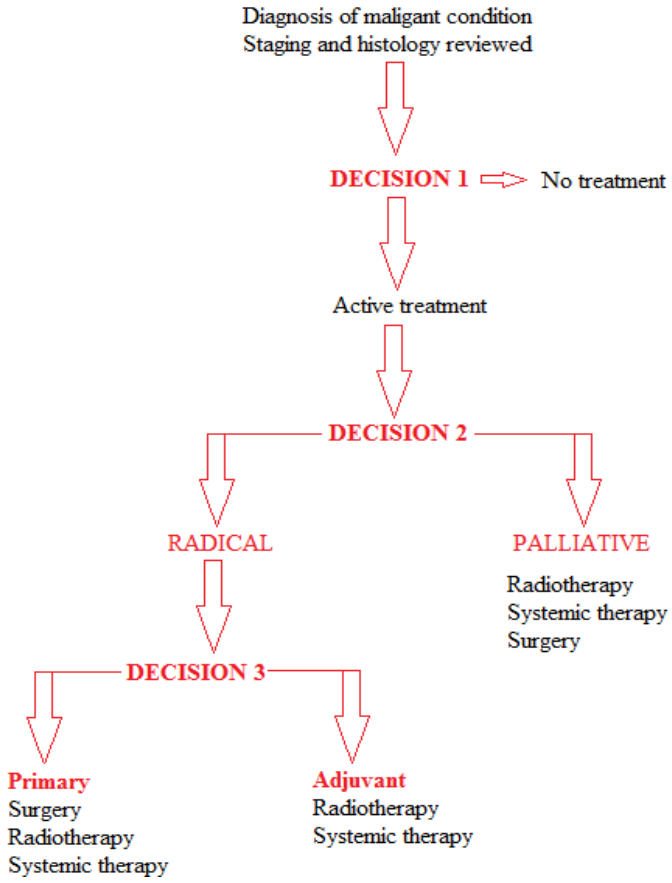

Figure 1.3 Treatment options adapted from Spence and Johnston, 2001.

1.4.1 Surgery

Surgery is one of the main treatments for cancer. It may be the only treatment needed and can be effective for cancer that is completely contained in one area and has not metastasized. The local treatment of malignant disease apart from the use of surgery, can also involve radiotherapy or a combination of the two. Surgery is essentially a local treatment while radiotherapy offers locoregional treatment covering a wider area less constrained by anatomical boundaries and the surgical technique. Optimum initial management of the primary tumor and regional metastases is vital if a later relapse is to be avoided.

1.4.2 Radiotherapy

1.4.1.1 General principles of radiotherapy

Radiation therapy involves the use of ionizing radiation for the treatment of patients with malignant neoplasia (and occasionally benign conditions). Ionizing radiation can be delivered by X-ray beams, beams of ionizing particles, e.g. electrons, or by beta or gamma irradiation produced from the decay of radioactive isotopes (Neal and Hoskin, 2009). The aim of radiation therapy is to treat a defined tumour volume under a precisely measured dose of radiation with minimal damage to surrounding healthy tissue, resulting in eradication of the tumour, better quality of life, and prolongation of survival. Once a diagnosis of cancer has been established, 50-70% of patients will receive radiation therapy at some point during their illness (Tannock et al., 2005).

1.4.1.2 Biological actions of ionizing radiation

1.4.1.2.1 Radiation-induced critical DNA damages

Alpha particles break the sugar phosphate backbone of the DNA, the beta particles break hydrogen bonds, and X-rays damage the bases. These three types of radiation in fact can lead to three types of direct damage. However, heavy charged particles such as alpha particles are more likely to cause direct damage compared to low charged particles such as X-rays, which inflict damage mostly by indirect effects. In addition to interacting directly with DNA, ionizing radiation can impair or damage cells indirectly by creating free radicals, such as hydroxyl radical, which can lead to the destruction of a cell.

Ionizing radiation causes a wide range of DNA lesions, including damages to nucleotide bases, DNA single-strand breaks (SSBs) and double-strand breaks (DSBs). The

damaged bases can be repaired through the base excision repair pathway. A SSB occurs when only one of the sugar phosphate backbones is broken. Most of the SSBs induced by ionizing radiation can be repaired via DNA ligation. DSBs are believed to be the most detrimental lesions produced in chromosomes by ionizing radiation (Jackson, 2002), because such breaks are more difficult to repair and thus more likely to result in permanent damage (Helleday et al., 2007).

1.4.1.2.2 Activation of radiation-response genes

Ionizing radiation causes cellular DNA damage affecting the expression of a number of genes involved in the DNA damage response in cells. Ionizing radiation induces the expression of early-response genes initialized by damage to the plasma membrane or to nuclear DNA. Transcription factors including c-myc, p53, c-fos/c-jun, and nuclear factor-kappa B (NF-$_k$B) proteins have been reported to be induced by cellular exposure to ionizing radiation (Hallahan et al., 1995; Ahmed, 2004; Ahmed et al., 1997). These proteins bind to specific DNA sequences and can in turn activate the transcription of cytokines, growth factors, and cell-cycle-related genes.

1.4.1.2.3 Radiation-induced cell- cycle arrest

Ionizing radiation can delay the cell cycle progression of mammalian cells. Such delays could allow for the repair of DNA damage in cells prior to undergoing either DNA replication or mitosis and could prevent the acquisition of genetic instability or mutant cellular phenotypes (Hartwell and Kastan., 1994; Schmitt et al., 2007). In fibroblasts, irradiation may cause loss of the reproductive potential by the induction of a permanent G_1 arrest (Little et al., 1994). However, the capacity for the p53 protein to mediate G_1 arrest is reduced in human tumour cells, suggesting that G_1-modulating factors may also

be important in the radiation-induced cell-cycle response of transformed cells (Li et al., 1995). Cell-cycle arrest during the S phase in irradiated cells is poorly understood, but probably involves inhibition of replicon initiation, which is required for DNA synthesis. The cyclin-B and the p34 ^{cdc2} protein kinase are associated with the control of the G_2 phase. Molecular alterations that have been associated with the onset and duration of the G_2 delay following radiation treatment include (1) decreased expression or stability of the cyclin-B protein; (2) altered phosphorylation of the p34 ^{cdc2} protein; and (3) cytoplasmic sequestration of the cyclin-B protein, thereby preventing the formation of nuclear cyclin-B/p34 ^{cdc2} complexes (Maity et a., 1994; Smeets et al., 1994; Royou et al., 2008; Metting and Little, 1995).

1.4.1.2.4 Radiation-induced cell death

The major objective of the irradiation of malignant tissue is the inhibition of the continued reproductive ability of cells. For the majority of normal and tumour cells, death secondary to mitotic catastrophe (a combination of deficient cell-cycle checkpoints and cellular damage) accounts for most of the cell kill following irradiation. However, irradiation to some radiosensitive cells such as lymphocytes, spermatocytes, thymocytes, and intestinal crypt cells leads to the cells undergoing an early (within a few hours) interphase death that can be associated with the biochemical and morphologic characteristics of apoptosis (i.e., cell membrane blebbing, the formation of nuclear apoptotic bodies, and specific DNA fragment patterns) (Radford and Murphy, 1994; Sarkaria and Bristow, 2008). The intracellular targets for the induction of the apoptotic response may be either the cell membrane or the DNA or both, depending on the cell type. The involvement of the cell membrane in triggering radiation-induced apoptosis is supported by the observation that ionizing radiation can initiate a

sphingomyelin-dependent signaling pathway within the cell membrane of endothelial cells which, in turn, can induce apoptosis in the absence of DNA damage (Verheij et al., 1996).

1.4.3 Chemotherapy

Medical oncology is the cancer speciality that focuses on the systematic management of the cancer patient with chemotherapy and other systemic treatments. The smallest size of tumour likely to be detectable is approximately 1 cm in diameter and contains about 10^8-10^9 tumour cells, depending on the contribution of the stroma and other elements to the tumour bulk. Such tumour lumps have significant potential to develop secondary tumours and metastatic disease at distant sites throughout the body, even at an early stage. Patients die due to the systemic spread of the disease rather than as a result of local recurrence in the primary organ. Therefore, anti-cancer treatment must include an effective systemic approach. Today, approximately 60-70% of cancer patients will require chemotherapy as part of the treatment of their disease (Rewari et al., 2004).

1.4.3.1 Adjuvant and neoadjuvant therapy

Cancer chemotherapy is the treatment of malignant disease with drugs rather than radiation or surgical removal. The drugs used are often highly toxic since they are not exclusively selective for cancer cells, resulting in unwanted side effects. Systemic therapy used after optimal locoregional therapy (surgery/radiotherapy) has been found to enhance local control and to reduce the potential of metastasis. The radiotherapy or systemic therapy is commonly given as adjuvant treatment after surgery for many types of cancer (e.g, breast and lung cancer). In certain circumstances chemotherapy is

administered prior to locoregional therapy in an attempt to significantly reduce the tumour cell burden. This approach is termed neoadjuvant therapy.

1.4.3.2 General principles of chemotherapy

The effective use of cancer chemotherapy requires an understanding of the tumour cell kinetics, the tumour cells' doubling time, cancer pharmacology and drug resistance. A variable proportion of the tumour cells will actively divide at any one time. This may range from 90% in some tumours, for example, lymphomas, to less than 20% in others such as certain solid tumours (e.g. colon and breast cancer). Cytotoxic chemotherapeutic agents are generally preferentially toxic towards actively proliferating cancer cells, however, they will also affect normal cells undergoing rapid proliferation (for example, cells of the buccal mucosa, bone marrow, gastrointestinal mucosa and hair folicles), contributing to the toxicity of chemotherapy (Gerber, 2008; Mitchison, 2012).

1.4.3.3 Classification of chemotherapeutic agents

1.4.3.3.1 Alkylating agents

Antitumour alkylating agents are the largest class of anticancer drugs. These cell cycle non-specific agents impair cell function by acting through the covalent bonding of alkyl groups ($R\text{-}CH_2$) to chemical moieties in DNA after being metabolized in the body (McCune and Slattery, 2002; reviewed in Hartley, 2001). In general, they act through the generation of highly reactive, positively charged intermediates, which then combine with an electron-rich nucleophilic groups such as an amino, carboxyl, sulfhydryl, phosphate or hydroxyl moiety (McCune and Slattery, 2002). Alkylating agents can be classified as either monofunctional or bifunctional, depending on whether they have one or two reactive groups. Alkylation by monofunctional agents produces monoadducts.

With bifunctional agents, an initial alkylation producing monoadducts is followed by a second reaction in which crosslinks are formed. The second reaction is often slow, and only around 1 in 20 monoadducts form crosslinks. DNA crosslinks can be formed within a single strand of DNA (intrastrand), between the two complementary strands of DNA (interstrand), or between a DNA base and a reactive group on a protein (DNA-protein) (Figure 1.4A and B) (McHugh et al., 2001).

1.4.3.3.1.1 Nitrogen Mustards

The first documented clinical use of chemotherapy was in 1942, when the alkylating agent nitrogen mustard (mechlorethamine) was used to obtain a brief clinical remission in a patient with lymphoma (Gilman, 1946). The family of drugs, deriving from the prototype alkylating agent nitrogen mustard, includes chlorambucil, cyclophosphamide, melphalan and ifosfamide. Chlorambucil is a phenylbutyric acid derivative of mechlorethamine and is relatively stable in aqueous solution and enters cells by simple diffusion. It is used to treat chronic lymphocytic leukaemia, lymphoma, Hodgkins disease and multiple myelomas (Takimoto, 2008). Cyclophosphamide is the most versatile and useful nitrogen mustard. It is a prodrug, requiring metabolic activation and conversion to an active nitrogen mustard, phorporamide mustard. It has a favourable therapeutic index and the broadest spectrum anti-tumour activity of all alkylating agents. It is mainly used for non-Hodgkins lymphomas (Moore, 1991; Ayash et al., 1992). Melphalan is the phenylalanine derivative of mechlorethamine and is less reactive due to its slower rate of chloride ionization. Each of them is bifunctional, with two chloroethyl groups that form the reactive electron-deficient groups responsible for alkylation of DNA. Ifosfamide is a prodrug and an analogue of cyclophosphamide that contains a chloroethyl group on the nitrogen atom of the oxazaphosphorine ring. It is

used primarily to treat sarcomas, and both testicular and non-small cell lung cancers (Takimoto, 2008).

A

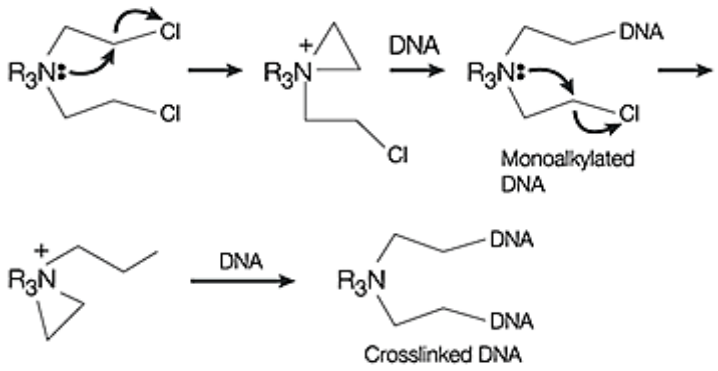

B

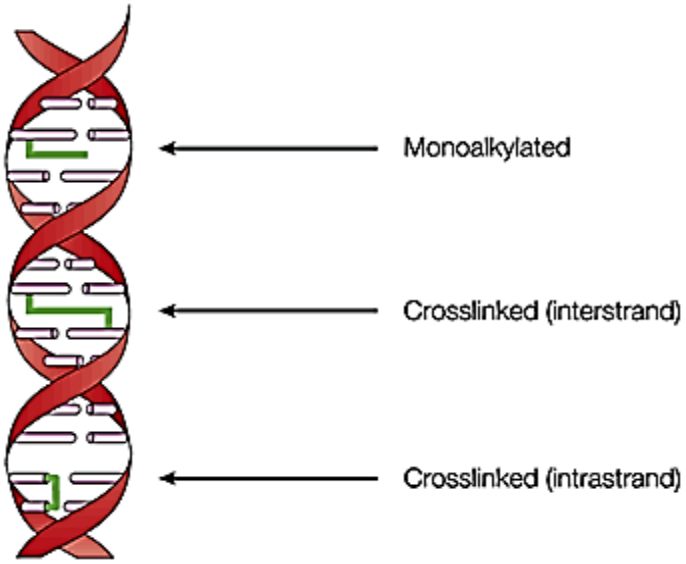

Figure 1.4 Monoalklation and crosslinking chemistry of bifunctional nitrogen mustards. **A**, Chlorine is a leaving group that facilitates nucleophilic attack of nitrogen to form an imminium ion (R_3N) in a strained ring system. This readily undergoes alkylation at N7 of guanine to form a monoalkylation adduct (see **B**). This process can then be repeated to form the DNA crosslink. Crosslinking can occur either between two complementary strands of DNA (interstrand) or within a strand of DNA (intrastrand) (see **B**) (adapted from Hurley, 2002).

1.4.3.3.2 Platinum-based compounds

Platinum compounds are amongst the most frequently used class of anti-cancer drugs, showing a mechanism of action that is similar to the mechanism of action of alkylating agents. The biological activity of cisplatin (cis-diamminedichloroplatium) was discovered serendipitously in 1965 by Rosenberg experimenting on the effect of electric fields on the cell division of bacteria (reviewed in Rosenberg et al., 1977). Cisplatin possesses two chloride ions, which can be displaced in aqueous solution to form a reactive electrophilic species (Figure 1.5A). The kinetics of cisplatin's chloride ligand displacement reactions lead to DNA crosslinking activities (Figure 1.5B), causing DNA bending and interfering with DNA replication, transcription and other nuclear functions and arresting cancer cell proliferation and tumour growth (Jakupec et al., 2003). Cisplatin primarily reacts with the N7 atom of purine bases in the DNA major groove resulting in the formation of 1,2-d(GpG) (~65%), 1,2-d(ApG) (~25%), and 1,3-d(GpNpG) (~6%) intrastrand cross-links, and interstrand cross-links (1-2%) between guanines in the complementary DNA strands (Figure 1.5B) (Damsma et al., 2007; Boulikas et al., 2007).

The use of cisplatin and its effectiveness in cancer chemotherapy has been thoroughly documented. It is used as a principal component for the treatment of testicular, ovarian and bladder cancer. In addition, cisplatin is being used as first line chemotherapy against cancers of the lung, head-and-neck, stomach, colon, bladder, cervix, uterus and as second line treatment against other advanced cancers such as cancers of the breast, pancreas, liver, kidney and prostate (Boulikas and Vougiouka, 2003; 2004). Cisplatin exhibits severe nausea and vomiting, renal damage and neurotoxicity. Analogues have been synthesized in an attempt to produce agents with the same high level of antitumour

activity but less intense side-effects. Of these analogues only carboplatin and oxaliplatin are widely used clinically. However, neither carboplatin or oxaliplatin have achieved the broad-spectrum effectiveness of cisplatin (Judson and Kelland, 2000; reviewed in Kelland, 2007).

1.4.3.3.3 Antimetabolites

Antimetabolites are structurally similar to naturally occurring metabolites, which interfere with normal cellular function, particularly involved in DNA and RNA synthesis. The cytotoxic activity of the antimetabolites derives either by competing with normal metabolites for the catalytic or regulatory site of a key enzyme or by substituting for a metabolite that is normally incorporated into DNA and RNA. As a result of this mechanism of action, antimetabolites exert their activity when cells are in the S phase and show little effect on resting cells. Therefore, these drugs are most effective against tumours that have a high growth fraction (Ruiz van Haperen and Peters, 1994). Many of the clinically useful antimetabolites are purine (e.g., 6-thioguanine) or pyrimidine (e.g., 5-fluorouracil) analogues that either inhibit the formation of the normal nucleotides or interact with DNA and prevent normal cell division from occurring (Moore et al., 1995; Pizzorno et al., 2000).

Most antimetabolites are cell cycle-specific and exhibit a nonlinear dose-response curve, such that after a certain dose, no more cells are killed despite increasing the drug dose (fluorouracil is an exception) (Pizzorno et al., 2000). As they do not interact directly with DNA, they do not cause problems such as carcinogenesis seen with DNA-binding drugs like the alkylating agents.

A

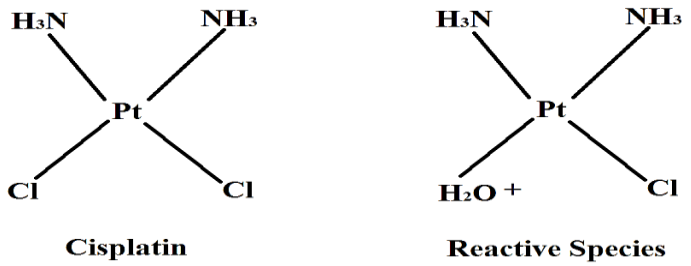

B

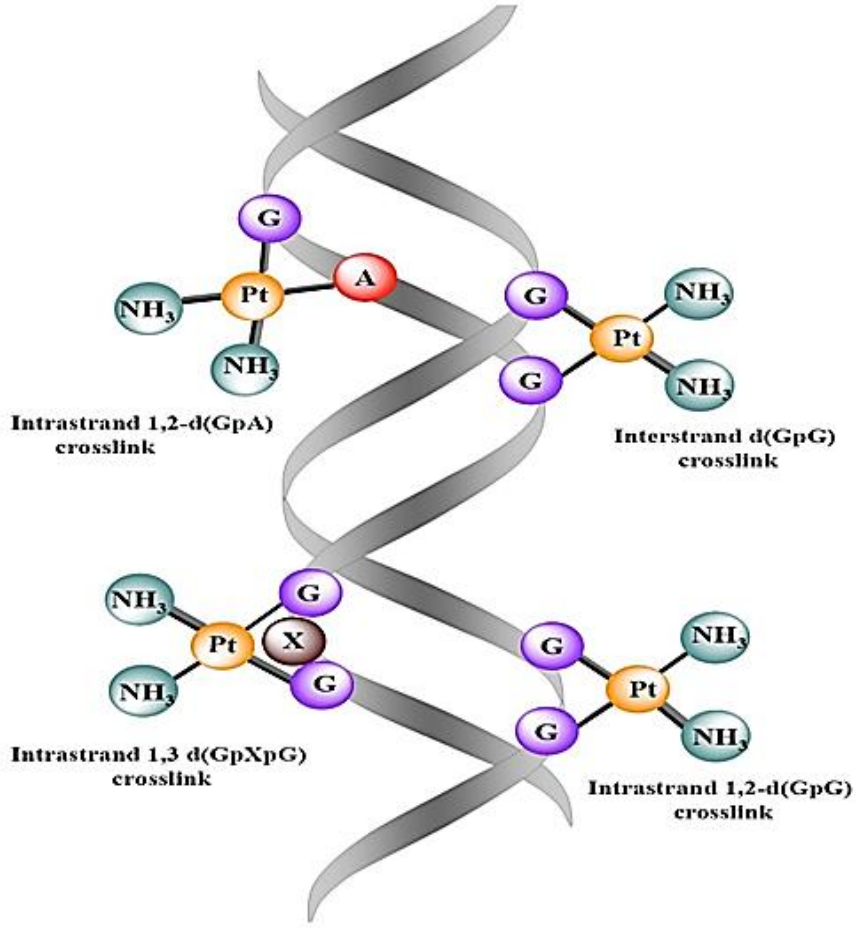

Figure 1.5 Structures of platinum compounds. A. Structures of cisplatin. In an aqueous solution, the chloride ions can be displaced to leave an electrophilic aquated species, which is the reactive form of these compounds. B. DNA adduct formation with cisplatin leaving two amino groups coordinated on the platinum atom (Boulikas et al., 2007).

1.4.3.3.4 Natural Products

Natural products are compounds isolated from plants, fungi, or bacteria or derivatives of such products. Within this category are drugs, which interfere with the topoisomerase I (topo I) (e.g., camptothecins) or topoisomerase II (topo II) (e.g., etoposide) enzymes, which bind directly to DNA (Baldwin and Osheroff, 2005; Bodley et al., 1989).

Camptothecin is an extract of the tree *Campotheca accuminata* that exerts antitumour activity by inhibiting topo I (Rothenberg, 1997). Topo I is an enzyme that catalyses the transient cleavage and resealing of a single strand of DNA during transcription and replication (Wang, 1991). A number of water-soluble Camptothecin semisynthetic derivatives have been investigated and demonstrated significant clinical activity, such as topotecan and irinotecan (CPT-11) (Rothenberg, 1997), which have well-established antitumour activities against various primary tumours (Timur et al., 2005; Wong and Berkenblit, 2004).

Etoposide is a semisynthetic glycoside derivative of the antimitotic agent podophyllotoxin derived from the mandrake plant. Podophyllotoxin binds to tubulin and inhibits polymerisation, however, etoposide inhibits the topo II enzyme and is widely used for treating various cancers (Baldwin and Osheroff, 2005). Topo II catalyzes a transient breakage and reunion of double-stranded DNA during transcription and replication, and is also responsible for chromosome segregation during mitosis (Cuvier and Hirano, 2003; Valkov and Sullivan, 2003). Two topo II isozymes have been identified in human cells namely, topo IIα and topo IIβ (Berger, 1996). Topo IIα is a homodimer which catalyses the ATP-dependent strand-passing reactions and functions in DNA replication and chromosome condensation and segregation (Li and Liu, 2001).

It contains two major domains, the N-terminal ATPase domain and the breakage/reunion C-terminal domain. Topo IIα is essential for cell growth and is a cell proliferation and tumour marker. Topo IIβ is also a homodimer which although exhibiting similar enzymatic activities to topo IIα *in vitro*, is constitutively expressed at a constant level throughout the cell cycle (Li and Liu., 2001; Burden and Osheroff, 1998; Baldwin and Osheroff, 2005).

1.5 DNA as an anti-cancer drug target

DNA has long been the molecular target for chemotherapeutic agents as illustrated in Figure 1.6. These drugs can block DNA replication and transcription either by direct binding to DNA or to DNA-binding proteins such as topoisomerases (Hurley, 1989). Many natural and synthetic anticancer agents with the ability to interact with DNA were discovered as a consequence of chemical warfare during World Wars I and II that spawned the modern era of cancer therapy (Kohn, 1996), but most have a limited degree of sequence specificity and often exhibit severe toxicity to normal tissue. Therefore, a new generation of chemotherapeutic agents that target DNA-associated processes is anticipated to be more specific, selective and effective (Hurley, 2002; Baraldi et al., 2007).

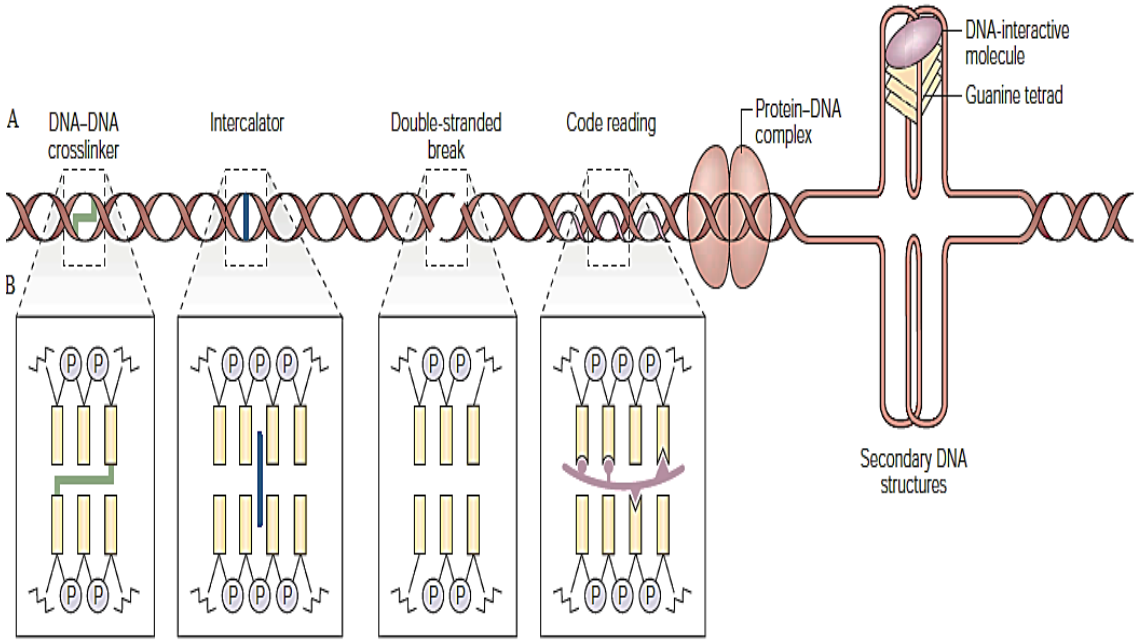

Figure 1.6 Types of DNA-interactive agents and their molecular interactions with DNA (adapted from Hurley, 2002).

1.5.1 Structure and biology of the DNA minor groove

The double helix of DNA is composed of two complementary, antiparallel polydeoxyribonucleotide strands associated by specific hydrogen bond interactions between nucleotide bases (Watson and Crick, 1953). The minor groove is narrow and shallow, approximately 10 Å in width in comparison with the deeper and wider major groove, which is about 24 Å in width (Figure 1.7A) (Saenger, 1984). The helical grooves are determined by the sugar phosphate backbone of double strands that stick out at 120 ° angles from each other instead of 180 ° (Saenger, 1984). The chemical features of the molecular surfaces in the DNA sequence provide the basis for molecular recognition by small molecules and proteins (Figure 1.7B) (Cai et al., 2009).

A

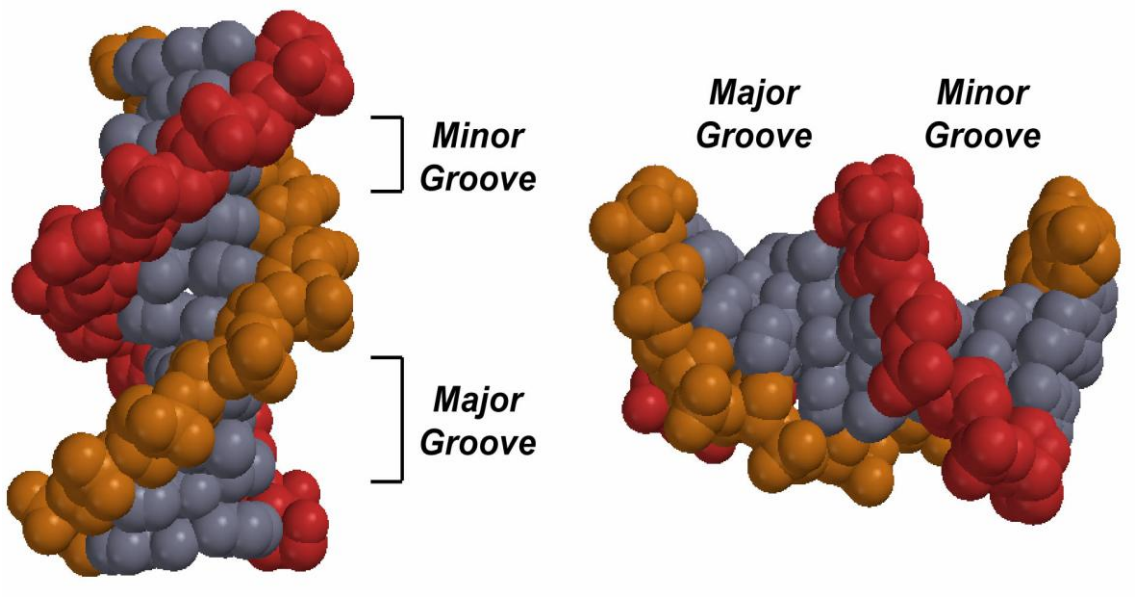

B

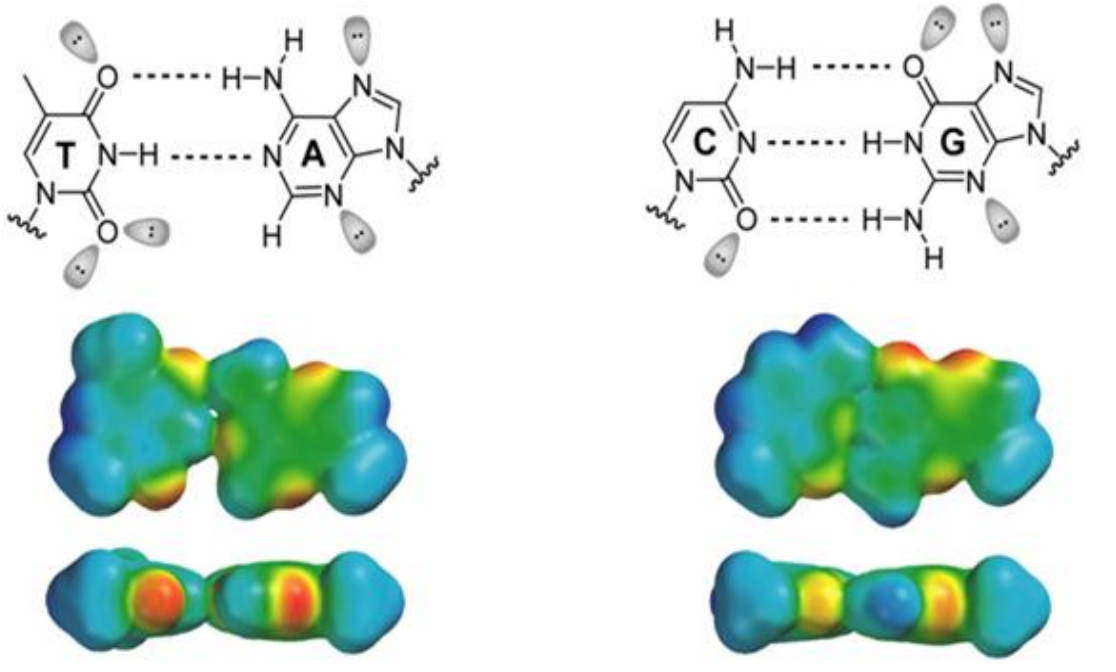

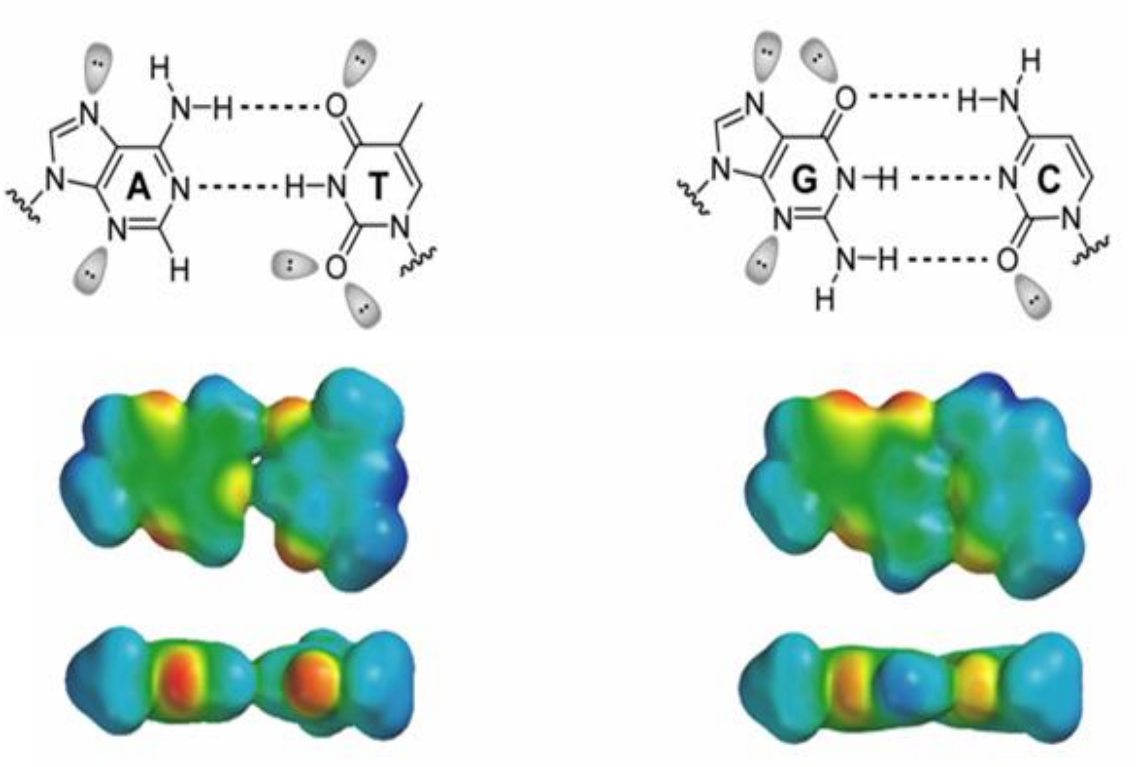

Figure 1.7 Structural features of the DNA double helix. **A** Molecular structure of double helical B-DNA showing major and minor groove. Sugar phosphate backbones are presented in red and orange. **B** Chemical features and electrostatic potential surfaces (red-negative electrostatic potential, blue-positive electrostatic potential, green-neutral) of Watson-Crick base pairings.

1.5.2 The DNA minor groove as a target

Proteins recognize hydrogen bond donors and acceptors as well as hydrophobic methyl groups (Panasik et al., 2005; Fleming and Rose, 2005). In nature, the minor groove represents a vulnerable site of attack, which is normally unoccupied or is bound by small molecules of less than 1000 Da, while most of the DNA interactive proteins bind to the major groove. The minor groove of double helical B-DNA has been considered as a target of great interest for developing new agents of non-covalent, reversible, highly specific interactions of small molecules at thymine-adenine (TA)-rich sequences, showing antibacterial and antiviral activities (Kielkopf et al., 1998; Baraldi et al., 2004).

The DNA minor groove binders have been widely studied and constitute an attractive lead for the design of novel antitumor molecules.

1.5.2.1 Diarylamides and their derivatives

Since the 1930s, the efficacy of diarylamides has been well known for the treatment of trypanosomiasis and leishmaniasis (Baraldi et al., 2004). In the early 1970s, diarylamides derivatives such as DAPI (DNA fluorochrome 4'-6-diamidine-2-phenyl indole), berenil, stilbamidine, and pentamidine were discovered with the aim of finding even more effective antiparasitic drugs. DAPI was shown to bind to the minor groove with the phenyl and indole rings parallel to the groove walls in the AT-rich regions of B-DNA (Larsen et al., 1989). However, the clinical use of DAPI as an anti-microbial agent has been constrained by its undesirable side effects. Berenil was characterized by high affinity for the three-base pair sequence ATT and has been used in veterinary medicine for the treatment of trypanosomiasis (Newton, 1975; Yoshida and Banville, 1990). Pentamidine is perhaps the most well-known anti-microbial DNA minor groove binder and has been shown to preferentially bind to AT-rich regions in the B-DNA minor groove containing at least five consecutive AT base pairs (Nguyen et al., 2002; Baraldi, 2004). The efficacy of pentamidine has been shown in the treatment of *Pneumocystis jiroveci*, although the mechanism of its action is still unclear. Yet, like the other anti-microbial minor groove binders, pentamidine displays toxicity such as nephrotoxicity, cardiotoxicity, and hepatotoxicity. Consequently, new pentamidine-type molecules have been sought with the aim of increasing the overall efficacy, decreasing the toxicity and improving the minor groove binding affinity to treat *Pneumocystis pneumonia* (Cai et al., 2009). The oncogenic PRL phophatases that have an essential role in many cancers has been shown to be a target of pentamidine.

1.5.2.2 Bis-bezimizazoles

Hoechst 33258 (also known as Pibenzimol) is a fluorescent reagent with a head-to-tail bis-benzimidazole and binds in the minor groove of B-DNA selective for AT sequences (Harshman and Dervan, 1985). Hoechst 33258 was initially founded to have moderate *in vivo* activity against murine leukemia (Gravatt et al., 1994). It is readily taken into cells (Bontemps et al., 1975) and binds extremely tightly to DNA (Loontiens et al., 1990), thus inhibiting transcription specific genes.

1.5.2.3 CC-1065 and Duocamycin

CC-1065 and Duocamycin are antitumour antibiotics, which exhibit their biological effect through binding to double-stranded B-DNA within the minor groove at AT-rich sequences and selectively alkylating the N-3 position of adenine (Krueger et al., 1991; Boger, 1995). CC-1065 exhibited high potency and a broad spectrum of antitumour activity, however it could not be used in humans because it results in delayed death in experimental models. Duocamycin, on the other hand, showed weaker antitumour activity, partially attributed to its low water solubility (Yasuzawa et al., 1988). Adozelesin was the first of the CC-1065 derivatives to enter clinical trials. A phase II study of adozelesin in untreated metastatic breast carcinoma was halted due to slow accrual and lack of efficacy (Cristofanilli et al., 1998). Later, studies have focused on the potential use of adozelesin or similar drugs as anti-malarial agents (Woynarowski et al., 2007). KW-2189 is a highly water-soluble derivative of Duocamycin B2. No objective responses were observed when treating patients with both advanced renal cells carcinoma and malignant melanoma in phase II trials (Small et al., 2000; Markovic et al., 2002).

1.6 Netropsin, distamycin A and derivatives

1.6.1 Netropsin and Distamycin A

A large number of minor groove binders have been designed and tested by researchers over the past decades. The majority of these were synthesized based on the naturally occurring netropsin and distamycin A agents originally termed lexitropsins. Netropsin and distamycin A are derived from the Streptomyces species *S. netropsis* and *S. distamyces* (Finlay et al., 1951; reviewed by Arcamone 1993), respectively. They comprise of two and three pyrrole moieties with either an N-terminal guanidinium or formyl group and a C-terminal propylamidine (Figure 1.8). Netropsin and distamycin A have shown potent biological effects exhibiting antiviral and antimalarial activities but without any significant antitumour properties (Arcamone, 1993; Sharma et al., 2002). They bind non-covalently to the minor groove of DNA, thereby preventing DNA and RNA synthesis by inhibition of the corresponding polymerase reaction and display pronounced sequence specificity (Zimmer et al., 1971; Chandra et al., 1972).

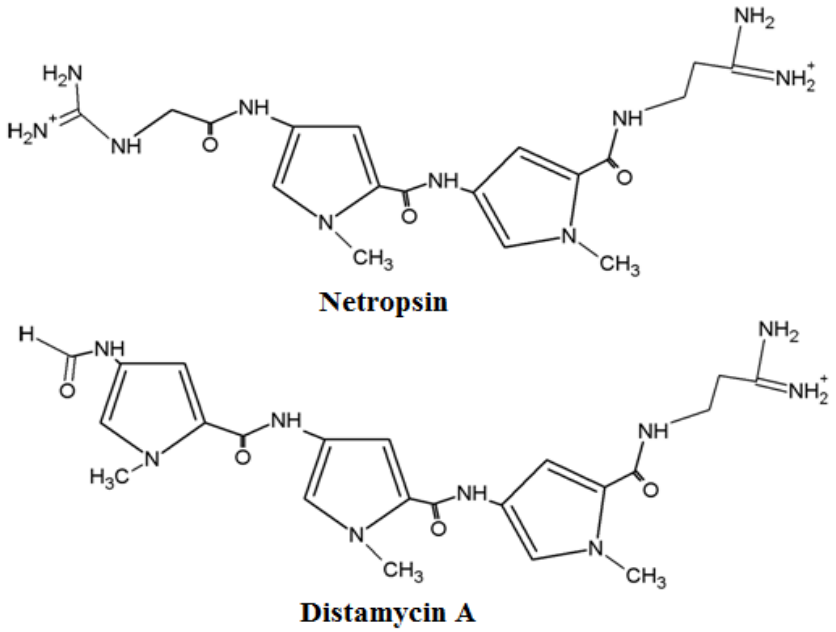

Figure 1.8 The minor groove binding antibiotics netropsin and distamycin A.

Netropsin and distamycin A show a highly selective reversible interaction with AT sequences containing four or five A/T base pairs, respectively (Lane et al., 1983; Fox and Waring 1984; Kielkopf et al., 1998). Binding is limited to AT tracts by netropsin and distamycin A due to the interruption of the guanine 2-amino group in the minor groove causing a steric clash with the N-methylpyrrole C3 hydrogen, preventing binding to GC-rich regions (Figure 1.9) (Wartell et al., 1974). Distamycin A, characterized by the presence of an oligopeptidic pyrrolecarbamoyl frame ending with an amidino moiety, has sequence specificity and high affinity due to a combination of interactions (Figure 1.10) including hydrogen bonding, van der Waals contacts and electrostatic interactions with a strong preferential binding to AT rich sequences in the minor groove of DNA (Pelton et al., 1989).

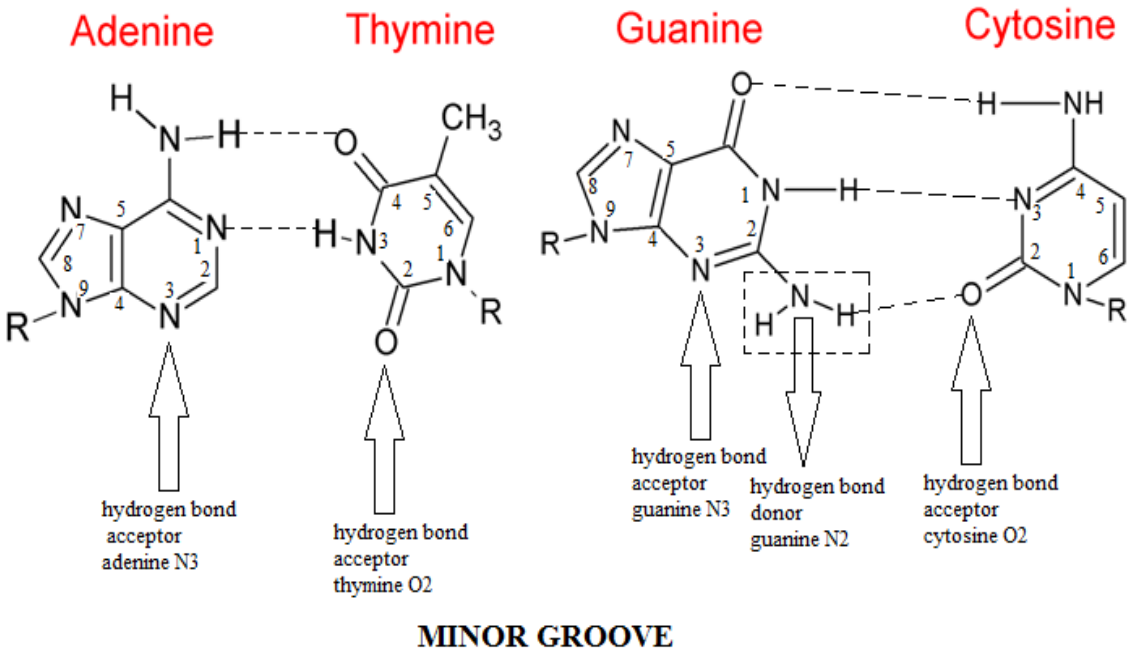

Figure 1.9 A schematic diagram showing the guanine 2-amino group protruded in the minor groove, as indicated by the dashed box. The available hydrogen bond donors and acceptors in the minor groove are also detailed.

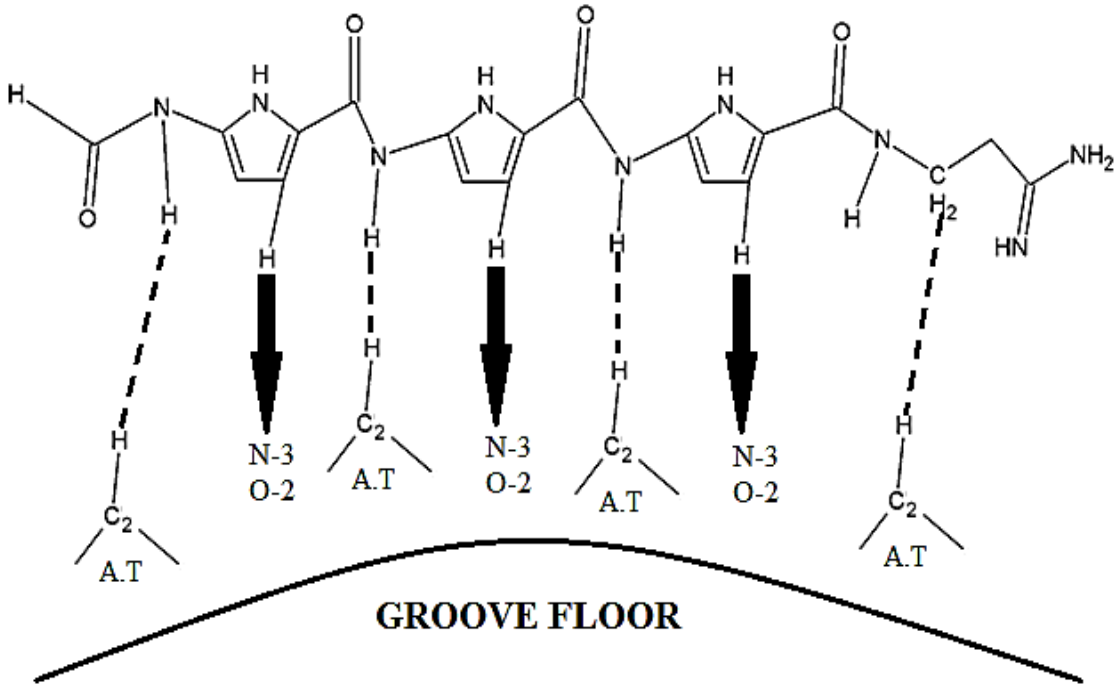

Figure 1.10 Bonding components contributing to the sequence-specific binding of distamycin A to $(AT)_5$ as adapted from Bailly and Chaires 1998. Heavy arrows indicate hydrogen bonding from donor to acceptor, whilst dashed lines indicate close van der Waals non-bonded contacts between the ligand and the DNA.

The cytotoxicity of netropsin and distamycin A limited their clinical use (Rehm et al., 2009; Pulido et al., 2009). However distamycin A was associated with the treatment of malarial and angiogenesis diseases based on gene expression of small molecules targeted sequence and control of gene switches. It is always the aim of the medicinal chemists to design and synthesize analogues of netropsin and distamycin A, having high DNA binding affinity and sequence selectivity so that these newly synthesized compounds can be used as drugs which have therapeutic value (reviewed in Khalaf, 2009).

1.6.2 Distamycin-derived nitrogen mustards

Netropsin and distamycin provide a platform for the rational design of DNA binding ligands (Dervan, 2001). The main representatives of minor groove binders that have been clinically tested in the past are tallimustine (TAM), a hybrid of a benzoic acid nitrogen mustard moiety and distamycin A (Figure 1.11) (Pezzoni et al., 1991; D'Incalci et al., 1997).

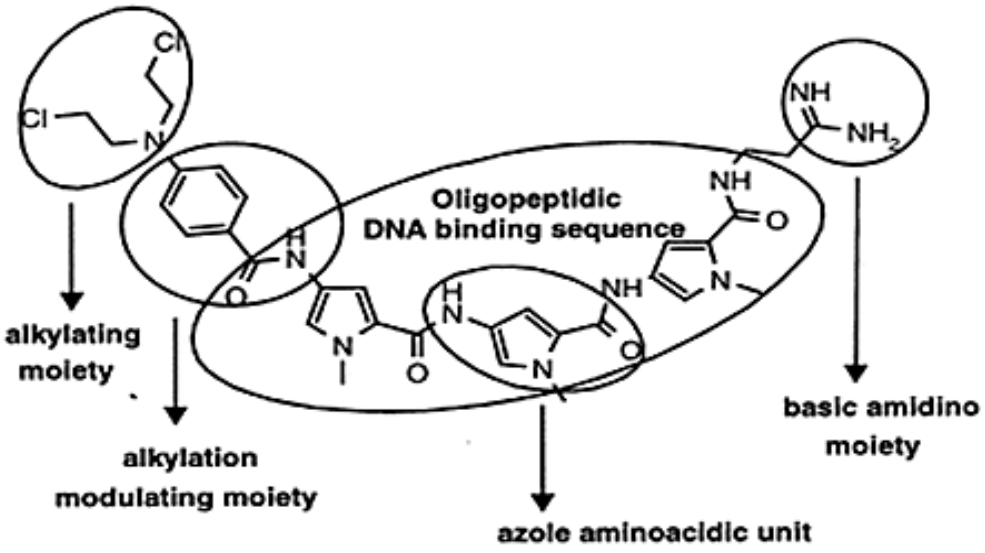

Figure 1.11 Chemical structure and different functional moieties of the benzoyl nitrogen mustard tallimustine (adapted from Cozzi et al., 2001).

DNA Footprinting and NMR studies showed that the pyrrole rings of TAM are stacked in the AT-rich domain of the B-DNA minor groove, so that the alkylating moiety of the benzoic acid nitrogen mustard would be able to alkylate the nucleotide residues present in the B-DNA minor groove (Marchini et al., 2001). Both of the components seem to contribute to the drug's biological properties as TAM possesses higher cytotoxicity against L1210 murine leukemia than distamycin A or classical benzoic acid nitrogen mustard (Arcamone et al., 1989; D'Allessio et al., 1994). The possibility could also be

considered that distamycin-driven DNA binding increases the TAM concentration near the DNA target, avoiding alkylation of other biological nucleophiles, e.g. glutathione (Denny et al., 2001). TAM showed promising antitumor activity in clinical development up to phase II, however, it exhibited severe myelotoxicity (Ghielmini et al., 1997) and its further development was discontinued. However, the utilization of TAM as a model compound advanced the design of new minor groove alkylating agents having demonstrated the possibility of gaining potent antitumor activity by combining a chemically reactive moiety (benzoic acid nitrogen mustard) with a DNA selective binding-frame. (Cozzi et al., 1997).

1.6.3 Distamycin-derived α-halogenoacrylamides

A class of cytotoxic distamycin derivatives possessing a potential alkylating moiety of low chemical reactivity such as α-bromo or chloro-acrylamido tethered to a distamycin A or distamycin A-like frame has been identified (D'Allessio et al., 1994; Cozzi et al., 2000). The first lead compound of this series, PNU-151807 (Figure 1.12A), the α-bromoacrylamido derivative of a four-pyrrole distamycin A analogue, revealed high cytotoxicity and in *vivo* activity. In addition, PNU-151807, unlike TAM, was unable to alkylate minor groove AT-rich sequences in different in *vitro* experiments but interacted non-covalently with the DNA minor groove, suggesting that α- bromoacryamido distamycin derivatives are a new class of minor groove binders acting through a mechanism distinct from direct DNA alkylation (Marchini et al. 1999).

Preclinical studies showed the antitumor activity of PNU-151807 with a significantly better cytotoxicity/myelotoxicity ratio over TAM. For instance, PNU-151807 in leukaemic cells was found to be a more potent agent compared with TAM and was also

demonstrated to block activity of cell-cycle dependent kinases at least in *vitro* while TAM or distamycin A were not (Marchini et al. 1999). As a result, the activity and the atypical mechanistic features of PNU-151807 elicited the synthesis of new halogenoacrylic derivatives of distamycin in the aim of optimising their toxicological profile and potentially helping to define their mechanism of action (Cozzi et al., 2000).

Brostallicin (PNU-166196) (Figure 1.12B), an α-bromoacrylamido-tetrapyrrolecarbamoyl derivative ending with a guanidino moiety, showed a outstanding favorable cytotoxicity/myelotoxicity ratio both in *vivo* and in *vitro*, and a broad spectrum of activity in tumor cell lines in *vitro* and tumor xenografts in *vivo* compared to other minor groove binders (e.g. TAM and PNU-151807) (Cozzi et al. 2000). Brostallicin has undergone phase I and phase II clinical trials in both Europe and the US involving more than 230 patients in single agent and combination trials (Leahy et al., 2007; Cai et al., 2009). Brostallicin has been generally well tolerated with mild to moderate, reversible myelosuppression being the primary adverse event. It has had predictable and predominantly hematologic toxicities, which rarely required growth factor support. Responses have been reported in metastatic soft tissue sarcoma and ovarian cancer resistant/refractory to platinum-based chemotherapty (Leahy et al., 2007; Lorusso et al., 2008). Brostallicin is therefore considered as a novel minor groove binder with unique pharmacological properties and a favorable toxicological profile.

1.7 Pyrrolobenzodiazepine hybrids and conjugates

The Pyrrolo[2,1-c][1,4]benzodiazepines (PBD) group of drugs includes the naturally occurring antitumor antibiotics anthramycin, sibiromycin, tomaymycin, neothramycin and DC-81 (Figure 1.13) produced by *Streptomyces* species. These agents exhibit their

DNA interactive activity and resultant biological effects through the N10-C11 carbinolamine/imine moiety in the central B-ring which is capable of covalently binding to the C2-NH_2 of guanine residues in the minor groove of DNA (Baraldi et al., 2007). X-ray and footprinting studies of covalent DNA-PBD adducts have demonstrated a high selectivity for 5'-purine-G-purine sequences (Kopka et al., 1994; Hertzberg et al., 1986; Hurley et al., 1988). Both anthramycin and sibiromycin were found to have antitumour activity against a range of transplanted tumours, however, the clinical use was limited due to dose-limiting cardiotoxicity, presumably due to the presence of a C9 oxygen (Korman and Tendler, 1965; Cargill et al., 1974). Many other naturally occurring PBDs do not include a C9 oxygen and exhibit cardiotoxicity. Only neothramycin has been tested clinically for the treatment of superficial carcinoma of the bladder (Tsugaya et al., 1986).

In the past decade, PBD hybrid or conjugate compounds, combining derivatives of PBD monomers with a distamycin A-like minor groove binder or intercalators (e.g. naphthalimides), have been designed, synthesized, and tested with the aim of combining high DNA binding affinity and sequence selectivity (Baraldi et al., 2000; Tietze et al., 2003; Wells et al., 2006). The numerous PBD hybrids and conjugates exhibited their antitumour activities against tumour cell lines and high DNA binding affinity *in vitro* (Cipolla et al., 2009). However, there is a lack of any *in* vivo data on these molecules. One exception is a PBD-indole conjugate, IN6CPBD (Figure 1.13), which induced apoptosis in human melanoma A375 cells *in vitro,* possessed enhanced DNA sequence selectivity, and also exhibited great efficacy and superior safety in suppressing the growth of established melanoma *in vivo* (Lee et al., 2009).

A

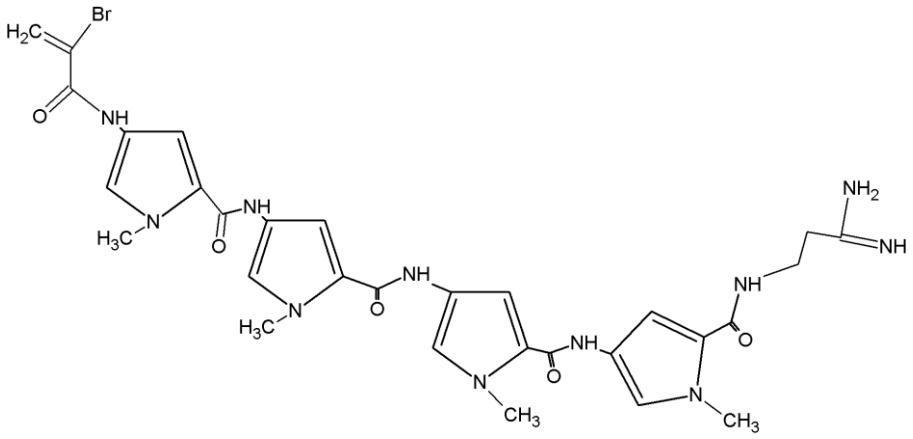

B

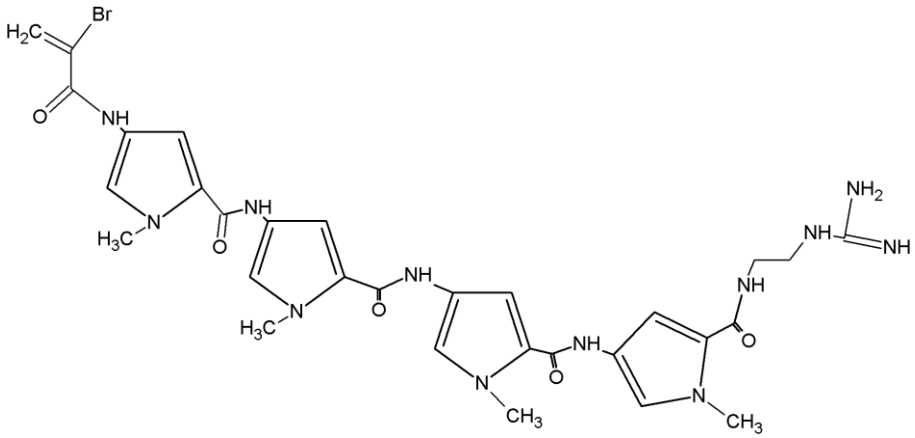

Figure 1.12 α-bromoacrylamido-tetrapyrrolecarbamoyl derivatives. A. PNU 151807 and B. Brostallicin.

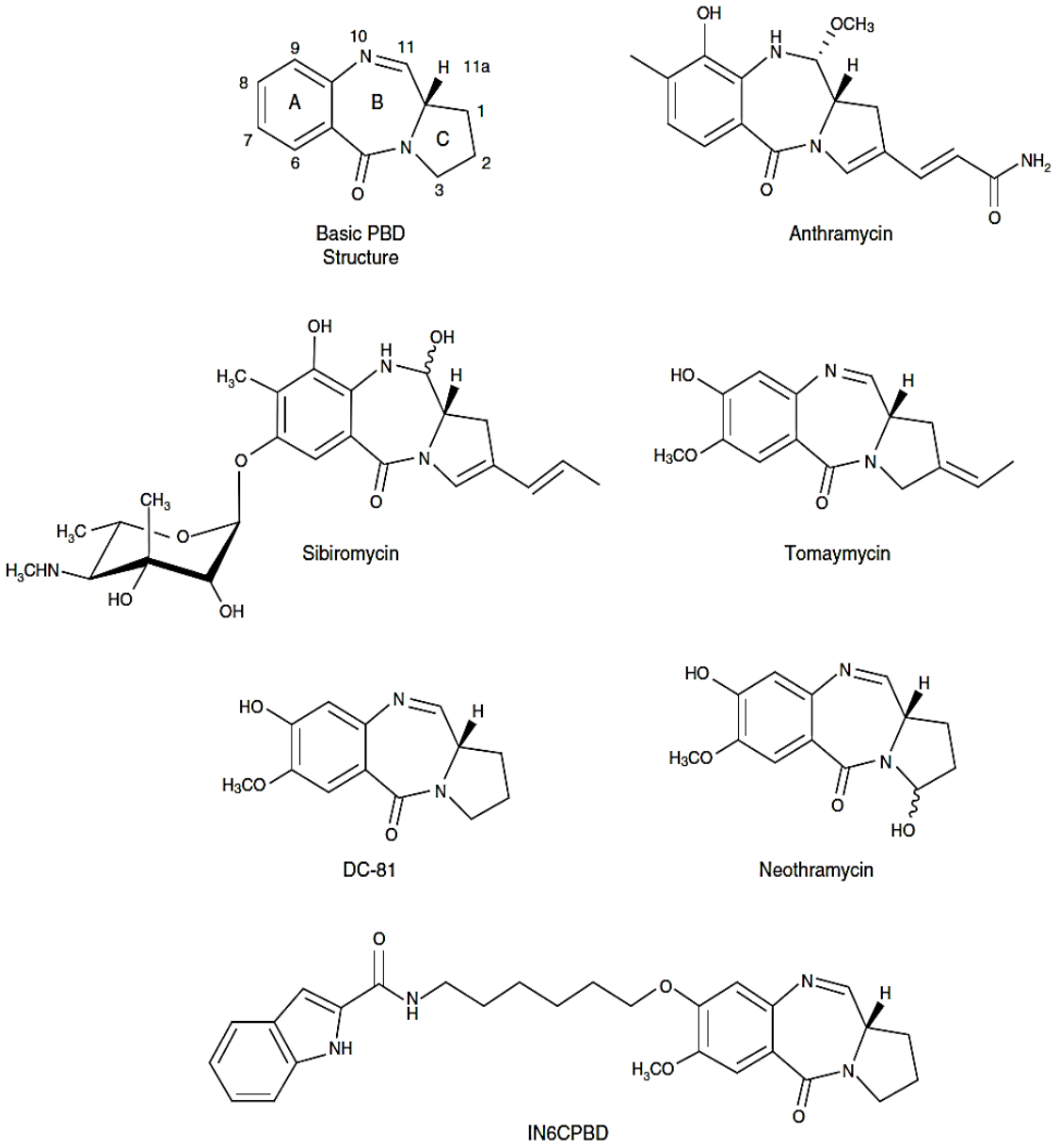

Figure 1.13 The basic pyrrolebenzodiazepine (PBD) structure, the structure of naturally occurring PBDs and PBD-indole conjugate IN6CPBD

1.8 Introduction of a GC recognition element

Polyamide structural derivatives of netropsin and distamycin A have been synthesized to capitalize on their strongly selective minor groove binding properties. Many research groups have reported more selective and specific polyamide molecules with the aim of

recognizing G/C base pairs alongside A/T (Kopka et al., 1985; Kielkopf et al., 1998; Dervan et al., 2001). Modification of the inherent specificity of netropsin for AT base pairs was achieved through the introduction of a GC recognition element, conducted by replacing the *N*-methylpyrrole rings of netropsin with imidazole, thiazole, triazole, pyrazole or oxazole heterocycles (Figure 1.14). Consequently, the modified compounds can bind selectively to DNA sequences with a mixed base pair content (Kopka et al., 1985; Lown et al., 1986; Kielkopf et al., 1998).

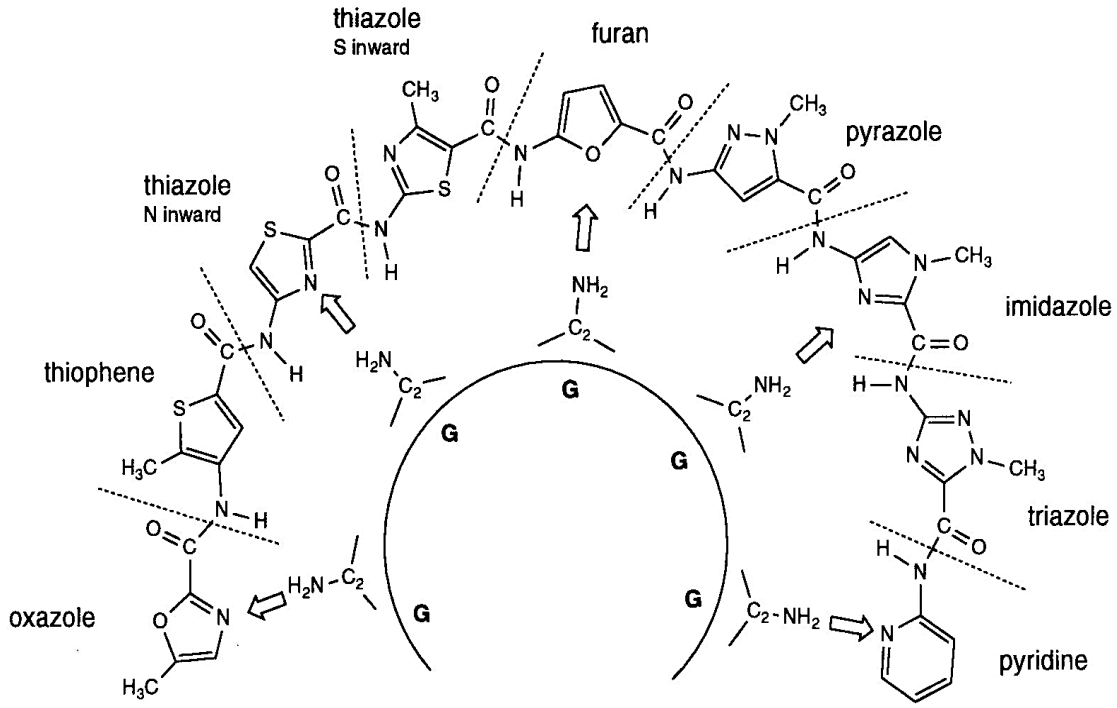

Figure 1.14 Representation of putative GC recognition heterocycles indicated by heavy arrows (Bailly and Chaires, 1998).

Imidazole was considered a favorable candidate for GC recognition as it is able to fit neatly alongside guanine in the minor groove, favouring the formation of a hydrogen bond between the guanine N2-amino and the imidazole nitrogen (Kopka et al., 1985;

Lown et al., 1986). DNA footprinting data have shown that mono-, di-, and triimidazole-containing oligopeptides (Figure 1.15) analogues of netropsin exhibited an increased ability to tolerate GC base pairs and a progressively decreasing preference for AT regions (Lown et al., 1986).

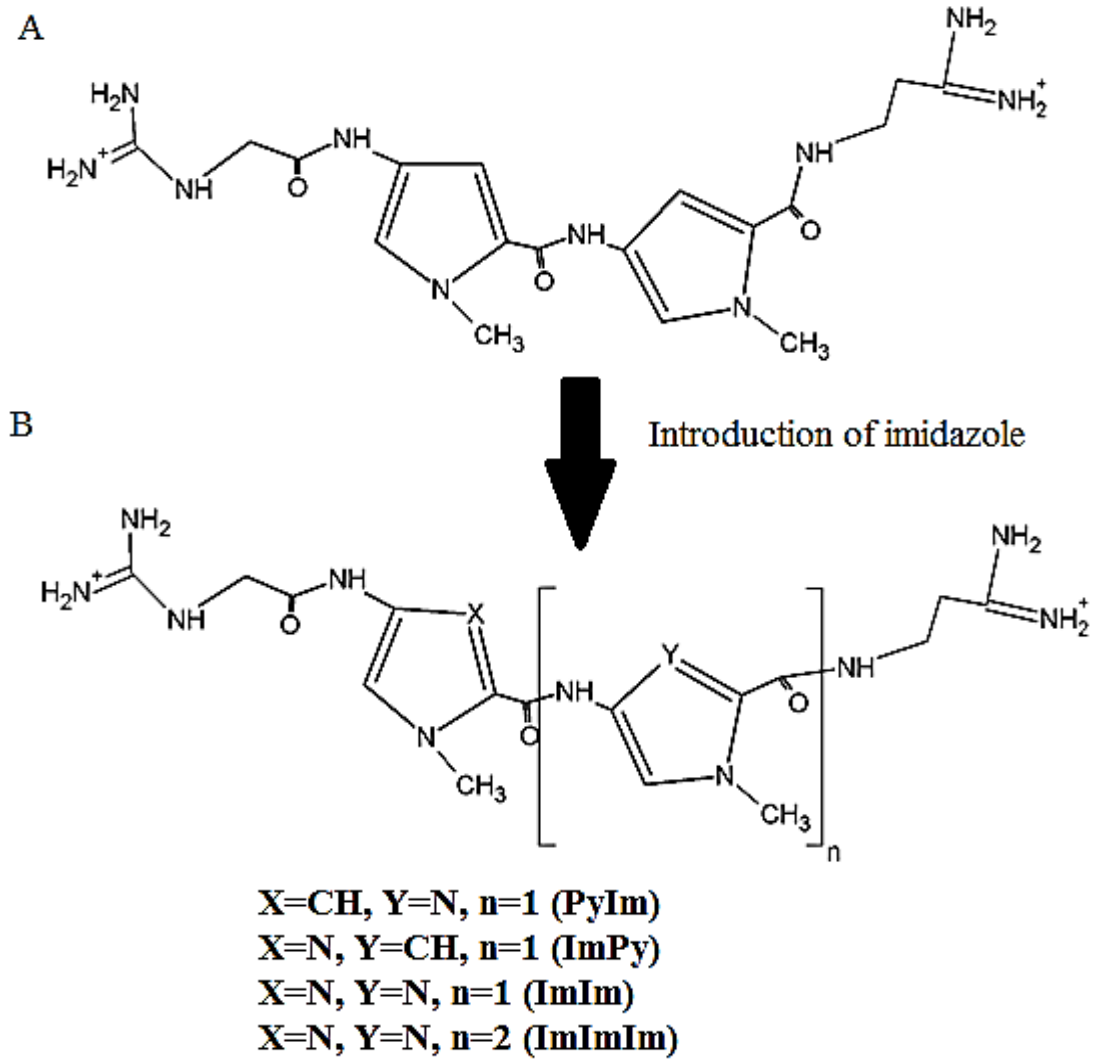

Figure 1.15 The development of GC recognition, showing the evolution of (A) netropsin into(B) a dicationic mono, di and triimidazole adapted from Lown et al, 1986.

1.9 Recognition of the DNA minor groove by pyrrole-imidazole polyamides

1.9.1 Pairing rules

Targeting predetermined DNA sequences by cell-permeable small molecules provides a promising approach for the regulation of gene expression (Gottesfeld et al., 1997, 2000). More than two decades of research in the laboratories of Peter Dervan led to the establishment of the 'pairing rules' for minor groove recognition by polyamides containing pyrrole (Py) and imidazole (Im) grooves (Wade et al., 1992; Mrksich et al., 1992; Gottesfeld et al., 1997; Dervan et al., 1999, 2003). The development of the pairing rules resulted from the surprising finding that the netropsin-based analogue, 1-methylimidazole-2-carboxamido-netropsin (2-ImN) (Figure 1.16), is bound to the 5bp sequence 5'-WGWCW-3' (where W=A or T) more strongly than that to the 5'-WGWWW-3', which was an anticipated site for a 1:1 polyamide-DNA complex (Wade et al., 1992; Dervan and Edelson, 2003). In addition, from affinity cleavage experiments 2-ImN binds with twofold symmetry rather than a single orientation as expected the 1:1 model. This surprising result was rationalized by NMR, which shows that distamycin can bind to DNA in a 2:1 as well as a 1:1 stoichiometry depending on the concentration (Pelton and Wemmer, 1989; Dervan and Burli, 1999).

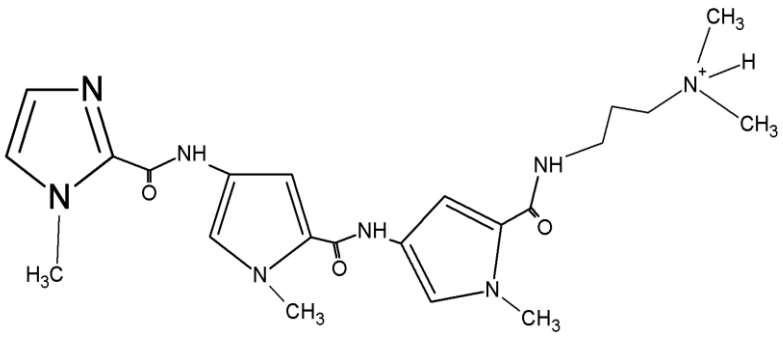

Figure 1.16 1-methylimidazole-2-carboxamido-netropsin (2-ImN)

The Im/Py pair has been extensively studied by analyses of binding in hundreds of different DNA sequence contexts and crystal structures, confirming the existence of a hydrogen bond between the imidazole nitrogen and the exocyclic amine of guanine (Kielkopf et al., 1998). On the basis of these results, the Dervan group formulated a set of 'pairing rules' for polyamides binding to DNA (Table 1.1) (Wade et al., 1992; White et al., 1997).

Table 1.1 Pairing code for minor groove recognition by polyamides*.

Pair	G•C	C•G	T•A	A•T
Im/Py	+	-	-	-
Py/Im	-	+	-	-
Py/Py	-	-	+	+
Hp/Py	-	-	+	-
Im/Im	+	+	-	-

* + favored recognition; - disfavored recognition.

A pyrrole opposite an imidazole (Im/Py) will specifically distinguish a GC from CG base pair, owing to the energetic preference for a linear hydrogen bond, coupled with unfavorable angle to an Im over the cytosine side of the base pair (Figure 1.17) (Kielkopf et al., 1998; Dervan et al., 2003). The antiparallel ring pairing of pyrrole stacked against pyrrole (Py/Py) in the corresponding ligand is partially degenerate and binds for A•T and T•A, due to the similarity of these bases in the minor groove. To break the A•T and T•A degeneracy by Py/Py, the *N*-methyl-3-hydroxypyrrole (Hp) monomer was designed as a thymine-selective recognition element when paired across from Py. An Hp/Py pairing was shown to specifically distinguish T•A from A•T, G•C

and C•G. The selectivity of Hp derives from a combination of hydrogen bond with the thymine O2 and the shape-selective discrimination of the asymmetric cleft between the thymine O2 and adenine C2 (Figure 1.17) (White et al., 1998; Kielkopf et al., 1998, 2000). Imidazole-imidazole paring (Im/Im) will bind either a GC or a CG base pair. DNA-binding polyamides containing *N*-methylpyrrole (Py), *N*-methylimidazole (Im), and *N*-methyl-3-hydroxypyrrole(Hp) are crescent-shaped and can bind to the minor groove as antiparallel dimers (2:1 model).

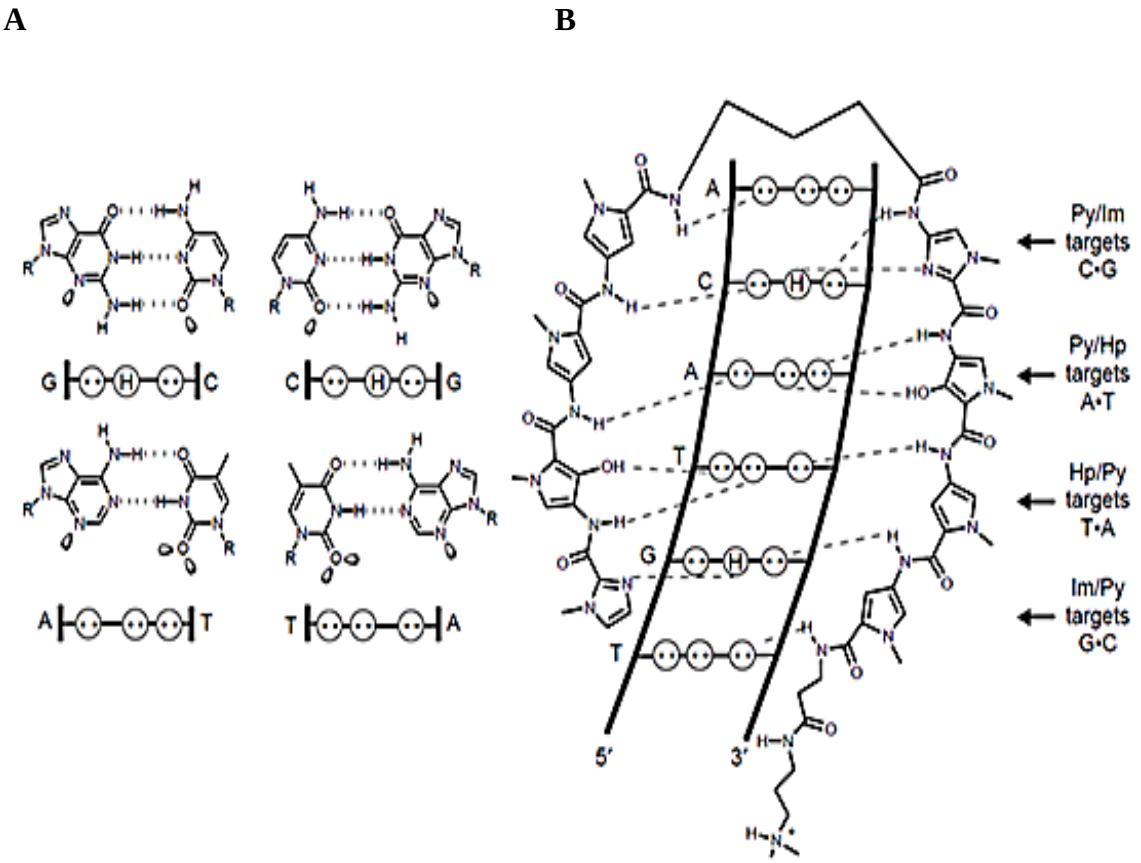

Figure 1.17 Molecular recognition of the minor groove of DNA. (**A**) Minor groove hydrogen-bonding patterns of Watson–Crick base pairs. Circles with dots represent lone pairs of N(3) of purines and O(2) of pyrimidines, and circles containing an H represent the 2-amino group of guanine. The R group represents the sugar–phosphate backbone of DNA. Electron lone pairs projecting into the minor groove are represented as shaded orbitals. (**B**) Binding model for the complex formed between ImHpPyPy-γ-ImHpPyPy-β-Dp and a 5'-TGTACA-3' sequence. Putative hydrogen bonds are shown as dashed lines (taken from Dervan and Burli, 1999).

1.9.2 The effects of a terminal formamido group on DNA sequence recognition

Pyrrole-imidazole-containing polyamides can bind the minor groove of DNA and selectively target specific DNA sequences through a stacked antiparallel dimer (Wemmer et al., 2000; Lacy et al., 2002). It has been suggested that there are two different low energy ways to form the stacked dimer: (i) a fully overlapped stacking mode in which the N-terminal heterocycles of the dimer stack on the amide groups between the two heterocycles at the C-terminal and (ii) a staggered stacking mode in which the N-terminal heterocycles are shifted by approximately one unit in the C-terminal direction (Figure 1.18) (Kopka et al., 1997; Lacy et al., 2002). The formamido (f-) group at the N-terminus of distamycin A and related triamides play a major role in controlling the staggered binding motif of a 2:1 ligand/DNA complex, while the unsubstituted analogues bind in the overlapped mode. Later studies of the binding of f-ImPyIm to its cognate sequences (5'-ACGCGT-3') showed its exceptionally high affinity and selectivity compared to its parent compound distamycin A and a non-formamido equivalent (Buchmueller et al., 2005). The order of the heterocycles at the 'core' of the triamide has been shown to be important for DNA binding affinity and selectivity in the staggered dimeric binding motif. Therefore, a set of central pairing rules have been developed with the two central units ranked as follows: -ImPy- > -PyPy- >> -PyIm- ≈ -ImIm- (Figure 1.18B) (Buchmueller et al., 2005).

Although monomer polyamides can form a 2:1 ligand/DNA complex within the minor groove, this is not always energetically favorable and there is also a concern that the monomers without a formamido group may split into the extended staggered motif, hence, creating a reading frame different to that they were designed for (Pelton et al.,

1990; Chen et al., 1994). In addition, the monomers may also bind in a mixed 2:1 and 1:1 motif, thus, reducing the overall affinity.

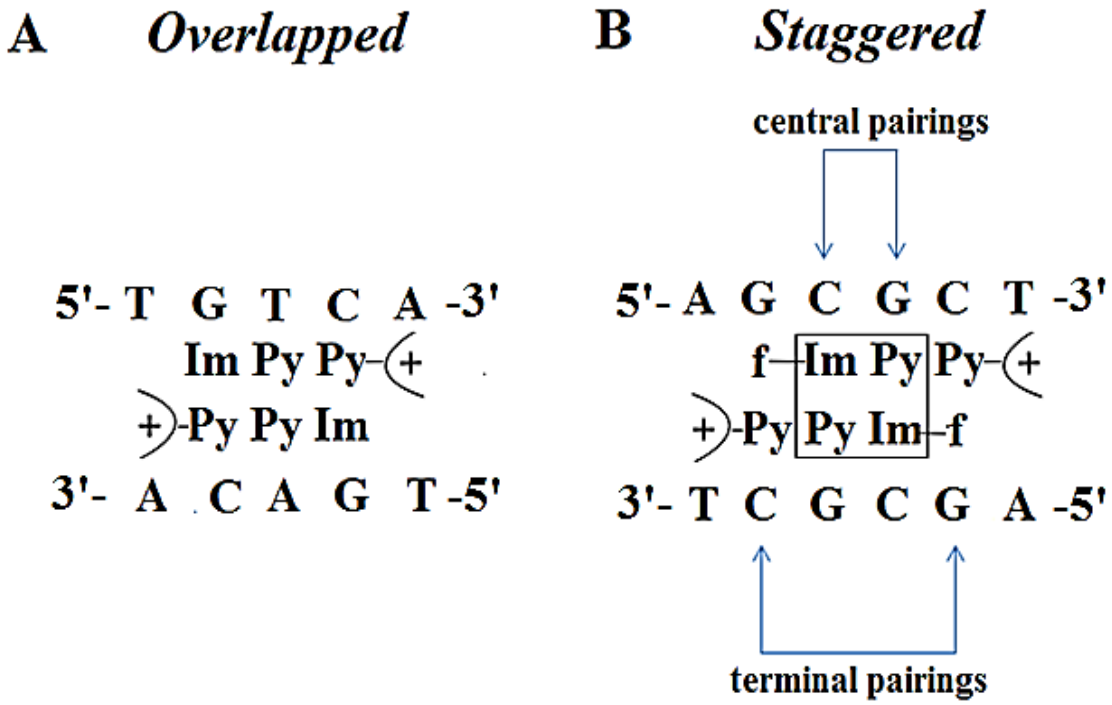

Figure 1.18 Staggered and overlapped orientations of triamide dimers that form within the DNA minor groove. (**A**) Overlapped dimers are preferred by non- formamido triamides. In the overlapped orientation, all three heterocycles are engaged in heterocycle–heterocycle stacking. (**B**) Staggered dimers are preferred by formamido triamides. In the staggered orientation, heterocycles stack (pair) to form the 'central pairing' (box). The central pairing is composed of two adjacent sets of stacked heterocycles. The C-terminal heterocyclic group is not included in the central pairing and is stacked on the formamido moiety, to form the 'terminal pairing'.

1.9.3 Affinity and specificity

The affinity and specificity of unlinked three-ring dimers are modest. To compete with nature's proteins, such as transcription factors, the affinity of these synthetic molecules had to be improved by about three orders of magnitude. Tethering two monomer polyamides with a suitable linker, as in the 'Hairpin' motif that covalently links two antiparallel polyamide strands, results in molecules with increased DNA affinity and

specificity. The 'standard' motif is the eight-ring hairpin, in which the monomers are linked ‘head’-to-‘tail’ using a flexible γ-aminobutyric acid moiety (Figure 1.17B, ImHpPyPy-γ-ImHpPyPy-β-Dp) (Dervan et al., 2003). Eight-ring hairpins targeting 6bp were found to have affinity and sequence specificity similar to that of DNA-binding proteins (i.e. K_d < 1nM) (Trauger et al., 1996). More selective hairpin polyamides have been developed by Dervan group (Dervan et al., 2001; 2003), which demonstrated excellent binding affinity but their usage has been restricted by problems of cellular and nuclear uptake and limited water solubility. An alternative motif is a cross-linked ‘H-pin’ structure where the central heterocycles of two polyamides are linked via either a methylene or preferably an ethylene glycol bridge (Figure 1.19A&B; ImPyIm H-pin and f-ImPyIm H-pin). H-pins without a formamido group at the N-terminus linked via alkyl chains of varying lengths (C_3-C_{12}) have been investigated as minor groove duplex DNA binders that interact in a 1:1 overlapped motif (the two polyamides’ constituent heterocycles are stacked against each other and the linker directly joins two central heterocycle across the polyamides, Figure 1.19A) (Chen et al., 1994; Mrksich et al., 1993;1994). Weak binding affinity of the former H-pin type was reported (Dervan et al., 1999, 2001) in comparison with the exceptional affinity of the linked monomer f-ImPyIm that binds to its cognate DNA sequence as a dimer in a staggered binding motif (the polyamide units are stacked in an off-centered staggered fashion and the linker joins two adjacent heterocycles in a diagonal arrangement, Figure 1.19B), covering more base pairs. In more recent biological studies (O'Hare et al., 2002), it has been demonstrated that at least a five-carbon linker for two f-ImPyIm ligands was required to cross the minor groove width and linkers of eight or nine carbons can further increase the already exceptional binding affinity (O'Hare et al., 2007). Poor cellular uptake of large H-pin polyamides has restricted their further utility as gene control agents,

although such H-pin polyamides have a great DNA-binding affinity and specificity. In a recent paper, it was reported that the f-PyImPy H-pin polyamides most likely does not enter the nucleus, because the anticipated biological effect (i.e. upregulation of topo IIα) was not observed in treated cells (Franks et al., 2010). In contrast, f-PyImPy was able to enter the nucleus, interact with the target site within the ICB2, inhibit NF-Y binding, and activate gene expression (Le et al., 2006).

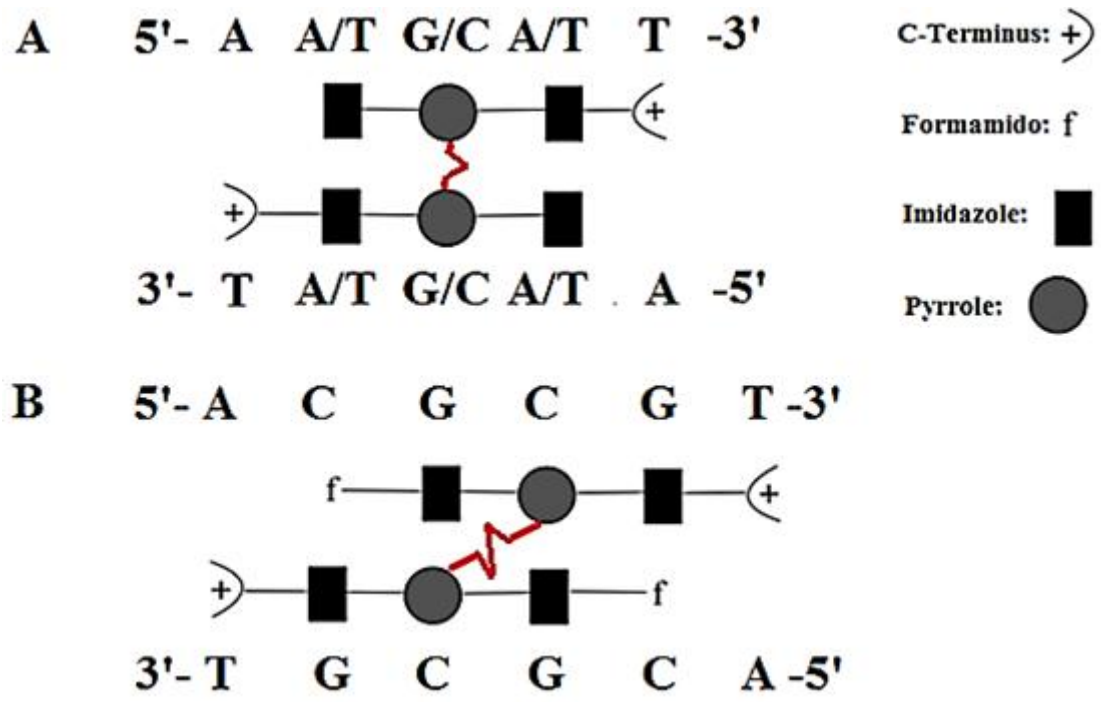

Figure 1.19 Diagram to show the overlapped H-pin motif (**A**), and staggered H-pin motif (**B**), the red line connecting the two polyamide unit's represents the H-pin linker.

1.9.4 Gene regulation by rationally designed polyamides

1.9.4.1 Inhibition of gene expression

According to the set of pairing rules, the optimal heterocycle pairs required for DNA sequence recognition at predetermined sites have been extensively studied and identified (Kielkopf et al., 1998; Wade et al., 1992; White et al., 1997, 1998). Such

sequence-reading polyamides have the potential to be used as gene control agents through inhibition of native transcription factors (Dervan et al., 2003; Melander et al., 2004). Figure 1.20 presents a model of how the inhibition of key transcription factor (TF) binding is derived by polyamide binding to TF sites within various promoters, thus interfering with the recruitment of RNA polymerases (Dervan amd Burli, 1999).

One of the examples reported was the transcription inhibition by blocking the 5S RNA gene-specific transcription factor TFIIIA binding to its cognate sequences by Py/Im hairpin polyamides. As a result, transcription of 5S RNA genes by RNA polymerase was suppressed *in vitro* and in cultured *Xenopus* kidney cells (Gottesfeld et al., 1997). Polyamides were later used to target viral genes transcribed by RNA polymerase II. The HIV-1 enhancer/promoter contains binding sites for multiple TFs, including TBP, Ets-1 and LEF-1. Two hairpin polyamides designed to bind DNA sequences immediately adjacent to the binding sites for these TFs specifically inhibited binding of each TF and HIV-1 transcription in a cell free assay (Dickinson et al., 1998). A polyamide-chlorambucil conjugate IR-Chl showed to be an inhibitor of cell proliferation in various cell lines with no apparent cytotoxicity and little or no murine animal toxicity (Dickinson et al., 2004; Tsai et al., 2007; Alvarez et al., 2006). IR-Chl targets the coding region of the histone *H4* gene both *in vitro* and in SW620 human colon carcinoma cells and down-regulates *H4* transcription (Dickinson et al., 2004; Chou et al., 2008). Later, newly synthesized conjugates between pyrrole-imidazole polyamides and the alkylating moiety *seco*-CBI were shown to alkylate within the coding regions of the histone *H4* genes. Chronic myelogenous leukemia K562 cells treated with a conjugate 5-CBI down-regulated the histone *H4* gene and induced apoptosis efficiently (Minoshima et al., 2010). Matsuda and co-workers further exhibited that a Py/Im polyamide targeted to the

transforming growth factor-β1 promoter inhibited gene expression *in vivo* (rat renal cortex) (Matsuda et al., 2011). Figure 1.21 presents examples of DNA-binding proteins that have been inhibited by Py/Im hairpin polyamides. The more recent studies by Dervan's group further demonstrated that Py/Im polyamides could inhibit DNA binding of transcription factors in cells. Py/Im hairpin polyamide [ImPyPyPy-(R)$^{\alpha\text{-amino}}$γ-ImPyPyPy] binds to the consensus sequence 5'-GGTACAnnnTGTTCT-3' in the androgen response elements (ARE) found in the prostate-specific antigen (PSA) promoter, inhibits expression of PSA and several other androgen receptor (AR)-regulated genes in cultured prostate cancer cells, and reduces AR occupancy at the PSA promoter and enhancer (Nickols et al. 2007). This polyamide was also found to bind to the consensus sequence in the glucocorticoid response elements (GRE) present in the promoter of the well-characterized GC-induced leucine zipper (*GILZ*) gene, inhibits expression of *GILZ* in cultured alveolar epithelial cells (A549), and reduces glucocorticoid receptor occupancy at the *GILZ* promoter *in vivo* (Muzikar et al., 2009). Another polyamide [ImImPyPy-(R)$^{\alpha\text{-amino}}$γ-PyPyPyPy] was designed to bind to κB sites, thus preventing nuclear factor κB (NF-κB) binding and consequently reducing the expression of various NF-κB-driven genes including *IL6* and *IL8* (Raskatov et al., 2012). The pharmacokinetics and toxicity of ImPyPyPy-(R)$^{\alpha\text{-amino}}$γ-ImPyPyPy and its analogue was tested in mice and micromolar levels were found in mouse plasma for up to 48 h following either intraperitoneal or subcutaneous injection (Synold et al., 2012). Jevgenij and co-workers further showed that a Py/Im hairpin polyamide is capable of trafficking to the tumour site following subcutaneous injection and represses *CCL2* and *SERPINE1* transcription *in vivo* (Raskatov et al., 2012).

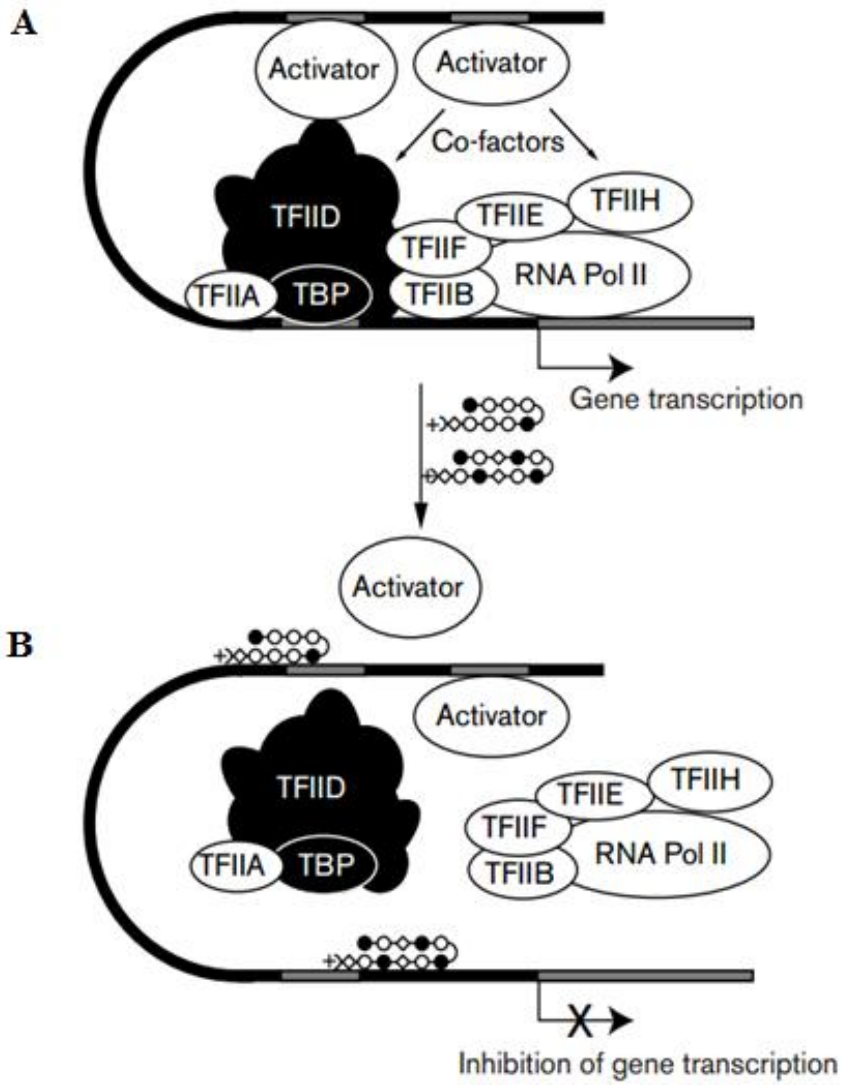

Figure 1.20 The inhibition of gene transcription by polyamides. (**A**) Model of the transcriptional machinery required for the initiation of gene transcription by RNA polymerase II (RNA Pol II). (**B**) Polyamides binding proximal to a transcription factor (TF) site within the promoter. Gene transcription is inhibited (Dervan amd Burli, 1999).

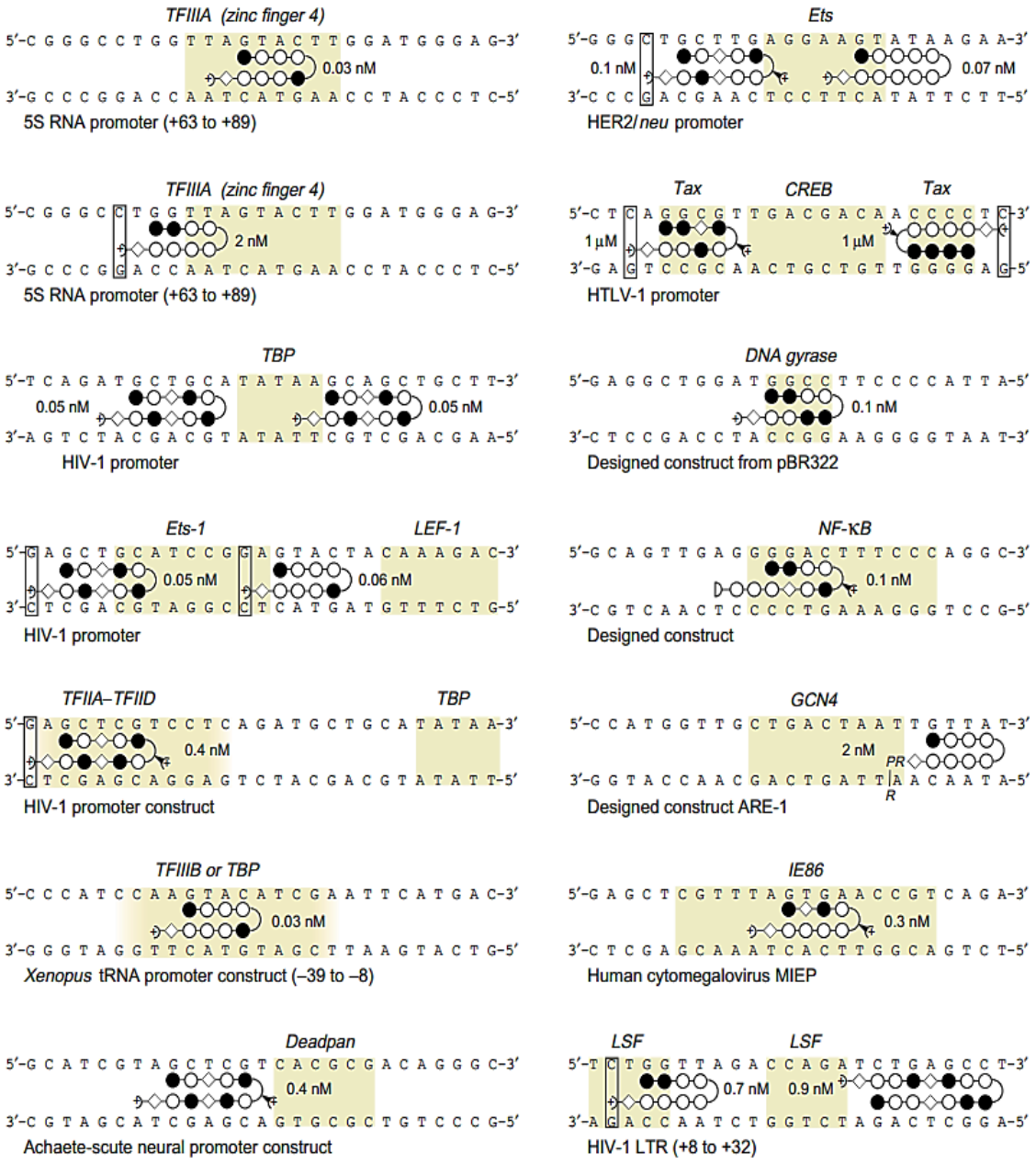

Figure 1.21 Examples of regulation of gene expression by competitive binding of Py-Im hairpin polyamides to binding sites of transcription factors. The coloured boxes indicate the binding site of the italicized protein. The promoter is identified below the DNA sequences. The back and open circles represent Im and Py rings respectively. Diamonds represent β-Ala residues. Plus signs next to diamonds represent 3-(dimethylamino)propylamine (Dp). The curved line connecting the sides of two circles represent the γ-turn. The half circle represents a propanolamine-NH(CH_2)CH_3OH group. Approximate Kd values are given next each polyamide. Open boxes indicate mismatches between the Dp tail and GC, base pairs (Dervan and Edelson, 2003).

1.9.4.2 Gene activation

Polyamides have also been used for upregulating transcription by recruiting or depressing the transcriptional machinery. For example, a hairpin polyamide was shown to block binding of the repressor IE86 to DNA, thereby upregulating transcription of the human cytomegalovirus MIEP (Dickinson et al., 1999). Polyamide-peptide conjugates can mediate transcriptional activation by functioning as artificial transcription factors (Mapp et al., 2000). Another example involves the expression of topoisomerase IIα (topo IIα) as a determinant of response to chemotherapeutic agents targeting this enzyme such as etoposide and doxorubicin (Burden et al., 1998). Confluent cancer cells express low levels of topo IIα that contributes to resistance to these agents (Isaacs et al., 1996; Tolner et al., 2001). The topo IIα promoter is regulated through transcription factors that interact with five inverted CCAAT boxes (ICBs) (Isaacs et al., 1996). In confluent cancer cells, repression of transcription is mediated mainly by the binding of the ubiquitously expressed CCAAT-binding protein NF-Y to ICB2 within the topo IIα promoter (Ronchi et al., 1995). Sequence-reading polyamides such as JH-37 and the pyrrolobenzodiazepine-polyamide conjugate GWL-78 have been designed to bind to the flanking regions of selected CCAAT sites within the topo IIα promoter, thus blocking the repressive binding of NF-Y , and upregulating topo IIα expression (Hochhauser et al., 2007; Kotecha et al., 2008).

1.10 Experimental aims:

A new class of unlinked polyamide precursors that contain appropriately designed pendant reactive and biocompatible functional groups was designed and is presented here. It was hypothesized that these relatively small polyamide precursors (molar mass ~500g/mol) will more readily penetrate cells compared to relatively large H-pin/hairpin polyamides, localize in the nucleus and bind to their DNA targets in the stacked, staggered motif, forming H-pin or Hairpin structures *in situ*.

The aim of the project is to test this approach of the *in situ* reaction of two rationally designed polyamide monomers capable of potentially forming either H-pin or Hairpin conjugates in the nucleus.

Additionally, the experimental work aims to investigate the effect of the presence of an additional amino group in selected polyamides on DNA binding affinity and specificity. The binding characteristics of PPPP(H)-N-dimethyl-3-aminopropylamine and IPPP(H)-N-dimethyl-3-aminopropylamine, and a novel fluorescent polyamide HxPI were also evaluated.

The sequence 5'-ACGCGT-3' (MCB) which occurs in the core HuDbf4 promoter is utilized in this thesis as a model system for investigating the effects of gene targeting by the polyamide f-IPI. The binding of f-IPI to the MCB *in vitro* and the cellular effects of f-IPI treatment (e.g. downregulation of HuDbf4, cell cycle effect, cell survival, proliferation and apoptosis) were assessed.

Subsequently, the targeting of the MCB in the promoter by the polyamides f-IP(C_3NH_2)I and f-IP(C_3Cl)I was assessed as part of the *in situ* formation of H-pin approach.

Lastly, polyamides containing the fluorescent Hx moiety were designed and tested with the aim of monitoring cellular uptake and nuclear localization. HxPI was additionally tested as a potential gene-control agent for the targeting of the HuDbf4 promoter model.

CHAPTER 2

MATERIALS AND METHODS

2.1 Materials

2.1.1 Primers for the generation of the probes for DNase I footprinting

Name	Sequence (5'-> 3')	Tm [℃]
Primer 17	GTCGTTAGGAGAGCTCACTTG	**60**
Primer 19	CTCCAGAAAGCCGGCAACTCAG	**64**

Table 2.1: List of primers

2.1.2 MCB oligonucleotides for the EMSA studies

Name	Dbf4 Promoter Sequence (5'-> 3')	Tm [℃]
MCB Wild Type forward	GCGTGACGCGTTTTCAAATCTTCAACC	**65**
MCB Wild Type reverse	GGTTGAAGATTTGAAAACGCGTCACGC	**65**
MCB Mutant forward	GCGTGAtGaGTTTTCAAATCTTCAACC*	**62**
MCB Mutant reverse	GGTTGAAGATTTGAAAAC*TCA*TCACGC*	**62**

Table 2.2: List of MCB oligonucleotides

* the italic font is mutated sequence

2.1.3 DNA sequences of the templates used for the PCR-generation of the fragments for footprint analysis

Polyamides	IM17/19 Sequence (5'-> 3')	Cognate site (5'-> 3')
f-IPI, f-IP(C_2NH_2)I, f-IP(C_3Cl)I, Ph-IPI, Ph-IP(C_3NH_2)I, Aza-HxPI, Aza-HxP(C_3NH_2)I and Aza-HxPI(C_3NH_2)	CTGTCCAGAAAGCCGGCACTCAGTCTACAA**ACGCGT**CATCTTGATCACCGGTGTTCACAGAAATTTCTCTAGATCTACACGTAACTCTAGTAGCGCTCTTCAAGCAAGTGGAGCTCTCCTAACCGAC sense	**ACGCGT**
f-IPI, f-IP(C_2NH_2)I, f-IP(C_3Cl)I, Ph-IPI,Ph-IP(C_3NH_2)I Aza-HxPI, Aza-HxP(C_3NH_2)I and Aza-HxPI(C_3NH_2)	GTCGGTTAGGAGAGCTCCACTTGCTTGAAGAGCGCTACTAGAGTTACGTGTAGATCTAGAGAAATTTCTGTGAACACCGGTGATCAAGATG**ACGCGT**TTGTAGACTGAGTGCCGGCTTTCTGGACAG anti-sense	**ACGCGT**

Table 2.3: List of polyamides, the targeted IM17/19 sequence and the cognate site [Pyrrole(P) and Imidazole (I)]

Polyamides	IM18/20 Sequence (5'-> 3')	Cognate site (5'-> 3')
f-IPP f-IP(C_3NH_2)P	CTGTCCAGAAAGCCGGCACTCAGTCTACA AACGCGTCATCTTGATC**ATGCAT**GTTCAC AGAAATTTCTCTAGATCTACACGTAACTCT AGTACTAGTCTTCAAGCAAGTGGAGCTCT CCTAACCGAC sense	**ATGCAT**
f-IPP f-IP(C_3NH_2)P	GTCGGTTAGGAGAGCTCCACTTGCTTGAA GACTAGTACTAGAGTTACGTGTAGATCTA GAGAAATTTCTGTGAAC**ATGCAT**GATCAA GATGACGCGTTTGTAGACTGAGTGCCGGC TTTCTGGACAG anti-sense	**ATGCAT**

Table 2.4: List of polyamides, the targeted IM18/20 sequence and the cognate site

Polyamides	HMC-click Sequence (5'-> 3')	Cognate site (5'-> 3')
PPP-b-NH_2 PPP-Benz-NO_2	CTGTCCAGAAAGCCGGCACTCAGTCTAC AAATAGATCATCTTGATCATATATGTTC ACAG**ACAGAT**CTCTAGATCTAGATATA ACTCTAGT**AAATTT**CTTCAAGCAAGTGG AGCTCTCCTAACCGAC sense	**ACAGAT** **AAATTT**
PPP-b-NH_2 PPP-Benz-NO_2	GTCGGTTAGGAGAGCTCCACTTGCTTGA AG**AAATTT**ACTAGAGTTATATCTAGATC TAGAG**ATCTGT**CTGTGAACATATATGA TCAAGATGATCTATTTGTAGACTGAGTG CCGGCTTTCTGGACAG anti-sense	**ATCTGT** **AAATTT**

Table 2.5: List of polyamides, the targeted HMC-click sequence and the cognate site

Polyamides	Click-6 Sequence (5'-> 3')	Cognate site (5'-> 3')
f-IP(C_3N_3)I, f-PP(C_3-alkyne)P, f-IP(C_3-alkyne)I and f-PP(C_3N_3)	CTGTGTCCAGAAAGCCGGCACTC AGCTACAA**ACGCGT**CATCGATC**A AATTT**GTTCACAGACTCATGTCTA GCTACACTTAAGTCTAGTCTCAAG TGTCATCTCACTAGTTCGTCAAGT GGAGCTCTCCTAACCGAC sense	**ACGCGT** **AAATTT** **WCWCWW***
f-IP(C_3N_3), f-PP(C_3-alkyne)P, f-IP(C_3-alkyne)I and f-PP(C_3N_3)	GTCGGTTAGGAGAGCTCCACTTG ACGAACTAGTGAGATGACACTTG AGACTAGACTTAAGTGTAGCTAG ACATGAGTCTGTGAAC**AAATTT**G ATCGATG**ACGCGT**TTGTAGCTGA GTGCCGGCTTTCTGGACACAG anti-sense	**ACGCGT** **AAATTT** **WCWCWW***

Table 2.6: List of polyamides, the targeted Click-6 sequence and the cognate site

***** Where W means A or T.

Polyamides	KM-A Sequence (5'-> 3')	Cognate site (5'-> 3')
PPPX IPPX	CTGTCCAGAAAGCCGGCACTCAGTCT ACAA**AAATTT**CATCTTGATCATATAT GTTCACAGAGCTCTCTCTAGATCT**AG ATCT**AACTCTAGT**ACATGT**CTTCAAG CAAGTGGAGCTCTCCTAACCGAC sense	**AAATTT** **AGATCT** **ACATGT**
PPPX IPPX	GTCGGTTAGGAGAGCTCCACTTGCTT GAAG**ACATGT**ACTAGAGTTAGATCT **AGATCT**AGAGAGAGCTCTGTGAACA TATATGATCAAGATG**AAATTT**TTGTA GACTGAGTGCCGGCTTTCTGGACAG anti-sense	**AAATTT** **AGATCT** **ACATGT**

Table 2.7: List of polyamides, the targeted KM-A sequence and the cognate site

Polyamides	Tope IIα Promoter Sequence (5'-> 3')	Cognate site (5'-> 3')
f-PIP f-P(C_3CN)IP f-PI(C_3N_3)IP f-PI(C_3NH_2)IP	CTGTCCAGAAAGCCGGCACTCAGTTTCCTC AGGAAAACGAAGCTAAGGCTCCCATTCCC CTCGCTAACAACGTCAGAACAGAGGACAG TTTTTAGATTTCAGGGATCTTAAATAGATT GGCAGTCCTGGAGAATAAACATCCTTTGC TTTTCTCCTGCACACTTTTGCCTCAGGCCA CCCCTTCCCGCTCCAAAGCCCATCTCTTCC AAGCTTTCCGCACGAGAAAACAAGTGAGC CCTTCTCATTGGCCAGATGCCCTGTCAATC TCTCCGCTATGACGCCGAGTGGTGCCTTTT GAAGCCTCTCTAGTCCCGCCTCCAGCTAAC CTGATTGGTTTATTCAAACAAACCCCGGCC AACTCAGCCGTTCATAGGTGGATATAAAA GGGCAAGC**TACGAT**TGGTTCTTCTGGACG GAGACGGTGAGAGCGAGTCAGGGATTGGC TGGTCTGCTCTCGGGCGGGCTAAAGGAAG GTTCAAGTGGAGCTCTCCTAACCGAC sense	**TACGAT** **(5'-flank of ICB2)**
f-PIP f-P(C_3CN)IP f-PI(C_3N_3)IP f-PI(C_3NH_2)IP	GTCGGTTAGGAGAGCTCCACTTGAACCTTC CTTTAGCCCGCCCGAGAGCAGACCAGCCA ATCCCTGACTCGCTCTCACCGTCTCCGTCC AGAAGAACCA**ATCGTA**GCTTGCCCTTTTA TATCCACCTATGAACGGCTGAGTTGGCCG GGGTTTGTTTGAATAAACCAATCAGGTTA GCTGGAGGCGGGACTAGAGAGGCTTCAAA AGGCACCACTCGGCGTCATAGCGGAGAGA TTGACAGGGCATCTGGCCAATGAGAAGGG CTCACTTGTTTTCTCGTGCGGAAAGCTTGG AAGAGATGGGCTTTGGAGCGGGAAGGGGT GGCCTGAGGCAAAAGTGTGCAGGAGAAA AGCAAAGGATGTTTATTCTCCAGGACTGC CAATCTATTTAAGATCCCTGAAATCTAAAA ACTGTCCTCTGTTCTGACGTTGTTAGCGAG GGGAATGGGAGCCTTAGCTTCGTTTTCCTG AGGAAACTGAGTGCCGGCTTTCTGGACAG anti-sense	**ATCGTA** **(5'-flank of ICB2)**

Table 2.8: List of polyamides, the targeted Tope IIα Promoter sequence and the cognate site

Polyamides	Dbf4 Promoter Sequence (5'-> 3')	Cognate site (5'-> 3')
f-IPI f-IP(C_2NH_2)I f-IP(C_3Cl)I	CTGTCCAGAAAGCCGGCACTCAGGC GTGAGACGGGGCGGGGCGCGCGTA TCGGCGCCGCGGCCGCGTG**ACGCG T**TTTCAAATCTTCAACCGCCGCAGC CCACTCGTTTCAAGTGGAGCTCTCCT AACCGAC sense	**ACGCGT**
f-IPI f-IP(C_2NH_2)I f-IP(C_3Cl)I	GTCGGTTAGGAGAGCTCCACTTGAA ACGAGTGGGCTGCGGCGGTTGAAGA TTTGAAA**ACGCGT**CACGCGGCCGC GGCGCCGATACGCGCGCCCCGCCCC GTCTCACGCCTGAGTGCCGGCTTTCT GGACAG anti-sense	**ACGCGT**

Table 2.9: List of polyamides, the targeted Dbf4 Promoter sequence and the cognate site

Polyamides	HxSeq (5'-> 3')	Cognate site (5'-> 3')
Hx-PI	CTGTCCAGAAAGCCGGCACTCAGTCT ACAAACGCGTCA**TCTTGA**TCATGCAT GTTCACAGAAATTTC**TCTAGA**TCTAC ACGTAACTCTAGT**ACTAGT**CTTCAAG CAAGTGGAGCTCTCCTAACCGAC sense	**WCWWCW** **W=A or T**
Hx-PI	GTCGGTTAGGAGAGCTCCACTTGCTT GAAG**ACTAGT**ACTAGAGTTACGTGT AGA**TCTAGA**GAAATTTCTGTGAACAT GCATGA**TCAAGA**TGACGCGTTTGTAG ACTGAGTGCCGGCTTTC TGGACAG anti-sense	**WGWWGW**

Table 2.10: List of polyamides, the targeted HxSeq sequence and the cognate site

2.2 Methods:

2.2.1 Generation of radiolabelled probe for DNase I footprinting analysis

The forward primer17 5'- GTCGTTAGGAGAGCTCACTTG-3' (4 µl pmol) was 5'-radioactively labeled with γ-[^{32}P] (3 µl), 1 µl of T4 polynucleotide kinase (NEB, UK), 2 µl of 10 × NEB buffer and 2 µl of water. The mixture was incubated at 37 ℃ for 1 hour during which an extra 0.5 µl of T4 kinase was added. T4 kinase was inactivated by heating at 65 ℃ for 20 min.

2.2.2 Polymerase chain reaction (PCR)

4 pmol of reverse primer19 5'-CTCCAGAAAGCCGGCAACTCAG-3', 2 µl of $MgCl_2$ (1 mM), 2 µl of 10 mM dNTPs (Promega, UK), 1 U Flexi GoTaq polymerase (Promega,UK), 10 µl of 5 × GoTaq buffer, 10 µl of γ-[^{32}p]-labeled forward primer17 and the DNA templates (20 ng each) (DNA fragment sequences are listed in the section 2.1) were mixed together in a final volume of 50 µl. The PCR reaction was performed as follows: an initial denaturation step for 3 min at 95 ℃, [1 min at 94 ℃, 1 min at 63 ℃, and 1 min at 72 ℃] for 35 cycles and 72 ℃ for 15 min. The resulting DNA products were purified using the Mermaid Kit (Q-biogene). DNA fragments greater than 200bp in length were purified using the GENECLEAN III kit (Q-biogene) according to the manufacturer's instructions.

2.2.3 DNase I footprinting experiments

DNase I reactions were performed in a total volume of 8 µl. The labeled DNA fragment (2 µl, 200 counts per second; cps) was incubated for 30 min at room temperature in 4 µl 1 × TN binding buffer (10 mM Tris Base, 10 mM NaCl, pH 7) containing the required drug concentration. The drug treated-DNA was then cleaved by the addition of 2 µl of DNase I solution (20 mM NaCl, 2 mM $MgCl_2$, 2 mM $MnCl_2$, DNase I 0.02 U/µl, pH 8.0) and the reaction was stopped after 3 min by freezing the samples on dry ice for a minimum of 30 min. The samples were subsequently lyophilized.

2.2.4 Polyacrylamide gel electrophoresis

DNA samples were resuspended in 5 µl of formamide loading dye (95% formamide, 20 mM EDTA, 0.05% bromophenol blue, and 0.05% cyanol blue), denatured by heating at 94 ℃ for 3.5 min and cooled on ice prior to loading a pre-run polyacrylamide (6% or 10%) gel (Sequagel, National Diagnostics, UK) containing urea (7.5 mM). Electrophoresis was conducted for 2 hours at 1650 V (~70 W, 50 ℃) in 1 × TBE buffer (89 mM Tris base, 89 mM boric acid, 2.5 mM Na_2EDTA, pH 8.3). The gel was then transferred onto Whatman 3MM paper and Whatman DE81 paper and dried under vacuum at 80 ℃ for 2 h. The gel was exposed overnight to medical X-Ray film in (Super RX, Fuji) and developed by Konica Medical Film Processor SRX-101A,

2.2.5 Cell culture

The human breast cancer cell line MDA-MB231 was cultured in Dulbecco's modified Eagle's minimal essential medium supplemented with 10% heat-inactivated fetal bovine serum (FBS) and 1% glutamine (Sigma, UK) in a 37 ℃ incubator with 5% CO2.

2.2.6 Nuclear protein extraction from MDA-MB231 cells

Nuclear extracts from exponentially growing MDA-MB231 cells obtained by using the Nuclear Extract Kit (Active Motif, UK) according to the manufacturer's instructions. Briefly, each flask was washed with 8 ml ice-cold phosphate buffered saline (PBS)/phosphatase inhibitors (1.6 ml of 10 × PBS, 13.6 ml of distilled water and 0.8 ml of phosphatase inhibitors). Cells were scraped off collected and split into pre-chilled 15 ml conical tubes. The cell suspension was centrifuged for 5 min at 500 rpm at 4 ℃ and the supernatant was discarded. The cell pellet was gently resuspended in 500 µl of 1×Hypotonic Buffer by pipetting up and down several times and the suspension was incubated for 15 min on ice in a pre-chilled microcentrifuge tube. 25 µl of detergent was added and vortexed 10 sec at highest setting. The suspension was centrifuged for 30 sec at 14,000×g in a pre-cooled microcentrifuge at 4 ℃ and the supernatant was discarded. The pellet was then resuspended in 50 µl of Complete Lysis Buffer and the suspension was incubated for 30 min on a 150 rpm rocking platform set at 4 ℃ and centrifuged for 10min at 14,000×g at 4 ℃. The supernatant (nuclear fraction) was transferred into a pre-chilled microcentrufuge tube and was stored at -80 ℃. The protein concentration of the nuclear extract was assayed by a Bio-Rad micro protein assay kit (Bio-Rad, USA).

2.2.7 Electrophoretic Mobility Shift Assay (EMSA)

2.2.7.1 Annealing and labeling of oligonucleotides

The Oligonucleotides (MWG biotech, Germany) containing the *Mlu*I Cell-cycle Box (MCB, *ACGCGT*) were used in EMSAs and their sequences are shown as below: MCB wild type, 5'-GCGTGACGCGTTTTCAAATCTTCAACC-3' (sense); MCB mutant, 5'-GCGTGA*TGA*GTTTTCAAATCTTCAACC-3' (sense, the italic font is mutated

sequence). Sense and antisense oligonucleotides were annealed at an equimolar ratio containing in the final volume of 50 µl. The mixture was incubated for 3 min at 95 ℃ and then 1 min at 30 ℃ and lastly stored at 4 ℃ overnight. The double-stranded oligonucleotides (0.5 µl) were 5'-end labeled with 1.5 µl of T4 kinase (NEB, UK) using 4 µl of γ-[^{32}p] ATP and mixed with 4 µl of 5 × NEB buffer made up with water to the final volume of 20 µl. They were incubated at 37 ℃ for 1 h and subsequently purified on Bio-Gel P-6 columns (Bio-Rad, UK).

2.2.7.2 Gel shift reactions

EMSAs reactions were conducted in a final volume of 20 µl. 0.4 pmol of radiolabeled probe was incubated for 30 min in a buffer containing 5 mM $MgCl_2$, 2.5 mM K-EDTA, 20% glycerol, 250 mM NaCl, 2.5 mM DTT, 50mM Tris-HCl (pH 7.5), and 0.9 µl of 1 mg/ml poly(dI-dC).poly(dI-dC) (Sigma, UK) and 1× protease inhibitor mix (Complete) (Roche, Germany) as well as the required drug concentration. Nuclear extracts (20 µg) were then added and the mixture was further incubated for 1 h. Subsequently, 5 µl of loading buffer [25 mM Tris-Cl (pH 7.5), 0.02% bromphenol blue, 10% glycerol] was added and the samples were separated on a 4% polyacrylamide gel in 0.5 × TBE containing 2.5% glycerol at 4 ℃. After drying the gels, the radioactive signal was visualized by exposing the gels to medical X-Ray film (Super Rx, Fuji) and developed by Konica Medical Film Processor SRX-101A.

2.2.8 Purification of total RNA from MDA-MB231 cells

MDA-MB231 cells grew in 60mm well at cell density of 2.5 × 10^6. RNA purification was carried out using RNeasy Mini kit (Qiagen, UK). Cells were trypsinized and collected as a cell pellet in a 15 ml falcon tube prior to lysis. 350 µl of buffer RLT was

added and the lysate was passed at least 5 times through a blunt 20-gauge needle (0.9 mm diameter) in order to homogenize. 350 µl of 70% ethonal was added to the homogenized lysate. 700 µl of the sample was transferred to an RNeasy spin colume and centrifuged for 15 s at 8000×g. The flow-through was discarded and 700 µl of buffer RW1 was added to the spin column and centrifuged for 15 s at 8000×g. 500 µl buffer RPE was added and centrifuged for 15 s at 8000×g and then another 500 µl was added and centrifuged for 2 min at 8000×g. The spin column was transferred with 30-50 µl of water and centrifuged for 1min at 8000×g. The flow-through was collected in a new 1.5 ml tube. The concentration of purified RNA was determined by measuring the absorbance at 260 nm.

2.2.9 Reverse transcription

Reverse transcription was carried out as described in the manufacturer's instructions (Qiagen). The reverse transcriptase reaction was carried out at 37℃ for 1 h using 2 µg of RNA, 2 µl of 10 × reverse transcriptase buffer (Qiagen), 2 µl of 5 mM dNTP mix (Qiagen), 2 µl of 10 µM Oligo-dT primer (Invitrogen), 0.5 µl of 20 U/µl RNase inhibitor (Applied Biosystems), 1 µl of Omnicript Reverse transcriptase (Qiagen), and nuclease-free water in a final volume of 20 µl.

2.2.10 Real-time PCR

2.2.10.1 Taqman primers/probe

Real-time PCR was carried out using an ABI PRISM 7000 Sequence Detection System from Applied Biosystems. Dbf4 forward and reverse primers and probe were designed by Taqman (Hs00988147_g1) and the primers to detect Dbf4 promoter yield an RT-

PCR product of 103bp. The cycling conditions used were 95 ℃ for 10 min to denature and 40 cycles of 95 ℃ for 15 s and 58 ℃ for 1 min to amplify the target (Dbf4) sequences. GAPDH primer/probe mix (1 µl; Applied biosystems) was used as an internal control in all reactions. The reaction mix was prepared using 10 µl of Taqman 2 × PCR master mix (Applied Biosystems), 1 µl of 20 × primer/probe mix and 1 µl of cDNA (1-100 ng) template in a final volume of 20 µl. The results were analyzed using the mathematical qualification approach described by PfaffI (PfaffI, 2001) and ABI user Bulletin 2 (ABI PRISM 7700 sequence detection system manual).

This statistical method is based on the relative expression ratio of the target gene (Dbf4) compared to that of internal control gene (GAPDH). Standard curves were constructed for both the internal and target genes, and slopes of these were used to ensure that both primer sets were equally efficient. The threshold cycle values (Ct) and the efficiencies of the reactions were used to compare the relative expression levels of the target gene in various samples. Levels of Dbf4 RNA in untreated, exponentially growing cells were set at a value of 100% and all test samples were expressed at values relative to this.

2.2.11 Western blot analysis

2.2.11.1 Cell line and culture conditions

MDA-MB231 cells were grown in DMEM (Autogen Bioclear, UK) supplemented with 10% FBS and 1% glutamine and incubated at 37 ℃ in 5% CO_2

2.2.11.2 Whole-cell protein extraction

MDA-MB231 cells were seeded in 6 well plates at 2×10^5 cells/ml and allowed to grow for 24 h before drug treatment. 24 h drug-treated and untreated cells were washed twice

with ice cold PBS and subsequently scraped from 6 well plates and then centrifuged in a 4℃ at 13,000 rpm for 5 min. The supernatant was discarded and the pellet was resuspended in 50-100 µl lysis buffer (25 × protease inhibitor, 10 × phosphatase inhibitor and 10 U/ µl Merck benzonase nuclease added in 1ml of sigma cell lytic M cell lysis reagent) and stored at -80 ℃.

2.2.11.3 Protein Assay

Protein was determined by the BCA assay (Pierce) according to the manufacturer's protocol using bovine serum albumin as a standard.

2.2.11.4 Immunoblotting

30-40 µg of protein lysate was mixed with 5× loading (laemelli) buffer (250 mM Tris HCl, pH 6.8, 500 mM DTT, 10% SDS, 0.5% Bromophenol Blue, 50% glycerol and distilled water were used to make a 5 times stock). The protein lysates were spun for a few seconds and boiled for 5 min at 100 ℃, and then centrifuged for 5 sec. The protein lysates were loaded on NuPAGE® Novex 10% Bis-Tris pre-casted mini gels (Invitrogen) along with a marker as a reference (Rainbow protein marker, GE healthcare, UK) and run in 1× NuPAGE® MOPS SDS Running Buffer using the XCell SureLock™ Mini-Cell module (Invitrogen).

The protein lysates were separated on the 10% Bis-Tris mini gel and were subsequently transferred electrophoretically (Trans-Blot cell, invitrogen) onto methanol activated polyvinylidene difluoride membranes (Immobilon-P, Sigma-Aldrich) and run in 1× transblot buffer [100 ml of running buffer stock × 10 (30.3 g Tris Base, 144.1 g Glycine

and distilled water to 1 litre-pH 8.30), 200 ml MetOH and distilled water to 2 litre] at 35 V for 2.5 h.

Membranes were blocked with 5% BSA in TBS buffer containing 0.1% Tween 20 (pH 7.5) for 1 hour. Proteins were probed using the appropriate primary antibody (see dilutions and preparation in Table 2.1.3) and incubated at 4 ℃ shaker overnight. Membranes were washed twice with TBS-Tween buffer in 30 min and subsequently were probed with HRP-conjugated polyclonal antibodies (Mouse or Rabbit – 1/1000, Cell Signaling) using 5% skimmed milk dissolved in TBS with 0.1% Tween 20 as blocking reagent for chemiluminescence detection (ECL system, Amersham Biosciences, UK). The chemiluminescent signal was visualized by exposing the blots to Kodak X-OMAT^{TM}LS film for various exposure times (15 seconds to 1 hour). For all experiments, calnexin was used as a loading control for the cytoplasmic fraction.

Stripping membranes to remove pre-bound antibody was done by rehydrating membranes in TBS-tween and washed 3 times for 5 min. Membranes were then incubated in Restore^{TM} Plus western blot stripping buffer (100mM β-mercaptoethanol, 2% SDS and 62.5 mM Tris HCl pH 6.8, Thermoscientific) for 15 min and washed in TBS-tween 3 times for 10 min. The membranes were blocked and reprobed as described above

Antibodies	Dilutions	Dilution buffer	Supplier
Anti-Dbf4	1/500	5% BSA	Abcam
Anti-Cdc7	1/1000	5% BSA	Cell signaling
Anti-Calnexin	1/1000	5% BSA	Cell signaling
Anti-Mouse (ab6728)	1/1000	5% Milk	Cell signaling
Anti-Rabbit (ab6721)	1/1000	5% Milk	Cell signaling

Table 2.10: List of antibodies

2.2.12 Cell cycle analysis

Cell cycle profiles were determined by propidium iodide (PI) staining of DNA content and flow cytometry. Exponentially growing cells were treated with required drug concentrations for 24 h. Untreated- and treated-cells were harvested by trypsinizing, pelleted by centrifugation for 5 min at 800 rpm, and ~1 $\times 10^6$ cells were washed in 2 ml ice cold PBS. Cell pellets were then fixed by drop-wise addition to 70% ice-cold ethanol and stored overnight at 4 ℃. The ethanol fixed cells were centrifuged for 5 min at 800 rpm, and the cell pellets were then resuspended in 1 ml staining solution containing 50 µg/ml of PI (Sigma) and 100 µg/ml of RNase A (Sigma) in 0.05% Triton X-100 PBS. After at least 30 min of incubation in the dark at room temperature, the cell suspension was analyzed by the CyAn ADP High-Performance Flow Cytometer. Data were analyzed by Summit V4.3 software.

2.2.13 Small interfering RNAs and Transfection

2.2.13.1 siRNA Transfection efficiency

Cells were plated in 100 µl of growth medium (DMEM supplemented with 10% FBS and 1% glutamine) in 96 well plate without antibiotics such that they would be 30-50% confluent at the time of transfection. For the transfection samples, a series of concentrations (1, 3, 5 and 10 pmol) of Silencer Fam GAPDH siRNA were diluted in 25 µl Opti-MEM® I Reduced Serum Medium (final concentration of siRNA when added to the cells is 33 nM). 0.25 µl of Lipofectamine 2000 reagent (invitrogen) was added in 25 µl Opti-MEM® I Reduced Serum Medium and incubated for 5 min at room temperature. After 5 min incubation, GAPDH siRNA diluent was incubated with Lipofectamine 2000 diluent for 20 min at room temperature. The GAPDH siRNA-Lipofectamine 2000 complexes were added to each well containing cells and medium and then mixed gently by rocking the plate back and forth. The transfected cells were observed and assessed using fluorescence microscopy.

2.2.13.2 Dbf4 siRNA transfection

siRNA specific to Dbf4 and scrambled control (Origene) were used on synchronized 0.8 × 10^5 cells. 10 pmol of Dbf4 siRNA (Origene) was optimized for each RNA interference in 96 well plates. Dbf4 siRNA transfection followed the same procedure as described above. 100 pmol of Dbf4 siRNA and 5 µl of Lipofectamine 2000 were diluted in 250 µl of Opti-MEM buffer for the RNA interference in 6 well plates. siRNA treatments were tested in cell survival, apoptosis and proliferation assay at the various time points.

2.2.14 CellTiter-Glo Luminescent cell viability assay

The CellTiter-Glo Luminescent cell viability assay (Promega, UK) is a homogeneous method to determine the number of viable cells in culture based on the quantitation of

the ATP present, which signals the presence of metabolically active cells. After Dbf4 siRNA transfection, cells were incubated with a volume of CellTiter-Glo reagent equal to the volume of cell culture medium present in each well for 10 min according to the manufacturer's protocol. The number of surviving cells was measured by luminometer (Thermo Scientific Varioskan Flash).

2.2.15 Caspase-Glo 3/7 apoptosis assay

The Caspase-Glo® 3/7 Assay is a homogeneous, luminescent assay that measures caspase-3 and -7 activities. The assay provides a luminogenic caspase-3/7 substrate, which contains the tetrapeptide sequence DEVD, in a reagent optimized for caspase activity, luciferase activity and cell lysis. After Dbf4 siRNA transfection, blank, negative control cells or treated cells in culture medium were incubated with Caspase-Glo 3/7 reagent in each well for 1.5 h according to the manufacturer's protocol. The number of apoptotic cells was then measured by luminometer (Thermo Scientific Varioskan Flash).

2.2.16 BrdU cell proliferation assay

The BrdU cell proliferation assay detects 5-bromo-2'-deoxyuridine (BrdU) incorporated into cellular DNA during cell proliferation using an anti-BrdU antibody. At Dbf4 siRNA post-transfection, cells were tested using BrdU cell proliferation assay kit (Cell signaling, UK) according to the manufacturer's protocol. Briefly, cells were incubated with BrdU solution for 18 h and then the medium was removed. 100 µl of fixing/denaturing solution were added to each well incubated for 30 min at room temperature before discarding the solution. 100 µl of BrdU detection solution were

added and kept at room temperature for 1 h prior to 3 times wash. Subsequently, anti-mouse lgG, HRP-linked antibody (100 µl, Cell signaling) was used to recognize the bound BrdU detection antibody. After 3 times wash, HRP substrate TMB (100 µl) was added to develop color. The magnitude of the absorbance for the developed color is proportional to the quantity of BrdU incorporated into cells, which is a direct indication of cell proliferation. The absorbance was measured at 450 nm by luminometer (Thermo Scientific Varioskan Flash).

2.2.17 Immunostaining for confocal microscopy

A total of 3×10^4 MDA-MB231 cells were plated in chambered slides. Cells were then treated with rationally designed polyamides at the various time points. Slides were fixed with 2.5% paraformaldehyde for 10 min followed by 3 times PBS washes, permeabilized with 0.5% Triton X-100 for 10 min followed by 3 times PBS washes, stained with 20 µg/µl propidium iodide (Sigma) for 3 min followed by 1 time PBS wash, and then incubated with water for 10 min before drying for 10-15 min at room temperature. Slides were covered with coverslips (24 × 60mm, VWR), which were sealed at the edge with clear nail varnish. Cells were visualized by confocal microscopy (objective: × 40; Leica TCS SP2). Nuclear slice images were acquired by sequential scanning by using the LAS AF Lite program.

CHAPTER 3

EVALUATION OF NOVEL POLYAMIDE CONTAINING BIOCAMPITABLE REACTIVE GROUPS FOR *IN SITU* H-PIN FORMATION

3.1 Introduction

Pyrrole (P)- and imidazole (I)-containing polyamide analogues of distamycin A bind in the minor groove of DNA in a stacked, antiparallel 2:1 (polyamide/DNA) motif (Mitra et al., 1999; Pelton and Wemmer, 1989,1990). Early studies have formulated a set of 'pairing rules' for DNA base pair recognition; A/T and T/A base pairs are recognized by P/P pairs, G/C base pairs by I/P pairs, and C/G base pairs by P/I pairs (Kopka et al., 1985; Mrksich et al., 1992; Wade et al., 1992; Lown et al., 1986). This recognition is analogous to a simple, single-letter language in which one heterocyclic pair reads one DNA base pair.

Formamido(f)-IPI binds selectively as a 2:1 stacked dimer in the minor groove of 5'-ACGCGT-3' (Buchmueller et al., 2006). Replacement of the f-group by a pyrrole or aryl groups at the N-terminus leads to binding in the overlapped fashion, with decreased binding affinity. Although the monomer polyamides can form a 2:1 polyamide/DNA complex within the minor groove, this is not always energetically favorable. There is also a concern that the monomers without a formamido group may split into an extended staggered motif, hence, creating a reading frame different to the one predicted (Pelton et al., 1990; Chen et al., 1994). In addition, the monomers may also bind in a mixed 2:1 and 1:1 motif, thus, reducing the overall affinity. To address the problem,

Hairpin and H-pin analogues have been designed, showing enhanced DNA binding affinity and selectivity. However, poor cellular uptake of large hairpin/H-pin polyamides has restricted their further development (Best et al., 2003; Dickinson et al., 2004; Franks et al., 2010).

A new class of unlinked polyamide precursors that contain appropriately designed pendant reactive and biocompatible functional groups was designed and synthesized by our collaborator Dr Moses Lee (Hope College). It was hypothesized that these relatively small polyamide precursors (molar mass ~500g/mol) will more readily penetrate cells in comparison with relatively large H-pin/hairpin polyamides, localize in the nucleus to their DNA target sequence in the stacked, staggered motif, and have the potential to form covalent H-pin or Hairpin structures *in situ*.

The aim of the project is to test the novel approach of *in situ* reaction of two rationally designed polyamide monomers capable of potentially forming either H-pin or Hairpin conjugates in the nucleus. The general approach is shown in Figure 3.1. There are four particular chemical reactions tested in the DNase I footprinting analysis. $-C_3NH_2$ reactive group could interact with $-C_3Cl$ through a nucleophilic substitution reaction; $-C_3N_3$ reactive group could interact with $-C_3CN$ through a 1,3-dipolar cycloaddition reaction; $-C_3N_3$ reactive group could interact with $-C_3$-alkyne through an azide-alkyne Huisgen reaction; $-NH_2$ reactive group could interact with carbamate carbonyl through an acyl transfer reaction (illustrated in Figure 3.1).

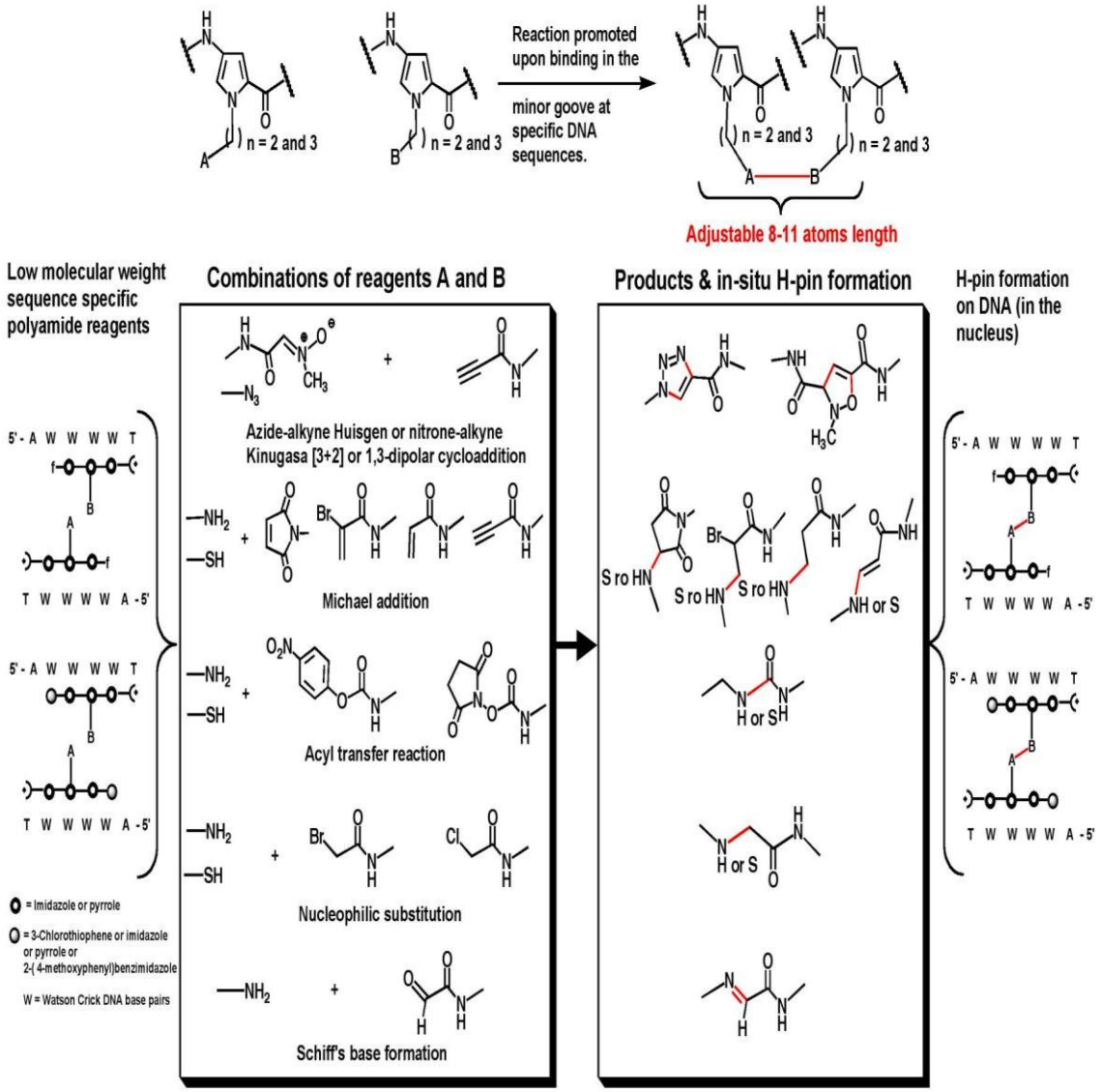

Figure 3.1 Biocompatible reactive groups for in-nucleus H-pin formation. Low molecular weight sequence selective polyamide reagents containing appropriate pendant reactive and biocompatible functional groups combine on the DNA *in situ* to form H-pin structures at specific DNA sequences.

3.2 Results

3.2.1 DNA sequence specific binding of f-IPI, analogues f-IP(C_3NH_2)I, f-IP(C_3Cl)I, and their combination

The binding of the formamido-imidazole-pyrrole-imidazole compound (f-IPI), its analogues f-IP(C_3NH_2)I, f-IP(C_3Cl)I, and their combination on a 127bp DNA fragment was investigated by DNase I footprinting. The chemical structure and DNA sequence binding models of f-IP(C_3NH_2)I, f-IP(C_3Cl)I, and their combination are shown in Figure 3.2A&B. The selectivity of these polyamides was determined in a DNA fragment engineered to contain the cognate site 5'-ACGCGT-3', the noncognate sites 5'-ACCGGT-3' and 5'-ACACGT-3', and the control AT-rich site 5'-AAATTT-3' (Figure 3.2C). Our footprinting studies of f-IPI have been reported previously (Buchmueller et al., 2006) and it is included here for comparison (Figure 3.3A). Binding of f-IP(C_3NH_2)I to the established cognate sequence (5'-ACGCGT-3') is observed at 0.05 μM similar to f-IPI. The stronger footprint for f-IP(C_3NH_2)I at this concentration suggests a slightly higher DNA binding affinity than that of f-IPI (Figure 3.3A&B). Binding of f-IP(C_3NH_2)I at the non-cognate binding site 5'-ACCGGT-3' and 5'-ACACGT-3' occurs at 1 μM while no significant binding is observed at the AT-rich site 5'-AAATTT-3' at concentrations <10 μM (Figure 3.3B).

Binding of f-IP(C_3Cl)I to the cognate sequence occurs at a higher dose (1 μM) than f-IP(C_3NH_2)I however f-IP(C_3Cl)I appears to have enhanced sequence selectivity as no significant binding is observed at any other sites at concentrations as high as 20 μM (Figure 3.3C). The different pendant groups on the central pyrrole unit of f-IPI can

therefore influcence DNA binding affinity while retaining specificity for the cognate sequence.

The combination (1:1 mixture) of f-IP(C_3NH_2)I and f-IP(C_3Cl)I (Figure 3.3D) was also tested with DNase I footprinting. The binding of the combination of the two polyamides to the cognate sequence occurs at 0.05 μM (Figure 3.3D). 0.025 μM of each polyamides f-IP(C_3NH_2)I and f-IP(C_3Cl)I was mixed to achieve the final concentration of the combined compound 0.05 μM.

These footprinting experiments showed that f-IP(C_3NH_2)I has comparable binding affinity to the cognate site as its parent compound f-IPI but exhibits 20-fold better binding affinity than f-IP(C_3Cl)I. When 0.025 μM of f-IP(C_3NH_2)I were mixed with 0.025 μM of f-IP(C_3Cl)I, binding occurs at 0.05 μM as was the case for f-IP(C_3NH_2)I alone. The question raised from these results is how the presence of the lower binding affinity compound f-IP(C_3Cl)I shows the same effect in the combination treated f-IP(C_3NH_2)I at half the concentration? One possibility is that f-IP(C_3NH_2)I and f-IP(C_3Cl)I combine *in situ* to form a favorable 2:1 structure, which can account for the higher binding affinity in the *in situ* reaction. However, it is difficult to prove whether the actual H-pin compound is covalently formed with just DNase I footprinting analysis.

A

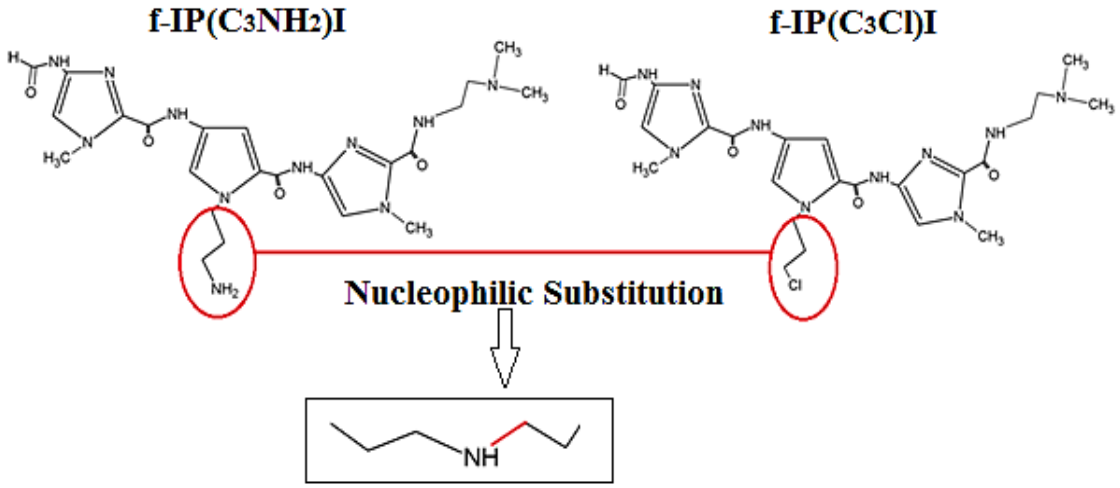
f-IP(C3NH2)I
f-IP(C3Cl)I
Nucleophilic Substitution
NH

B

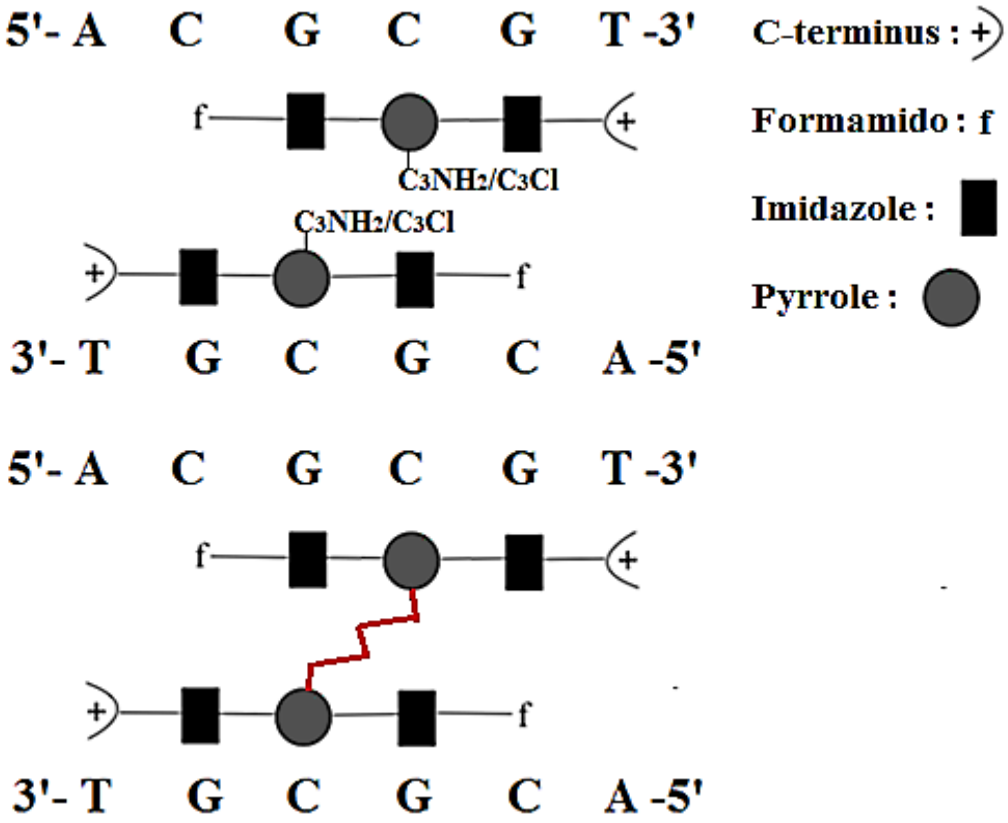
5'- A C G C G T -3'
C-terminus : +
f
+
C3NH2/C3Cl
Formamido : f
C3NH2/C3Cl
Imidazole :
+
f
Pyrrole :
3'- T G C G C A -5'
5'- A C G C G T -3'
f
+
+
f
3'- T G C G C A -5'

C IM17/19

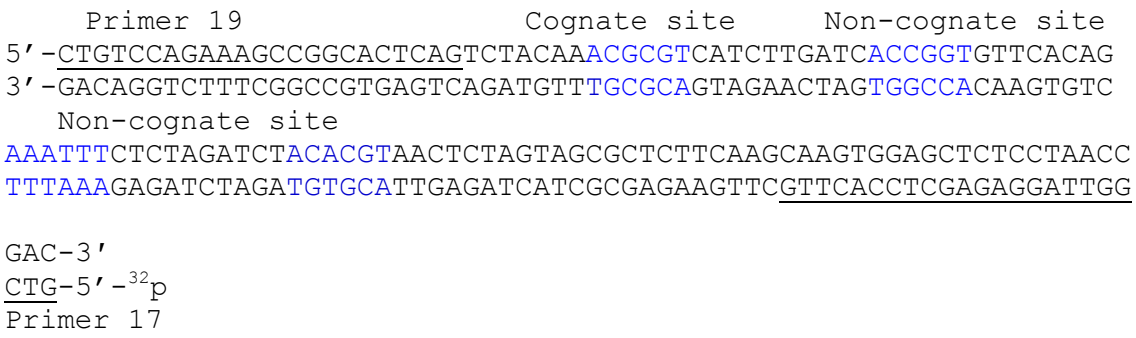

Figure 3.2 A, Chemical structures of f-IP(C_3NH_2)I and f-IP(C_3Cl)I, and reactive groups (red) of the two monomer polyamides designed to form H-pin structure through a nucleophilic substitution reaction **B**, Binding models of f-IP(C_3NH_2)I, f-IP(C_3Cl)I and potentially formed hybrid. **C**, DNA fragment IM17/19. The bottom strand is 5'-labelled with ^{32}P. DNA cognate and non-cognate sequence binding sites are labeled with blue color.

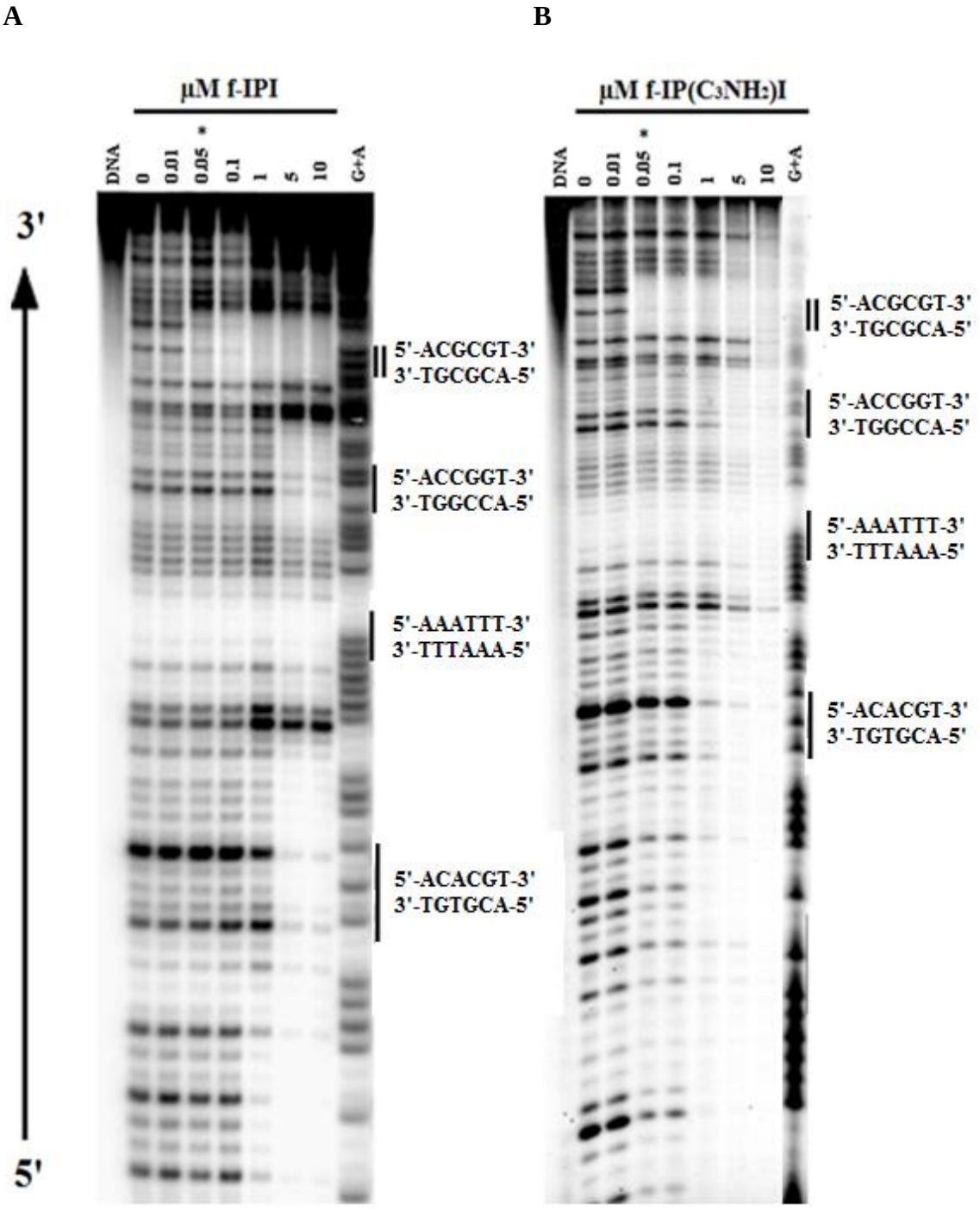
A
B
μM f-IPI
μM f-IP(C3NH2)I
DNA
0
0.01
0.05 *
0.1
1
5
10
G+A
3'
5'
5'-ACGCGT-3'
3'-TGCGCA-5'
5'-ACCGGT-3'
3'-TGGCCA-5'
5'-AAATTT-3'
3'-TTTAAA-5'
5'-ACACGT-3'
3'-TGTGCA-5'

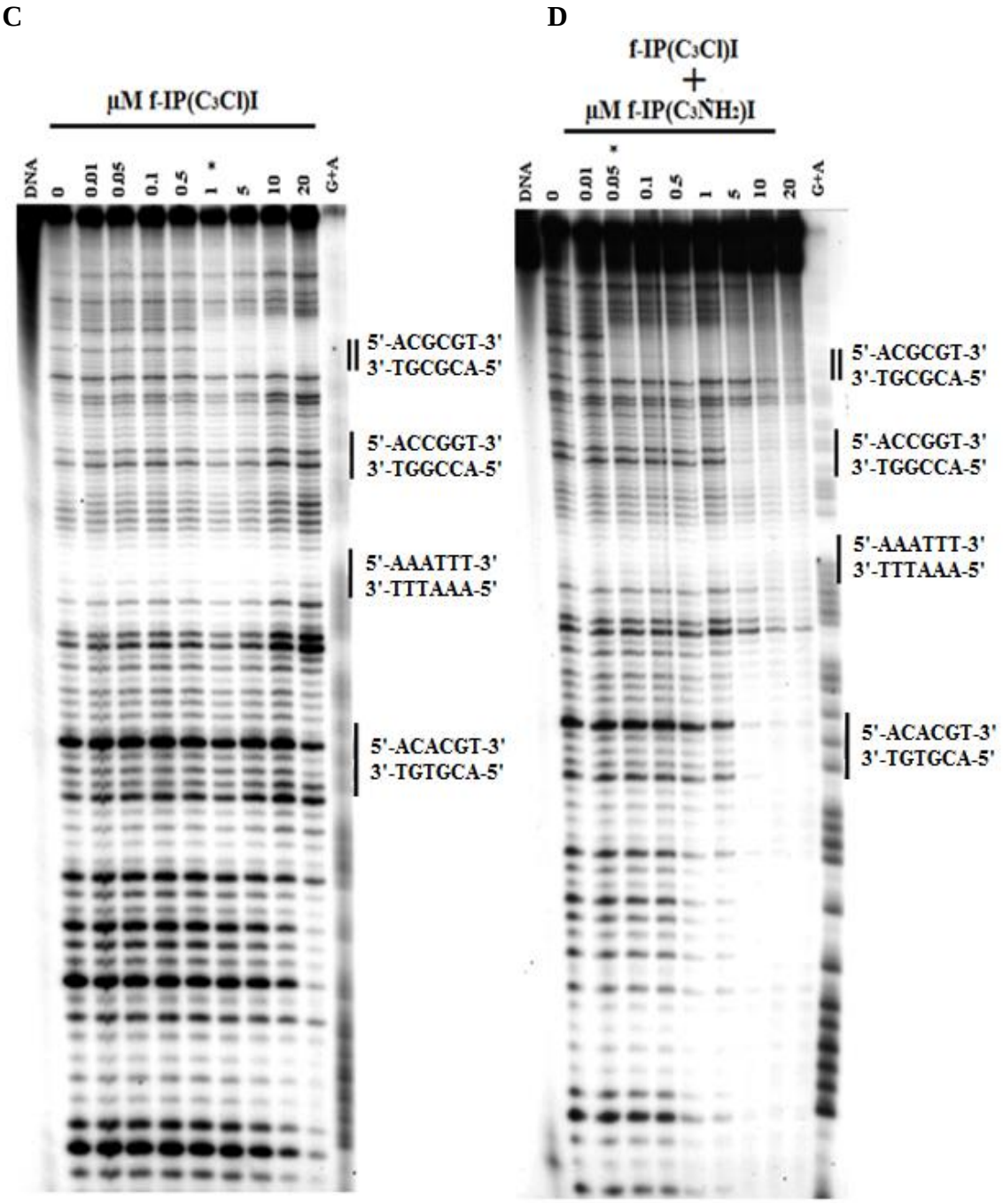

Figure 3.3 DNase I footprinting was performed with a radiolabeled probe containing the IM17/19 DNA sequences. The probe was incubated with increasing concentrations of f-IPI (**A**), f-IP(C_3NH_2)I (**B**), f-IP(C_3Cl)I (**C**) and combination of f-IP(C_3NH_2)I and f-IP(C_3Cl)I (0.01-20 µM) (**D**). Asterisks indicated the concentration of polyamide at which cleavage protection is initially observed. The cognate sequence binding sites are highlighted by double solid bars. Control DNA lanes lack DNase I treatment and G+A lanes denote the position of the purine nucleotides.

3.2.2 DNA sequence binding affinity of f-PIP, analogues f-P(C_3CN)IP, f-P(C_3N_3)IP and their combination

The chemical structures and DNA sequence binding models of f-P(C_3CN)IP, f-P(C_3N_3)IP and their combination are shown in Figure 3.4A&B. DNase I footprinting studies of f-PIP binding to a DNA fragment corresponding to the topo IIα promoter (Figure 3.4C) have been previously reported and the titration experiment indicated that a footprint at the 5'-TACGAT-3' site (5'-flank of ICB2 shown in Figure 3.4B) begins to appear at a concentration of 30 μM (Le et al., 2006). f-PIP is included here for comparison purposes with its derivatives (Figure 3.5A). The autoradiograms given in Figure 3.5B&C showed that both f-P(C_3CN)IP and f-P(C_3N_3)IP footprint at the 5'-TACGAT-3' site at 30 μM, revealing similar affinity to f-PIP. However, nonspecific binding of f-P(C_3N_3)IP occurs at 30 μM. The combination (1:1 mixture) of f-P(C_3CN)IP and f-P(C_3N_3)IP (Figure 3.5D) was also tested with DNA footprinting. The binding of the combination of the two polyamides to the cognate sequence occurs at 30 μM polyamides (Figure 3.5D), by adding and mixing 15 μM of each polyamides f-P(C_3CN)IP and f-P(C_3N_3)IP to achieve the final concentration of the combined compounds 30 μM. Identical binding affinity is therefore observed with all the compounds. Consequently, it is difficult to prove that the two unlinked monomers form a covalent H-pin structure, and do not just bind in a 2:1 motif. Unlike f-IPI and its analogues f-IP(C_3NH_2)I and f-IP(C_3Cl)I, the two different pendant reactive groups (-C_3CN and -C_3N_3), retain the same DNA binding affinity as the parent compound f-PIP. In this case, the pendant groups are on the first heterocycle of f-PIP adjacent to the formamido group suggesting that modification at this position does not affect binding affinity.

A

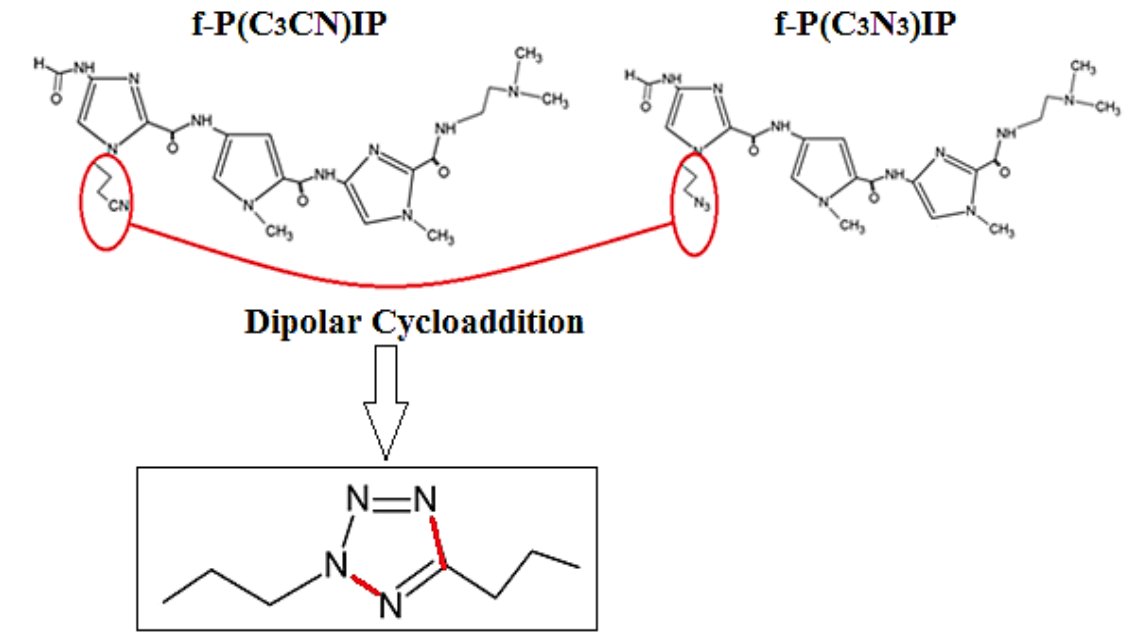
f-P(C3CN)IP
f-P(C3N3)IP
Dipolar Cycloaddition

B

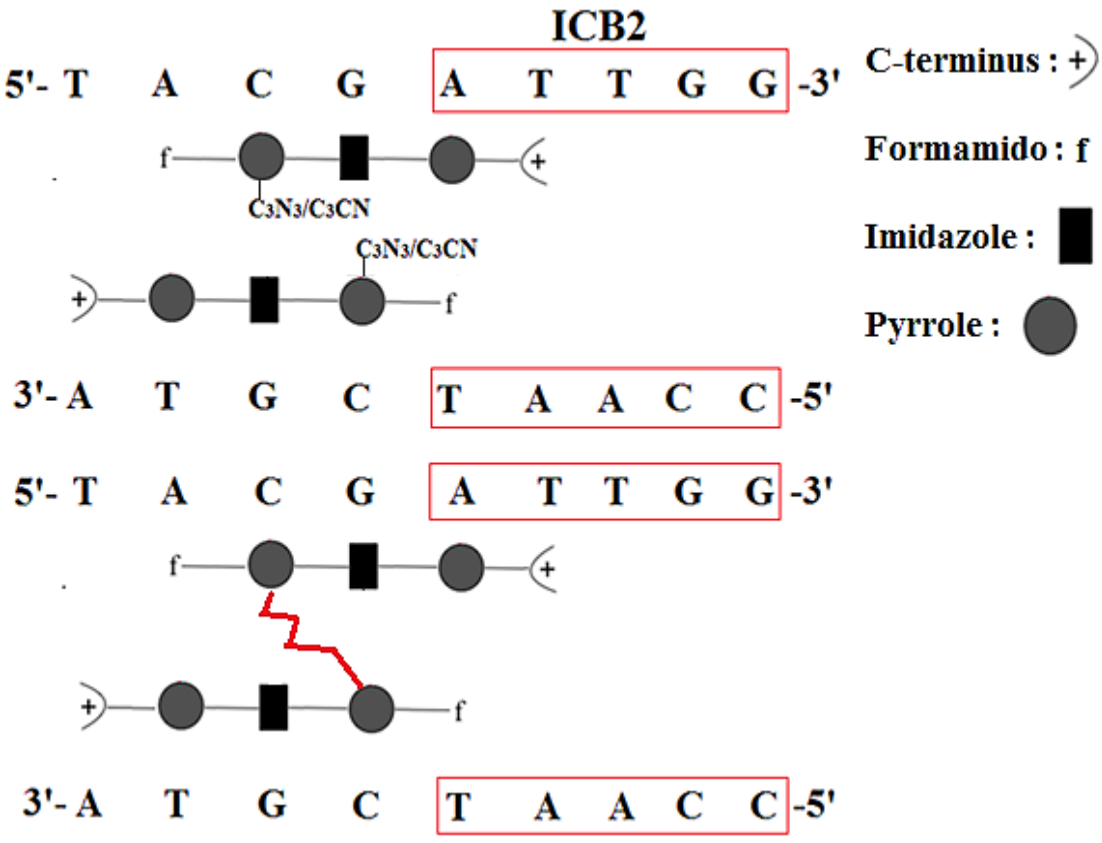
ICB2
5'- T A C G A T T G G -3'
f
+
C3N3/C3CN
C3N3/C3CN
+
f
3'- A T G C T A A C C -5'
5'- T A C G A T T G G -3'
f
+
+
f
3'- A T G C T A A C C -5'
C-terminus : +
Formamido : f
Imidazole :
Pyrrole :

C

Topo IIα promoter

Figure 3.4 A, Chemical structures of f-P(C_3CN)IP and f-P(C_3N_3)IP, and reactive groups (red) of the two monomer polyamides designed to form H-pin structure through a dipolar cycloaddition reaction. **B**, Binding models of f-P(C_3CN)IP, f-P(C_3N_3)IP and potentially formed hybrid at the 5'-TACGAT-3' site (5'-flank of ICB2). ICB2 labeled. **C**, The 496bp topo IIα promoter. The bottom strand is 5'-labelled with ^{32}P. The ICB1, ICB2, ICB3, and ICB4 sites are indicated. ICB1, 5'-CAGGG*ATTGG*CTGG-3'; ICB2, 5'-CTACG*ATTGG*TTCTT-3'; ICB3, 5'-ACCTG*ATTGG*TTTAT-3'; ICB4, 5'-TTCTC*ATTGG*CCAGA-3'. DNA binding sites are labeled with blue color.

A

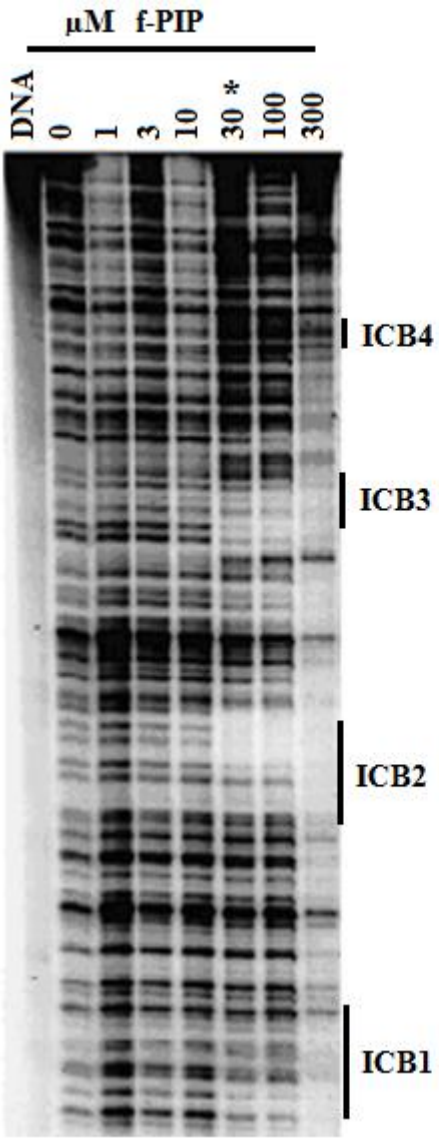
µM f-PIP
DNA
0
1
3
10
30 *
100
300
ICB4
ICB3
ICB2
ICB1

B

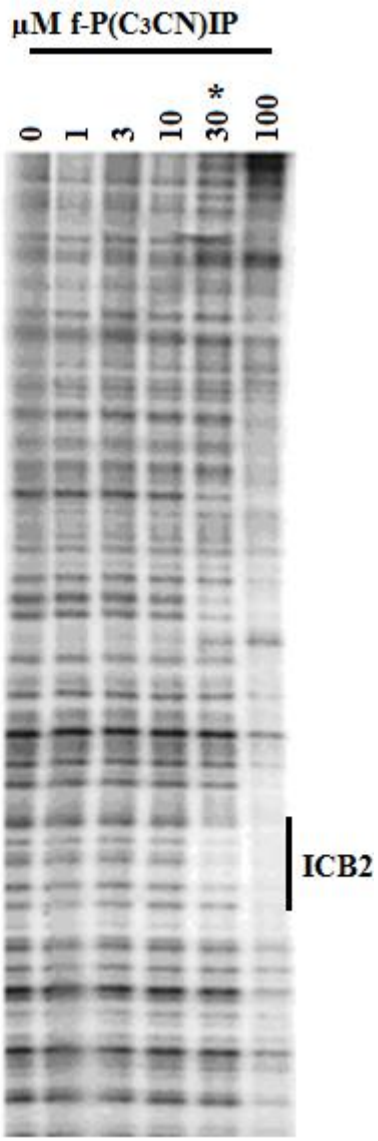
µM f-P(C3CN)IP
0
1
3
10
30 *
100
ICB2

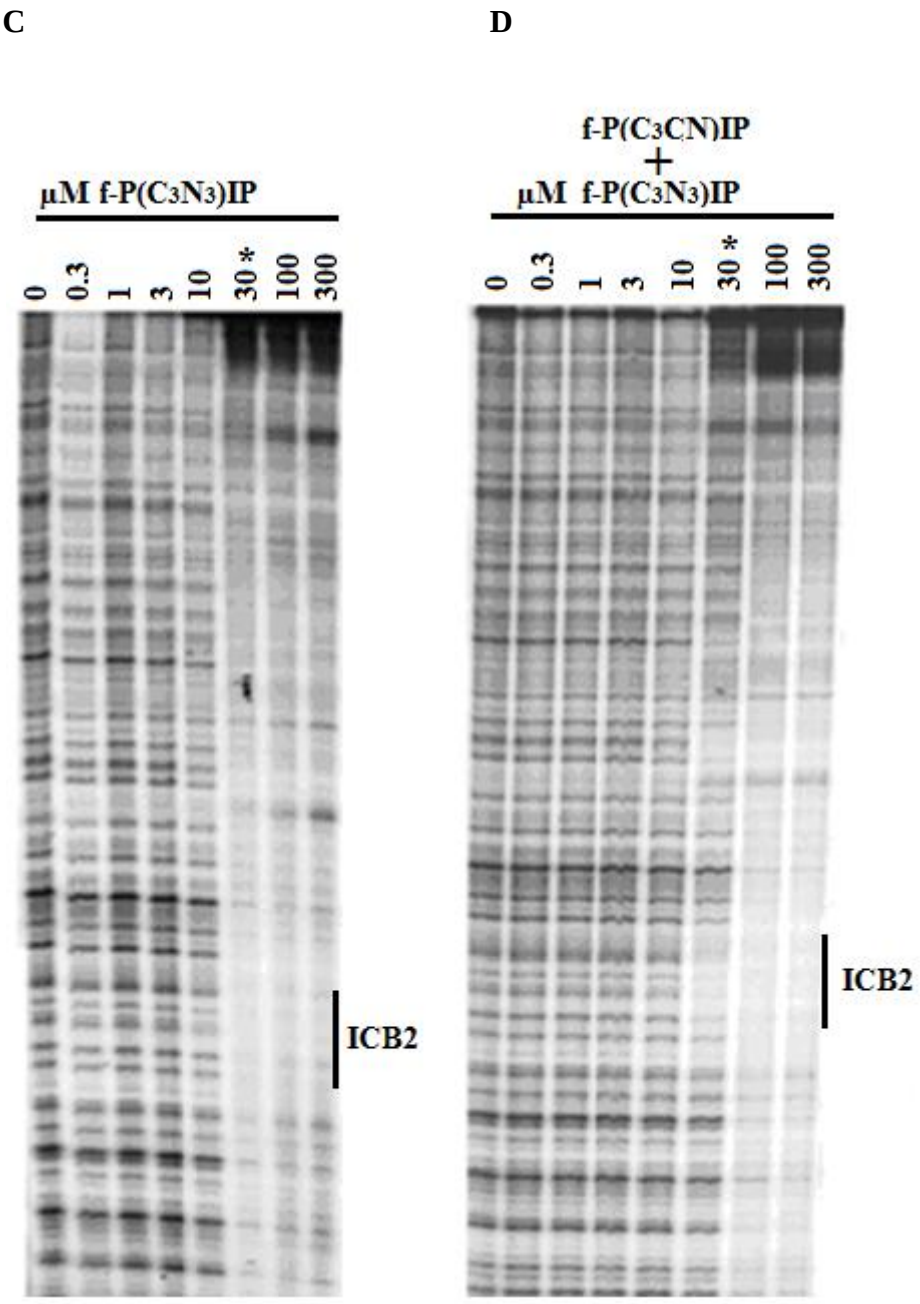

Figure 3.5 DNase I footprinting was performed with a radiolabeled probe corresponding to the *topo IIα* promoter. The probe was incubated with increasing concentrations of f-PIP (**A**), f-P(C_3CN)IP (**B**), f-P(C_3N_3)IP (**C**) and combination of f-P(C_3CN)IP and f-P(C_3N_3)IP (**D**), respectively (0.3-300 µM).

3.2.3 DNA sequence specific binding of f-IP(C_3N_3)I, f-PP(C3-alkyne)P, and their combination

The combination of two polyamide monomers f-IP(C_3N_3)I and f-PP(C_3-alkyne)P can potentially form an H-pin heterodimer and therefore target a new binding site, as the heterodimer has a cognate sequence different to those of the two monomers as illustrated in Figure 3.6A. The chemical structures of f-IP(C_3N_3)I and f-PP(C_3-alkyne)P and their binding models are shown in Figure 3.6A&B. DNase I footprinting was performed to assess the DNA sequence selectivity and binding affinity of f-IP(C_3N_3)I, f-PP(C_3-alkyne)P, and their combination using a 136bp base pair 5'-[^{32}P]-radiolabeled fragment (Figure 3.6C) containing the corresponding cognate sequences 5'-ACGCGT-3', 5'-AAATTT-3', and 5'-WCWCWW-3' (where W is A or T), respectively. The autoradiogram depicted in Figure 3.7A indicates that binding of f-IP(C_3N_3)I to its cognate sequence 5'-ACGCGT-3' is initially observed at 5 μM while nonspecific binding begins to appear at the 5'-ACTCAT-3', 5'-ACACTT-3', 5'-TCTCAA-3' and 5'-TCACTA-3' sites at concentrations >20 μM. Cleavage protection at the cognate sequence (5'-AAATTT-3') for f-PP(C_3-alkyne)P is observed at 5 μM and nonspecific binding occurs at the 5'-ACACTT-3' (15 μM) and 5'-TCACTA-3' site (>10 μM) (Figure 3.7B). The potential hybrid generates a footprint at 10 μM at the cognate sites 5'-ACTCAT-3', 5'-ACACTT-3', 5'-TCTCAA-3' and 5'-TCACTA-3' by adding and mixing 5 μM of each polyamides f-IP(C_3N_3)I and f-PP(C_3-alkyne)P to achieve a 10 μM final concentration of the combined compound (Figure 3.7C). The hybrid heterodimer has a higher binding affinity for the cognate sites 5'-ACTCAT-3', 5'-ACACTT-3', 5'-TCTCAA-3' and 5'-TCACTA-3' (10 μM) than either f-IP(C_3N_3)I or f-PP(C_3-alkyne)P. These results suggest that the two monomers f-IP(C_3N_3)I and f-PP(C_3-alkyne)P can interact to form a heterodimer.

A

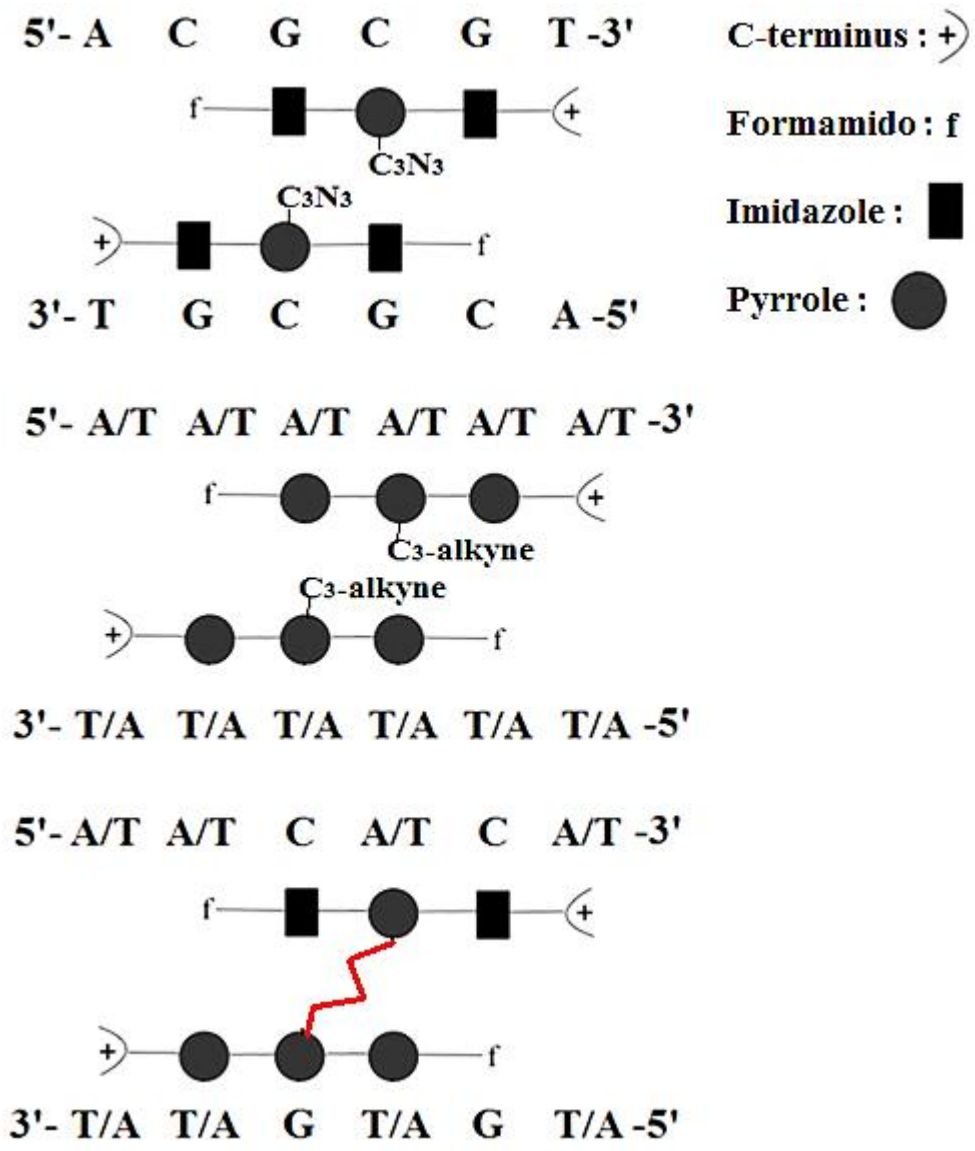
5'- A C G C G T -3'
f
+
C3N3
C3N3
+
f
3'- T G C G C A -5'
C-terminus : +
Formamido : f
Imidazole :
Pyrrole :
5'- A/T A/T A/T A/T A/T A/T -3'
f
+
C3-alkyne
C3-alkyne
+
f
3'- T/A T/A T/A T/A T/A T/A -5'
5'- A/T A/T C A/T C A/T -3'
f
+
+
f
3'- T/A T/A G T/A G T/A -5'

B

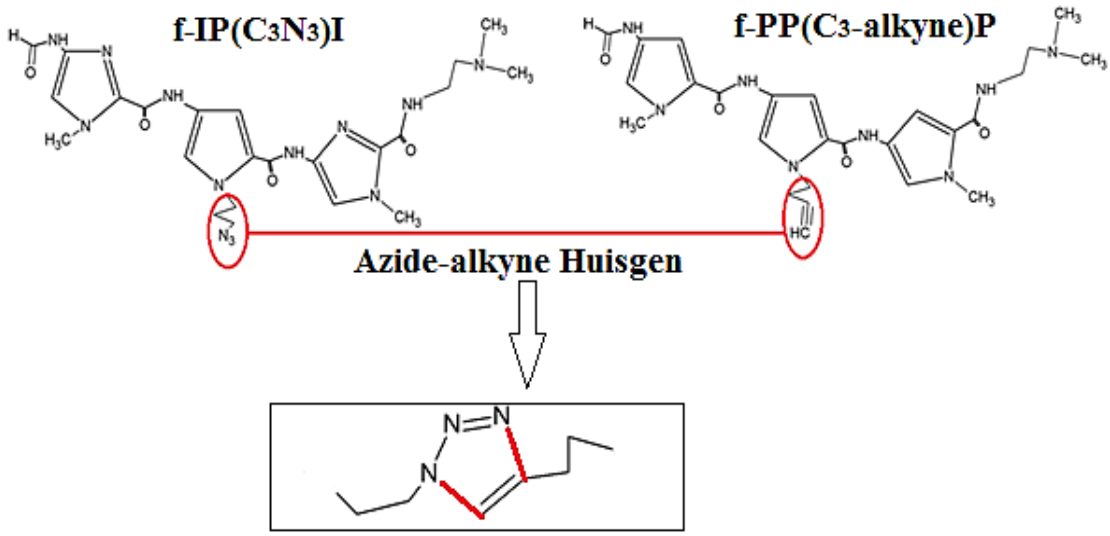

C

DNA fragment Click 6

f-IP(C_3N_3) cognate site

f-PP(C3-alkyne)P cognate site

Primer 19

```
5′-ACTGTGTCCAGAAAGCCGGCACTCAGCTACAAACGCGTCATCGATCAAATTTGTTCACAGAC
3′-TGACACAGGTCTTTCGGCCGTGAGTCGATGTTTGCGCAGTAGCTAGTTTAAACAAGTGTCTG

TCATGTCTAGCTACACTTAAGTCTAGTCTCAAGTGTCATCTCACTAGTTCGTCAAGTGGAGCTCT
AGTACAGATCGATGTGAATTCAGATCAGAGTTCACAGTAGAGTGATCAAGCAGTTCACCTCGAGA
                                                    Primer 17

CCTAACCGACTTT-3′
GGATTGGCTGAAA-5′-32p
```

Figure 3.6 A, Binding models of f-IP(C_3N_3)I, f-PP(C_3-alkyne)P and potentially formed hybrid. **B**, Chemical structures of f-IP(C_3N_3)I and f-PP(C_3-alkyne)P, and reactive groups (red) of the two monomer polyamides designed to form H-pin structure through an azide-alkyne Huisgen reaction. **C**, DNA fragment Click-6. The bottom strand is 5'-labelled with ^{32}P. DNA cognate sequence binding sites of the hybrid are labeled with blue color.

A

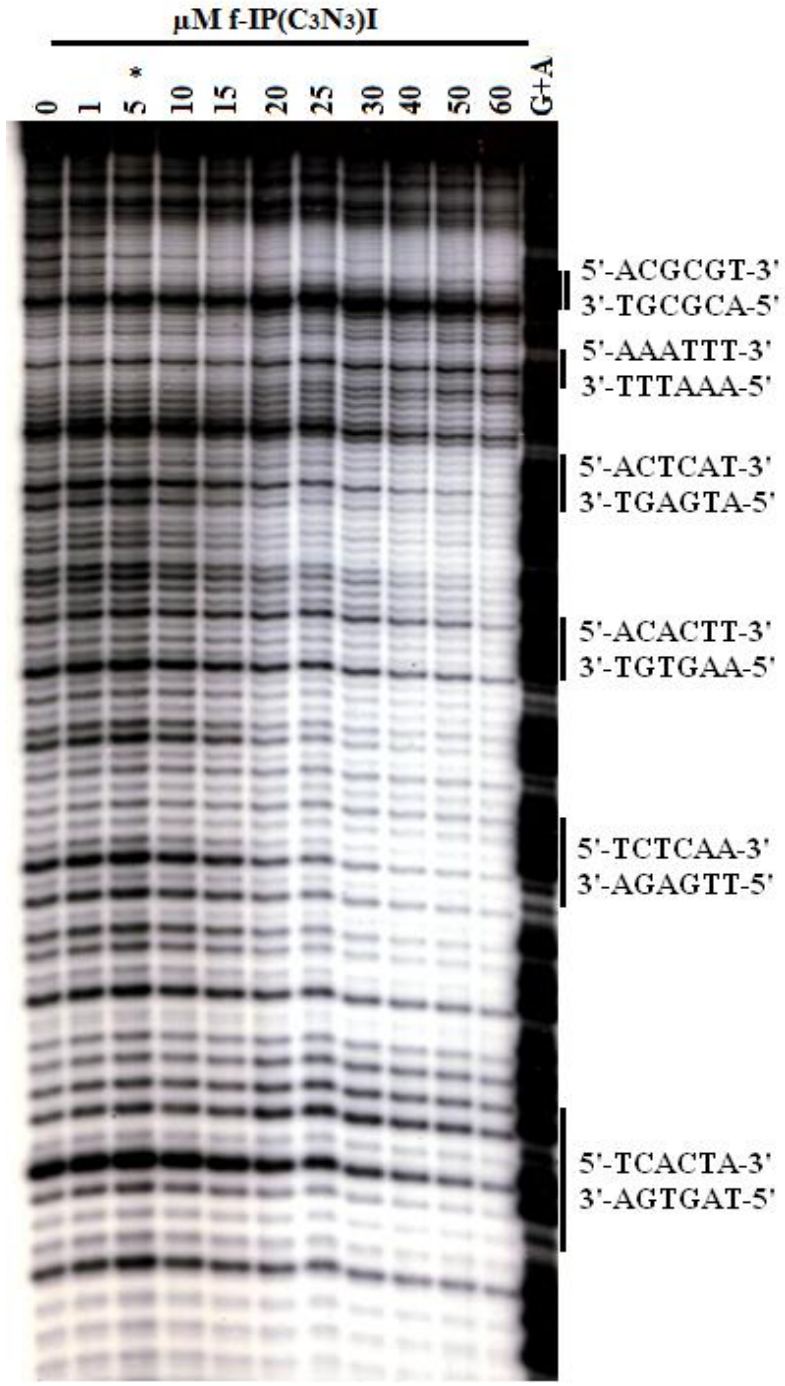
μM f-IP(C3N3)I
0
1
5 *
10
15
20
25
30
40
50
60
G+A
5'-ACGCGT-3'
3'-TGCGCA-5'
5'-AAATTT-3'
3'-TTTAAA-5'
5'-ACTCAT-3'
3'-TGAGTA-5'
5'-ACACTT-3'
3'-TGTGAA-5'
5'-TCTCAA-3'
3'-AGAGTT-5'
5'-TCACTA-3'
3'-AGTGAT-5'

B

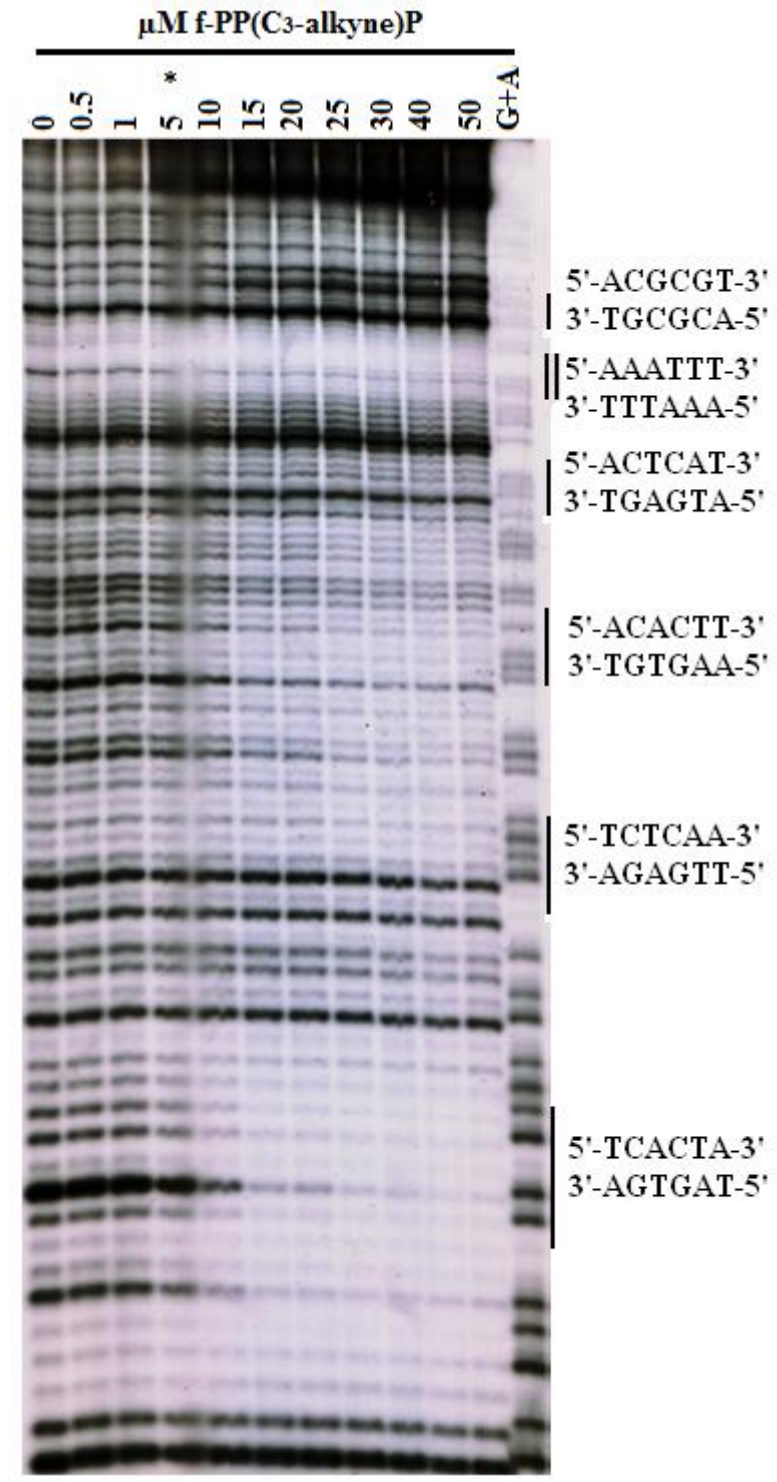
µM f-PP(C3-alkyne)P
0
0.5
1
5
*
10
15
20
25
30
40
50
G+A
5'-ACGCGT-3'
3'-TGCGCA-5'
5'-AAATTT-3'
3'-TTTAAA-5'
5'-ACTCAT-3'
3'-TGAGTA-5'
5'-ACACTT-3'
3'-TGTGAA-5'
5'-TCTCAA-3'
3'-AGAGTT-5'
5'-TCACTA-3'
3'-AGTGAT-5'

C

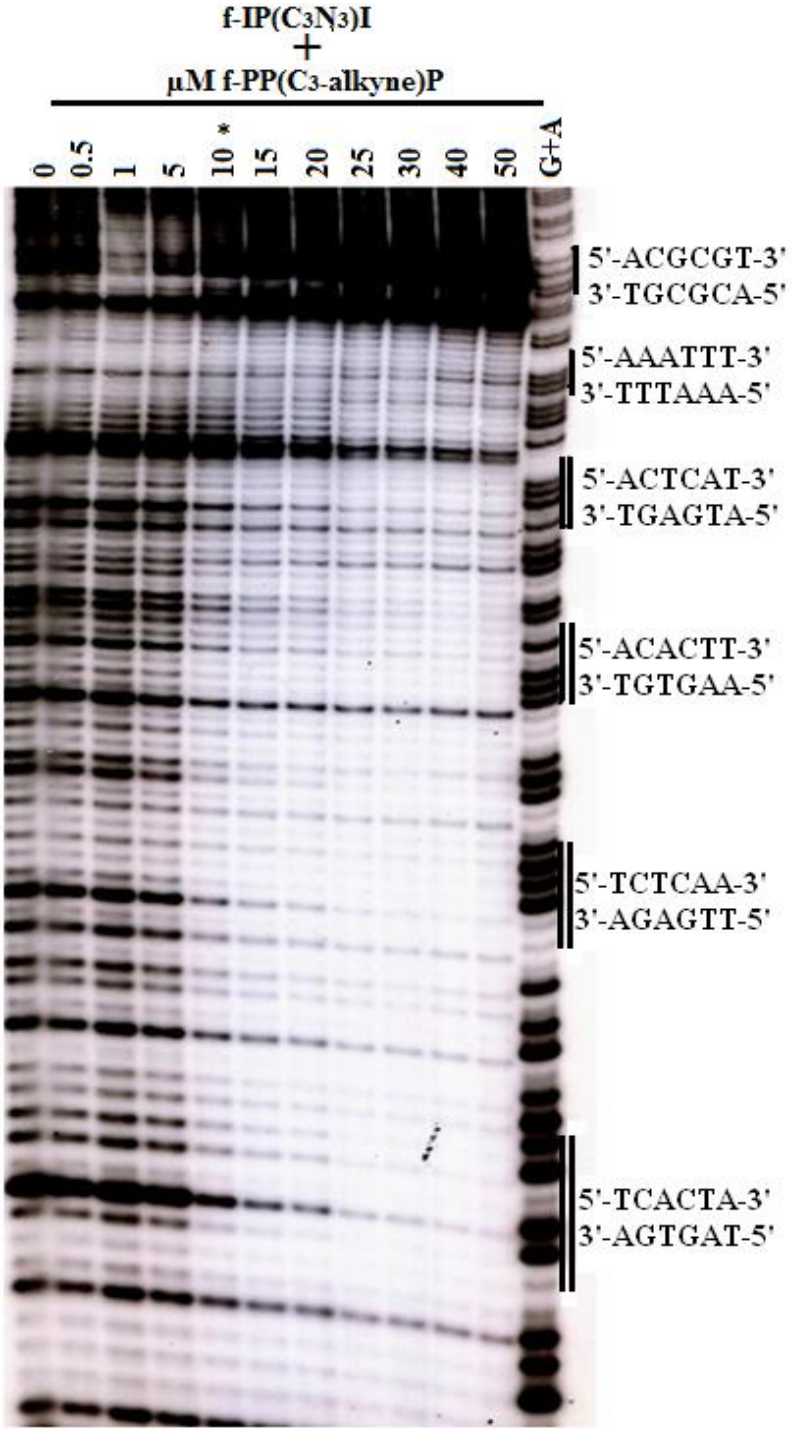

Figure 3.7 DNase I footprinting was performed with a radiolabeled probe containing the Click-6 sequences. **A, B and C**, The probe was incubated with increasing concentrations of f-IP(C_3N_3)I (**A**), f-PP(C_3-alkyne)P (**B**), and their combination (**C**), respectively (0.5-50 µM). Asterisks indicated the concentration of polyamide at which cleavage protection is initially observed. The cognate sequence binding sites are highlighted by double solid bars. G+A lanes denote the GA nucleotides.

3.2.4 DNA sequence specific binding of f-IP(C3-alkyne)I, f-PP(C_3N_3)P, and their combination

The chemical structures and the DNA binding models of f-IP(C_3-alkyne)I, f-PP(C_3N_3)P and their combination are shown in Figure 3.8A&B. These compounds were designed with the same reactive groups alternated, compared to the compounds previously presented. As a result, they share the same corresponding cognate sequences 5'-ACGCGT-3', 5'-AAATTT-3', and 5'-WCWCWW-3' (Figure 3.6C). Figure 3.9A indicates that binding of f-IP(C_3-alkyne)I to the cognate sequence 5'-ACGCGT-3' is observed at 10 μM and therefore has a two-fold lower binding affinity than f-IP(C_3N_3)I (Figure 3.7A). However, nonspecific binding of f-IP(C_3-alkyne)I begins to appear at 30 μM, indicating this compound's greater selectivity compared to f-IP(C_3N_3)I. This result suggests that the -C_3N_3 reactive group attached to the pyrrole group of f-IPI has a better binding affinity for the cognate site 5'-ACGCGT-3' compared to that of the -C_3-alkyne reactive group, but reduces the DNA sequence selectivity. Cleavage protection at the cognate sequence (5'-AAATTT-3') for f-PP(C_3N_3)P is observed at 5 μM while non-specific binding occurs at the 5'-ACACTT-3' and 5'-TCACTA-3' sites at ~10 μM (Figure 3.9B). The -C_3N_3 reactive group attached to the middle pyrrole of f-PPP shows a similar binding affinity for the cognate site 5'-AAATTT-3' at ~5 μM, as the -C_3-alkyne reactive group, while also sharing a similar pattern of non-specific binding to the 5'-ACACTT-3' and 5'-TCACTA-3' sites at concentrations >10 μM (Figure 3.7B and 3.9B). The combination of f-IP(C_3-alkyne)I and f-PP(C_3N_3)P produces clear footprints (15-20 μM) at the cognate sequences 5'-ACTCAT-3', 5'-ACACTT-3', 5'-TCTCAA-3' and 5'-TCACTA-3' by adding and mixing equimolar concentration of each polyamides f-IP(C3-alkyne)I or f-PP(C_3N_3)P to achieve the final concentration of the combined compound (Figure 3.9C). The potential hybrid shows a higher binding affinity for the

cognate sites 5'-ACTCAT-3' and 5'-TCTCAA-3' at concentrations >15 μM than either of the parent compounds f-IP(C3-alkyne)I or f-PP(C_3N_3)P. However, binding at the 5'-ACGCGT-3' and 5'-AAATTT-3' sites are still observed at 15 μM and 10 μM respectively. This study suggests that the combination of f-IP(C_3-alkyne)I and f-PP(C_3N_3)P could form a heterodimer, yet both heterodimer and homodimer mixtures of the two compounds are evident.

The pendant reactive group -C_3N_3 on the central pyrrole of f-IPI shows a higher DNA binding affinity but less selectivity than the -C_3-alkyne group, while no DNA binding affinity and selectivity differences are observed with the same pendant reactive groups when attached to the central pyrrole of f-PPP. The combination of f-IP(C_3N_3)I and f-PP(C_3-alkyne)P exhibits a higher binding affinity than the combination of f-IP(C_3-alkyne)I and f-PP(C_3N_3)P but with a similar selectivity, suggesting that -C_3N_3 reactive group on the central pyrrole of f-IPI contributes more binding affinity to the heterodimer.

A

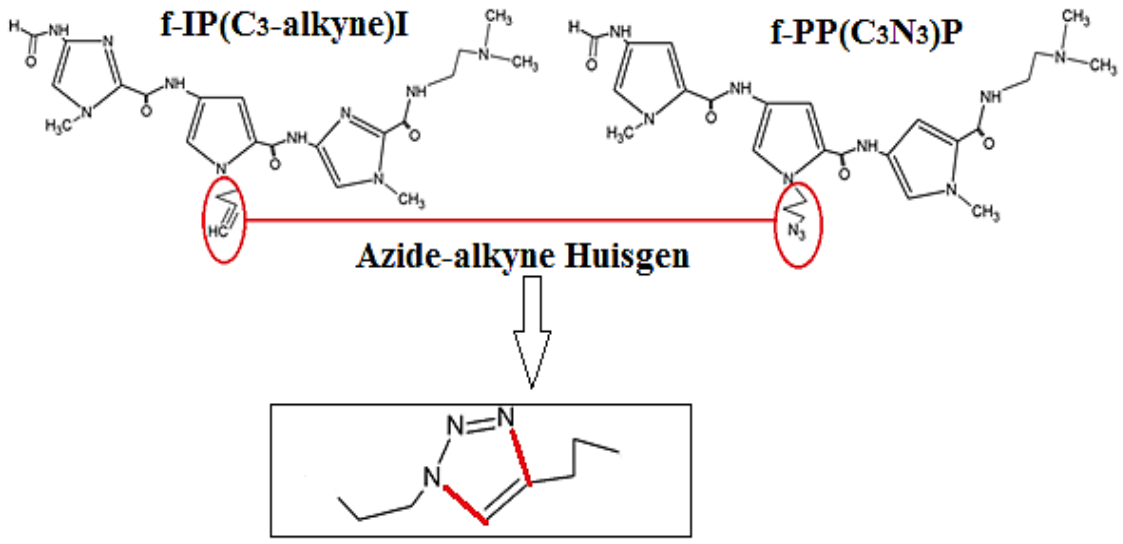

B

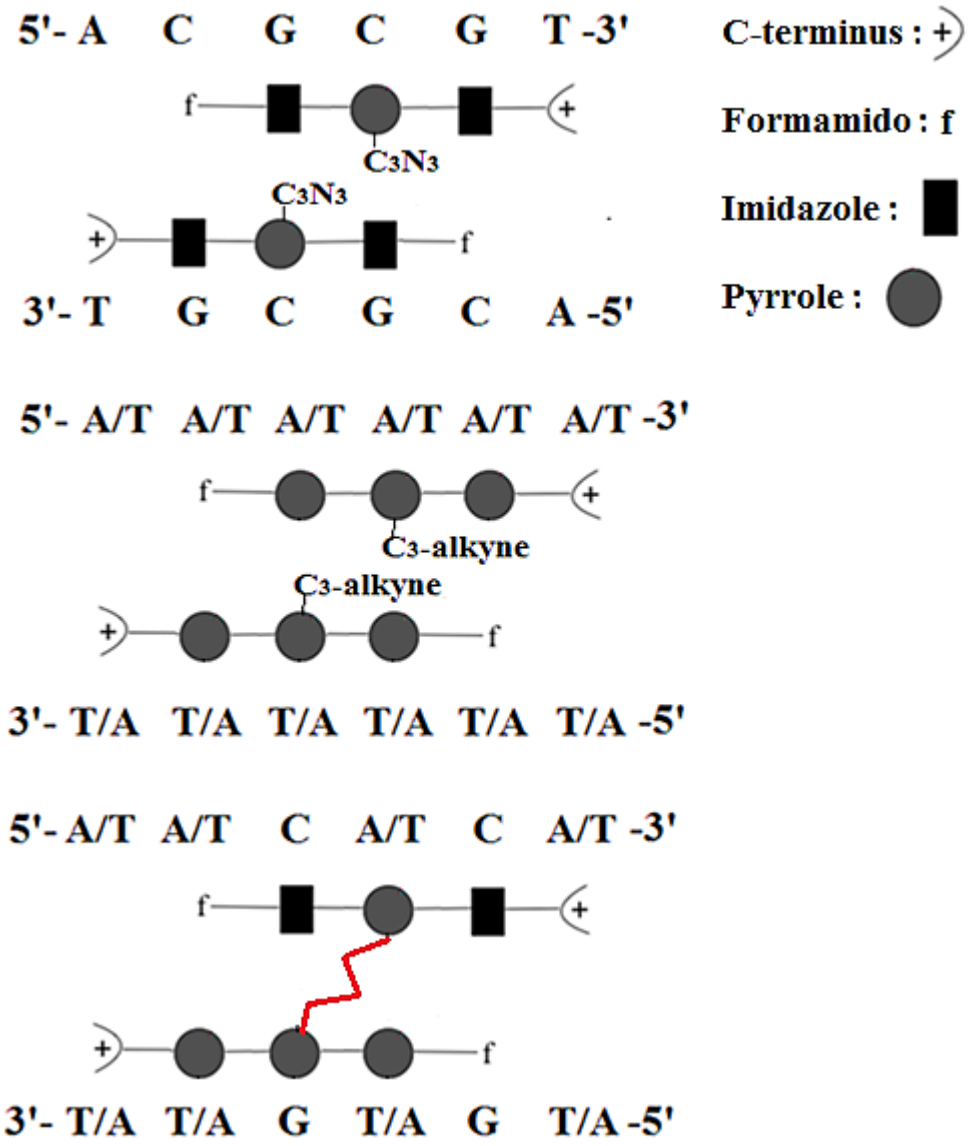

Figure 3.8 A, Chemical structures of f-IP(C3-alkyne)I and f-PP(C_3N_3)P, and reactive groups (red) of the two monomer polyamides designed to form H-pin structure by an azide-alkyne Huisgen reaction. **B**, Binding models of f-IP(C3-alkyne)I, f-PP(C_3N_3)P and potentially formed hybrid.

A

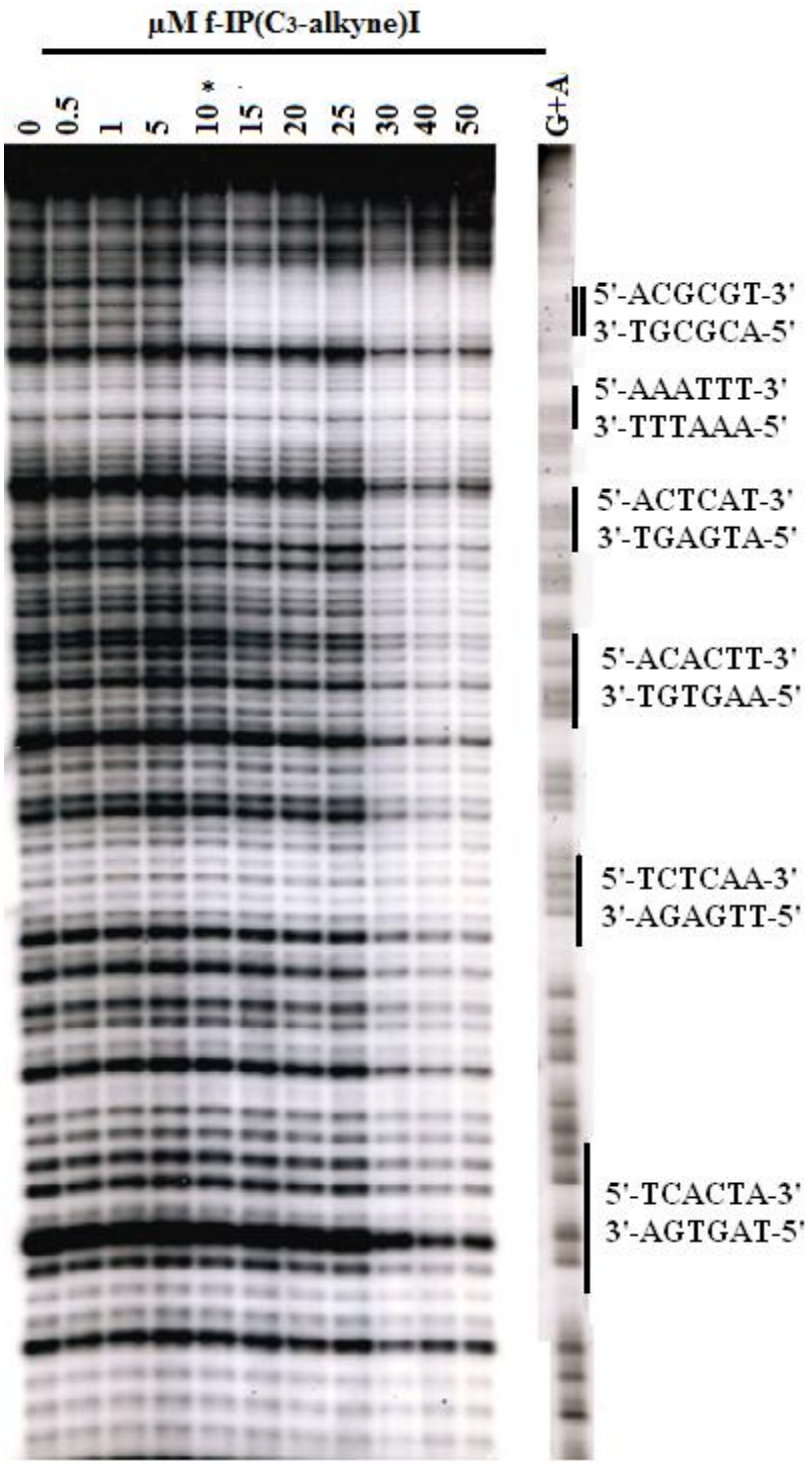
µM f-IP(C3-alkyne)I
0
0.5
1
5
10 *
15
20
25
30
40
50
G+A
5'-ACGCGT-3'
3'-TGCGCA-5'
5'-AAATTT-3'
3'-TTTAAA-5'
5'-ACTCAT-3'
3'-TGAGTA-5'
5'-ACACTT-3'
3'-TGTGAA-5'
5'-TCTCAA-3'
3'-AGAGTT-5'
5'-TCACTA-3'
3'-AGTGAT-5'

B

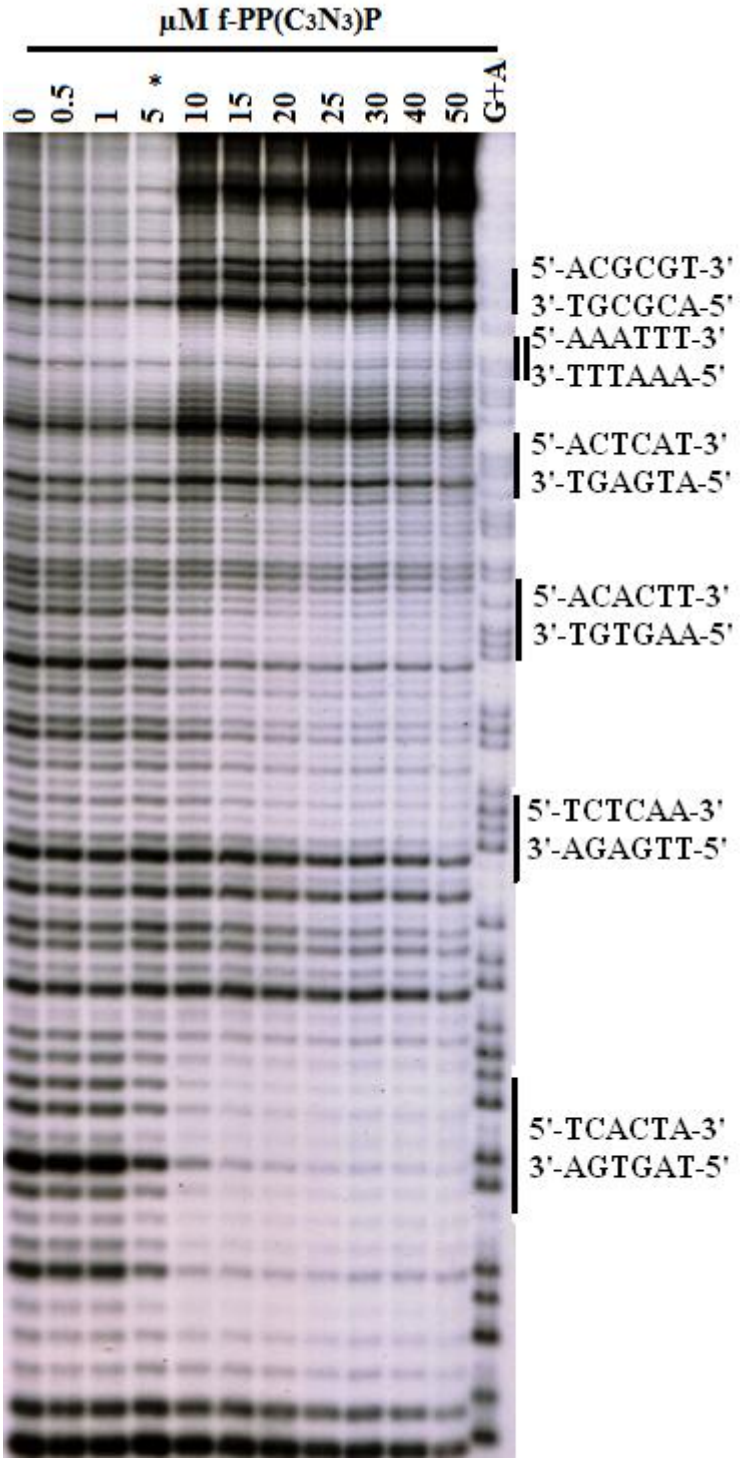
µM f-PP(C3N3)P
0
0.5
1
5 *
10
15
20
25
30
40
50
G+A
5'-ACGCGT-3'
3'-TGCGCA-5'
5'-AAATTT-3'
3'-TTTAAA-5'
5'-ACTCAT-3'
3'-TGAGTA-5'
5'-ACACTT-3'
3'-TGTGAA-5'
5'-TCTCAA-3'
3'-AGAGTT-5'
5'-TCACTA-3'
3'-AGTGAT-5'

C

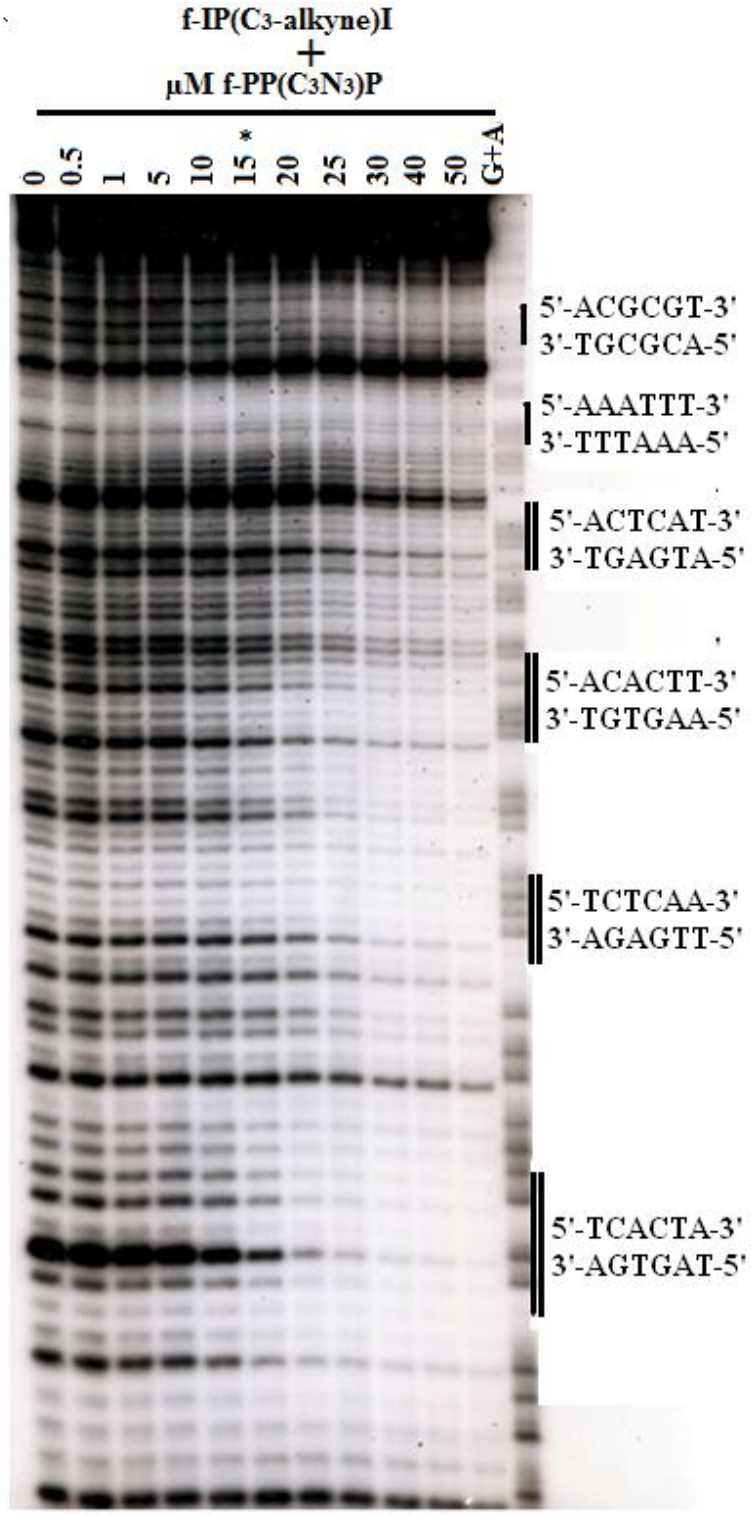

Figure 3.9 DNase I footprinting was performed with a radiolabeled probe containing the Click-6 sequences. **A, B and C**, The probe was incubated with increasing concentrations of f-IP(C_3-alkyne)I (**A**), f-PP(C_3N_3)P (**B**), and their combination (**C**), respectively (0.5-50 μM). Asterisks indicated the concentration of polyamide at which cleavage protection is initially observed. The cognate sequence binding sites are highlighted by double solid bars. G+A lanes denote the GA nucleotides.

3.2.5 DNA sequence specific binding of PPI-b-NH_2, PPP-Benz-NO_2, and their combination

The aim of this experiment was to further probe the binding of the combination of two polyamide monomers, which in this case can potentially form a hairpin structure by the connection between 'Head' and 'Tail' groups of the two monomer polyamides. This time the two monomers should form heterodimers and therefore target a different cognate sequence-binding site compared to that of the parent compound homodimer. The chemical structures and DNA sequence binding models of PPI-b-NH_2, PPP-Benz-NO_2 and their combination are shown in Figure 3.10A&B. The cognate sequences of PPI-b-NH_2, PPP-Benz-NO_2, and the combination of PPI-b-NH_2 and PPP-Benz-NO_2 are 5'-AGACA-3', 5'-AAATT-3' and 5'-AGATA-3', respectively (Figure 3.10C). The combination of PPI-b-NH_2, and PPP-Benz-NO_2 can potentially form a hairpin heterodimer through an acyl transfer reaction (Figure 3.10A), and thus target a new sequence 5'-AGATA-3' (described in Figure 3.10B). The autoradiogram given in Figure 3.11A reveals no significant specific binding of PPI-b-NH_2 for its cognate sequence at concentrations up to 50 μM and non-specific binding occurs at 100 μM. This was consistent with the binding pattern of the combination of PPI-b-NH_2 and PPP-Benz-NO_2 (Figure 3.11C). No significant specific binding of PPP-Benz-NO_2 for its cognate sequence appeared at concentrations <10 μM and non-specific binding occurs at >30 μM (Figure 3.11B).

A

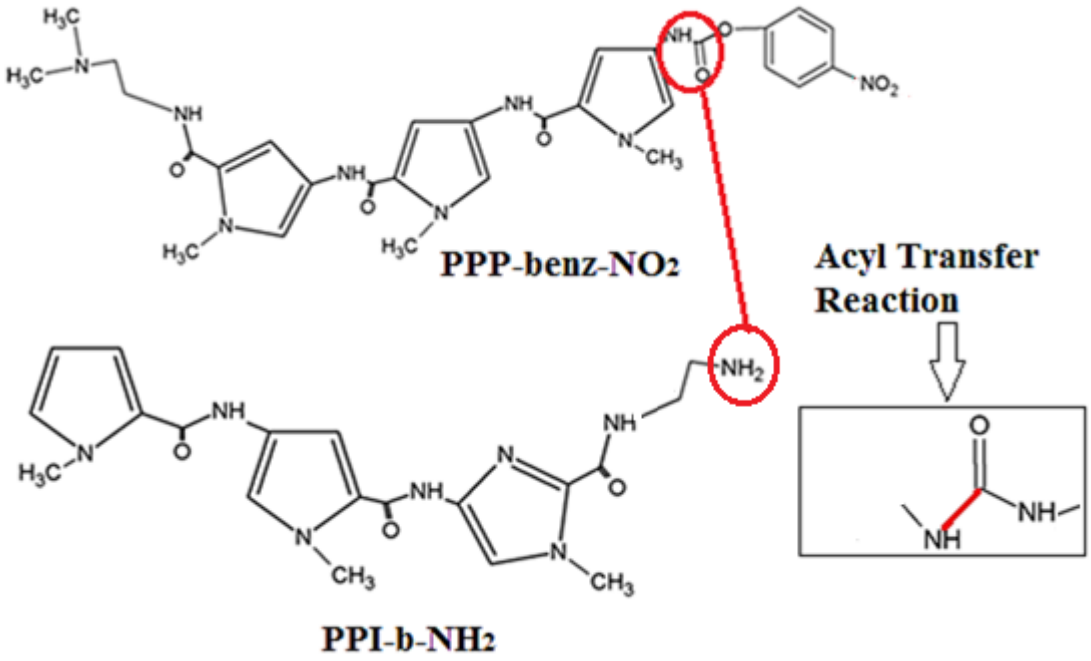
PPP-benz-NO2
Acyl Transfer Reaction
PPI-b-NH2

B

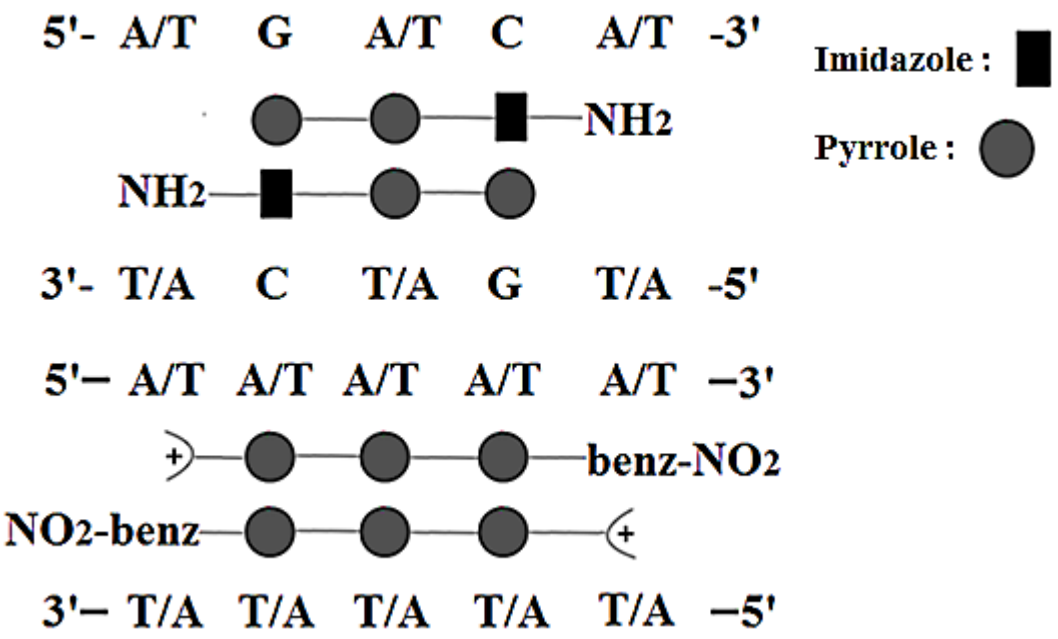
5'- A/T G A/T C A/T -3'
NH2
NH2
3'- T/A C T/A G T/A -5'
5'– A/T A/T A/T A/T A/T –3'
benz-NO2
NO2-benz
3'– T/A T/A T/A T/A T/A –5'
Imidazole :
Pyrrole :

B continued

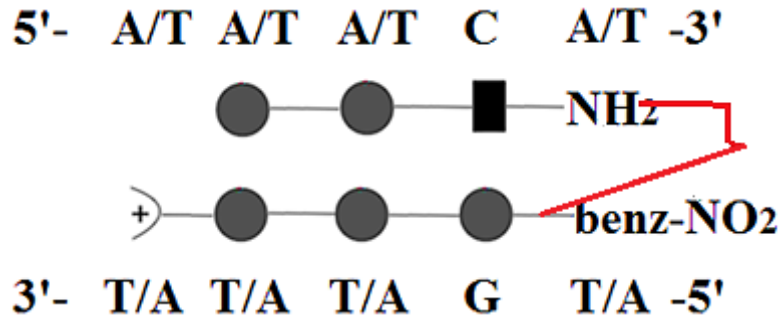

C

DNA fragment HMC-click

```
     Primer 19
5′-CTGTCCAGAAAGCCGGCACTCAGTCTACAAATAGATCATCTTGATCATATATGTTCACAG
3′-GACAGGTCTTTCGGCCGTGAGTCAGATGTTTATCTAGTAGAACTAGTATATACAAGTGTC
```

PPI-b-NH_2 Hairpin PPP-Benz-NO_2

```
Cognate site   Cognate site   Cognate site
AGACATCTCTAGATCTAGATATAACTCTAGTAAATTTCTTCAAGCAAGTGGAGCTCTCCTAACC
TCTGTAGAGATCTAGATCTATATTGAGATCATTTAAAGAAGTTCGTTCACCTCGAGAGGATTGG
                                                    Primer 17
GAC-3′
CTG-5′-32P
```

Figure 3.10 A, Chemical structures of PPI-b-NH_2 and PPP-Benz-NO_2, and 'Head' and 'Tail' groups of the two monomer polyamides designed to form Hairpin structure through an acyl transfer reaction. **B,** Binding models of PPI-b-NH_2 and PPP-Benz-NO_2 and potentially formed hybrid at the respective 5'-AGACA-3', 5'-AAATT-3' and 5'-AGATA-3' sites. **C**, DNA fragment HMC-click. The bottom strand is 5'-labelled with ^{32}P. DNA binding sites are labeled with blue color.

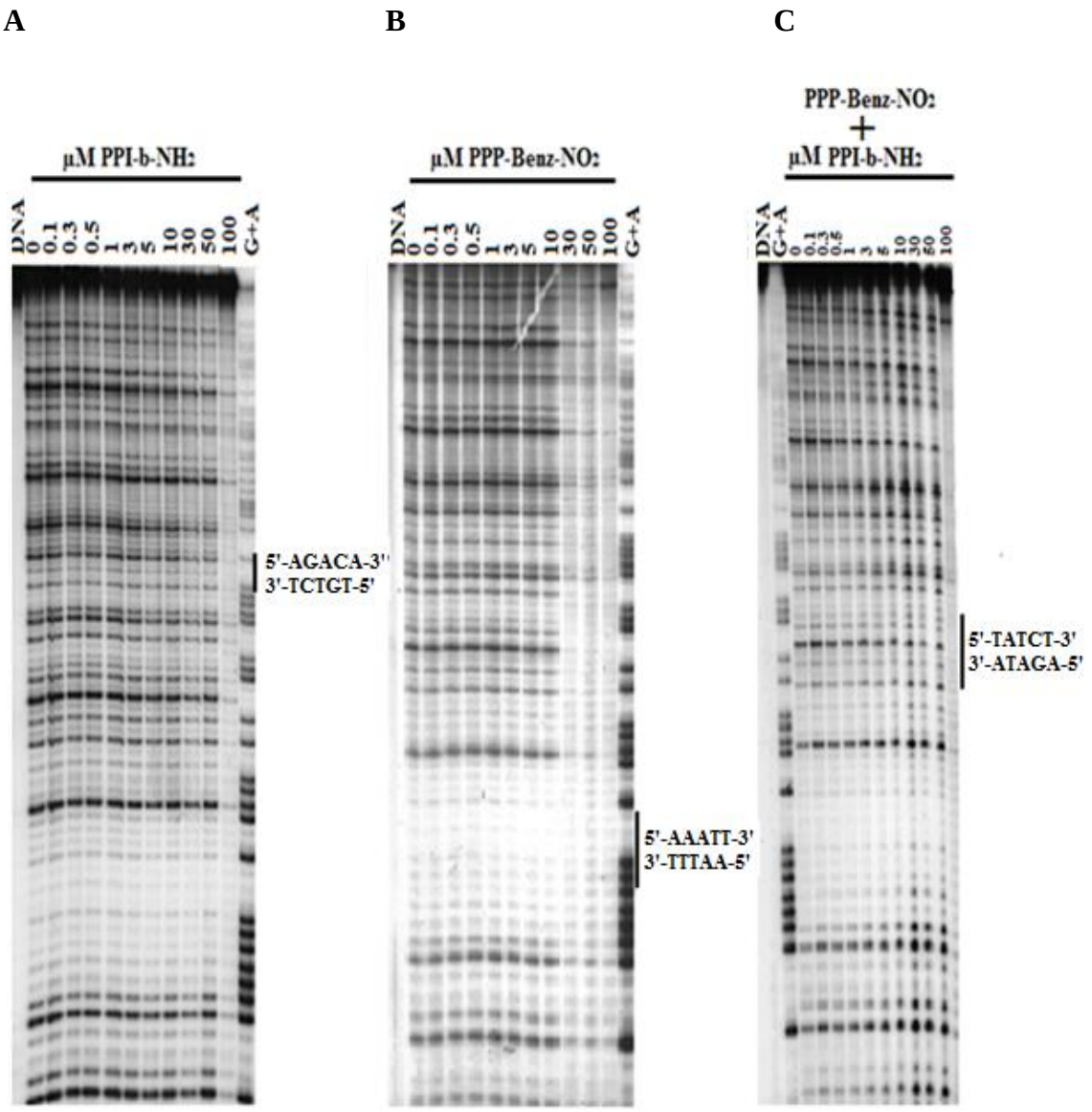

Figure 3.11 DNase I footprinting was performed with a radiolabeled probe containing the HMC-click sequences. The probe was incubated with increasing concentrations of PPI-b-NH_2 (**A**), PPP-Benz-NO_2 (**B**), and their combination (**C**), respectively (0.1-100 μM).

3.3 Discussion

In the early studies of DNA-small molecule complexes, a large number of minor groove binders were synthesized based on netropsin and distamycin A (Pelton and Wemmer, 1989, 1990; Wemmer et al., 2000). The discovery that distamycin A could form an antiparallel dimer in the minor groove of some AT sequences initiated the rational design of the original DNA sequence reading polyamides (Lown et al., 1993; Lee et al., 1993; Dervan and Burlii, 1999). The Dervan group formulated a set of rules for Watson-Crick base pair recognition by the dimer motif as described in the introduction (White and Dervan, 1997; Dervan and Burlii, 1999). A wide range of synthetic monomer polyamides and covalently linked dimers have been synthesized over the years offering a paradigm for the development of small molecules for sequence specific recognition of DNA. Such sequence-reading polyamides have the potential to be used as gene control agents by inhibition of native transcription factors at the predetermined site (Dervan et al., 2003).

The study of the interaction of the formamido-imidazole-pyrrole-imidazole (f-IPI) compound to its cognate sequences (5'-ACGCGT-3') has shown the enhanced DNA binding affinity of this polyamide compared to its non-formamido equivalent (PIPI), attributed to the formamido group (Brown et al., 2008). This is not surprising since the formamido group is known to confer enhanced DNA binding affinity. However, the formamido bearing monomers may also bind in a mixed 2:1 and 1:1 fashion, which can reduce the overall binding affinity. Hairpin and H-pin analogues have been designed and synthesized to ensure the equivalent of the 2:1 binding mode, but the size of these compounds results in poor cellular uptake, thus limiting their development (Best et al., 2003; Dickinson et al., 2004; Franks et al., 2010).

To investigate the influence of the size of the Hairpin and H-pin polyamides on their cellular uptake and nuclear localization, we have developed a new class of unlinked precursors that contain appropriately designed pendant reactive and biocompatible functional groups. An orthogonally positioned diamino polyamide f-IP(C_3NH_2)I, in which P-C_3NH_2 is the *N*-(3-aminopropyl)pyrrole moiety, was designed to interact with f-IP(C_3Cl)I, in which P-C_3Cl is the *N*-(3-chloropropyl)pyrrole moiety, with the potential to produce *in situ* an H-pin molecule through a nucleophilic substitution reaction (Figure 3.2A). The DNase I footprinting experiments demonstrated that f-IP(C_3NH_2)I has the same binding affinity for the cognate site (5'-ACGCGT-3') as f-IPI (Figure 3.3A&B). Surface plasmon resonance (SPR) experiments, however, showed that the diamino polyamide displays a binding constant of 2.4×10^8 M^{-1} for the cognate sequence 5'-ACGCGT-3', which is 4 times higher than that of its monoamino counterpart f-IPI (5.4×10^7 M^{-1}) (Satam et al., 2012). The sequence specificity of f-IP(C_3NH_2)I was found to be comparable to that of f-IPI. In addition, incorporation of the aminopropyl group in the polyamide backbone of f-IP(C_3NH_2)I offers a significant benefit over its monomer triamide f-IPI in terms of enhanced water solubility. In contrast, the chloro containing polyamide f-IP(C_3Cl)I possesses a reduced DNA binding affinity for the cognate sequence 5'-ACGCGT-3' (1 μM) (Figure 3.3C). When 0.025 μM of f-IP(C_3NH_2)I was mixed with 0.025 μM of f-IP(C_3Cl)I, their combination's binding, as detected by the onset at a footprint, occurs at 0.05 μM (Figure 3.3D). When f-IP(C_3NH_2)I was used alone, it also produced a footprint at 0.05 μM. The question raised from these results is how f-IP(C_3NH_2)I when used at half the concentration (0.025 μM) in combination with f-IP(C_3Cl)I (0.025 μM), which has a lower binding affinity, produces the same results (i.e cleavage inhibition) at 0.05 μM as when f-IP(C_3NH_2)I is used alone at double the concentration (0.05 μM). One possibility is that

f-IP(C_3NH_2)I does react with f-IP(C_3Cl)I to form a favorable H-pin compound, which can compensate for the lower binding affinity of f-IP(C_3Cl)I in the *in situ* reaction. However, it is difficult to prove whether the stable 2:1 complex is covalently formed with just the DNase I footprinting analysis.

An orthogonally positioned azido polyamide f-P(C_3CN)IP, in which P-C_3CN is the *N*-(3-cyanopropyl)pyrrole moiety, was designed to potentially react with f-P(C_3N_3)IP, in which P-C_3N_3 is the *N*-(3-azidopropyl)pyrrole moiety, with the potential to produce *in situ* a homodimer H-pin molecule through a dipolar cycloaddition reaction (Figure 3.4A). The DNase I footprinting data show that f-P(C_3CN)IP, f-P(C_3N_3)IP and the 'combined compound' have the same binding affinity for 5'-TACGAT-3' (5'-flank of ICB2) site, however again this cannot prove whether any binding occurs as a true H-pin or just in a 2:1 motif (Figure 3.5). It is clear, however, that the position of the pendant reactive groups, in this case on the heterocycle adjacent to the formamido group, does not significantly alter the ability to form dimer complexes *in situ*.

One limitation of these experiments is that the individual polyamide and resulting potential combined molecule target the same DNA sequence, making quantification of the different binding possibilities impossible.

The study of heterodimer formation therefore was investigated. An orthogonally positioned azide polyamide f-IP(C_3N_3)I, in which P-C_3N_3 is the *N*-(3-azidopropyl)pyrrole moiety, was designed to react with f-PP(C_3CH)P, in which P-C_3CH is the *N*-(3-alkynopropyl)pyrrole moiety, with the potential to produce *in situ* a heterodimer H-pin molecule through an azide-alkyne Huisgen reaction (Figure 3.6B).

The hybrid heterodimer H-pin structure potentially formed by the combination of f-IP(C_3N_3)I and f-PP(C_3CH)P targets the new sequence 5'-WWCWW-3', which differs from the parent compounds. The DNase I footprinting experiments showed that the combination of polyamides does target the cognate sequences 5'-ACTCAT-3', 5'-ACACTT-3', 5'-TCTCAA-3', 5'-TCACTA-3', with higher binding affinity than either f-IP(-C_3N_3)I or f-PP(-C_3CH)P alone (Figure 3.7A-C). These results suggest that the two monomers f-IP(C_3N_3)I and f-PP(C_3CH)P can interact *in situ* to form a heterodimer.

Alternating the reactive groups between f-IPI and f-PPP [f-IP(C_3CH)I and f-PP(C_3N_3)P] was also tested by DNase I footprinting (Figure 3.9). The data showed that the combination of f-IP(C_3CH)I and f-PP(C_3N_3)P targets the same cognate sequences 5'-ACTCAT-3', 5'-ACACTT-3', 5'-TCTCAA-3', 5'-TCACTA-3' as the combination of f-IP(C_3N_3)I and f-PP(C_3CH)P. However, in this case the hybrid polyamide f-IP(C_3CH)I and f-PP(C_3N_3)P binds with a higher affinity than the monomers only at the 5'-ACTCAT-3' and 5'-TCTCAA-3' sites (Figure 3.9). Although these results are encouraging and clearly demonstrate that the orthogonally positioned pendant groups can allow *in situ* interaction of both homodimer and heterodimer polyamides, footprinting analysis does not confirm the formation of proposed covalent H-pins. It is clear that the different pendant reactive groups, in this case on the central pyrrole of f-IPI, can influence DNA binding affinity. However, there is no alteration of binding affinity found in f-PPP analogues f-PP(C_3CH)P and f-PP(C_3N_3)P.

The study of heterodimer hairpin formation was also investigated. PPI-b-NH_2 and PPP-Benz-NO_2 were designed to potentially form a hairpin heterodimer through an acyl transfer reaction (Figure 3.10A). In this case the resulting combined compound would

target the new sequence 5'-AGATAT-3'. However, these compounds failed to show any significant binding up to 30 μM for their respective cognate sequences (Figure 3.11).

Overall, the resulting H-pin homodimer targets the same cognate sequence as its parent compounds, thus causing quantification of the different binding possibilities impossible. In contrast, the resulting heterodimer targets a different cognate sequence compared to its parent compounds, therefore solving the previous problem and allowing to identify the H-pin formation. However, DNA footprinting analysis is not enough to determine how the H-pin structure is formed (e.g. covalently), so further investigation is required using other techniques such as mass spectrometry.

Only the additional amino group among the pendant reactive groups on the selected polyamides showed a slightly enhanced binding affinity compared to the respective parent compounds. Therefore, the study of positioning the additional amino group at different sites of the polyamides was carried out and will be discussed in the chapter 4.

CHAPTER 4

EVALUATION OF NOVEL POLYAMIDES ON DNA BINDING AFFINITY, SPECIFICITY AND SEQUENCE RECOGNITION

4.1 Introduction

The modification of novel polyamides needs to be further studied with the aim of the newly synthesized polyamides possessing excellent sequence specificity, stronger binding affinity, high solubility in biological media and enhanced cell penetration and nuclear localization properties. It has been previously reported that pyrrole-imidazole-containing polyamides with multiple cationic groups exhibit binding affinity for A/T rich sequences due to attraction to the negative molecular electrostatic potential in the minor groove of A/T rich sequences (Nickols et al. 2007; Edelson et al., 2004). In addition, Satz and Bruice showed that polyamides containing a pyrrole-N1-alkyl spermine/spermidine group target A/T rich sequences and bind with high affinity (Satz and Bruice, 2002). These polyamides effectively inhibit transcription factors bound to dsDNA compared to other minor groove binders lacking an alkyl-multiamino side chain. It was suggested that the additional cationic groups were attracted to the negatively charged phosphodiester groups of DNA (Satam et al., 2012). An orthogonally positioned diamino polyamide f-IP(C_3NH_2)I was synthesized and demonstrated an increased DNA binding affinity over its monoamino/monocationic counterpart f-IPI by DNA footprinting as shown in Chapter 3. F-IP(C_3NH_2)I also exhibits a four-fold higher binding constant than f-IPI by surface plasmon resonance (SPR) studies (Satam et al., 2012). The sequence specificity of f-IP(C_3NH_2)I was found

to be comparable to that of f-IPI (Chapter 3). Incorporation of the second amino group in f-IP(C_3NH_2)I also offers a significant benefit over f-IPI in terms of increased water solubility. In order to investigate the benefits of having a second positively charged group in the form of an orthogonally positioned alkylammonium side chain, the diamino compounds f-I(C_3NH_2)PI, f-P(C_3NH_2)IP, f-IP(C_3NH_2) P and Phenyl-IP(C_3NH_2)I were synthesised.

The pyrrole (P) heterocyclic moieties in distamycin stack as a 2:1 antiparallel dimer in the DNA minor groove and can bind indiscriminately to an A/T or a T/A base pair (Wade et al., 1992; 1993; Pelton and Wemmer, 1990). Alternatively, an imidazole (I) heterocycle moiety can be paired opposite a pyrrole to selectively target a G/C base pair (Kopka et al., 1985). In addition, 3-hydroxy-1H-pyrrole (Hp) has been paired opposite P and shown to selectively target T/A base pairs but with a significant loss in binding affinity. The bulky hydroxyl group on an Hp-containing polyamide (which forms an additional hydrogen bond to the O-2 group of thymine), makes the 2:1 complex formed in the minor groove sterically encumbered leading to unfavorable binding (Kielkopf et al., 2000). Accordingly, the additional hydrogen bonding to thymine O-2 could be critical for distinguishing A/T from T/A. We envisaged that a polyamide containing a reversed conformation P moiety [P(H) or 2,5-linked N-methylpyrrole-2-carboxamide] stacked over a polyamide containing P [P(H)/P] may recognize a T/A base pair. In an attempt to test this hypothesis, our collaborator Dr Moses Lee synthesized two polyamides PPPP(H)-N-dimethyl-3-aminopropylamine and IPPP(H)-N-dimethyl-3-aminopropylamine. The new molecules incorporated only one P(H) moiety into each polyamide, as previous studies have shown that incorporation of multiple 2,5-linked (Marques et al., 2002) or 2,4-linked P(H) units may result in a loss in sequence

specificity, thus allowing for an increased tolerance of G/C base recognition (Bremer et al., 2000).

Over the past decade, the development of DNA recognition elements that exhibit fluorescence while maintaining high sequence specificity and binding affinity has been demanding. Such compounds would provide an intrinsic probe for monitoring the cellular uptake of the molecule and ultimately the binding to nuclear DNA. The incorporation of fluorescent dyes such as thiazole orange, fluorescein and bodipy on hairpin polyamides exhibited fluorescence while maintaining a high degree of DNA binding affinity and specificity (Fechter et al., 2005; Best et al., 2003; Belitsky et al., 2002). However, limited nuclear localization of such dye-containing hairpin polyamides restricted their usefulness. In addition, the behavior of the nonfluorescing hairpins did not always mimic that of its fluorescing counterpart (Chavda et al., 2011). Therefore, polyamide fluorophores are needed with enhanced cell and nuclear penetration abilities.

The bis-benzimidazole fluorophores, such as bisbenzimide or Hoechst 33258, are known to selectively recognize A/T-rich sequences in the DNA minor groove and are capable of crossing certain cellular and nuclear membranes (White et al., 2001). On the basis of the sequence specificity and high affinity of the formamido-containing polyamides for the minor groove as ascertained from previous studies (Brown et al., 2007; Buchmueller et al., 2005; Le et al., 2005; Liu and Wilson, 2010), our group envisioned the incorporation of the p-anisylbenzimidazolecarboxamido (Hx) moiety of Hoechst 33258 attached to imidazole pyrrole heterocyclic units (Chavada et al., 2011). Therefore, Hx-containing compounds were designed, synthesized and evaluated.

Chapter aims:

The aim of this part of the study was therefore to contribute to the development of novel polyamides by evaluating 1) whether an additional amino group on polyamides can increase DNA binding affinity and specificity; 2) a binding preference of a P/P(H) pairing and a I/I(H) pairing; 3) binding characteristics of HxPI.

4.2 Results

4.2.1 DNA sequence specific binding of mono- and diamino-polyamides: f-I(C_3NH_2)PP, f-P(C_3NH_2)IP and f-IP(C_3NH_2)P

As shown in section 3.2.1, the monoamino polyamide f-IPI has a slightly lower binding affinity for the cognate sequence than its diamino counterpart f-IP(C_3NH_2)I but shows much higher binding affinity than its chloro counterpart f-IP(C_3Cl)I. The presence of a second amino group improves the water solubility of f-IPI without compromising its DNA sequence selectivity encouraging us to further investigate the effect of an additional amino group on the polyamides.

The chemical structure and DNA binding model for f-I(C_3NH_2)PI are shown in Figure 4.1. DNase I footprinting studies were performed using a 125 bp 5'-[^{32}P]-radiolabeled engineered DNA fragment containing the DNA sequences 5'-ACGCGT-3', 5'-ACCGGT-3', 5'-AAATTT-3' and 5'-ACACGT-3'. The results depicted in Figure 4.2A provide direct evidence of footprinting at the cognate site 5'-ACGCGT-3' emerging at 0.05 μM and becoming strong at 0.1 μM. In contrast, no footprint at the other three non-cognate sites was apparent. However, f-IP(C_3NH_2)I shows a clear footprint at the non-cognate sites 5'-ACCGGT-3' and 5'-ACACGT-3' at 1 μM (Figure 3.3B). These results therefore demonstrate an enhanced sequence specificity of f-I(C_3NH_2)PI for its cognate sequence over its isomer f-IP(C_3NH_2)I. The onset of a footprint at the cognate site 5'-ACGCGT-3' for f-I(C_3NH_2)PI (0.05-0.10 μM) (Figure 4.2A) was slightly higher than that for f-IP(C_3NH_2)I (strong at 0.05 μM) (Figure 3.3B), suggesting a slightly reduced binding affinity (Satam et al., 2012). In Figure 3.3A, f-I(C_3NH_2)PI shares a similar binding affinity and sequence specificity to f-IPI. The binding affinities varied

according to the order: f-IP(C_3NH_2)I > f-IPI = f-I(C_3NH_2)PI, suggesting that the second amino group on the different positions can affect binding affinity, thus its position within the polyamide is important.

A

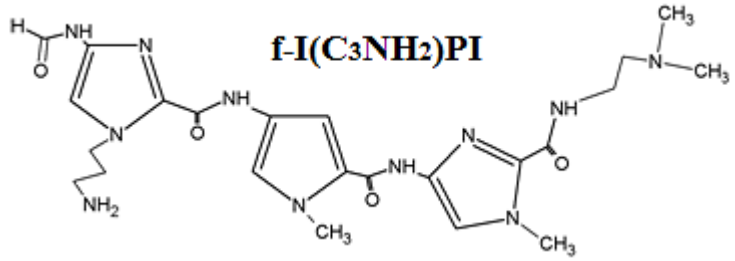

B

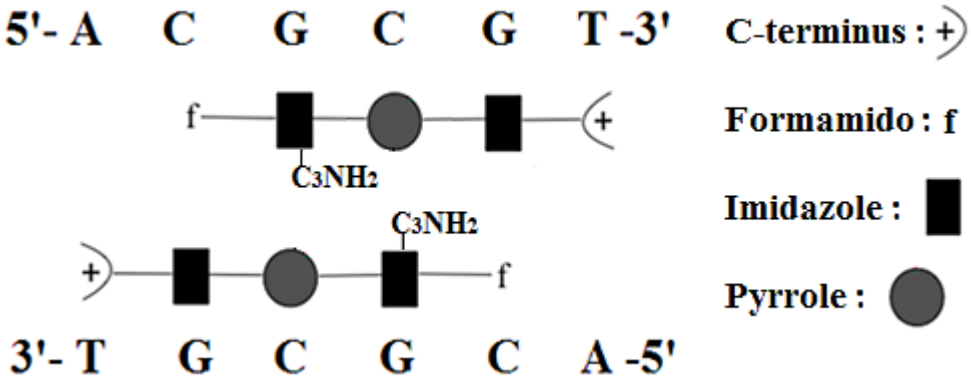

Figure 4.1 A, Chemical structures of f-I(C_3NH_2)PI. **B**, Binding model of f-I(C_3NH_2)PI at the sequence 5'-ACGCGT-3'

A

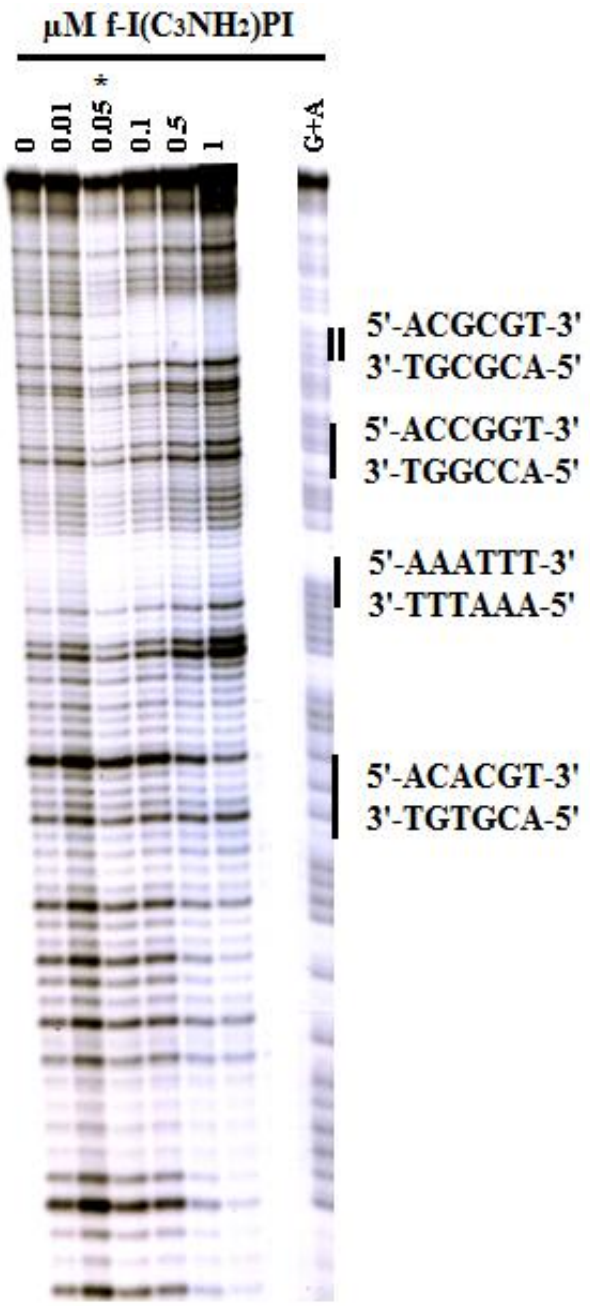

Figure 4.2 DNase I footprinting was performed with a radiolabeled probe containing the IM17/19 DNA sequences. The probe was incubated with increasing concentrations of f-I(C_3NH_2)PI (**A**) (0.01-1 μM). Asterisks indicated the concentration of polyamide at which cleavage protection is initially observed. The cognate sequence binding sites are highlighted by double solid bars. G+A lanes denote the GA nucleotides.

The chemical structures and DNA binding models for f-P(C_3NH_2)IP and f-IP(C_3NH_2)P are shown in Figure 4.3 and 4.5. The DNA sequence selectivity and binding affinity of the monoamino polyamide f-PIP and its diamino analogue f-P(C_3NH_2)IP, as well as the monoamino polyamide f-IPP and its diamino counterpart f-IP(C_3NH_2)P were investigated by DNase I footprinting using a 496bp (described in Figure 3.4C) and a 127bp 5'-[^{32}P]-radiolabeled DNA fragment, respectively (Figure 4.5C). The DNA sequence specificity of f-IPP and f-IP(C_3NH_2)P for the cognate site 5'-ATGCAT-3', and the non cognate GC-rich 5'-ACGCGT-3', AT-rich site 5'-AAATTT-3' and 5'-ACTAGT-3' sites were examined and are presented in Figure 4.5 and Figure 4.6.

The autoradiogram depicted in Figure 4.4A shows that f-P(C_3NH_2)IP produces a footprint at the 5'-TACGAT-3' site (5'-flank of ICB2) beginning at 10 μM, having a 3-fold higher binding affinity than the monoamino parent compound f-PIP. Both compounds exhibit similar sequence specificity for the ICB2 flank site. The autoradiogram depicted in Figure 4.6A indicates that binding of f-IPP to the corresponding cognate sequence 5'-ATGCAT-3' is initially observed at 3 μM, which presents a 3-fold lower binding affinity than its diamino counterpart f-IP(C_3NH_2)P. However, extensive non-specific binding of f-IP(C_3NH_2)P is observed at concentrations >1.5 μM, indicating poor DNA sequence selectivity especially when compared to f-IPP, which shows some degree of selectivity towards 5'-ACTAGT-3' .

The footprinting results of the diamino polyamides f-P(C_3NH_2)IP and f-IP(C_3NH_2)P show better binding affinity than their respective monoamino counterparts due to the presence of the additional amino group.

A

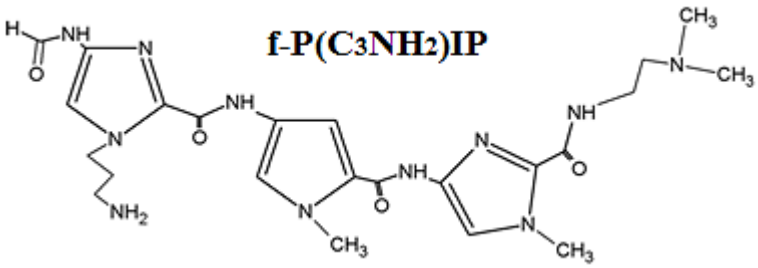

B

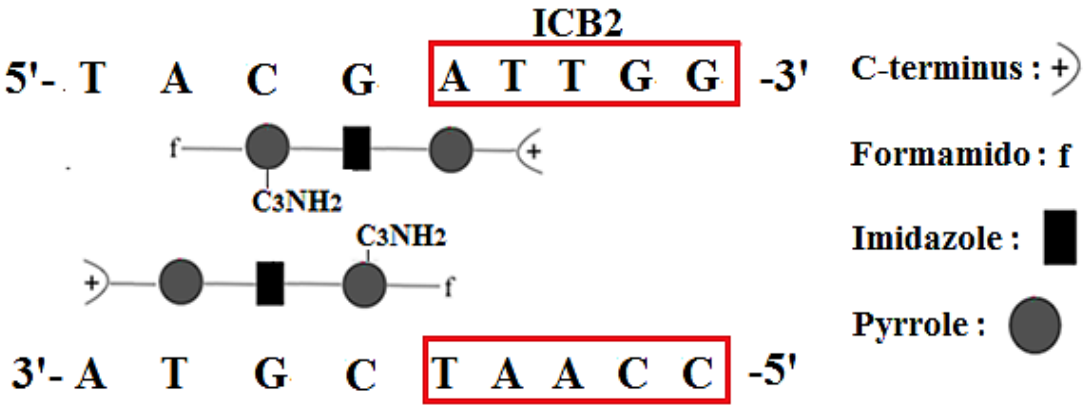

Figure 4.3 A, Chemical structures of f-P(C_3NH_2)IP. **B**, Binding model of f-P(C_3NH_2)IP at the 5'-TACGAT-3' site (5'-flank of ICB2 in the human topo IIα promoter). ICB2 labeled in the red box. .

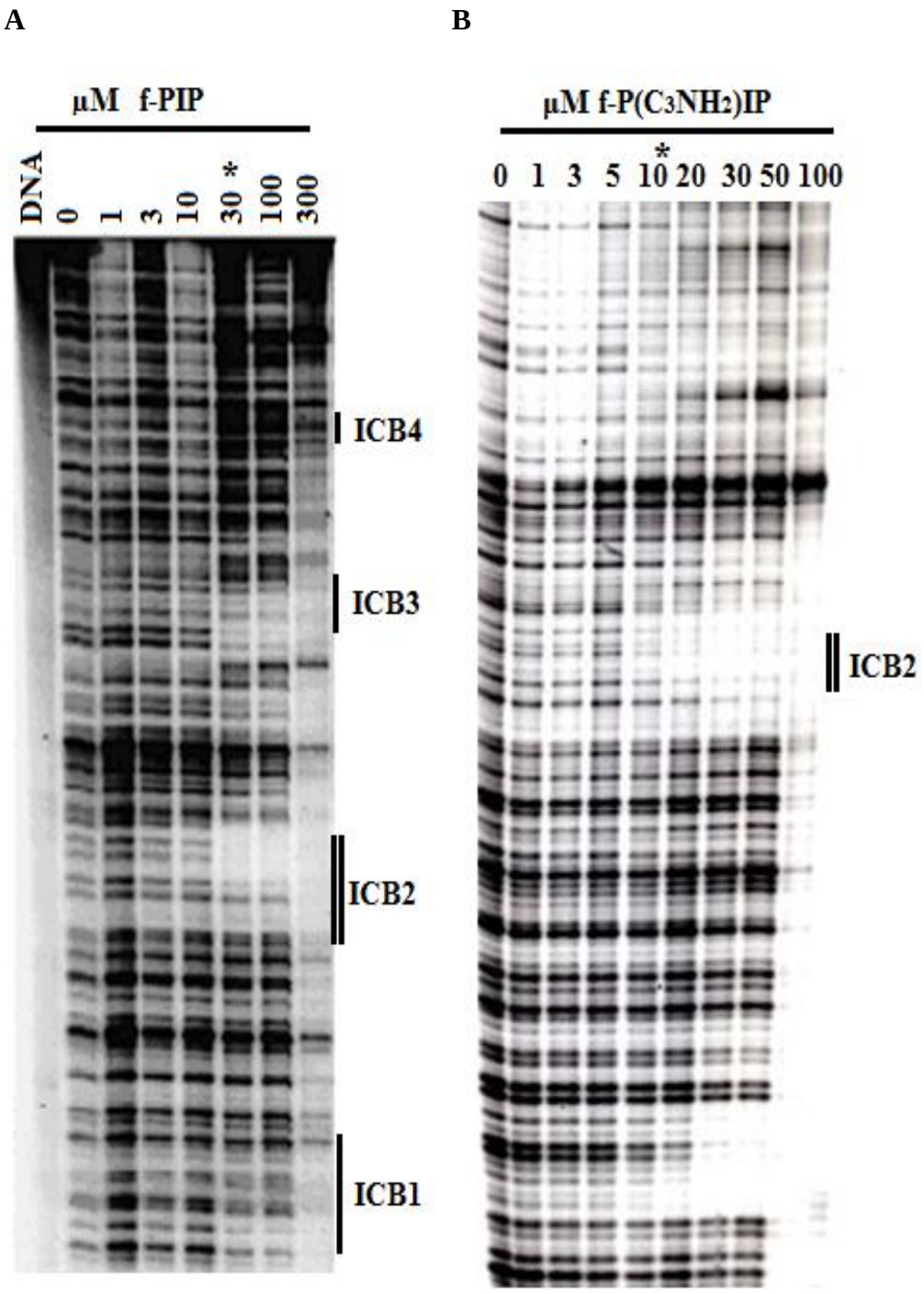

Figure 4.4 DNase I footprinting was performed with a radiolabeled probe containing the 496bp topo IIα promoter. The probe was incubated with increasing concentrations of f-PIP (**A)** and f-P(C_3NH_2)IP (1-300 µM) (**B**). Asterisks indicated the concentration of polyamide at which cleavage protection is initially observed. The cognate sequence binding sites are highlighted by double solid bars.

A

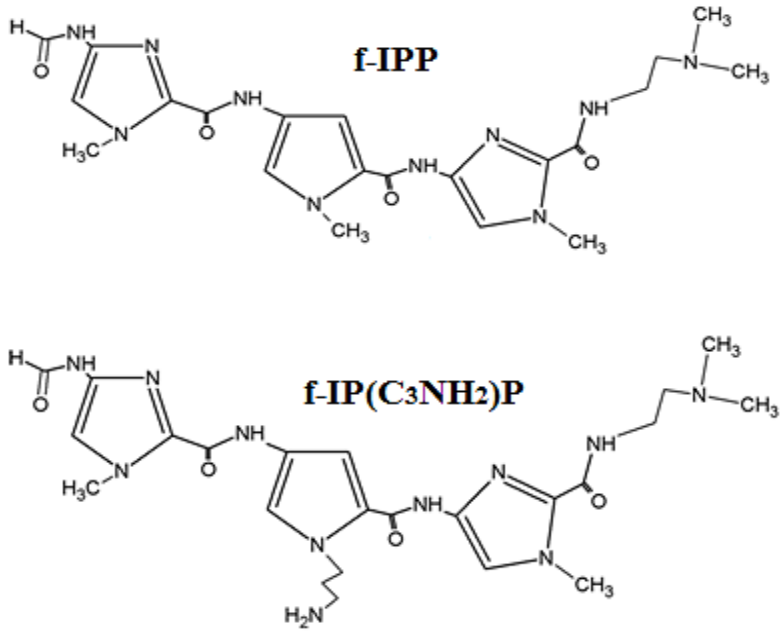

B

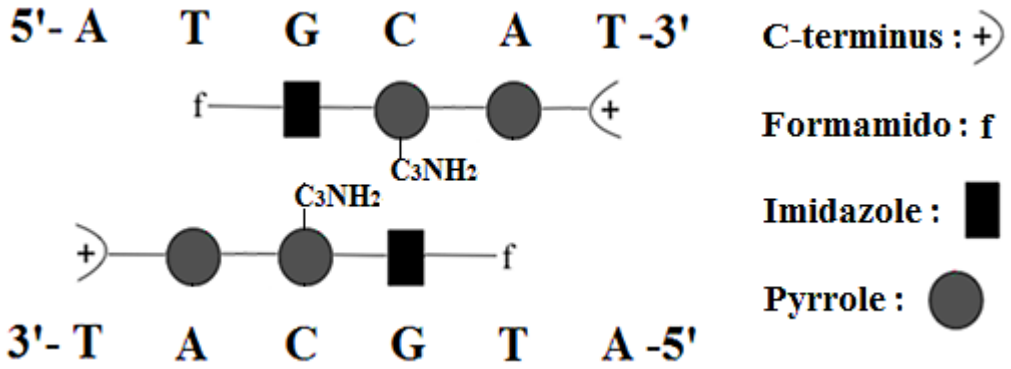

C Primer 19

5′-CTGTCCAGAAAGCCGGCACTCAGTCTACAAACGCGTCATCTTGATCATGCATGTTCACAG
3′-GACAGGTCTTTCGGCCGTGAGTCAGATGTTTGCGCAGTAGAACTAGTACGTACAAGTGTC

AAATTTCTCTAGATCTACACGTAACTCTAGTACTAGTCTTCAAGCAAGTGGAGCTCTCCTAACC
TTTAAAGAGATCTAGATGTGCATTGAGATCATGATCAGAAGTTCGTTCACCTCGAGAGGATTGG

GAC-3′
CTG-5′-^{32}p
Primer 17

Figure 4.5 A, Chemical structures of f-IPP and f-IP(C_3NH_2)P. **B**, Binding model of f-IP(C_3NH_2)P. **C**, DNA fragment IM18/20. The bottom strand is 5'-labelled with ^{32}P. DNA cognate and non-cognate sequence binding sites are labeled with red color and blue color, respectively.

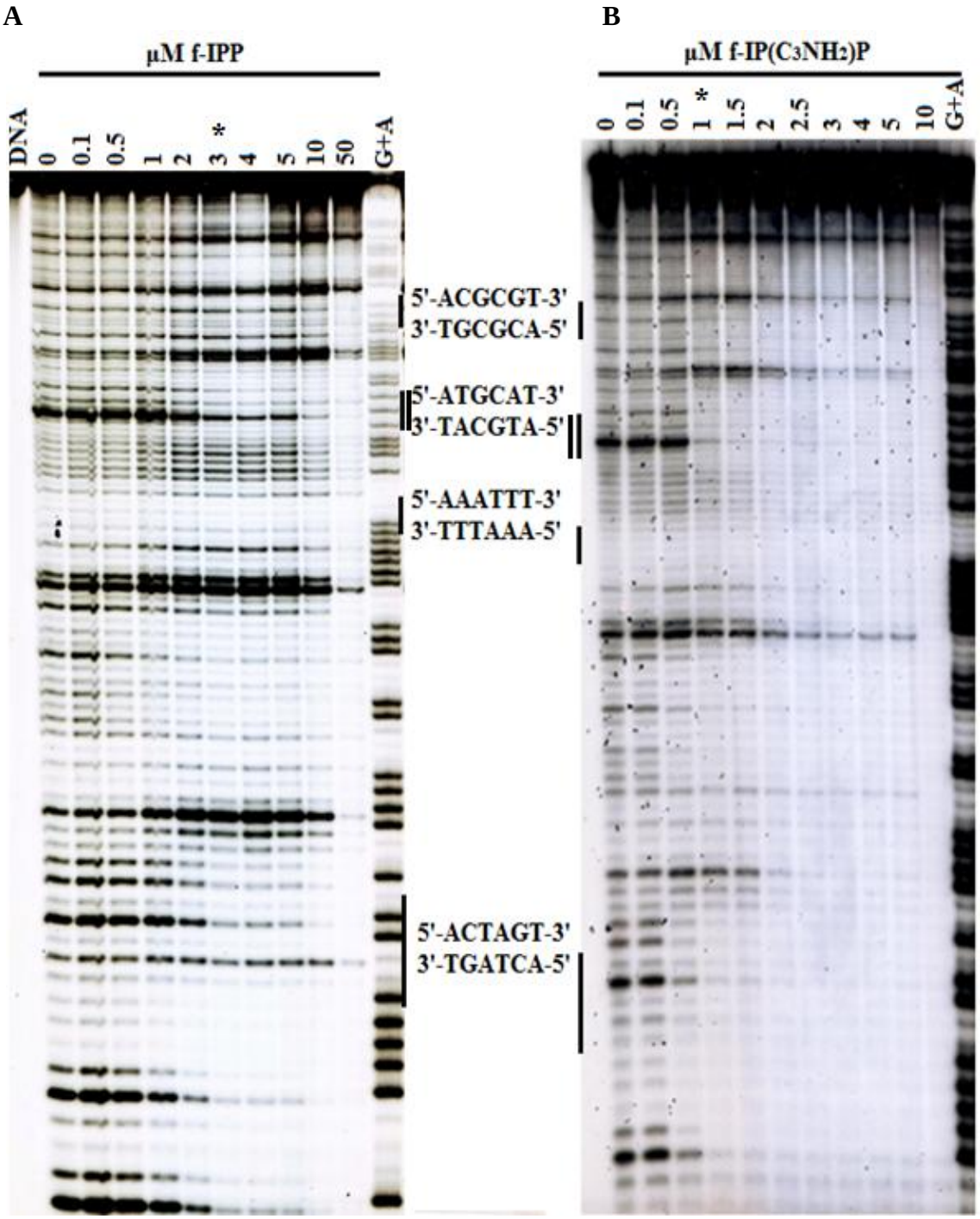

Figure 4.6 DNase I footprinting was performed with a radiolabeled probe containing the IM18/20 DNA sequences. The probe was incubated with increasing concentrations of f-IPP (**A**) and f-IP(C_3NH_2)P (**B**), respectively (0.1-50 μM). Asterisks indicated the concentration of polyamide at which cleavage protection is initially observed. The cognate sequence binding sites are highlighted by double solid bars. Control DNA lanes lack DNase I treatment and G+A lanes denote the GA nucleotides.

4.2.2 DNA binding studies of mono- and diamino non-formamido polyamides- Phenyl-IPI and Phenyl-IP(C_3NH_2)I

The chemical structures and the DNA binding models of the polyamides Ph-IPI and Ph-IP(C_3NH_2)I are shown in Figure 4.7. The sequence selectivity and binding affinity of the monoamino polyamide Ph-IPI and its diamino counterpart Ph-IP(C_3NH_2)I were investigated by DNase I footprinting using a 127bp 5'-[^{32}P]-radiolabeled DNA fragment containing the shared cognate sequence 5'-ACGCGT-3', and the non-cognate 5'-ACCGGT-3', 5'-ACACGT-3' and 5'-AGCGCT-3' control sites (described in Figure 3.2C). The autoradiogram depicted in Figure 4.8A shows that Ph-IPI produces a footprint at the 5'-ACGCGT-3' site at 20 μM, and no other footprints are apparent even at 100 μM. The results for the diamino polyamide Ph-IP(C_3NH_2)I demonstrate markedly superior binding affinity compared to Ph-IPI. The footprint at 5'-ACGCGT-3' for the diamino polyamide Ph-IP(C_3NH_2)I emerges at 0.5 μM, representing a 40-fold higher binding affinity compared to that of the parent polyamide Ph-IPI (Figure 4.8A) (Satam et al., 2012). Overall, the gain in the DNA binding affinity of Ph-IP(C_3NH_2)I over Ph-IPI is achieved without compromising the DNA sequence selectivity, suggesting that the second amino group can enhance DNA binding affinity, particularly in the non-formamido containing polyamides.

In the DNA footprinting analysis, Ph-IPI shows an increased sequence specificity but with a 400-fold lower binding affinity compared to f-IPI (Figure 3.3A and Figure 4.8A). This is not surprising since the formamido group is known to confer enhanced binding affinity (Lacy et al., 2002; Buchmueller et al., 2005).

A

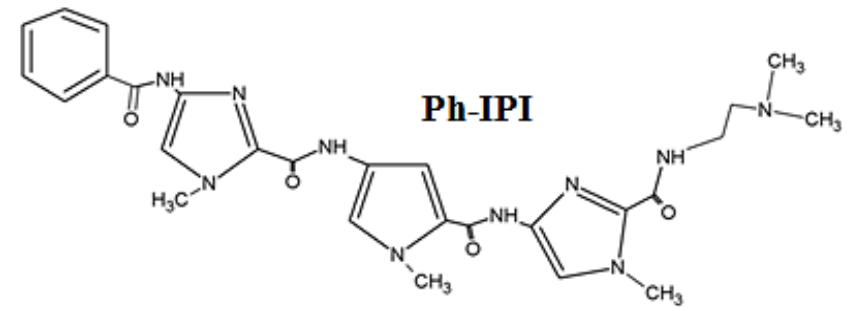

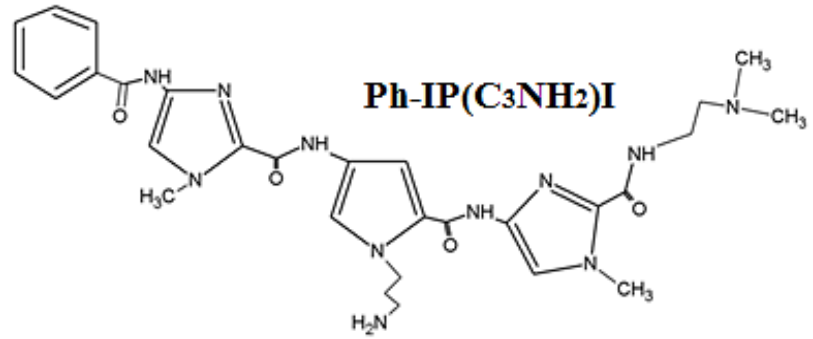

B

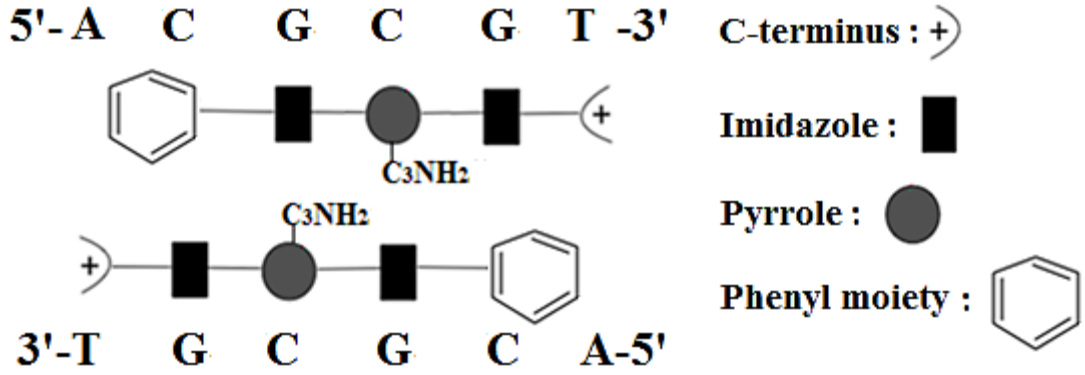

Figure 4.7 A, Chemical structures of Ph-IPI and Ph-IP(C_3NH_2)I. **B**, Binding model of Ph-IP(C_3NH_2)I.

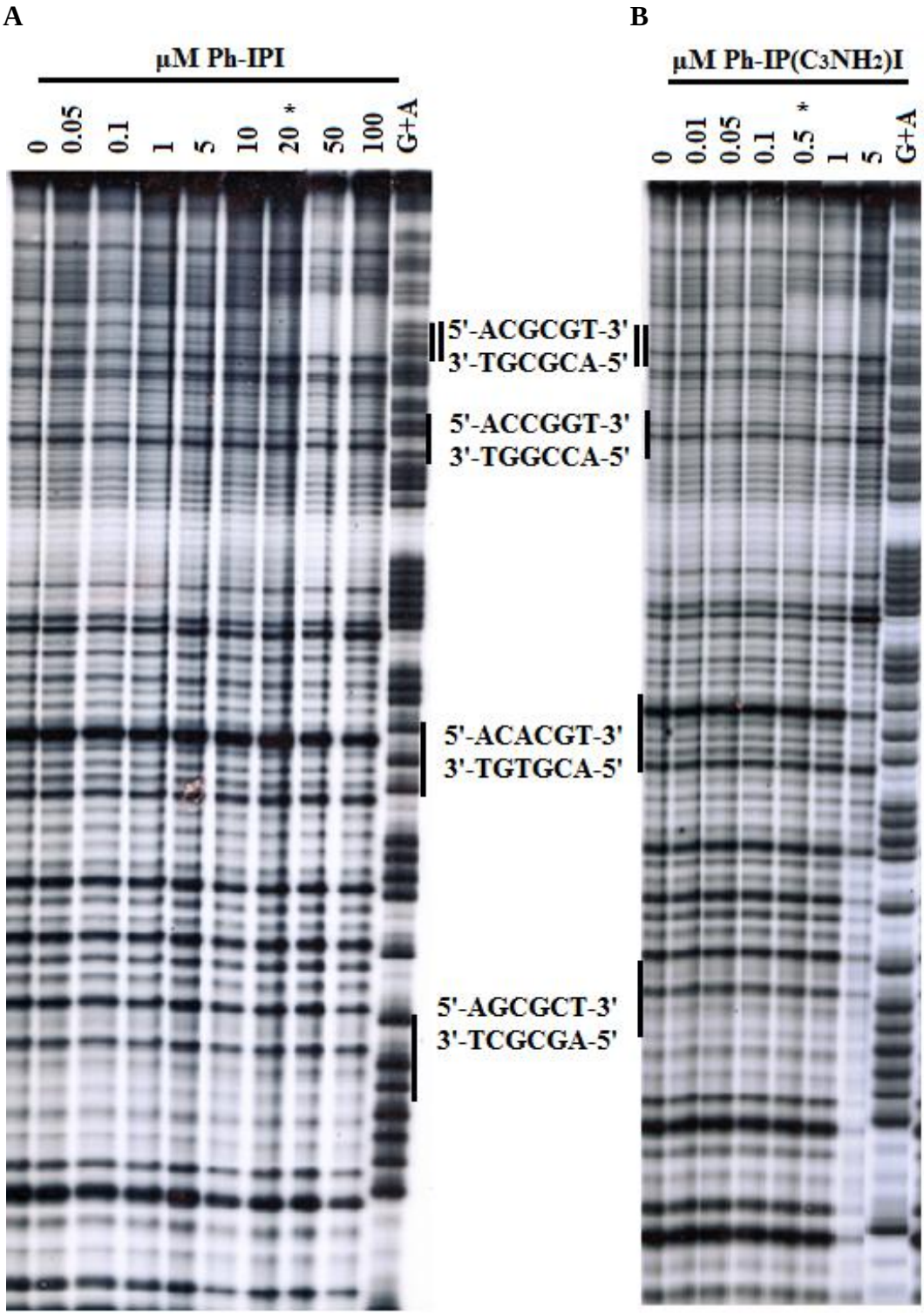

Figure 4.8 DNase I footprinting was performed with a radiolabeled probe containing the IM17/19 DNA sequences. The probe was incubated with increasing concentrations of Ph-IPI (**A**) and Ph-IP(C_3NH_2)I (**B**) (0.01-100 μM). Asterisks indicated the concentration of polyamide at which cleavage protection is initially observed. The cognate sequence binding sites are highlighted by double solid bars respectively. G+A lanes denote the GA nucleotides.

4.2.3 DNA sequence specific binding of Pyrrole(H) based polyamides

Two polyamides PPPP(H)-N-dimethyl-3-aminopropylamine (PPPX) and IPPP(H)-N-dimethyl-3-aminopropylamine (IPPX) designed to test the binding preference of a P/P (H) pairing [P/X] and a I/P(H) pairing [I/X]. The chemical structure and the DNA binding models for the polyamides PPPX and IPPX are shown in Figure 4.9. DNase I footprinting experiments were performed using a 127bp 5`-[$^{32}$P]-radiolabelled DNA fragment containing the following sequences: 5`-AAATTT-`3; 5`-ATATAT-`3; 5`-ACATGT-`3; 5`-AGATCT-`3 and 5`-AGAGCT-`3 (Figure 4.9C). The autoradiogram shown in Figure 4.10A shows that PPPX exhibits good sequence specificity for the $A_3T_3$ sequence and a clear footprint appears at 20 μM. PPPX displays negligible binding to 5`-ATATAT-`3 as shown by the appearance of a weak footprint at 100 μM. In contrast, IPPX shows better binding towards the sequences tested but poorer DNA sequence selectivity. The autoradiogram indicates that for IPPX, there is some binding to the 5`-AAATTT-`3, 5`-ATATAT-`3, 5`-AGATCT-`3 and 5`-ACATGT-`3 sites at concentration ~6 μM, indicative of poor sequence selectivity, in contrast to PPPX which shows some degree of sequence selectivity towards A_3T_3 DNA but with lower binding affinity. This study therefore shows that PPPX containing the P/X pairing has a weaker binding affinity for its cognate sequences but retains some DNA sequence selectivity as observed in DNase I footprinting studies. PPPX reveals no preference for T/A over A/T base pairs. In contrast, IPPX containing an I/X pairing indicates no preference towards G/C over C/G base pairs (Chavda et al., 2010).

A

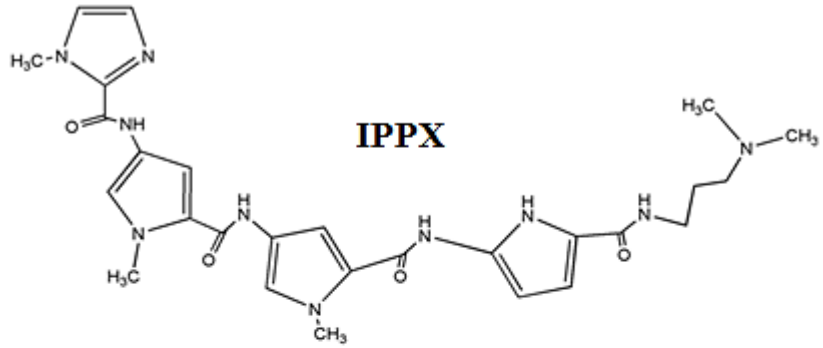
IPPX

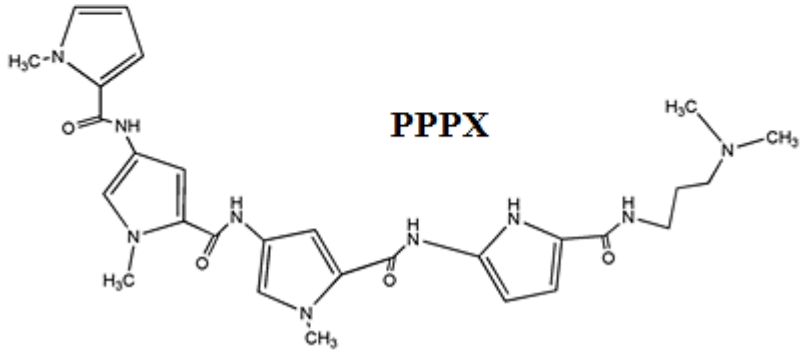
PPPX

B

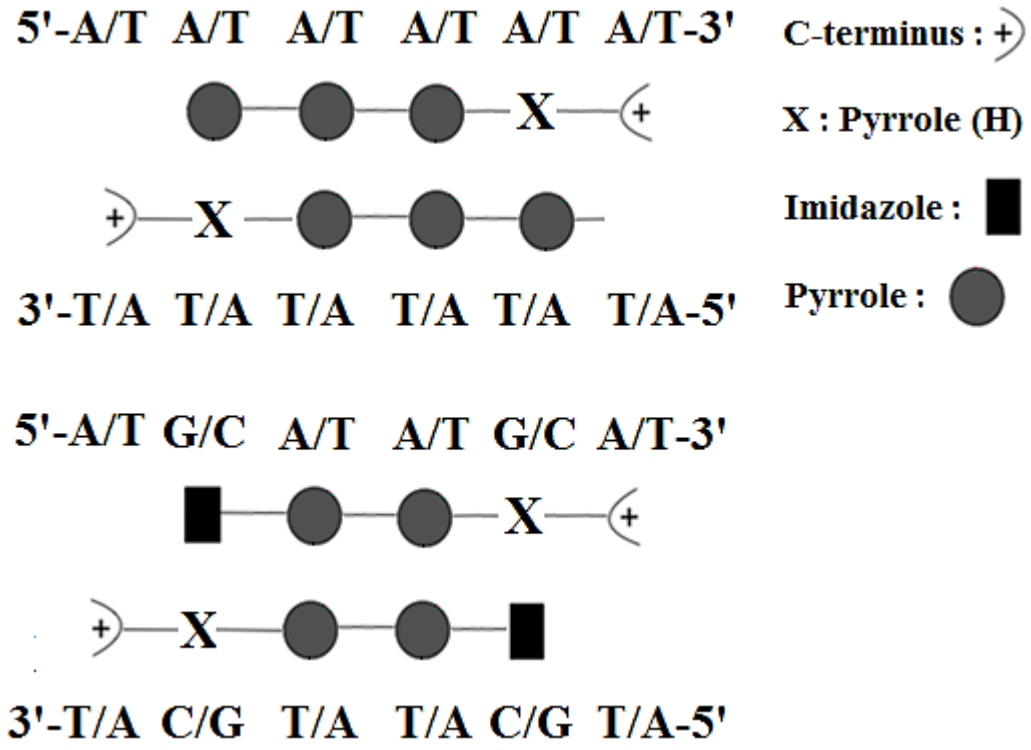
5'-A/T A/T A/T A/T A/T A/T-3'
X
+
+
X
3'-T/A T/A T/A T/A T/A T/A-5'
C-terminus : +
X : Pyrrole (H)
Imidazole :
Pyrrole :
5'-A/T G/C A/T A/T G/C A/T-3'
X
+
+
X
3'-T/A C/G T/A T/A C/G T/A-5'

C

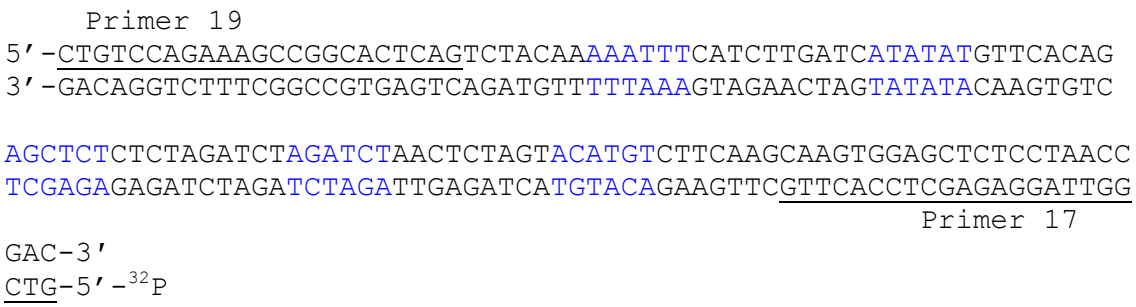

Figure 4.9 A, Chemical structures of PPPX and IPPX. **B**, DNA sequences binding models of PPPX and IPPX. **C**, DNA fragment KM-A used for the footprinting experiment. The bottom strand is 5'-labelled with [^{32}P]. DNA cognate and non-cognate sequence binding sites are labeled with blue color.

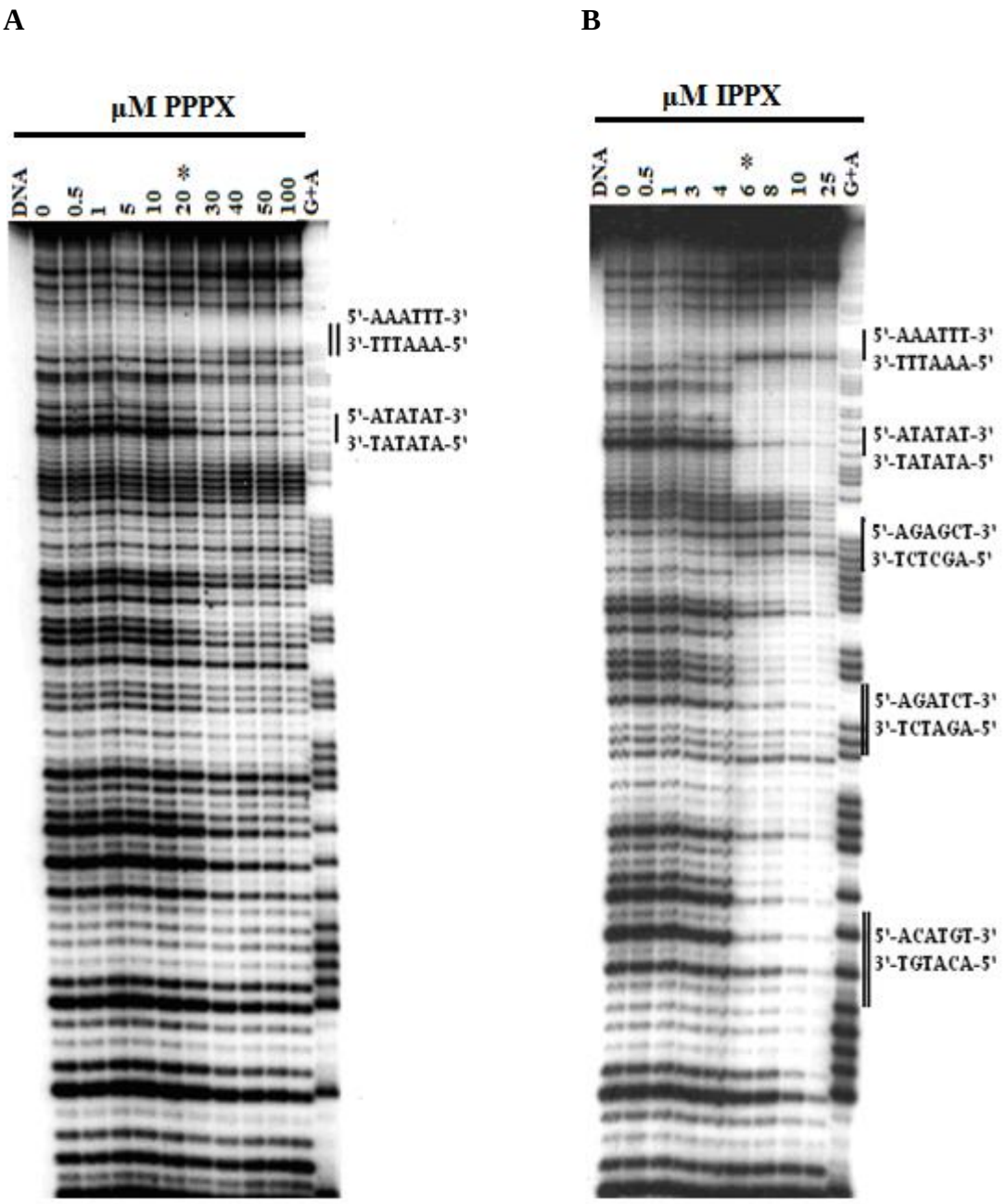

Figure 4.10 DNase I footprinting was performed with a radiolabeled probe containing the KM-A DNA sequences. The probe was incubated with increasing concentrations of PPPX (**A**) and IPPX (0.5-100 μM) (**B**). Asterisks indicated the concentration of polyamide at which cleavage protection is initially observed. The cognate sequence binding sites are highlighted by double solid bars. Control DNA lanes lack DNase I treatment and G+A lanes denote the GA nucleotides.

4.2.4 DNA Binding Properties of p-Anisylbenzimidazolecarboxamido (Hx) imidazole/pyrrole-containing polyamides

The chemical structure of p-anisylbenzimidazolecarboxamido-pyrrole-imidazole (Hx-PI) is shown in Figure 4.11A. The proposed DNA binding model was shown in Figure 4.12B. Hx moiety exhibits fluorescence and thus would provide an intrinsic probe for monitoring the cellular uptake of the molecule and ultimately the binding to nuclear DNA. Footprinting experiments were performed using a 127bp 5'-[^{32}P]-radiolabeled DNA fragments containing the following sequences: 5'-TCTTGA-3', 5'-TCTAGA-3' and 5'-ACTAGT-3' (Figure 4.11C). The autoradiograms in Figure 4.12A shows binding of HxPI at the 5'-ACTAGT-3' and 5'-TCTTGA-3' cognate sites at 20 μM. The binding to the 5'-TCTAGA-3' site occurs at a slightly higher concentration (~30 μM) (Figure 4.12).

A

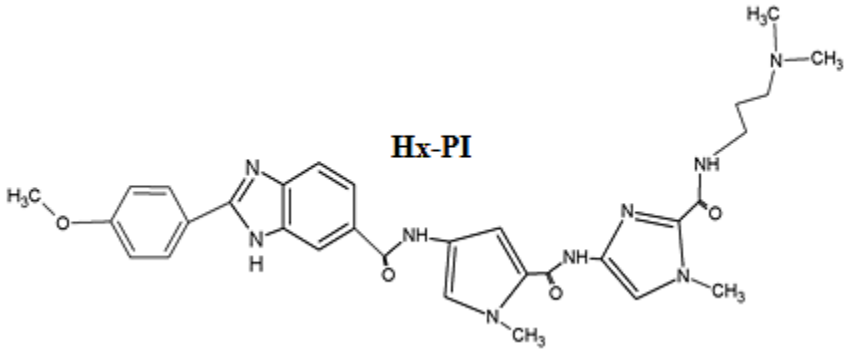

B

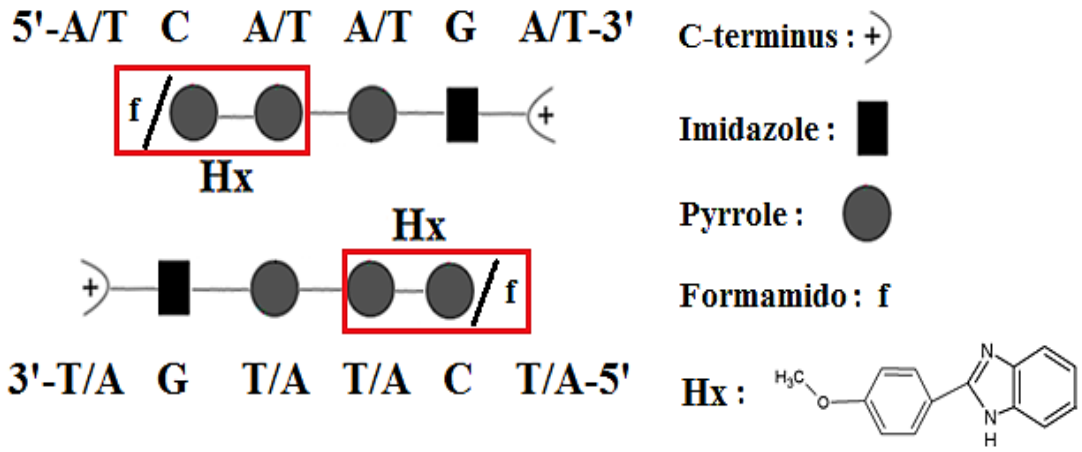

C Hx Seq

```
Primer 19
5′-CTGTCCAGAAAGCCGGCACTCAGTCTACAAACGCGTCATCTTGATCATGCATGTTCACAG
3′-GACAGGTCTTTCGGCCGTGAGTCAGATGTTTGCGCAGTAGAACTAGTACGTACAAGTGTC

AAATTTCTCTAGATCTACACGTAACTCTAGTACTAGTCTTCAAGCAAGTGGAGCTCTCCTAACC
TTTAAAGAGATCTAGATGTGCATTGAGATCATGATCAGAAGTTCGTTCACCTCGAGAGGATTGG


GAC-3′
CTG-5′-32p
Primer 17
```

Figure 4.11 A, Chemical structure of Hx-PI. **B**, DNA sequences binding model of HX-PI. **C**, DNA fragment Hx Seq. The bottom strand is 5'-labelled with ^{32}P. DNA sequence binding sites are labeled with blue color.

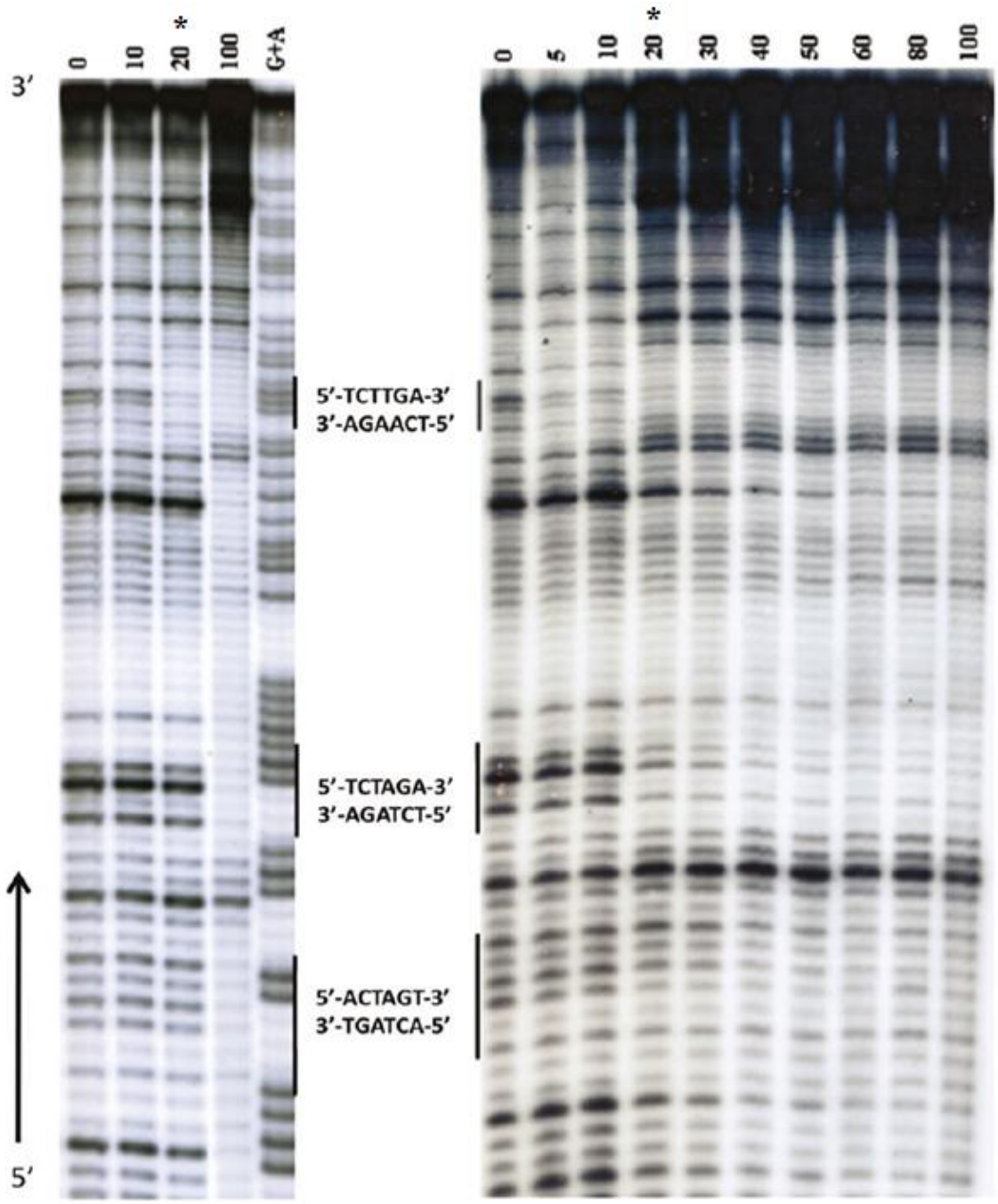

Figure 4.12 DNase I footprinting was performed with a radiolabeled probe containing the Hx DNA sequences. The probe was incubated with increasing concentrations of Hx-PI (5-100 μM). Asterisks indicated the concentration of polyamide at which protection is initially observed. The cognate sequence binding sites are highlighted by solid bars respectively. G+A lanes denote the GA nucleotides.

4.3 Discussion

The polyamide f-IPI has been previously studied (Buchmueller et al., 2006) and in this project f-IPI was further modified by the addition of a series of pendant reactive groups such as $–C_3NH_2$, $-C_3Cl$, $-C_3N_3$ and $–C_3CN$ on its pyrrole. f-IP(C_3NH_2)I shows a higher DNA binding affinity for the cognate sequence 5'-ACGCGT-3' than f-IPI (Figure 3.3A&B). The position of pendant group $–C_3NH_2$ was altered and is added on the imidazole adjacent to the formamido group. f-I(C_3NH_2)PI had a similar binding affinity to f-IPI (Figure 4.2A) (Satam et al., 2012). The binding affinities varied according to the order: f-IP(C_3NH_2)I > f-IPI = f-I(C_3NH_2)PI, suggesting that the second amino group can affect binding affinity, thus its position within the polyamide is important. However, the other f-IPI analogues exhibit at least a 10-fold reduced DNA binding affinity (Figure 3.3C, Figure 3.7A and Figure 3.9A). Therefore, we focused on investigating the effect of the *N*-(3-aminopropyl) reactive group on a series of polyamides including f-P(C_3NH_2)IP and f-IP(C_3NH_2)P. The DNase I footprinting data showed that the diamino polyamides f-P(C_3NH_2)IP and f-IP(C_3NH_2)P demonstrate better binding affinity than their respective monoamino counterparts (Figure 4.4 and 4.6). The study was further extended to explore non-formamido polyamides, including diamino polyamides e.g phenyl-IP(C_3NH_2)I [Ph-IP(C_3NH_2)I] (Figure 4.8). Compared to its monoamino counterpart Ph-IPI, the diamino polyamide Ph-IP(C_3NH_2)I demonstrated a higher DNA binding affinity for the cognate sequence 5'-ACGCGT-3' (Figure 4.8). In agreement, parallel SPR studies showed that the diamino polyamide Ph-IP(C_3NH_2)I displays a binding constant of 1.5×10^7 M^{-1} for the cognate sequence 5'-ACGCGT-3', which is ~3-fold higher than that of its monoamino polyamide (4.8×10^6 M^{-1}) (Satam et al., 2012). The side chain of these diamino polyamides is found to offer a significant benefit over the monocationic triamide in terms of enhanced water solubility as evidenced by

the ease in dissolving diamino polyamide over monoamino polyamide. Overall, it is evident that the incorporation of an orthogonally positioned aminopropyl side chain in the polyamide backbone can afford favorable physicochemical and DNA binding properties.

The novel polyamides containing the 2,5-linked N-methylpyrrole-2-carboxamide, or pyrrole(H) [P(H) or X] moiety, were designed. The two polyamides PPPP(H) (PPPX) and IPPP(H) (IPPPX) tested the binding preference of a P/X pairing and an I/X pairing. Studies utilizing circular dichroism, thermal denaturation, biosensor-surface plasmon resonance and the DNase I footprinting (Figure 4.10) show that an I/X pairing prefers a G/C or C/G pairing whilst a P/X pairing tolerates A/T or T/A base pairs and avoids a G/C base pair (Chavda et al., 2010).

Our latest efforts include polyamides which exhibit increased fluorescence upon binding to DNA. Such compounds provide an intrinsic probe for monitoring the cellular uptake of polyamides and ultimately their binding to nuclear DNA. The footprinting results showed that Hx-PI binds to the sequence 5'-WCWWGA-3' (W= A/T), suggesting that the Hx moiety behaves as PP or f-P (Figure 4.12A). This is consistent with the finding that Hx-PP and Hx-IP bind to their respective DNA sequences as their counterparts PPPP and PPIP (Chavda et al., 2011). In addition to the Hx-PP and Hx-IP footprinting, complementary biophysical studies (thermal denaturation, circular dichroism and surface plasmon resonance) also indicate that the Hx moiety behaves similarly to two consecutive pyrrole heterocyclic moieties or formamido-pyrrole. Fluorescence emission studies were performed on HxPP and HxIP to confirm the pattern of induced fluorescence of the Hx fluorophore upon binding to DNA (Chavda et al., 2011). .

CHAPTER 5

INVESTIGATION INTO *IN VITRO* BINDING CHARACTERISTICS OF F-IPI AND ITS ANALOGUES TO THE HUDBF4 AND THEIR CELLULAR EFFECTS IN MDA-MB231 CELLS

5.1 Introduction

5.1.1 Protein kinases as drug targets

5.1.1.1 Protein kinase inhibitors

Protein phosphorylation caused by protein kinases regulates most aspects of cell life, whereas abnormal phosphorylation is a cause or consequence of disease. Protein kinases have become the second most intensively pursued class of drug targets after G-protein-coupled receptors. There are numerous small molecule inhibitors of protein kinases that have been approved or are nearing approval for clinical use, mainly for treatment of cancer (reviewed in Cohen, 2013, table 5.1). However, other diseases, including diabetes, rheumatoid arthritis, neurodegeneration and immunosuppression are also linked to the deregulation of protein kinase-meditated cell signalling pathways (Cohen, 2013).

It was more than 30 years ago when Ray Erikson found that the transforming factor of the Rous sarcoma virus was a protein kinase (Collett and Erikson, 1978). In the later years, Hiroyoshi Hidaka developed the first protein-kinase inhibitors, Naphthalene sulphonamides, which were already used as antagonists of the calcium-binding protein

calmodulin (Hidaka et al., 1984). However, at higher concentrations they were able to inhibit several protein kinases. When the naphthalene ring was replaced by isoquinoline, the derivatives lost the calmodulin antagonistic ability, but surprisingly could still act as protein kinase inhibitors. Subsequently many other isoquinolinesulphonamides were developed with relatively low potency and non-specificity, but only HA1077 (also known as AT877 or fasudil hydrochloride) was investigated in human clinical trials in the early 1990s and consequently was approved for the treatment of cerebral vasospasm after surgery in Japan in 1995 (Shibuya et al., 1992; reviewed in Cohen, 2002). HA1077 inhibits several protein kinases, such as the RHO-dependent protein kinase ROCK, but it is unclear whether its clinical efficacy results from inhibition of this or other protein kinases, or whether it is due to a non-kinase effect (Cohen, 2002). In 2009, it was demonstrated that peripheral administration of the ROCK inhibitor HA1077 could also be used to enhance memory and improve the prognosis of Alzheimers patients (Huentelman et al., 2009).

Rapamycin, also known as sirolimus, was first discovered as a product of the bacterium *Streptomyces hygroscopicus* in soil samples from Easter Island and characterized more than 40 years ago. It was later developed as an antifungal agent. However, this use was terminated when it was discovered to have potent immunosuppressive and antiproliferative properties (Garber, 2001). In September 1999, rapamycin was approved for clinical use by the FDA as an immunosuppressant drug.

Name	Structure	Reported target	Company	Approved for clinical use
Eril		ROCK	Eisai	1995 cerebral vasospasm (Japan)
Rapamune	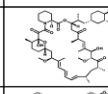	mTOR	Wyeth Pfizer	2000 kidney transplantation
Temsirolimus	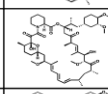	mTOR	Wyeth Pfizer	2007 advanced renal cell carcinoma
Everolimus	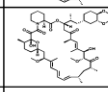	mTOR	Novartis	2009 several cancers
Imatinib	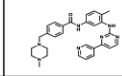	Bcr-Abl c-KIT PDGFR	Novartis	2001 chronic myelogenous leukaemia
Gefitinib	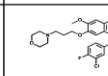	EGFR	Astra Zeneca	2005 lung cancer
Erlotinib	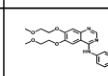	ErbB1	Genetech Roche	2005 lung,pancreatic and others cancers
Sorafenib	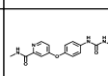	Multiple Tyrosine kinases targeted	Onyx Bayer	2005 renal cancer
Dasatinib	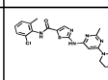	Multiple Tyrosine-kinases targeted	Bristol Myers Squibb	2006 chronic myeloenous leukaemia, All
Sunitinib	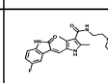	Multiple Tyrosine-kinases targeted	SUGEN Pfizer	2006 renal cancer and GIST
Nilotinib	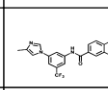	Bcr-Abl	Novartis	2007 chronic myelogenous leukaemia
Lapatinib	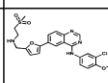	Her2 EGFR	GlaxoSmith Kline	2009 renal cancer
Pazopanib	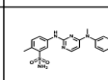	VEGFR2 PDGFR c-KIT	GlaxoSmith Kline	2009 renal cancer
Ruxolitinib	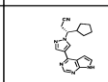	JAKs	Incyte	2011 myelofibrosis
Crizotinib	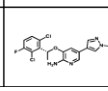	ALK/Met	Pfizer	2011 NSCLC with Alk mutation

Name	Structure	Reported target	Company	Approved for clinical use
Vemurafenib	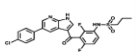	BRAF	Roche	2011 melanoma
Vadetinib	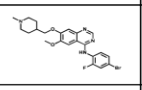	Multiple Tyrosine kinases targeted	Caprelsa IPR Pharms	2012 thyroid cancer
Axitinib	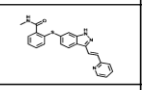	VEGFRs PDGFRB c-KIT	Pfizer	2012 renal cell carcinoma
Bosutinib	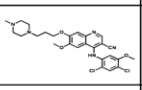	BcrAbi SRC	Pfizer	2012 chronic myelogenous leukemia
Tivozanib	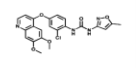	VGFRs	AVEO Pharms	2012 kidney cancer
Tofacitinib	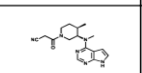	JAKs	Pfizer	2012 rheumatoid arthritis
Regorafenib	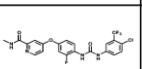	Multiple Tyrosine kinases targeted	Stivarga Bayer	2012 thyroid cancer
Lenvatinib	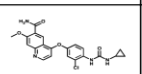	VEGFR2/ VEGFR2	Eisai	2012 thyroid cancer (Japan)
Toceranib	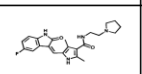	Multiple Tyrosine kinases targeted	Pfizer	2009 canine mastocytoma
Masivet Kinavet	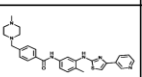	c-KIT PDGFR	AB Science	2010 canine mastocytoma
Cabozantinib	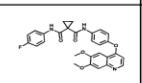	VEGFRs KIT / Axl	Cometriq Exelixis	2012 canine thyroid cancer
Afatinib	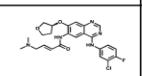	Her2 EGFR	Boehringer Ingelheim	Not yet NSCLC
Dabrafenib	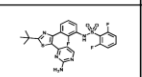	BRaf	GlaxoSmith Kline	Not yet metastatic melanoma
Trametinib	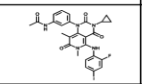	MEK1/2	GlaxoSmith Kline	Not yet metastatic melanoma

Table 5.1 Small molecule inhibitors of protein kinases approved for clinical use or in advanced clinical trials (Taken from Cohen, 2013).

Rapamycin was the first cytostatic agent to be identified and be approved for clinical use that exerts its effects by specifically inhibiting a protein kinase (Davies et al., 2000). The intracellular receptor for rapamycin is the FK-binding protein (FKBP) and the molecular target of rapamycin-FKBP in yeast was identified as a protein kinase, which was termed the 'target of rapamycin' (TOR) by Heitman (Heitman et al., 1991). Subsequently the mammalian homologue, called mTOR or the FKBP-rapamycin-associated protein (FRAP), was identified and was shown to have an important role in the phosphatidylino-3-kinase-dependent signaling pathway that regulates cell-cycle progression from G_1 to S phase (Neshat et al., 2001; Podsypanina et al., 2001; Ballou and Lin, 2008). Dysregulation of the mTOR signaling pathway occurs frequently in a variety of human tumors, and thus, mTOR has emerged as an important target for the design of anticancer agents. However, rapamycin showed very poor water solubility and chemical stability, severely limiting its bioavailability (Huang and Houghton, 2003; Huang et al., 2003). Therefore, several rapamycin analogues with better pharmacokinetic properties and lower immunosuppressive effects, including temsirolimus (CCI-779), everolimus (RAD001), and deforolimus (AP23573), have been developed (Ballou and Lin, 2008; Rizzieri et al., 2008). Temsirolimus and everolimus were recently approved by the FDA for the treatment of advanced/metastatic renal cell carcinoma (Motzer et al., 2008; Hess et al., 2009).

The human genome encodes approximately 518 protein kinases that regulate virtually every signal transduction stage through a phosphotransfer cascade: from the receptor tyrosine kinases that initiate intracellular signaling, to the kinases that regulate cell cycle

and are involved in cellular fate (Cohen et al., 2002; Fabbro et al., 2002; Levitzki et al., 2003; Zhang et al., 2009).

5.1.1.2 The Cyclin-dependent kinases

The Cyclin-dependent kinases (CDKs) are serine/threonine protein kinases which mediate the cell cycle progression, regulating transition from G_1 to S phase and G_2 to M phase. CDK activity is tightly dependent on binding and activation by cyclins and CDK inhibitors (Malumbres, 2005; Malumbres and Barbacid, 2005; Barbacid et al., 2005). A subset of CDK-cyclin complexes is directly involved in driving the cell cycle. This subset includes: CDK1 which predominantly regulates the transition from G_2 to M phase, and CDK2/4/6 which regulates the transition from G_1 to S phase (Malumbres and Barbacid, 2009); CDK7 on the other hand has dual roles as a CDK-activating kinase and a regulator of the transcriptional machinery. In addition to cell cycle regulatory functions of the CDKs, CDK9 plays a key role in the control of RNA polymerase II-mediated transcription (Krystof et al., 2010; Krystof and Uldrijan, 2010). CDK inhibitors has been considered as relevant drug candidates for cancer therapy owing to their potential role in restoring control of the cell cycle (Malumbres et al., 2008; Shapiro et al., 2006). A new generation of CDK inhibitors undergoing clinical trials is listed in table 5.2 (Malumbres and Barbacid, 2009).

5.1.1.3 Association between the CDKs and Cdc7 kinase

The highly conserved Cdc7 (cell division cycle 7) kinase, a serine/threonine kinase, is essential for cell cycle progression, and has several structure-function connections with the CDKs, making it an important target for drug development.

Compound	Primary target(s)	Clinical trials	Sponsor
AG-024322	CDK1, CDK2 CDK4	Phase I, advanced cancer: Discontinued (2007)	Pfizer
AT-7519	CDK1, CDK2 CDK4, CDK5	Phase I/II, advanced or metastatic tumours	Astex
P276-00	CDK1, CDK4 CDK9	Phase I/II, advanced refractory neoplasms	Piramal
P1446A-05	CDK4	Phase I, advanced refractory malignancies	Piramal
PD-0332991	CDK4, CDK6	Phase I, advanced cancer	Pfizer
R547	CDK1, CDK2 CDK4, CDK7	Phase I, advanced solid tumours	Hoffmann -LaRoche
Roscovitine	CDK2, CDK7 CDK8, CDK9	Phase II, non-small cell lung cancer, nasopharyngeal cancer, haematological tumours	Cyclacel
SNS-032	CDK1, CDK2 CDK4, CDK7 CDK9	Phase I, B-lymphoid malignancies Phase I, solid tumours	Sunesis

Table 5.2 Examples of specific CDK inhibitors in clinical trials (single-agent trials) adapted from Malumbres and Barbacid, 2009.

5.1.1.3.1 Functional similarities

Cyclin D/CDK4, cyclin E/CDK2 and cyclin A/CDK2 play important regulatory roles in the regulation of the G_1/S progression. Activation of these kinases leads to the phosphorylation of the retinoblastoma protein (pRb) and its related family members, p107 and p130 (Kiess et al., 1995; Paggi et al., 1996; Suzuki-Takahashi et al 1995). This phosphorylation releases the E2F transcription factors, inducing the expression of other genes required for DNA synthesis (Ohtani et al., 1995). CDK2 and Cdc7, required for the CDC45-dependent loading of DNA polymerases, operate in a separate pathway to activate the origin replication complexes and progress DNA replication through modulation of Mcm2 (Jares et al., 2000; Zou et al., 2000). The CDK2-interacting protein (CINP) was proposed to be the functional link between CDK2 and Cdc7 during

firing of the origins of replication. CINP is a component of the active cyclin A/Cdk2, and also interacts with Cdc7 while it is phosphorylated by Cdc7. The association of CINP with the pre-replicative complex (pre-RC) binds to chromatin in a replication-dependent manner (Swords et al., 2010; Figure 5.1).

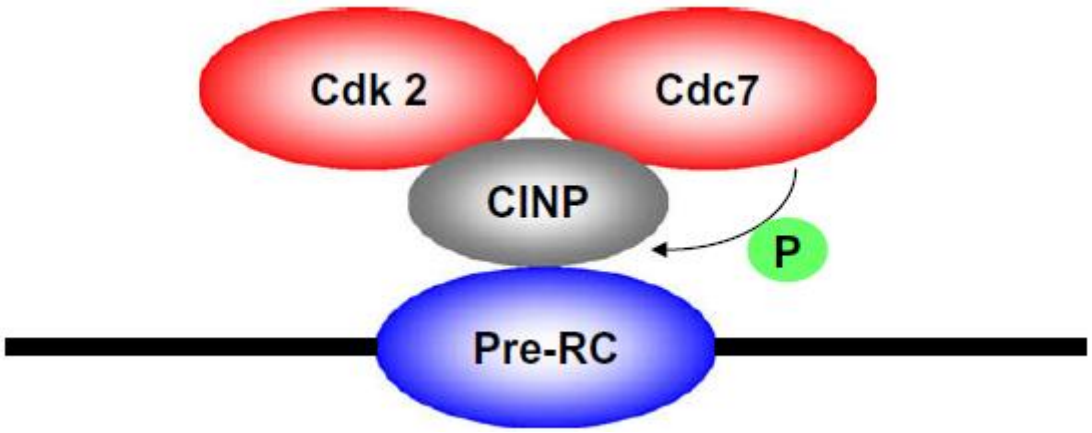

Figure 5.1 Functional relationship between Cdc7 and CDKs. CINP interacts with both Cdk2 and Cdc7 but is phosphorylated only by Cdc7. CINP binds to chromatin in a replication-dependent manner, and associates with the Pre-RC. CINP is a part of the Cdc7-dependent mechanism of origin firing and becomes a functional and physical link between Cdk2 and Cdc7 complexes at these sites on DNA (taken from Swords et al., 2010).

5.1.1.3.2 Similarities in regulation

The regulation and activation of the Cdc7 kinase is similar to that of the CDKs by their cyclin partners. In general, cyclins are unstable, appearing briefly in the cell cycle and regulating CDKs activity at crucial points. Their function has been best characterized in yeast, where they regulate transition from G_1 to S phase and G_2 to M phase. Both the Cdks and Cdc7 are dependent on the levels of associated protein subunits which fluctuate during the cell cycle and correspond to the kinase activities of Cyclin-Cdk and Cdc7-Dbf4/Drf1, respectively (Swords et al., 2010). Like Cyclin-CDKs, Cdc7 and Dbf4 are also conserved from yeast to humans (Johnston et al., 1999; Sclafani, 2000).

5.2.1 Cdc7 characteristics

5.2.1.1 Structural features of the ATP-binding domain of Cdc7 kinase

Hydrogen bonds link ATP to the ATP-binding pocket at a hinge region connecting the N- and C-terminal lobes of the kinase catalytic domain (Figure 5.2; Sawa and Masai, 2009). The hinge region with additional interactions with two hydrophobic regions (sites B and E in Figure 5.2) adjacent to the ATP-binding pocket has been also reported as a target of most kinase inhibitors. Due to the size of a single residue in the interior of the hydrophobic region I (site E in Figure 5.2), this region termed the gatekeeper is commonly referred to as the selectivity pocket and is an essential determinant of inhibitor sensitivity (Cherry and Williams, 2004; Vieth et al., 2004).

Approximately 90 kinases contain a small threonine gatekeeper, and 190 kinases possess a large methionine residue according to the in-house human kinome database. Sawa and Nasai built in-house a homology model of Cdc7 indicating that the large gatekeeper residue (Met134) results in a very narrow entrance to the hydrophobic region I, and the back pocket of this site is in possession of residues Val120 and I1e132 (Figure 5.3; Sawa and Masai, 2009). The formation of the adenine-binding region by a hydrophobic sandwich with two residues (Met118 and I1e64) at the central portion suggested that a flat hydrophobic core is perhaps preferred as an inhibitor scaffold. In the same region, typical hydrogen bonds may be formed with the backbone of the hinge region. The potential targets of two ionic residues (Lys90 and Asp196) could be useful for the design of potent inhibitors (Sawa and Masai, 2009).

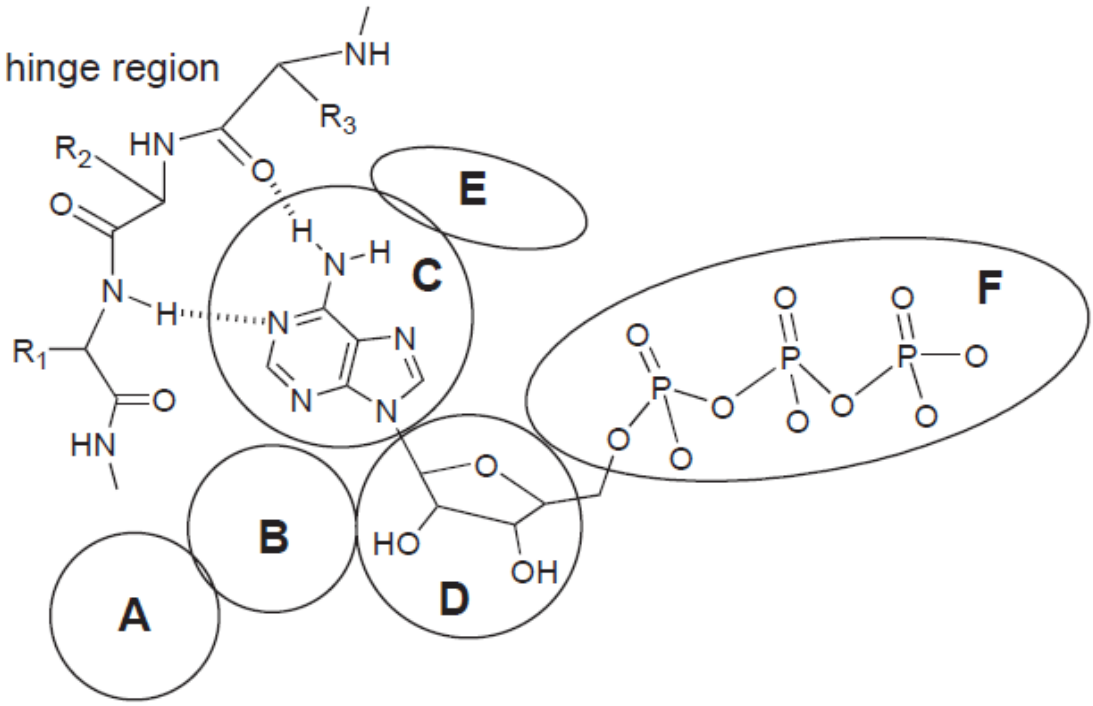

Figure 5.2 Schematic representation of general binding of ATP; interactions with specific segments of protein kinases: **A** solvent accessible region, **B** hydrophobic region II, **C** adenine-binding region, **D** sugar pocket, **E** hydrophobic region I, **F** phosphate-binding region (taken from Sawa and Masai, 2009).

A

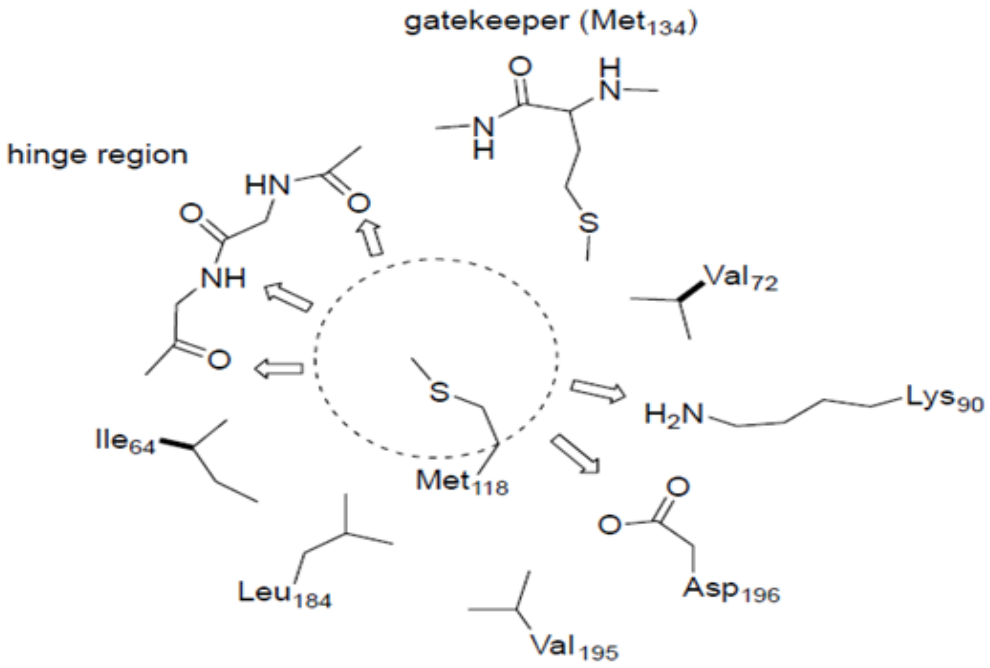

B

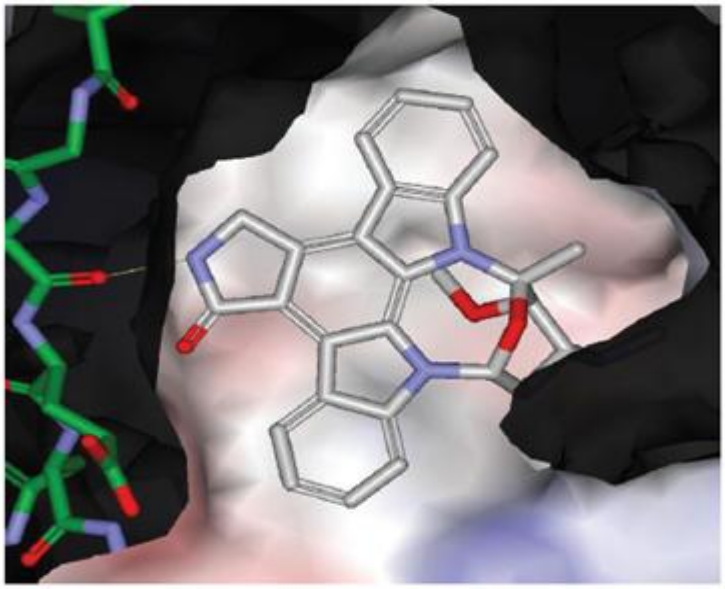

Figure 5.3 A homology model of Cdc7 kinase. **A,** mapping of important residues within the ATP-binding pocket of Cdc7 kinase. The formation of hydrophobic area (adenine-binding region) by a hydrophobic sandwich with two residues (Met118 and I1e64) is labeled with the dotted circle area. The arrows mark possible hydrogen bonds between an inhibitor and the ATP-biding site of Cdc7. **B,** the association of a model of staurosporine with the ATP-binding site of Cdc7 by Van der Waals surfaces. The negatively and positively charged regions are indicated in pink and blue respectively. Oxygen and nitrogen are shown in red and blue respectively. The carbon atoms in the ligand (staurosporine) and in the protein are shown in white and green respectively (Sawa and Masai, 2009).

5.2.1.2 The role of Cdc7 in the initiation of DNA replication

The highly conserved Cdc7 was initially identified by Hartwell in studies of a temperature-sensitive mutant in budding yeast, in which Cdc7 is required for the initiation of DNA replication (Hartwell et al., 1971; Patterson et al., 1986). The human homologue Cdc7 was identified almost 20 years later and comprises a distinct group in the kinase family (Figure 5.4A; Masai et al., 1995; Sawa and Masai, 2009).

Cdc7 is critical for viability in yeast. The Kim group first indicated that the knockout of murine Cdc7 results in early embryonic death. Subsequently it was found that knockout of Cdc7 genes in murine embryonic stem cells led to S-phase arrest, accumulation of nuclear DNA damage, and eventual p53-dependent cell death (Kim et al., 2002). These results suggest that Cdc7 kinase plays an important role in DNA replication through S-phase, which is conserved across species, including *Xenopus*, mouse and human (Jiang and Hunter, 1997; Sato et al., 1997; Kim et al., 1998). The initiation of Eukaryotic DNA replication is originally fired by binding of ORC (origin recognition complex) to replication origins. Mcm (minichromosome maintenance complex) is delivered to the origins of replication after association with Cdc6 and Cdt1 as a result of generation of pre-RC (pre-replicative complex). Phosphorylation of Mcms (N-terminal tails of Mcm2, mcm4 and mcm6 proteins) by Cdc7 and Cdk facilitates the association of Cdc45, Mcms and GINs complex (Masai et al 2000, 2006). The generation of active replication forks occurs at the origin in response to the association of DNA polymerases (Sawa and Masai, 2009). This step is crucial for the generation of active and efficient replication fork structures (Figure 5.5).

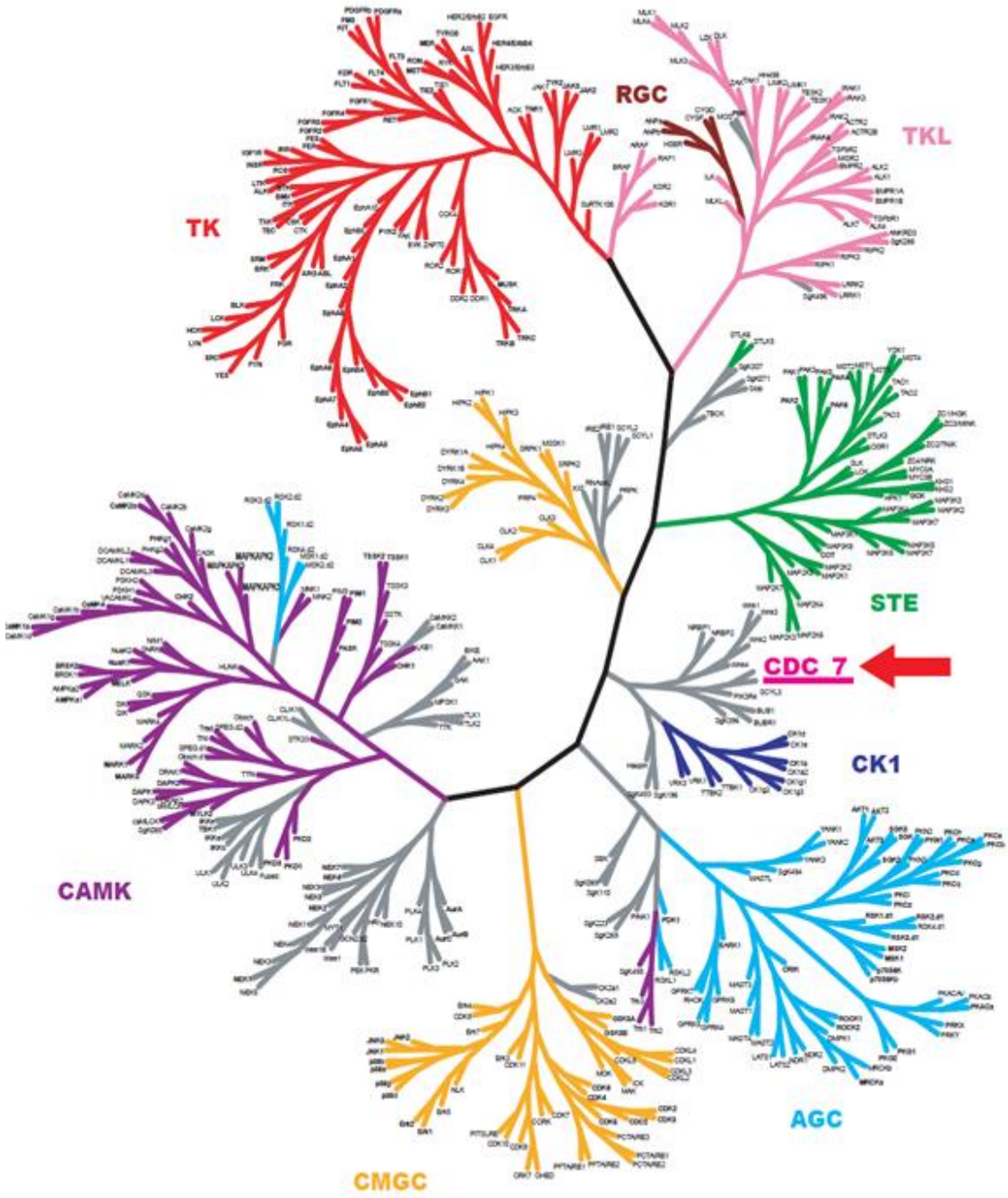

Figure 5.4 Homology analysis of human Cdc7 kinase. CAMK (calcium/calmodulin-depedent kinase group), TK (tyrosine kinase group), RGC (receptor guanylyl cyclase group), TKL (tyrosine kinase-like group), STE (sterile phenotype kinase group), CKI (cell kianse I/casein kinase I group), AGC (protein kinaseA, G and C group), CMGC (cyclin-depedent-kinase (CDK), mitogen-activated-kinase (MAPK), glycogen-synthase-kinase (gsk) and CDK-like kinase group. The human kinome tree (taken from Sawa and Masai, 2009).

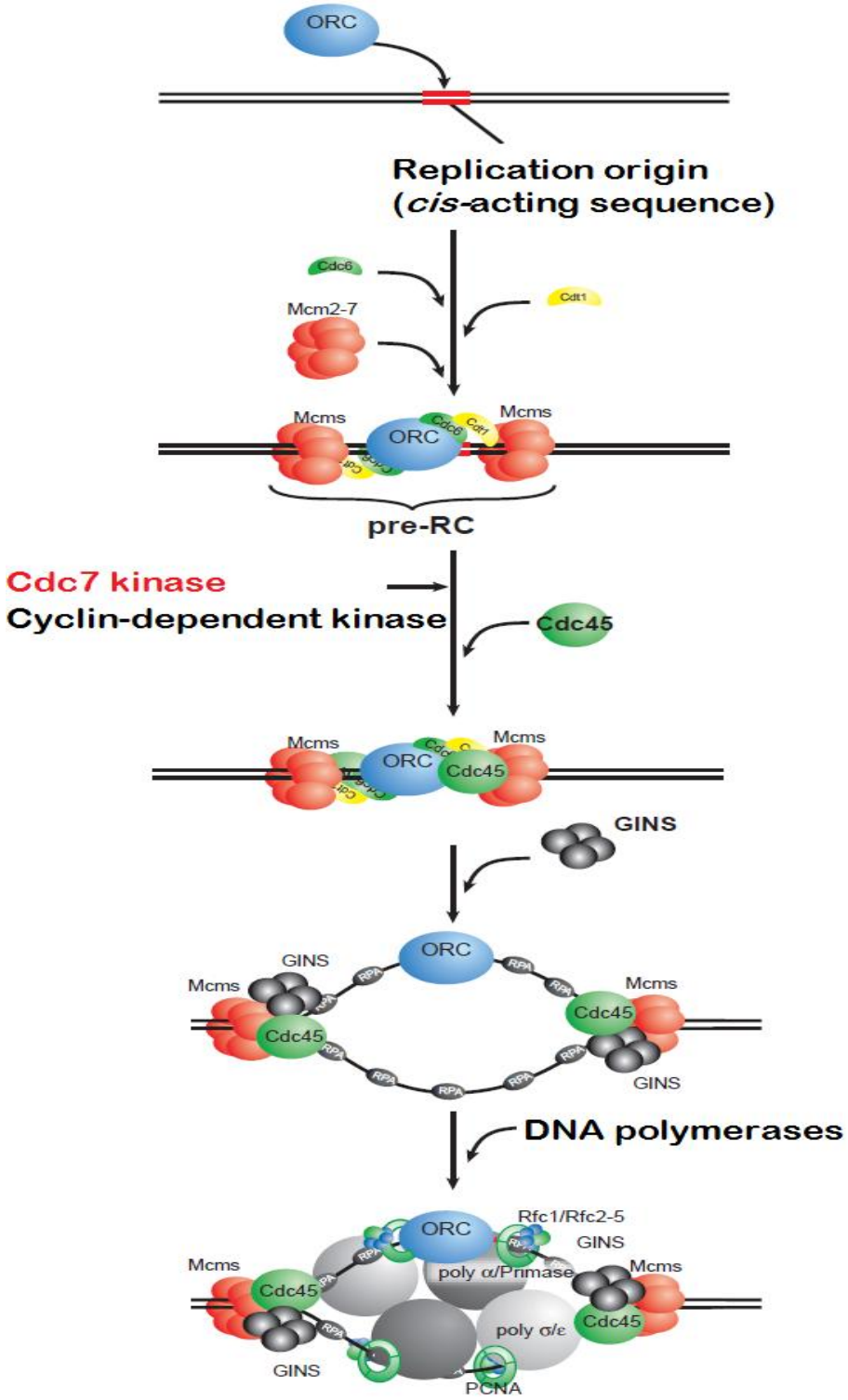

Figure 5.5 Scheme of the initiation of eukaryotic DNA replication and the role of Cdc7. The binding of ORC to replication origin initiates DNA replication. The binding of Mcm to ORC results from the association of both Cdc6 and Cdt1, generating pre-RC. Both Cdc7 and Cdk2 phosphorylate elements of the MCM complex, which leads to loading of other accessory factors such as Cdc45 and the GINs complex. Active replication forks are then generated by the association of DNA polymerases that results in the semiconservative replication of DNA (Sawa and Masai, 2009)

5.2.1.3 The role of Cdc7 in checkpoint regulation

Highly conserved DNA-repair and cell-cycle checkpoint pathways are critical for the viability of cells as they are continuously subjected to both endogenous and exogenous damage (Sonoda et al., 1998). The proper processing of stalled replication forks and the resumption of DNA replication is key to the stable inheritance of genetic information through generations. Cells respond to DNA damage and stalled replication forks by regulation of checkpoint reactions. A defect in checkpoint regulation causes serious threats to genomic stability. Mutations in checkpoint regulators have been demonstrated to be responsible for various tumours or diseases (D'Andrea and Grompe 2003; Michelson and Weinert, 2000).

The checkpoint responses consist of four phases; the sensor, the mediator, the transducer and the effector phases (Niida and Nakanishi 2006; Nakanishi and Shimada, 2006). It has been indicated that Cdc7 kinase is critically involved in the mediator phase (activating the checkpoint effect) of DNA replication checkpoint responses (Kim et al., 2008). Cdc7 is required for activation of the ATR (ataxia-telangiec-tasia-mutated-Rads-related)-Chk1 checkpoint pathway through the hyperphosphorylation of Claspin (a mediator) in response to stalled replication forks (Kim et al., 2008). In addition, a critical role of Cdc7 kinase is also found in the effector phase (executing the checkpoint effects) suggested by the fact that Cdc7 is inactivated in *xenopus* egg extracts in response to etoposide, which generated single-strand DNA gaps. It was found that replication protein A (RPA) binding to single-stranded DNA in these gaps induces an ATR-dependent checkpoint that blocks origin firing by inactivation of Cdc7 kinase (Costanzo et al., 2003). Dierov's group showed that Cdc7 is inactivated by etopside in

human cells (Dierov et al., 2004). Accumulating evidence suggests the dual roles of Cdc7 kinase in the mediator and effector phases of checkpoint responses. However, it is not clear that these functions of Cdc7 are as critical in human cells, as Cdc7 activity remains unaltered by stalled replication fork in human cells (Tenca et al., 2007). What is clear however is that the knockout of Cdc7 in actively proliferating cells leads to replication fork arrest in response to DNA damage, and simultaneously causes defective checkpoint activation.

5.2.1.4 The effects of Cdc7 depletion in cancer cells

siRNA-mediated downregulation of Cdc7 expression has been investigated in various cancer cell lines. Following retardation of S phase progression caused by Cdc7 depletion, cancer cells accumulate nuclear damage, presumably induced by replication fork arrest, and then undergo chromosome fragmentation and die. This occurs in both p53-positive and -negative cells, indicating that cell death is p53-independent (Montagnoli et al., 2004; Yoshizaw-Sugata et al., 2005; Im and Lee 2008; Kim et al., 2008). In contrast, in normal fibroblasts, a p53-dependent cell cycle checkpoint actively prevents progression through a lethal S phase in the absence of Cdc7 kinase (Montagnoli et al., 2004).

The precise mechanisms of cancer-specific cell death are not clear. Depletion of Cdc7 can cause defects in firing of the replication origins as well as acute destabilization of replication forks which eventually collapse. Furthermore, checkpoint defects may trigger uncoupling of the M phase with the S phase. Therefore it is suggested that the combined effect of replication fork arrest and deficient checkpoint responses might

cause cell death by inducing aberrant cell cycle progression. Whereas normal cells have backup checkpoint mechanisms, cancer cells, in which checkpoint mechanisms are very often dysregulated, would suffer from aberrant M phase progression. It has been reported that ATR-induced activation of p38 MAP kinase causes caspase activation in Cdc7-depleted cancer cells (Im and Lee 2008).

5.3.1 The roles of Cdc7/Dbf4 in yeast and mammalian cells

5.3.1.1 Function of Cdc7/Dbf4 during origin activation

The activation of the eukaryotic replication origins contains two steps. The first step consists of the sequential assembly onto replication origins of the origin recognition complex (ORC), Cdc6 and Mcm2-7 (the MCM proteins). This assembly occurs during late mitosis and $G_{1,}$ causing the origin to become 'licensed' for DNA replication (Figure 5.6). In the second step, licensed replication origins fire at different times during S phase to each initiate a pair of replication forks. The two kinases CDKs and Cdc7/Dbf4 are involved in this step (reviewed in Jares et al., 2000; Lee et al., 2012).

Cdc7 is a serine/threonine kinase, conserved from yeast to humans (reviewed in Johnston et al., 1999; Sclafani, 2000). It is activated by binding to its regulatory protein Dbf4 (Jackson et al., 1993; Jiang et al., 1999). Cdc7 kinase activity reaches the highest levels at G_1/S transition, although Cdc7 protein levels remain approximately constant through the cell cycle (Jackson at al., 1993; Yoon et al., 1993). This cyclic control of activity reflects changes in the abundance of Dbf4 (Brown and Kelly, 1999; Cheng et al., 1999). Although Cdc7 kinase was first identified in budding yeast, orthologs of Cdc7 and Dbf4 have been also found in the fission yeast *Aspergillus, Drosophila*, *Xenopus,*

mice, and human, where Dbf4 is also called the activator of S phase kinase (ASK) (Sato at el., 1997; Takeda et al., 1999; Jiang et al., 1999). This subunit is referred to as Dbf4 in the thesis. The levels of Dbf4 oscillate during cell cycle and Dbf4 accumulates in the nuclei of late G_1, S and M phase cells (Cheng et al., 1999; Jiang et al., 1999; Oshiro et al., 1999). Dbf4 levels are degraded in late mitosis and early G_1 by a functional anaphase-promoting complex (Cheng et al., 1999; Weinreich and Stillman, 1999; Ferreira et al., 2000). Cdc7/Dbf4 is required for initiation to fire at early- and late-replication origin rather than acting as a global sensor for progression into S phase. Consistent with this proposal, Cdc7 along with its interacting factor Dbf4, have been shown to associate with chromatin (Weinreich and Stillman, 1999), whilst Dbf4 localise to a replication origin in the budding yeast (Dowell et al., 1994).

In *saccharomyces cerevisiae*, Dbf4 binds to chromatin at the G_1/S transition and remains attached during S phase, whilst Cdc7 shows association with chromatin through the cell cycle (Weinreich and Stillman, 1999). Pasero et al reported that the association of Dbf4 with chromatin in G_1 phase depends on the presence of ORC but does not require Cdc6 or Mcm(2-7) (Figure 5.6A ; Pasero et al., 1999). However, in the *xenopus* cell-free system, Jares and Blow showed that Cdc7 also binds to chromatin during the G_1 and S phase. Its association with chromatin does not require the continued presence of *xenopus* ORC or Cdc6. Once origin licensing is completed, Cdc7/Dbf4 appears to depend on the presence of Mcm (2-7) (i.e. licensed origin) (Figure 5.6B ; Jares and Blow, 2000). These results suggest that yeast and *xenopus* may recruit Cdc7/Dbf4 to replication fork origins differently.

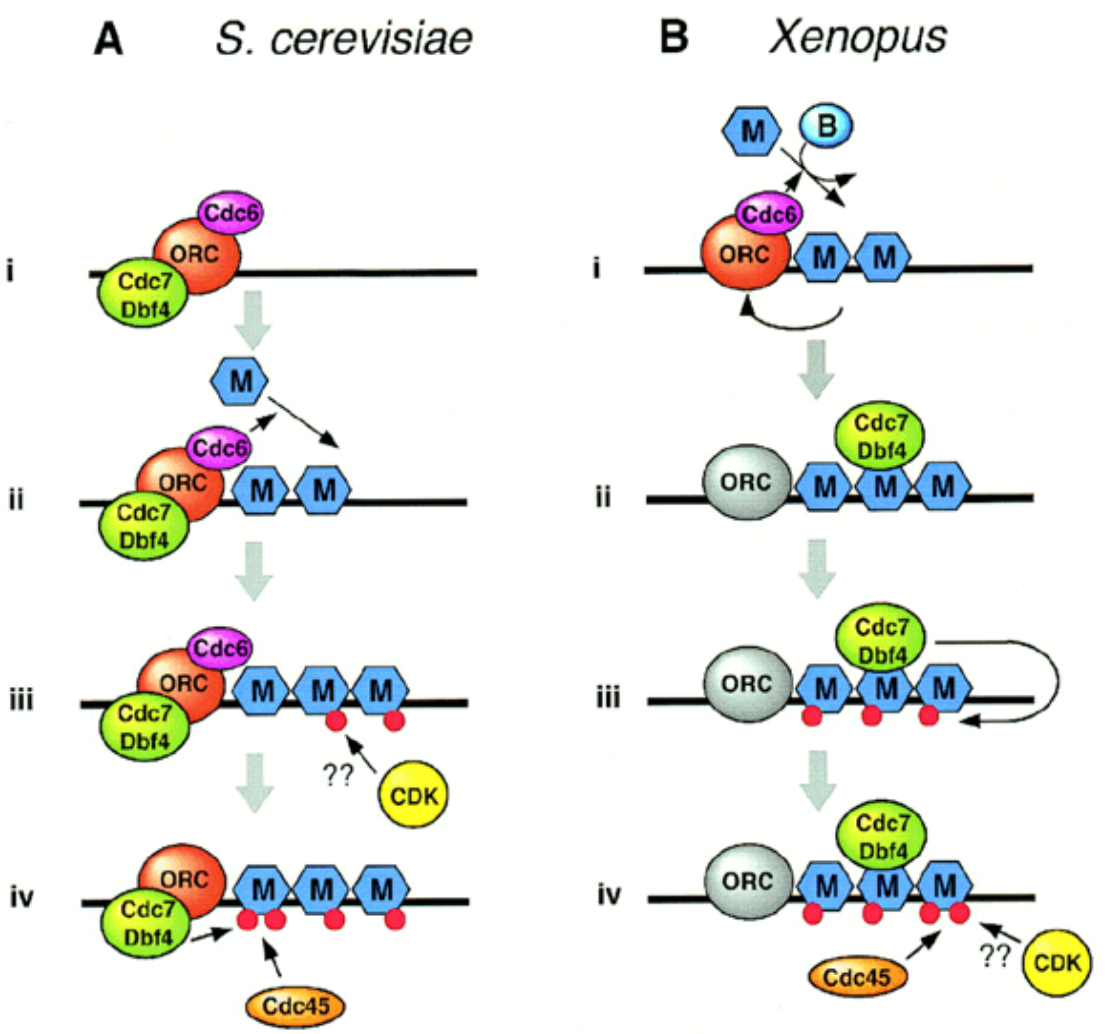

Figure 5.6 Comparison of proposed Cdc7/Dbf4 function in *S. cerevisiae* and *Xenopus.* 'M' refers to the Mcm (2-7) heterohexamer and 'B' refers to RLF-B component for the replication licensing system. **A** (i) Cdc6 and Cdc7/Dbf4 bind to ORC separately at a replication origin. (ii) Cdc6-delivering Mcm (2-7) onto origin. (iii) Phosphorylation of Mcm (2-7) possibly by CDK-dependent step occurs prior to Cdc7/Dbf4 function. (iv) Cdc7/Dbf4 function results in assembly of Cdc45 onto the origin. **B** (i) ORC, Cdc6 and RLF-B regulate the origin licensing DNA, which once bound to Mcm (2-7) leads to displacement of Cdc6 and destabilization of ORC. (ii) Mcm (2-7) but not ORC or Cdc6 is required for Cdc7/Dbf4 bound to the origin. (iii) Cdc7/Dbf4 phosphorylated Mcm (2-7) can occur in the absence of CDKs. (iv) Cdc45-delivering to the origin depends on both Cdc7 and CDK activity (Taken from Jares et al., 2000).

The association of Cdc7/Dbf4 with replication fork origins suggests that their substrates may also be origin-attached. Previous reports showed that the S phase-promoting kinase Cdc7/Dbf4 and the putative DNA replicative helicase Mcm (2-7) play essential roles in the initiation of DNA replication in all eukaryotes. Mcm2 subunit of the Mcm complex that is selectively phosphorylated by Cdc7/Dbf4 is an excellent substrate both in *vivo* and in *vitro*, suggesting that Cdc7/Dbf4 may be directly involved in the initiation of DNA replication by targeting Mcm2 (Lei et al., 1997; Sato et al., 1997; Brown and Kelly, 1998; Jiang et al., 1999; Roberts et al., 1999; Jares and Blow, 2000). To determine the importance of the Cdc7/Dbf4 phosphorylation of Mcm2 in the initiation of DNA replication, Tsuji et al mapped Cdc7/Dbf4 phosphorylation sites in human Mcm2. Three major sites (Ser27, Ser41, and Ser139) and two minor sites (Ser43 and Ser108) of Mcm2 were found to be phosphorylated in *vivo*. Those major sites are specifically phosphorylated by purified Cdc7/Dbf4 in *vitro* and their phosphorylation in *vivo* was significantly decreased in Cdc7 siRNA treated cells, thereby strongly suggesting that Ser27, Ser41, and Ser139 are in *vivo* Cdc7/Dbf4 phosphorylation sites in Mcm2 (Tsuji et al., 2006). They also examined chromatin recruitment and phosphorylation of chromatin-bound Mcm2 by Cdc7/Dbf4. Mcm2 accumulated on chromatin and was not phosphorylated by Cdc7/Dbf4 until G_1/S transition and early S phase, which coincided with the initiation of DNA replication. In late S and G_2/S transition, phosphorylated Mcm2 gradually disassociated from chromatin. Suppression of Mcm2 expression in Mcm2 siRNA-treated cells inhibits DNA replication in Hela cells. The inhibition of DNA replication by Mcm2 siRNA can be rescued by co-expression of Mcm2. This confirms the essential role of phosphorylation of Mcm2 by Cdc7/Dbf4 kinase is involved in the initiation of DNA replication in human cells (Tsuji

et al., 2006), however, it alone is not sufficient (Owens et al., 1997; Zou and Stillman, 1998; Tercero et al., 2000).

A model for the regulation of the initiation of DNA replication by Cdc7/Dbf4 phosphorylation of Mcm2 in human cells has been proposed on the basis of previous results (Bell and Dutta, 2002; Mendez and Stillman, 2003; Forsburg, 2004; Tsuji et al., 2006). Mcm2 is not phosphorylated by Cdc7/Dbf4 in G_1, where Cdc7/Dbf4 kinase activity remains at a minimum. Association of unphosphorylated Mcm2 with other Mcms (Mcm2-7 complex) occurs on chromatin, presumably on the replication origins by the Cdc6 and Cdt1 (DNA replication loading factors) to establish pre-RCs. Activation of Cdc7/Dbf4 kinase during G_1/S transition and early S phase leads to the phosphorylation of chromatin-attached Mcm2. Cdc7/Dbf4 phosphorylation of Mcm2 in the Mcm (2-7) complex elicits the conformational change of the complex and activation of its helicase, which is crucial for DNA replication. MCM2-7 helicase works at a distance from the replication forks, pumping DNA along its helical axis by ATPase-coupled rotation. In late S and G_2/S transition, Mcm (2-7) complex is released from chromatin, seemingly by additional post-translational modifications to prevent DNA re-replication (Tsuji et al., 2006).

5.3.1.2 Cdc7/Dbf4 in cell cycle checkpoints

In addition to its crucial function in the initiation of DNA replication, the Cdc7/Dbf4 kinase is a target of the S-phase checkpoint pathway, and it plays an essential role in growth recovery from DNA damage in multiple organisms (Takeda et al., 1999; Weinreich and Stillman, 1999). The ATR- and Chk1- dependent S checkpoint inhibits

the initiation of DNA replication in response to UV irradiation, which is biochemically distinct from that induced by ionizing radiation. The UV irradiation-induced S checkpoint is offset by overexpression of Dbf4 and Chk1 phosphorylated Dbf4 in *vitro*, suggesting that Dbf4-dependent kinase is a possible downstream target of ATR- and Chk1- checkpoint kinases in response to UV irradiation in human cells where its activity may be inhibited to prevent replicon initiation (Heffernan et al., 2007). Costanzo's group demonstrated that a DNA damage (ATR- and Chk1-) checkpoint targets Cdc7/Dbf4 kinase, although it is not clear if Cdc7 or Dbf4 are direct targets of either ATR or Chk1/2 (Costanzo et al., 2003). Cdc7/Dbf4 is thereby an important cell cycle regulator that is also important for genome integrity in response to replication fork stalling or DNA damage.

5.3.1.3 Overexpression of Cdc7/Dbf4 in multiple cancers

Changes in Cdc7/Dbf4 protein abundance or activity might arise during tumorigenesis and might have an important impact on cell survival (Bardelli et al., 2003; Greenman et al., 2007). Nambiar's group showed that overexpression of Dbf4 protein is observed in primary cutaneous melanoma and cutaneous melanoma metastases, and proposed that up-regulated Dbf4 bound to Cdc7 in the nucleus is a novel determinant of the cutaneous melanoma development with prognostic value (Nambiar et al., 2007). Furthermore, Bonte et al found that the Cdc7 protein has a relatively low or undetectable abundance in normal tissues and cell lines while is highly expressed in ~50% of 62 human tumor cell lines tested (Bonte et al., 2008). They also found a tight correlation between the expression levels of Cdc7 and Dbf4. Most cell lines with increased Cdc7 protein levels also possess increased levels of Dbf4 protein. Seven of 14 ovarian, breast, and prostate

tumor cell lines tested were found to have an extra copy of the Dbf4 gene (Bonte et al., 2008). Therefore, all the observations suggest that increased Cdc7/Dbf4 abundance is a common occurrence during tumorigenesis and may offset recovery or repair of replication forks arrest to enhance survival of some tumor cells.

5.3.1.4 Importance of the MCB elements in the human Dbf4 promoter

The mammalian homologues share many properties of the yeast Dbf4. For example, both mammalian and yeast Dbf4 proteins are crucial for initiation of DNA replication. Like in yeast, the human Dbf4 (HuDbf4) mRNA levels dramatically rise in late G_1, peak at the G_1/S boundary, and remain high in S phase (Jiang et al., 1999; Kumagai et al., 1999). Overall HuDbf4 mRNA levels reflect those of HuDbf4 protein as is the case in yeast (Jiang et al., 1999). HuDbf4 protein levels correspond to the formation of the Cdc7-Dbf4 protein complex which correlates with Cdc7 kinase activities (Jiang et al., 1999; Kumagai et al., 1999). It was found in both *in vitro* and *in vivo* assays that HuDbf4-HuCdc7 kinase can effectively phosphorylate HuMcm2 protein (Lei et al., 1997; Nougarede et al., 2000). Accumulating data suggest that Dbf4-Cdc7 kinase is directly involved in the regulation of DNA replication initiation for both yeast and mammals (Guo and Lee, 2001).

In order to further gain a understanding of how the transcription of Dbf4 is regulated, HuDbf4 has been cloned and characterized (Figure 5.7) and its core promoter activity was found within the nucleotide 211 to 285 upstream of the translation start-codon (i.e. -211 to -285). This 75bp DNA segment contains a putative *M1uI* cell cycle Box (MCB) with a 5'-ACGCGT-3' sequence among others (Sp1 as positive regulator, HES-1 as

repressor and TFIIB). A point change of the 'C' residue (adjacent to A) within the putative MCB to 'T' significantly reduced the promoter activity, suggesting that this element is critically important for the HuDbf4 core promoter activity (Wu and Lee, 2002).

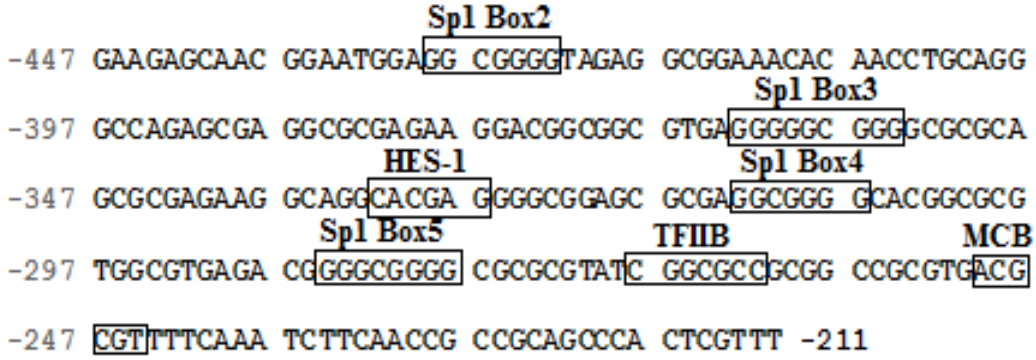

Figure 5.7 Diagram showing the alignment of human Dbf4 promoter sequence from -211 to -447. The putative transcription-factor binding sites are indicated in the boxes. The 75bp core promoter -211/-285 contains a putative MCB element (Wu and Lee, 2002).

MCB elements were also found in the promoter of most DNA synthesis genes in budding yeast, whose transcription in late G_1 depends on copies of a short sequence (MCB elements; ACGCGTNA). MCB elements are regulated mainly by MBF (MCB binding factor), which consists of Mbp1 and Swi6 (Koch et al., 1993; Koch and Nasmyth, 1994). In addition, SCB elements (Swi4 cell cycle boxes) also constitute important sequences present in the promoter like the MCB elements and are regulated by the transcription factor SBF (SCB binding factor) composed of Swi4 and Swi6 (Breeden and Nasmyth, 1987; Andrews and Moore, 1992). Downregulation of MCB genes is caused by inactivation of MBF. The deletion of both MBF and SBF leads to a lethal arrest, indicating that transcriptional activation by MBF and SBF is involved in controlling cell cycle progression (Nasmyth and Dirich, 1991; Koch et al., 1993).

5.4.1 Aims of the project

The sequence 5'-ACGCGT-3' (MCB) which occurs in the core HuDbf4 promoter is utilized in this thesis as a model system for investigating the effects of gene targeting by the polyamide f-IPI. The binding of f-IPI to the MCB *in vitro* and the cellular effects of f-IPI treatment (e.g. downregulation of HuDbf4, cell cycle effect, cell survival, proliferation and apoptosis) were assessed.

Subsequently, the targeting of the MCB in the promoter by the polyamides f-IP(C_3NH_2)I and f-IP(C_3Cl)I was assessed as part of the *in situ* formation of H-pin approach.

Lastly, polyamides containing the fluorescent Hx moiety were designed and tested with the aim of monitoring cellular uptake and nuclear localization. HxPI was additionally tested as a potential gene-control agent for the targeting of the HuDbf4 promoter model.

5.2 Results

In vitro binding characteristics of f-IPI to the Dbf4 and its cellular effects in MDA-MB231 cells

5.2.1 *In vitro* binding of f-IPI to the Dbf4 promoter

The chemical structures of f-IPI and its binding model have been described in Figure 3.2A&B. The binding model of f-IPI H-pin is the same as f-IPI and its chemical structure is shown in Figure 5.8A. F-IPI targets 5'-ACGCGT-3' the *MIuI* Cell cycle Box (MCB), which is a critical site for transcription factor binding and activation of expression of the HuDbf4 core gene in mammalian cells. A DNA fragment containing the core HuDbf4 promoter sequences (i.e. -285/-211) including the MCB as designed for footprinting analysis and is shown in Figure 5.8B.

To identify the pattern of f-IPI binding to the HuDbf4 promoter, DNase I footprinting was carried out using the fragment shown in Figure 5.8B. The autoradiograms presented in Figure 5.8C and D show the titration results for the two polyamides f-IPI and f-IPI H-pin. A clear footprint is observed for both polyamides over the MCB site at 0.1 and 0.05 μM respectively, indicating that the f-IPI H-pin exhibits a stronger DNA binding affinity than f-IPI (Figure 5.8C&D). A noticeable footprint at the site 5'-ACGCGC-3' is also observed for f-IPI and f-IPI H-pin at 0.5 μM and 0.1 μM respectively, because this sequence also contains the central sequence 5'-CGCG-3' required by f-IPI.

A

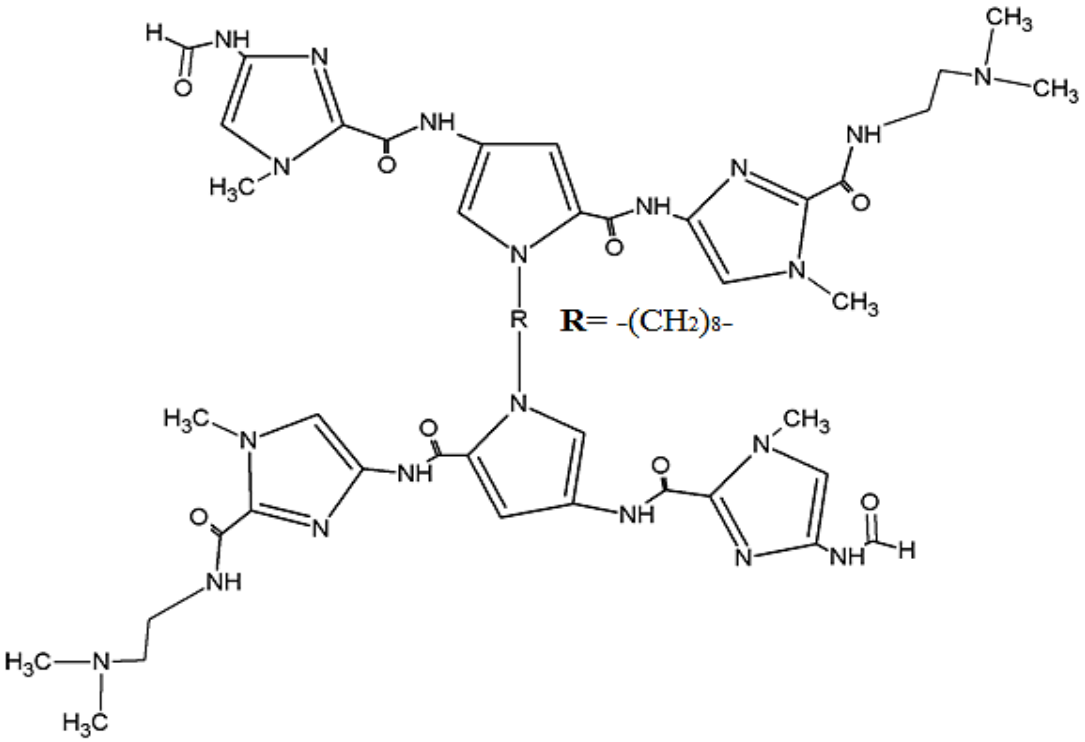
R= -(CH2)8-

B

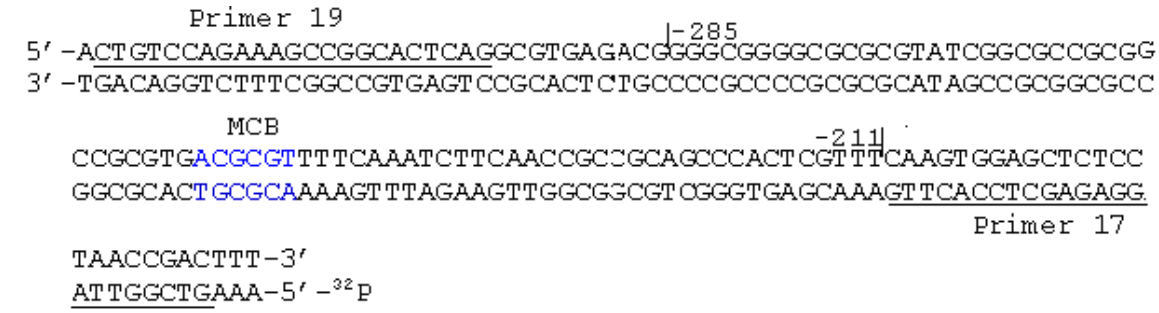
Primer 19
-285
5′-ACTGTCCAGAAAGCCGGCACTCAGGCGTGAGACGGGGCGGGGCGCGCGTATCGGCGCCGCGG
3′-TGACAGGTCTTTCGGCCGTGAGTCCGCACTCTGCCCCGCCCCGCGCGCATAGCCGCGGCGCC
MCB
-211
CCGCGTGACGCGTTTTCAAATCTTCAACCGCCGCAGCCCACTCGTTTCAAGTGGAGCTCTCC
GGCGCACTGCGCAAAAGTTTAGAAGTTGGCGGCGTCGGGTGAGCAAAGTTCACCTCGAGAGG
Primer 17
TAACCGACTTT-3′
ATTGGCTGAAA-5′-32P

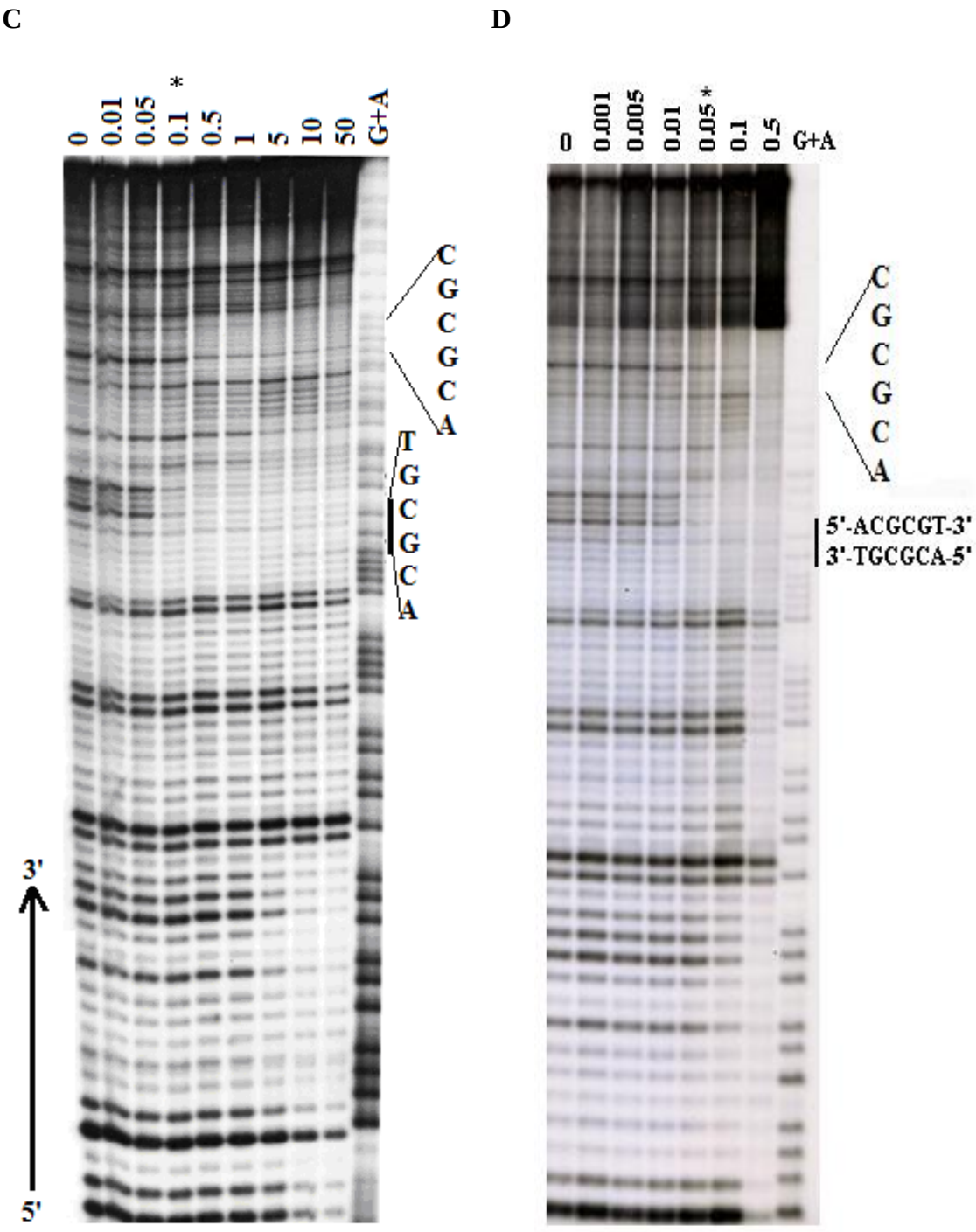

Figure 5.8 A The chemical structure of f-IPI-H-pin. DNase I footprinting was performed using (**B)** a 131bp 5'-[γ-^{32}P]-radiolabeled DNA fragment containing the Dbf4 promoter**.** Footprint gels show the DNA sequence specific binding of f-IPI (**C)** and f-IPI H-pin (**D)** to the cognate, target sequence 5'-ACGCGT-3' within the Dbf4 promoter. Asterisk indicates the concentration of polyamide at which protection from DNase I cleavage is initially observed. The cognate binding site is highlighted by solid bar. G+A refers to the sequencing lane.

To further demonstrate that f-IPI can bind to the MCB motif and potentially affect the HuDbf4 promoter activation, electrophoretic mobility shift assay (EMSA) studies were carried out using radiolabeled oligonucleotides containing the MCB sequence, incubated with f-IPI and nuclear extracts from MDA-MB231 cells. As shown in Figure 5.9A, pre-incubation of the radioactive oligonucleotides containing the MCB sequence (5'-ACGCGT-3') with f-IPI, for 1 h and subsequent addition of nuclear extracts results in the inhibition of protein binding to the MCB at drug concentrations >0.1 μM. No effect was observed when reactions are incubated with an excess of unlabeled mutated oligonucleotide (labeled M in Figure 5.9A-C, sequence as shown in Figure 5.9D), while shifted bands (denoted by the arrows) are competed out with an excess of unlabeled wild-type oligonucleotide, confirming the specificity of binding (labeled C in Figure 5.9). A supershift reaction (S1 labeled in Figure 5.9A) did not produce a supershifted band when incubating with the MCB transcription factor antibody (yeast anti-MBP1) with nuclear extracts from MDA-MB231 cells (Figure 5.9A). However, the disappearance of the band suggests that the MCB protein is part of the protein complex when compared to the band presents after treatment with a negative antibody (S2 labeled in Figure 5.9A). There are no other specific MCB antibodies commercially available and therefore it is difficult to further test the effect of f-IPI on protein-DNA interaction. A similar EMSA study of f-PPP was considered as a negative control because f-PPP cannot target the MCB motif. As expected no effect was observed by f-PPP at doses up to 100 μM (Figure 5.9B).

An EMSA study of f-IPI H-pin was also carried out due to its great binding affinity observed by DNase I footpinting. As shown in Figure 5.8C, the inhibition of protein binding is found with treatment with f-IPI H-pin and the effect was observed at 0.05

μM, suggesting an approximately10-fold enhanced binding affinity at the MCB site compared to f-IPI. The EMSA results are consistent with the DNase I footprinting studies, which also revealed the enhanced effect of f-IPI H-pin over f-IPI on DNA binding affinity. The same experiments were repeated with nuclear extracts allowed to react with the radioactive oligonucleotides first, for 1 h, before the addition of the three polyamides. The protein binding inhibition patterns are identical (data not shown) suggesting that these polyamides can not only compete but also displace transcription factors already bound to DNA, including MCB.

A

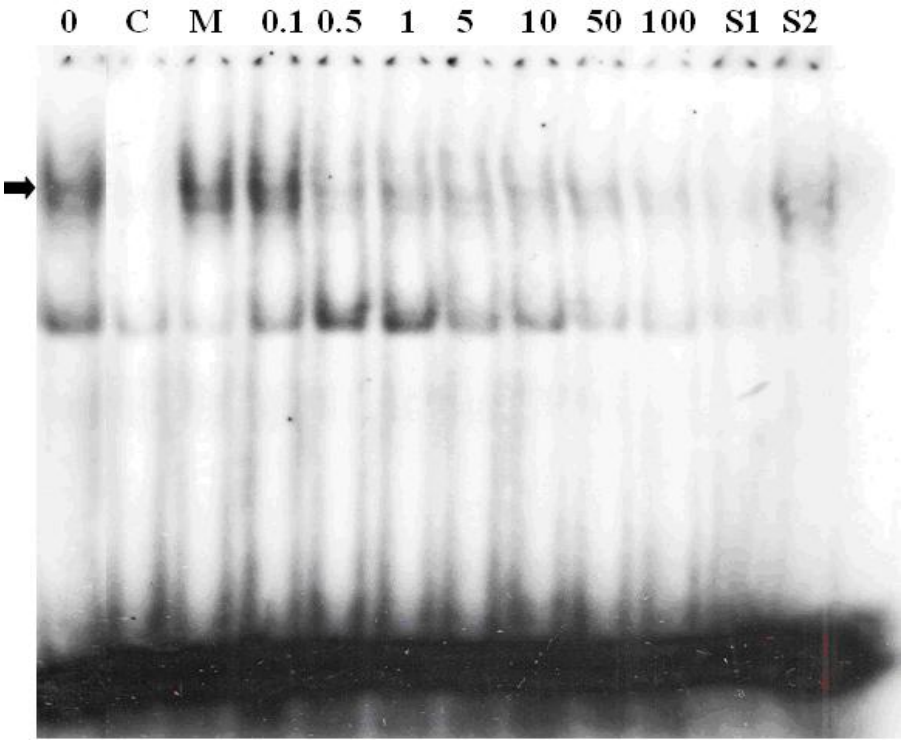

f-IPI

B

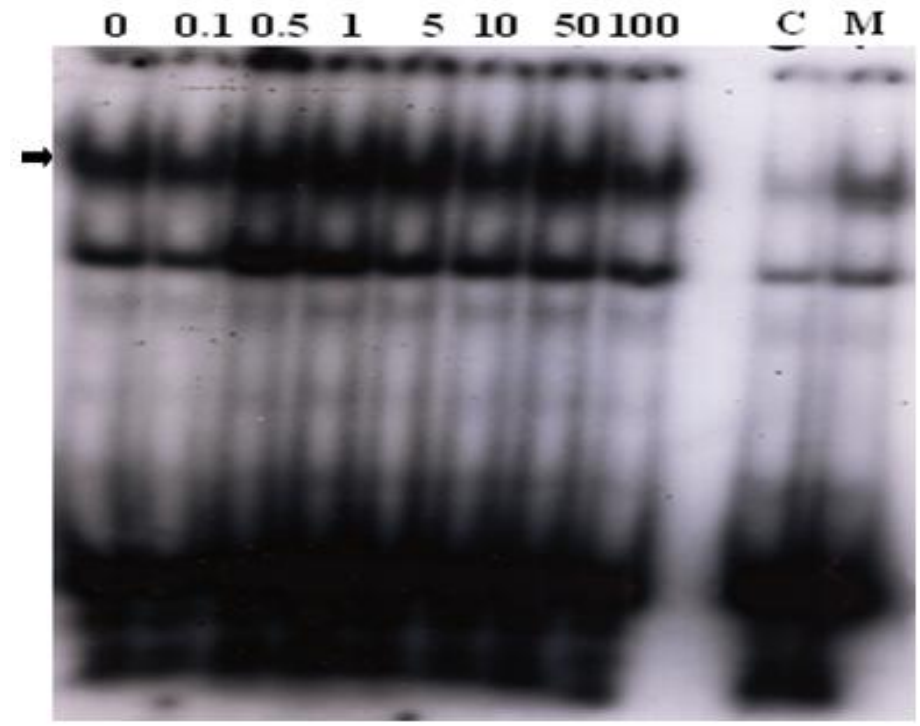

f-PPP

C

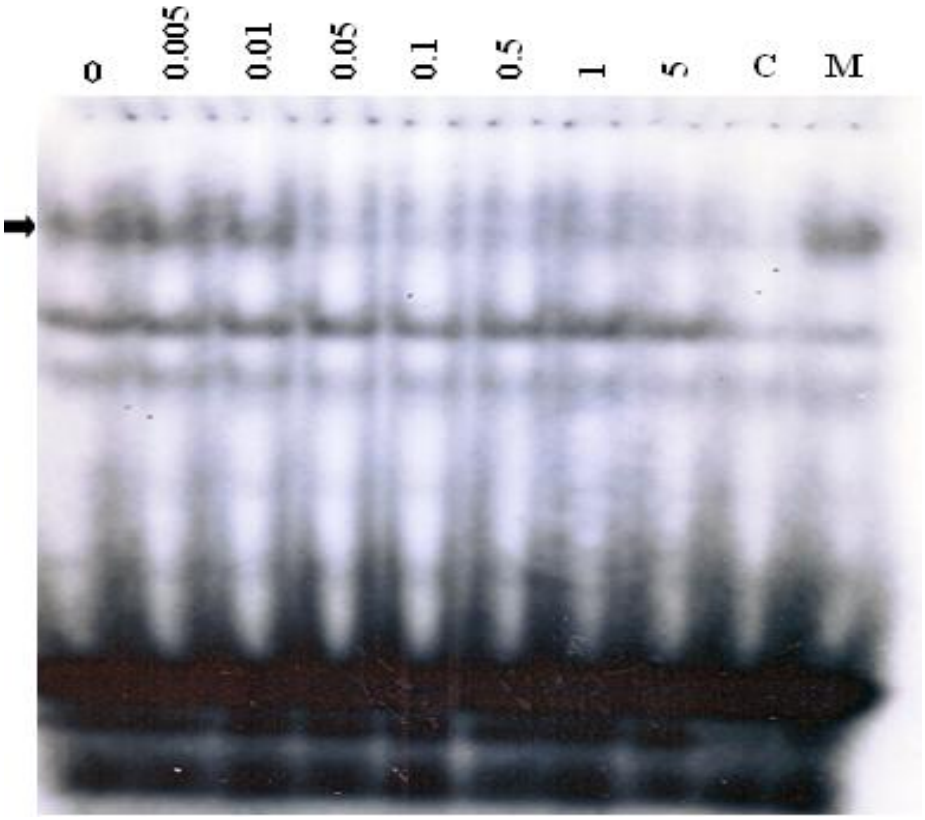

f-IPI H-pin

D

MCB wild type oligo: 5'-GCGTGACGCGTTTTCAAATCTTCAACC-3'
MCB mutant oligo: 5'-GCGTGAC*TA*GTTTTCAAATCTTCAACC-3'

Figure 5.9. Interaction of f-IPI and its analogues with the MCB in the HuDbf4 promoter. **A**, **B** and **C**, Electrophoretic Mobility Shift Assay studies (EMSAs) were carried out using 10 µg MDA-MB231 nuclear extracts and the radioactive DNA probe shown in (**D**). The arrow denotes the DNA-protein complex. A dose-dependent inhibition of protein binding to the MCB by f-IPI (**A**), f-PPP (**B**) and f-IPI H-pin (**C**) was observed, respectively. Lane C and M represent reactions with unlabeled and mutated MCB oligonucleotides. S1 represents reaction using anti-MCB antibody (yeast) and S2 was treated with a negative antibody.

5.2.2 Validation of $\Delta\Delta C_t$ method for RT-PCR experiments

Before using the $\Delta\Delta C_t$ (C_t is cycle threshold) method for quantitation, a validation experiment was performed as shown in Figure 5.10 to demonstrate that efficiencies of target gene (e.g Dbf4 Figure 5.10A) and reference gene (e.g. GAPH Figure 5.10B) are approximately equal. The absolute value of the slope of log input amount vs.ΔCT should be < 0.1. The slope in Figure 5.10C is 0.0936 with acceptable limits. The $\Delta\Delta C_t$ calculation method can subsequently be used for the relative quantitation of the target gene without running standard curves on the same plate.

A

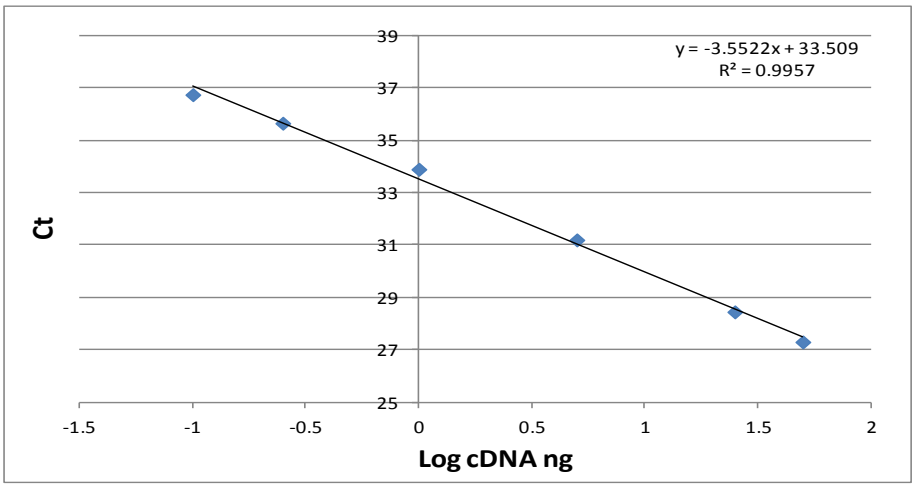

B

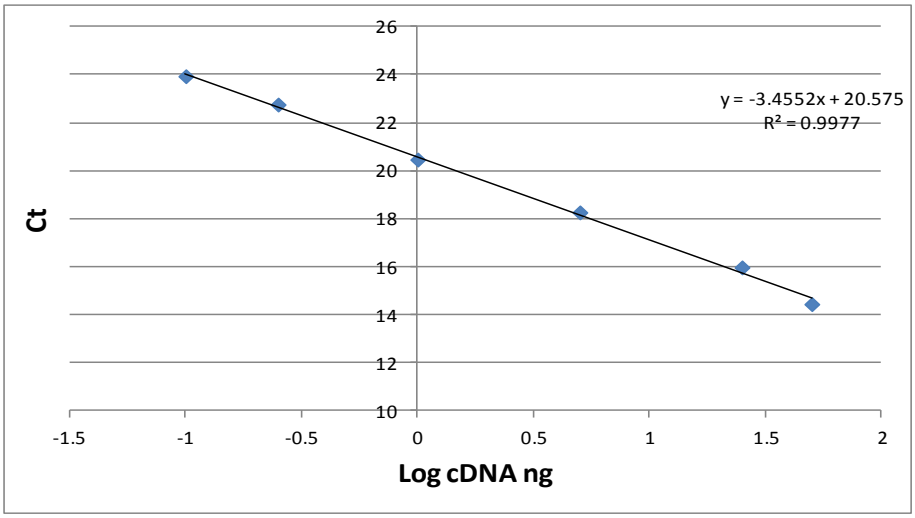

C

Input Amount ng Total cDNA	Dbf4 Average Ct	GAPDH Average Ct	ΔCt Dbf4 -GAPDH	Log cDNA
50	27.3028	14.4503	12.8525	1.69897
25	28.45625	15.97895	12.4773	1.39794
5	31.20035	18.27155	12.9288	0.69897
1	33.90815	20.4684	13.43975	0
0.25	35.65765	22.762	12.89565	-0.60206
0.1	36.74585	23.9423	12.80355	-1

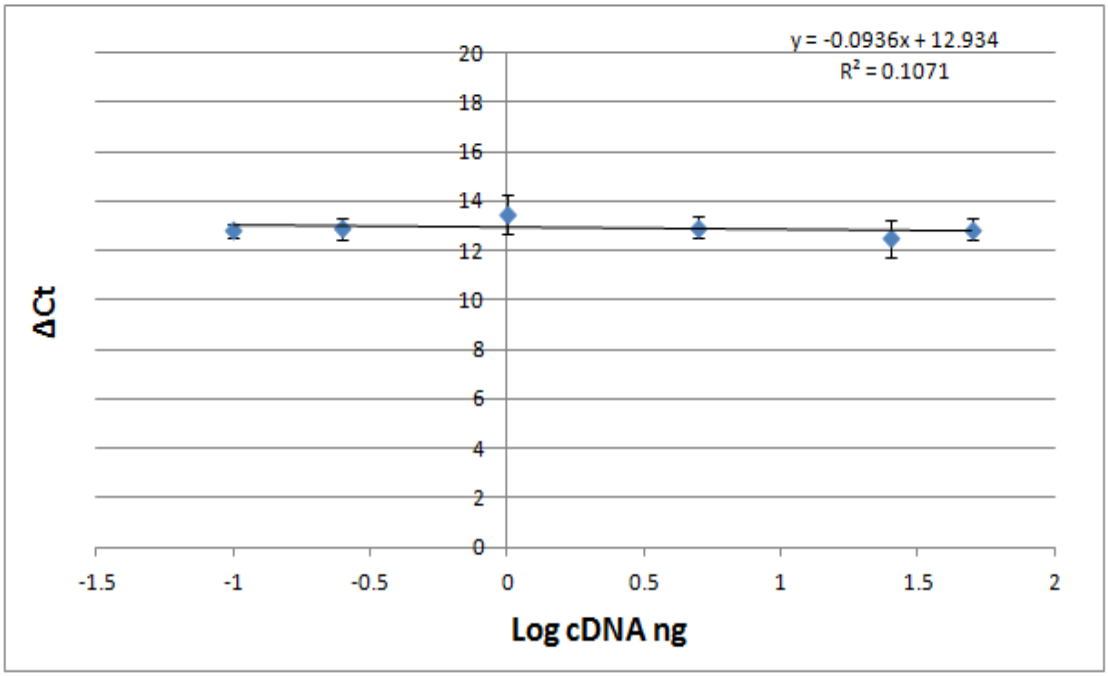

Figure 5.10. Standard curve of Dbf4 and GAPDH. **A**, The standard curve of amplification of the Dbf4 target detected using FAM-labeled probe. **B**, The standard curve of amplification of the GAPDH endogenous control detected using FAM-labeled probe. **C**, Relative efficiency plot of Dbf4 and GAPDH

5.2.3 Effects of f-IPI and f-IPI H-pin on the cellular levels of HuDbf4: RT-PCR and western blot analysis

The effects of f-IPI on Dbf4 expression were analyzed in exponentially growing MDA-MB231 cells. Following incubation of exponentially growing cells with 50, 100 and 200 μM of f-IPI, there was a 32%, 50% and 57% reduction in Dbf4 mRNA levels at 24 h, respectively, compared to untreated cells (Figure 5.11A). However, no reduction of Dbf4 mRNA levels occurred at 24 h after incubation with 50 and 100 μM of f-IPI H-pin (Figure 5.11B).

In order to further demonstrate whether polyamides could be developed as cellular gene control agents, the ability of f-IPI monomer and f-IPI H-pin to enter the nucleus of cells and subsequently affect protein levels was investigated using western blotting. Exponentially growing MDA-MB231 cells were incubated with 50 μM and 100 μM of f-IPI and f-IPI H-pin for 24 h. Western blot analysis of treated cells was performed and the results are shown in Figure 5.12A and B. The results demonstrate that f-IPI inhibits Dbf4 protein expression after 24 h of exposure in a dose-dependent fashion (Figure 5.11A). This is in contrast to f-IPI H-pin, which even at 100 μM did not affect Dbf4 protein levels after a 24 h incubation (Figure 5.11B). As a loading control, the levels of calnexin in the cells were probed with the appropriate antibody, and they were found to be unaffected. This indicates that the cells were viable and the overall gene expression machinery was not impaired. In addition, the Cdc7 protein levels remained unchanged even when cells were treated with the highest concentration (100 μM) of f-IPI.

A

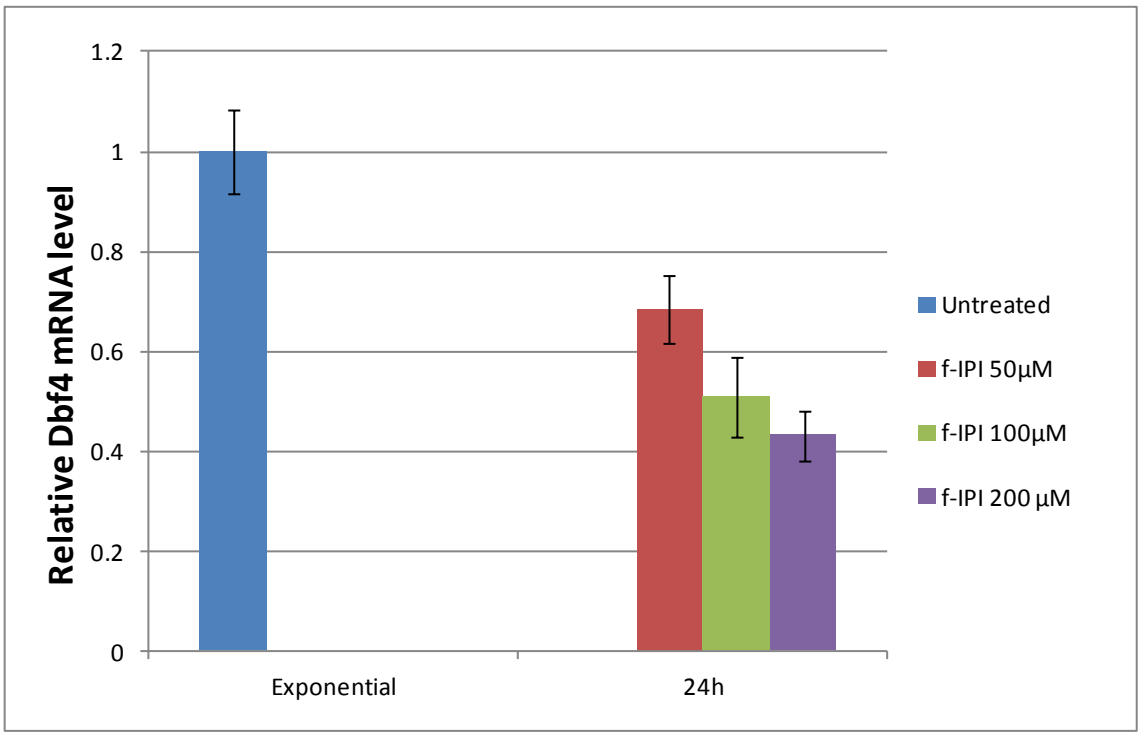

B

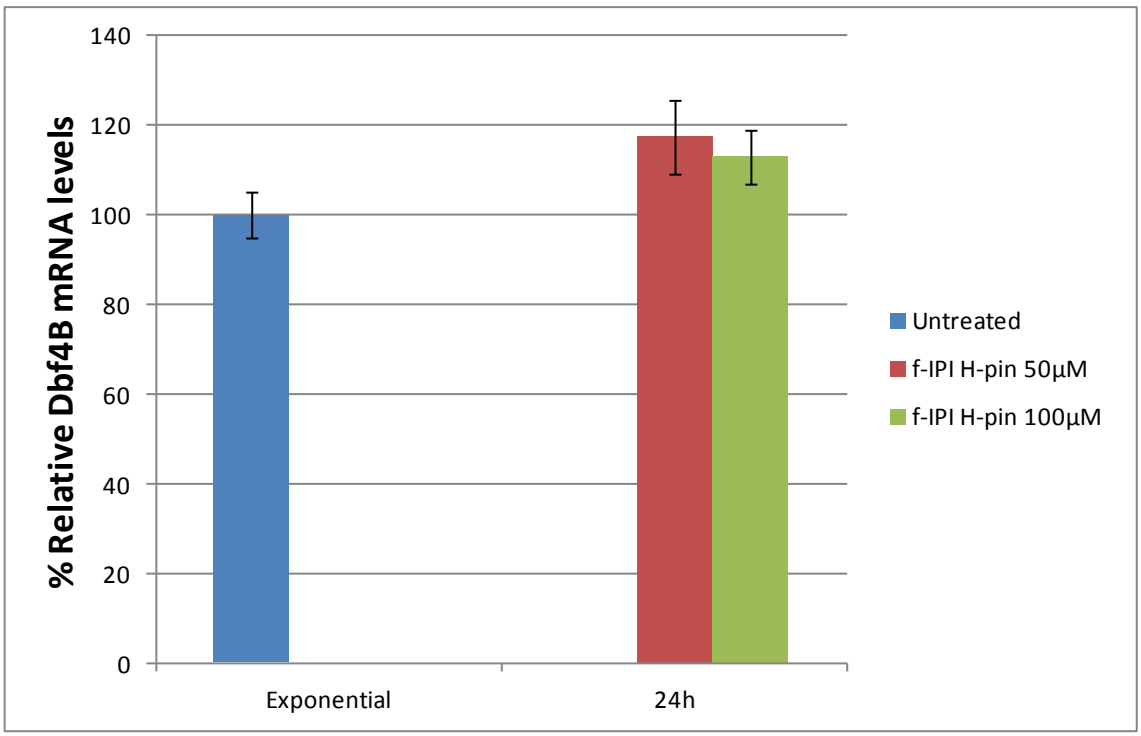

Figure 5.11. Exponentially growing MDA-MB231 cells were treated with f-IPI (**A**) and f-IPI H-pin (**B**) for 24 h. mRNA levels in f-IPI and f-IPI H-pin-treated cells were expressed relative to untreated cells. Results are the mean of three independent experiments with error bars showing the standard deviation of the mean.

A

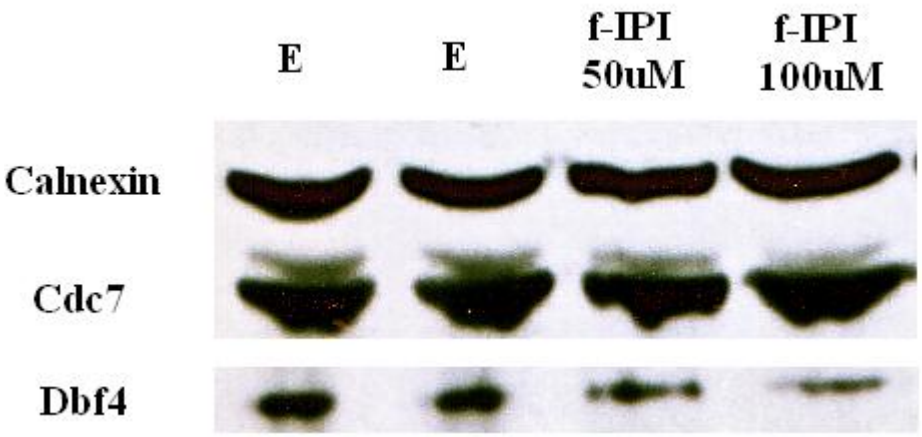

B

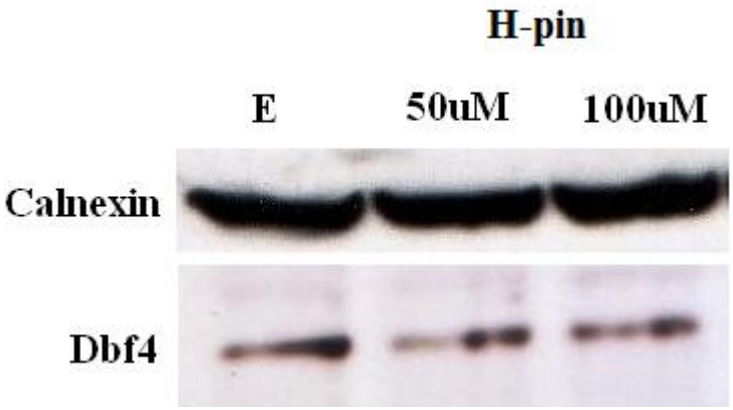

Figure 5.12 Western blot analysis of exponentially growing MDA-MB231 cell extracts following treatment with f-IPI (**A**) and f-IPI H-pin (**B**). Exponential cells were treated with 50 and 100 μM f-IPI and f-IPI H-pin respectively and analysis was carried out on samples collected after 24 h of drug treatment as indicated. Calnexin is shown as a loading control. Protein and RNA samples from exponentially growing cells (E).

5.2.4 Validation of Dbf4 siRNA knockdown

In order to elucidate the role of Dbf4 in MDA-MB231 cells, a siRNA-mediated strategy to knock down the endogenous levels of Dbf4 was employed. The efficiency of Dbf4 siRNA knockdown was assessed at the mRNA level, as determined by RT-PCR (Figure 5.13A). The Figure 5.13A shows the 80-90% reduction of Dbf4 mRNA levels at 24, 48, 72 and 96 h post-transfection with the Dbf4 siRNA.

A

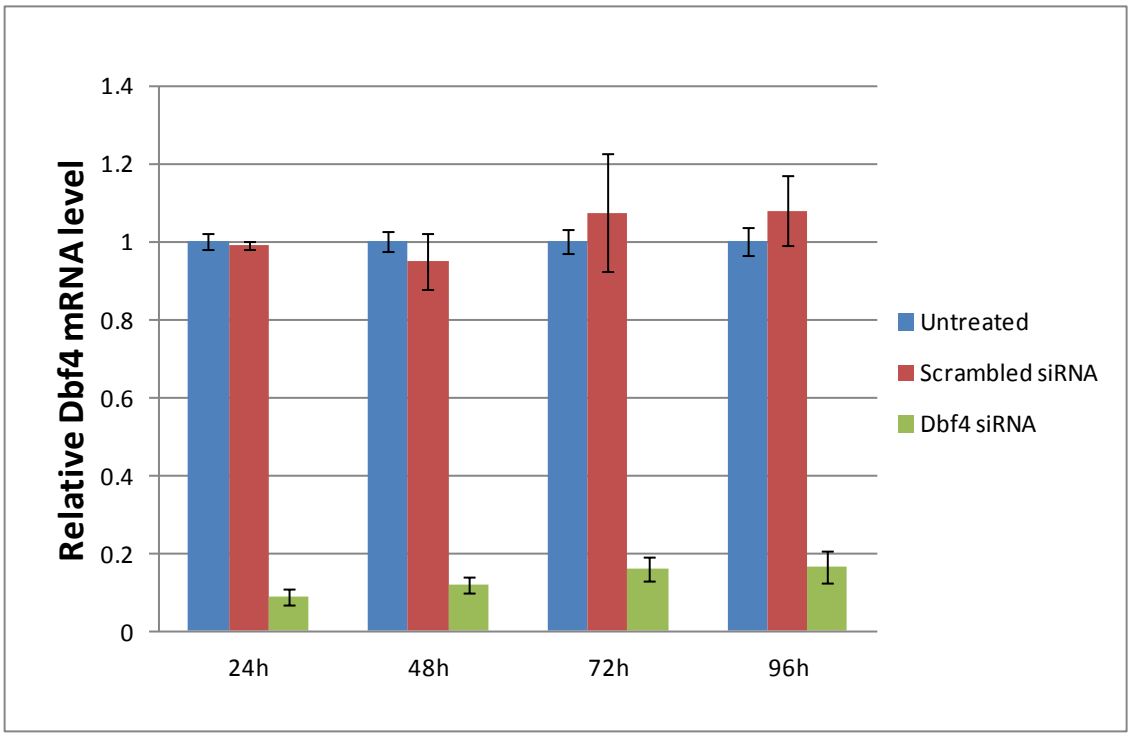

Figure 5.13. **A**, Dbf4 mRNA levels were quantified via RT-PCR after siRNA knockdown at 24, 48, 72 and 96 h. mRNA levels in scrambled and Dbf4 siRNA knockdown cells relative to untreated-exponentially growing cells. Results are the mean of two independent experiments with error bars showing the standard deviation of the mean.

5.2.5 Effects of the depletion of endogenous Dbf4 by siRNA in MDA-MB231 cells

To elucidate the association between loss of endogenous Dbf4 and MDA-MB231 cell growth, proliferation and apoptosis, the kinetics of cell viability, cell proliferation and cell apoptosis were measured by the presence of ATP (CellTiter-Glo assay), BrdU incorporation (BrdU assay), and Caspase3/7 activity (Caspase3/7 assay), respectively.

The luminescence levels of Dbf4 siRNA-treated MDA-MB231 cells in the cell viability assay (CellTiter-Glo assay) are proportional to the number of metabolically active cells. Figure 5.14A shows the luminescence levels of Dbf4 siRNA-treated cells which were then converted to the relative percentage of cell viability (Figure 5.14B). There is a 11.4%, 14% and 16.6% reduction of cell viability compared to the scrambled siRNA-treated control at 24, 48 and 72 h post-transfection, respectively (Figure 5.14B). The luminescence levels of Dbf4 siRNA treated cells in the cell apoptosis assay (Caspase3/7 assay) represent the number of dead cells. Figure 5.14C and D show the luminescence levels of treated cells with the resulting percentages of cell apoptosis. The Dbf4 siRNA-treated cells show higher levels of apoptosis compared to the untreated, transfection reagent treated and scrambled siRNA-treated cells at 24, 48 and 72 h, however the percentage of apoptosis is <3% at each time point, suggesting that siRNA-mediated knockdown of Dbf4 is not significantly cytotoxic (Figure 5.14D).

The absorbance of Dbf4 siRNA-treated MDA-MB231 cells in the proliferation assay (BrdU assay) is proportional to the cellular DNA content. Figure 5.14E shows the absorbance of Dbf4 siRNA treated cells, converted to the relative percentages of cell proliferation in Figure 5.14F. Figure 5.14F shows the decreased proliferation of treated

cells (~10%) compared to the scrambled siRNA treatment at 24, 48 and 72 h, respectively.

A

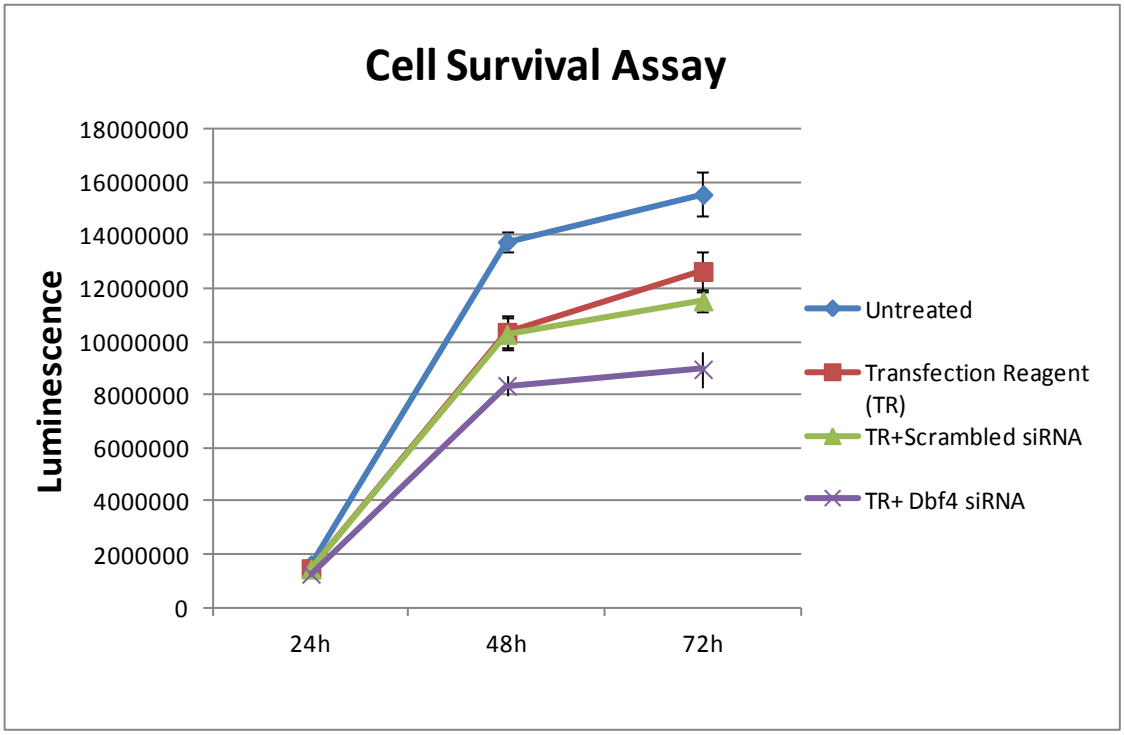

B

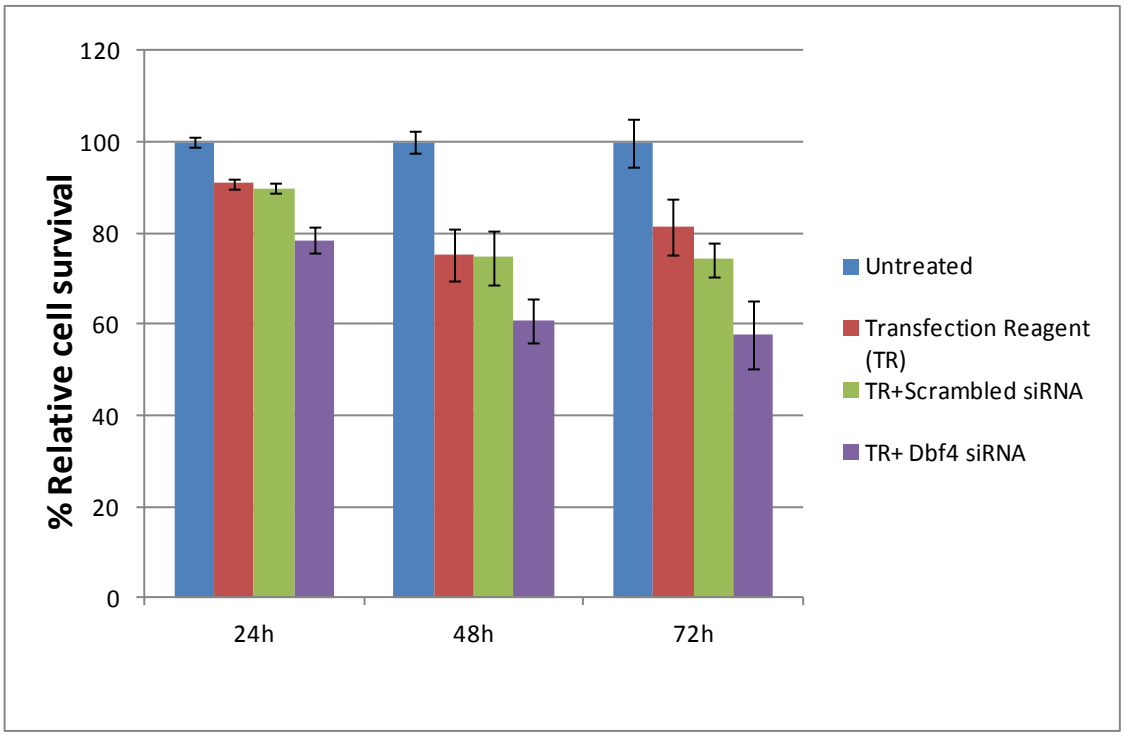

C

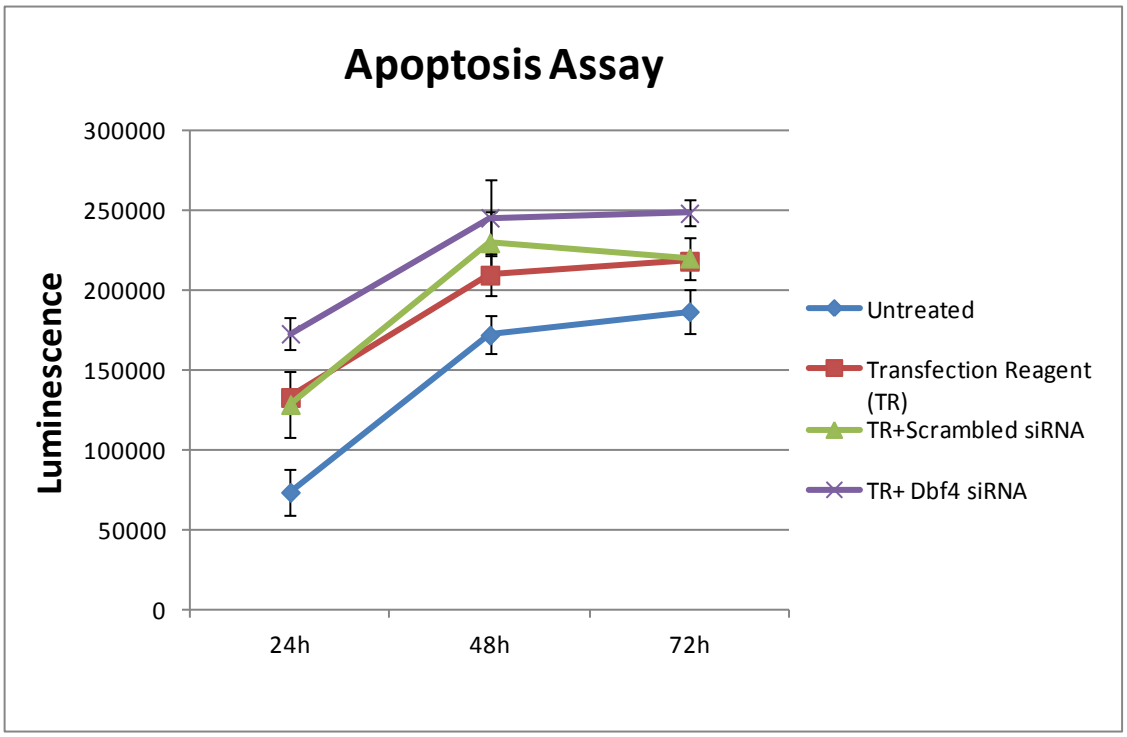
Apoptosis Assay
Luminescence
300000
250000
200000
150000
100000
50000
0
24h
48h
72h
Untreated
Transfection Reagent (TR)
TR+Scrambled siRNA
TR+ Dbf4 siRNA

D

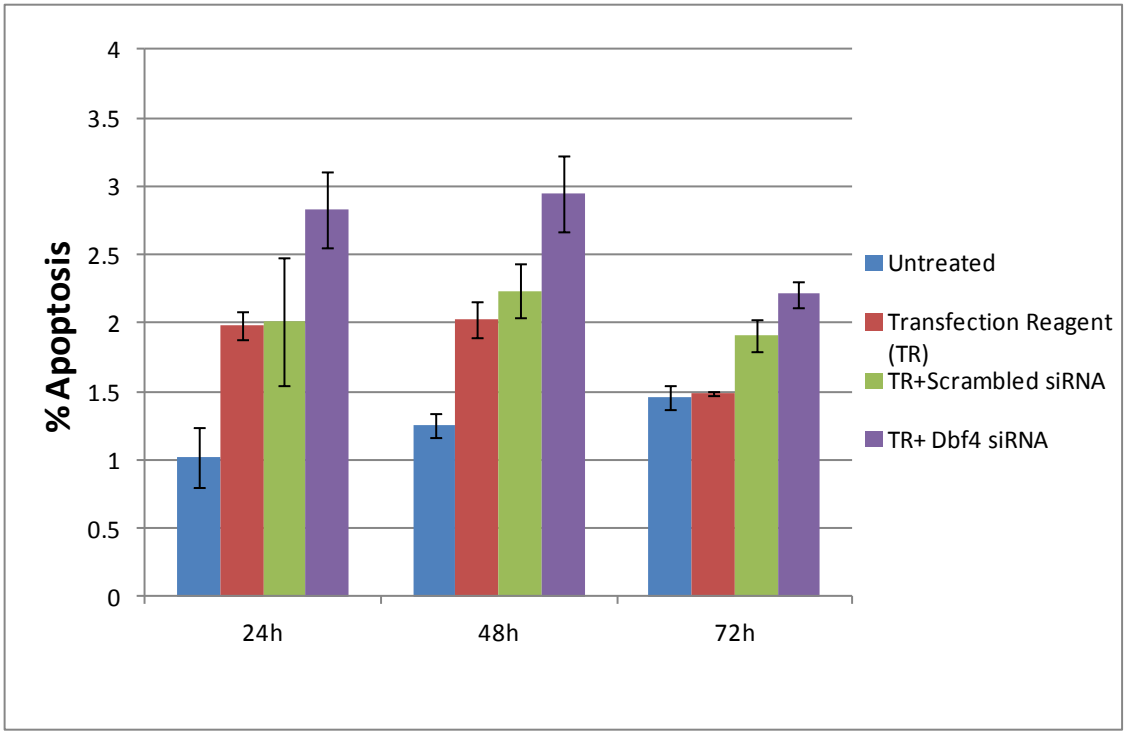
% Apoptosis
4
3.5
3
2.5
2
1.5
1
0.5
0
24h
48h
72h
Untreated
Transfection Reagent (TR)
TR+Scrambled siRNA
TR+ Dbf4 siRNA

E

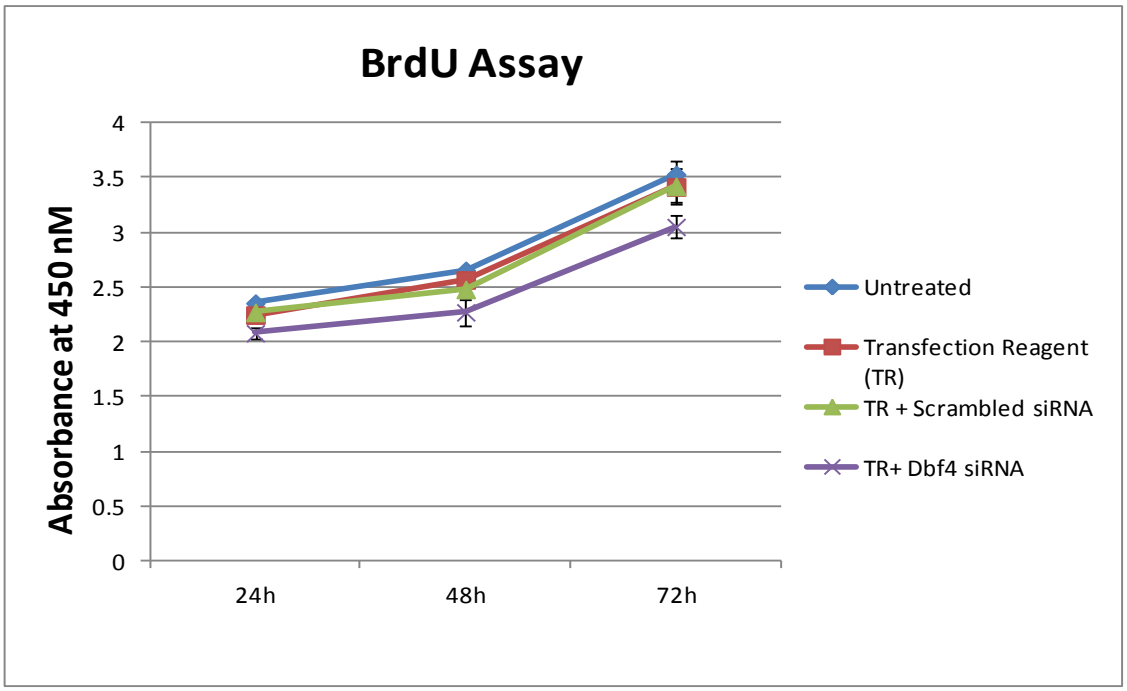

F

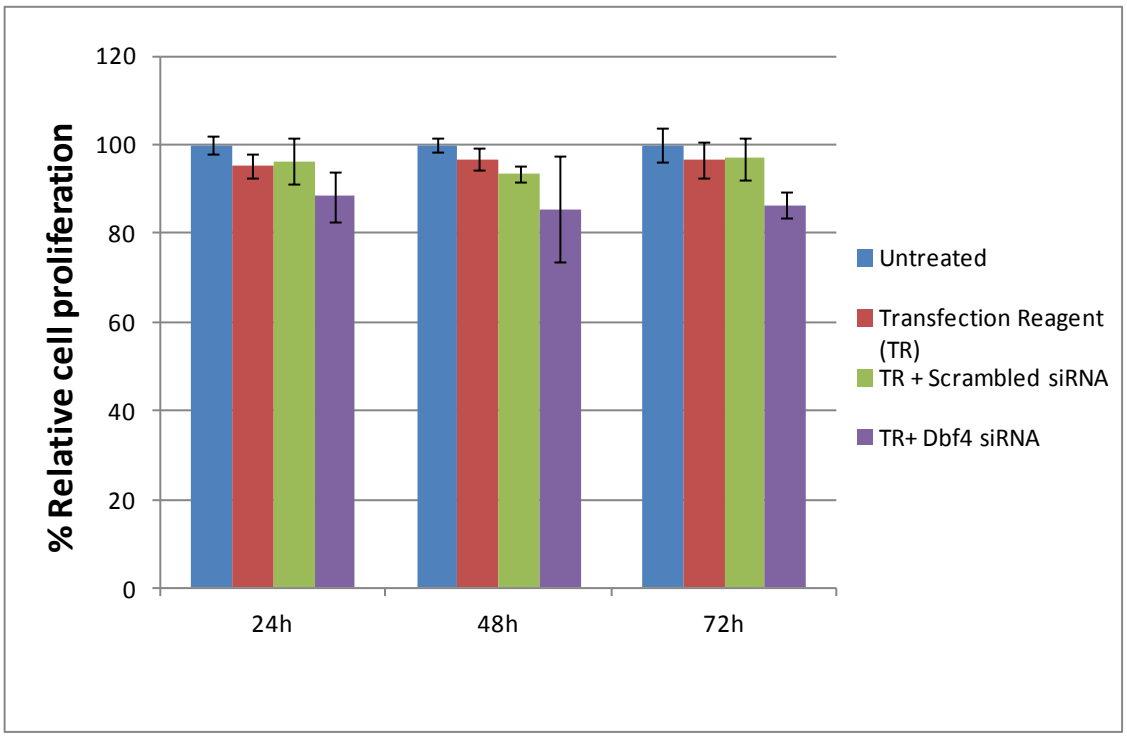

Figure 5.14 Cell survival, apoptosis and proliferation analysis of siRNA-treated MDA-MB231 cells. **A**, Kinetics of cell survival after siRNA treatment of MDA-MB231 cells (CellTiter-Glo assay at 24, 48 and 72 h). **B**, Relative percentage of viable cells at 24, 48 and 72 h after siRNA treatment. **C**, Kinetics of cell apoptosis after siRNA treatment of MDA-MB231 cells (Caspase-Glo 3/7 assay at 24, 48 and 72 h). **D**, Percentage of apoptotic cells at 24, 48 and 72 h after siRNA treatment. **E**, Kinetics of cell proliferation after siRNA treatment of MDA-MB231 cells (BrdU incorporation assay at 24, 48 and 72 h). **F**, Relative percentage of cell proliferation at 24, 48 and 72 h after siRNA treatment. Results are the mean of three independent experiments with error bars showing the standard deviation of the mean.

5.2.6 Dbf4 siRNA knockdown-induced G_1 arrest in MDA-MB231 cells

To further investigate the effect of Dbf4 on the MDA-MB231 cells, cell cycle analysis of untreated, scrambled-control and Dbf4 siRNA knockdown cells was performed after 24 and 48 h post-transfection. Harvested cells were subjected to analysis by flow cytometry, which used DNA content as a measure of progression in the cell cycle. There was no significant difference in the percentage of cells in each phase of the cell cycle between different treatments, 24 h post-transfection (Figure 5.15A). However, at 48 h, there was an 8% increase in the number of Dbf4 siRNA treated cells at G_1 compared to scrambled control (Figure 5.15B). The data suggest that the Dbf4 siRNA knockdown induces a small G_1 arrest in MDA-MB231 cells. This is consistent with the previous finding that Dbf4 is required for the initiation of DNA replication and presents high levels in G_1/S, thus the downregulation of Dbf4 could result in G_1 arrest of cells.

5.2.7 Effects of f-IPI treatment on the cell growth, proliferation and apoptosis in the MDA-MB231 cells

To investigate the effects of f-IPI in MDA-MB231 cells, the same assays as in section 5.2.5 were carried out.

The luminescence levels of f-IPI treated cells in the viability assay gradually reduce in response to increasing concentrations of f-IPI at 24, 48 and 72 h, respectively (Figure 5.16A). The relative percentages of cell viability are presented in Figure 5.16B. The dose-dependent treatments of f-IPI (50 µM, 100 µM and 200 µM) exhibit respective 70%, 40% and 22% cell survival at 72 h compared to the untreated control (Figure 5.16B). Similarly, the luminescence levels in the apoptosis assay increase in response to

increasing concentrations of f-IPI at 24, 48 and 72 h, respectively (Figure 5.16C). As shown in Figure 5.16D, 200 μM f-IPI treatment induces the highest levels of apoptosis at each time point. f-IPI treatments are much more cytotoxic than siRNA knockdown.

The absorbance of f-IPI treated cells in the cell proliferation assay decreases in response to increasing concentrations of f-IPI at 24, 48 and 72 h, respectively (Figure 5.16E). The relative percentages of cell proliferation are shown in Figure 5.16F. There is a 32%, 35% and 37% decrease of cell proliferation in the 200 μM f-IPI treated cells at 24, 48 and 72 h, respectively (Figure 5.16F).

5.3.8 f-IPI treatment-induced G_1 arrest in MDA-MB231 cells

Cell cycle analysis of control and f-IPI treated-cells was performed at 24 h (Figure 5.17). 7% and 10.3% increase of cells in G_1 were observed at 24 h after f-IPI treatments compared to the untreated-control (Figure 5.17 middle and lower panel). F-IPI treatment-induced G_1 arrest in MDA-MB231 cells might therefore be associated with alteration of the Dbf4 protein levels, downregulated by f-IPI binding to the MCB site in the Dbf4 promoter.

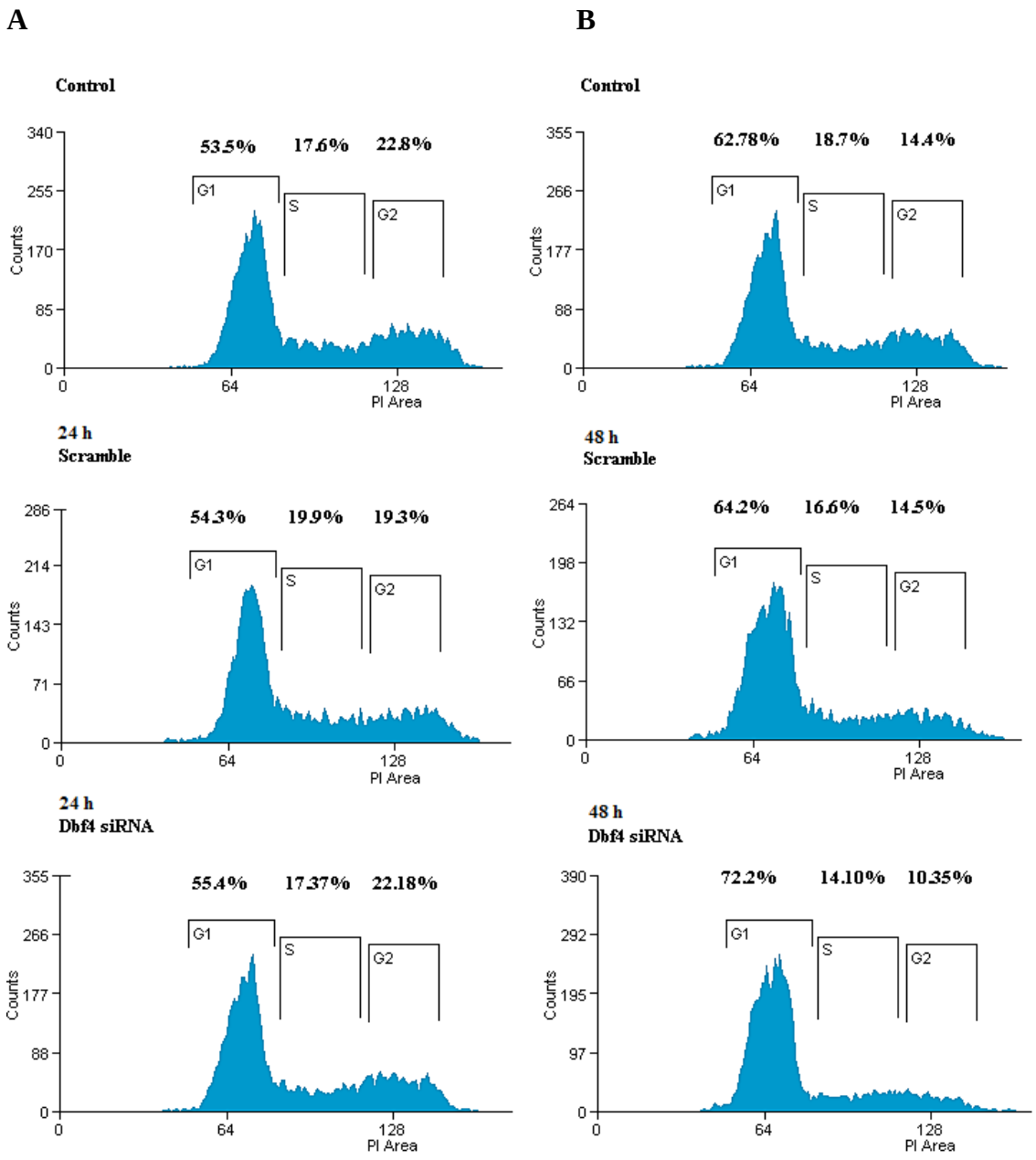

Figure 5.15. Flow cytometry analysis after siRNA treatment of MDA-MB231 cells. **A** and **B**, untreated-(upper panel), scrambled siRNA (middle panel) and Dbf4 siRNA (lower panel) treated- MDA-MB231 cells 24 h and 48 h post-transfection, respectively. Percentage of cells at different phases of the cell cycle was counted using Summit 4.3 software.

A

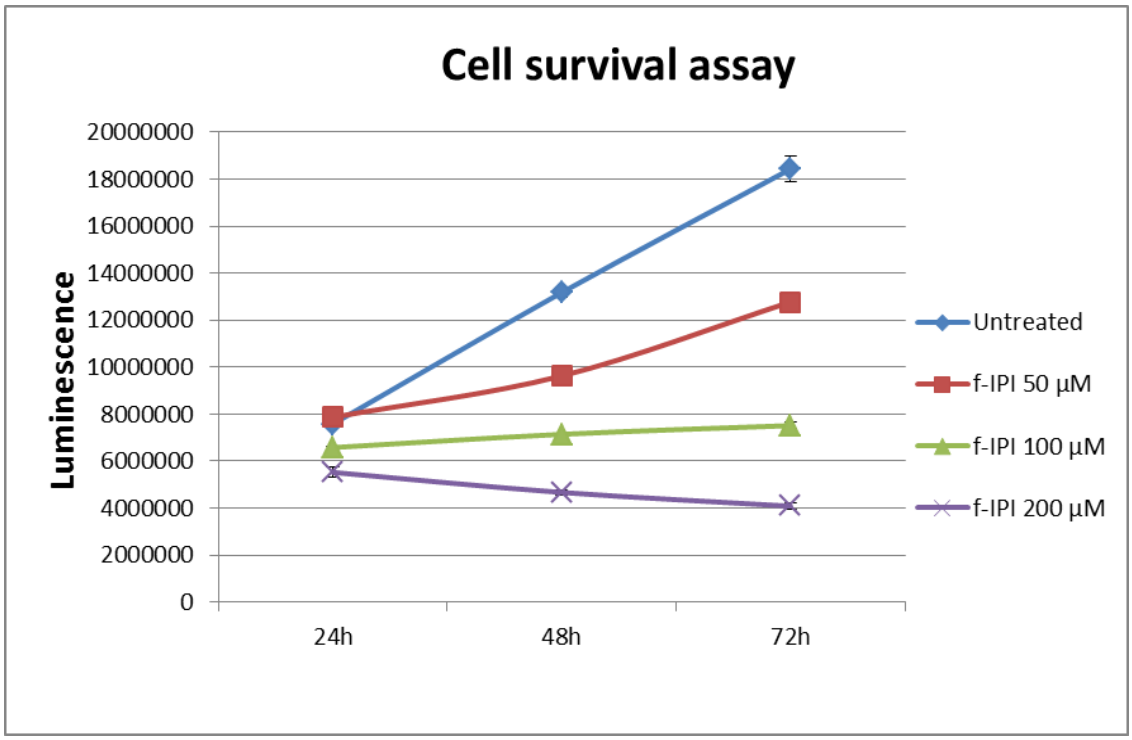
Cell survival assay
Luminescence
20000000
18000000
16000000
14000000
12000000
10000000
8000000
6000000
4000000
2000000
0
24h
48h
72h
Untreated
f-IPI 50 µM
f-IPI 100 µM
f-IPI 200 µM

B

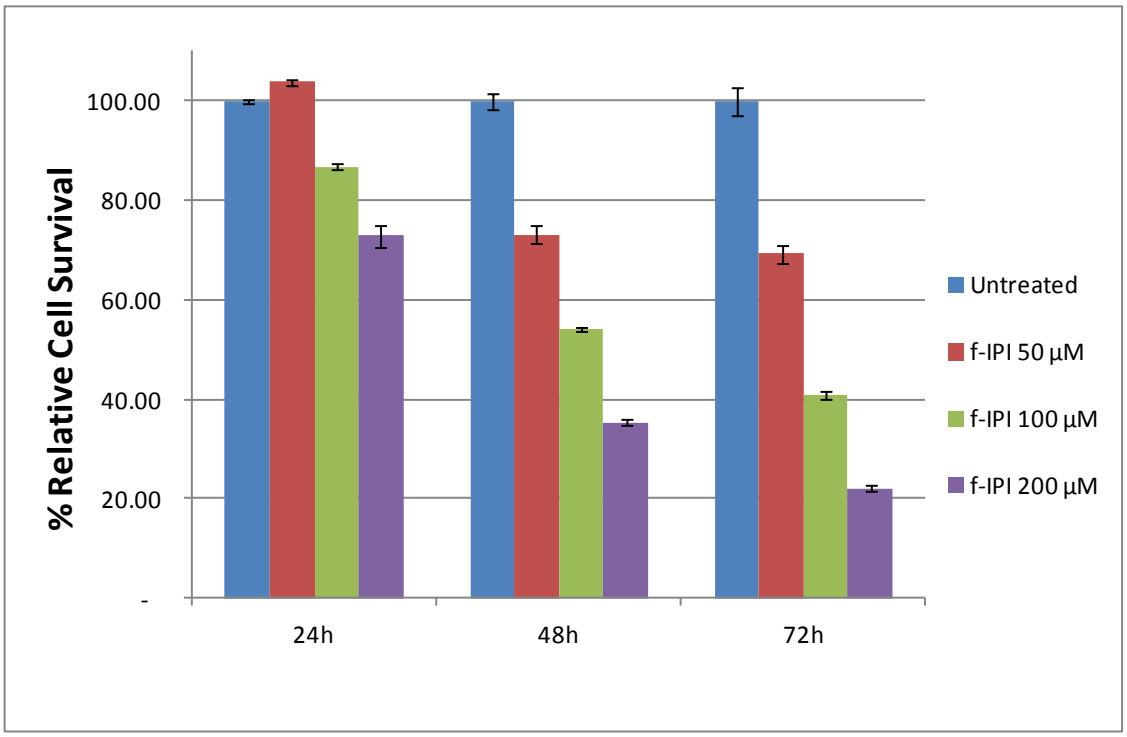
% Relative Cell Survival
100.00
80.00
60.00
40.00
20.00
-
24h
48h
72h
Untreated
f-IPI 50 µM
f-IPI 100 µM
f-IPI 200 µM

C

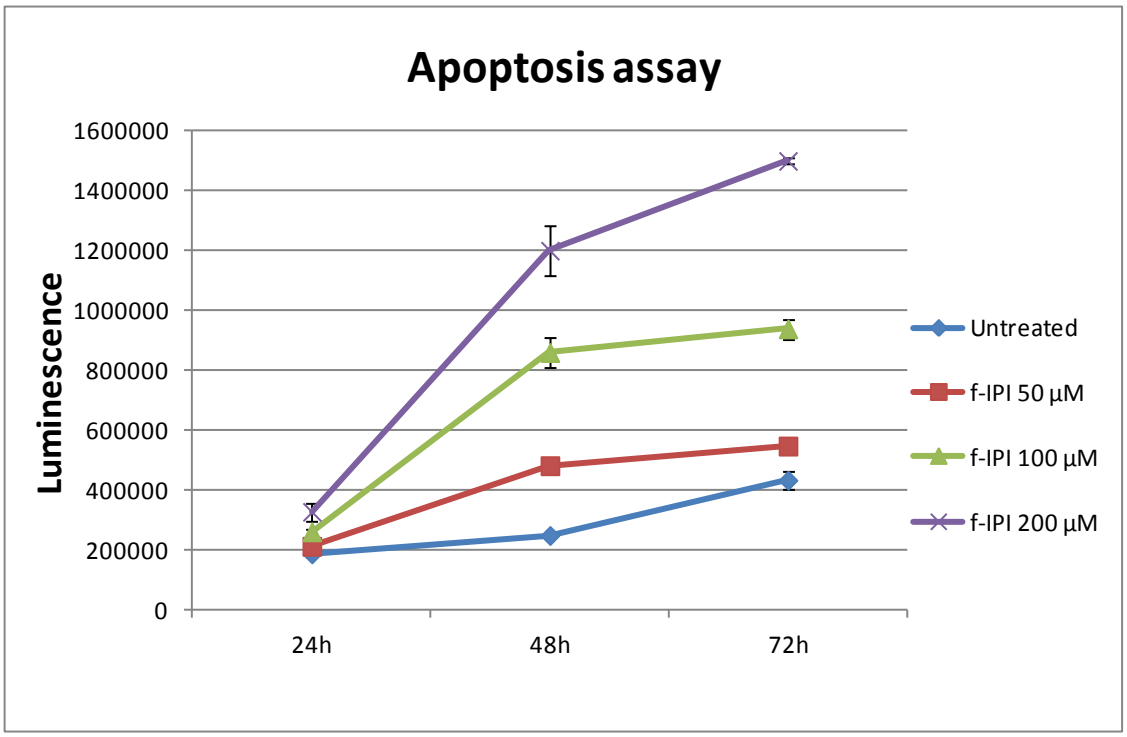
Apoptosis assay
Luminescence
1600000
1400000
1200000
1000000
800000
600000
400000
200000
0
24h
48h
72h
Untreated
f-IPI 50 µM
f-IPI 100 µM
f-IPI 200 µM

D

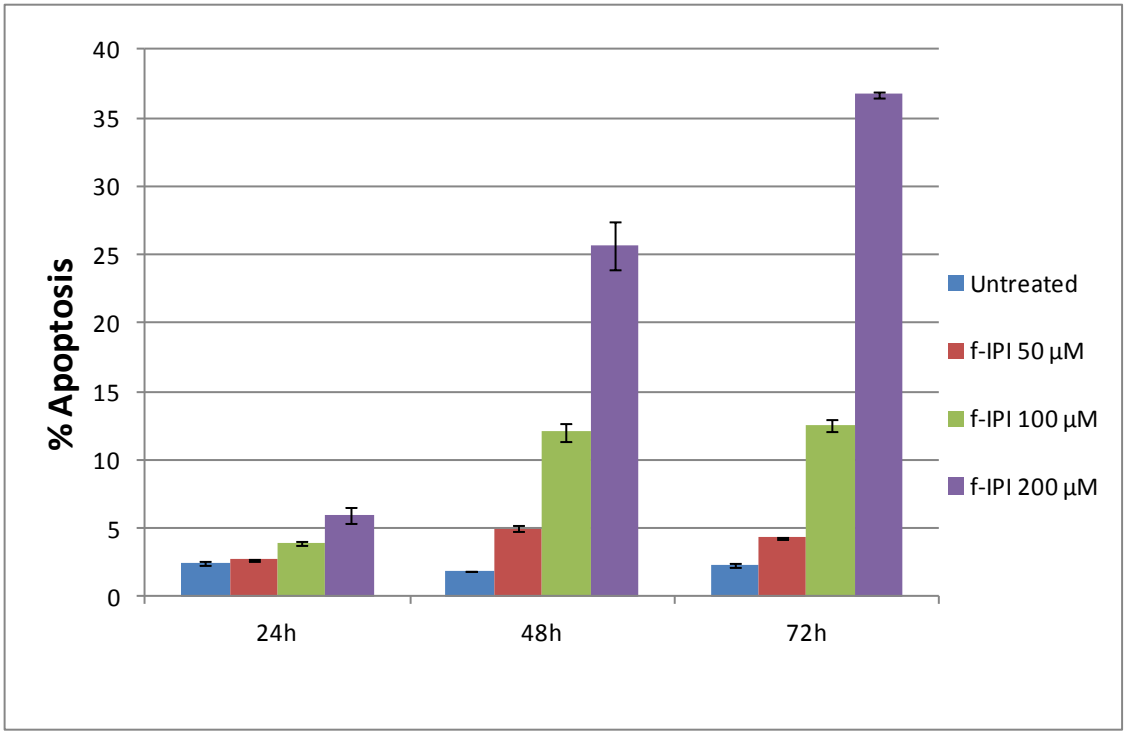
% Apoptosis
40
35
30
25
20
15
10
5
0
24h
48h
72h
Untreated
f-IPI 50 µM
f-IPI 100 µM
f-IPI 200 µM

E

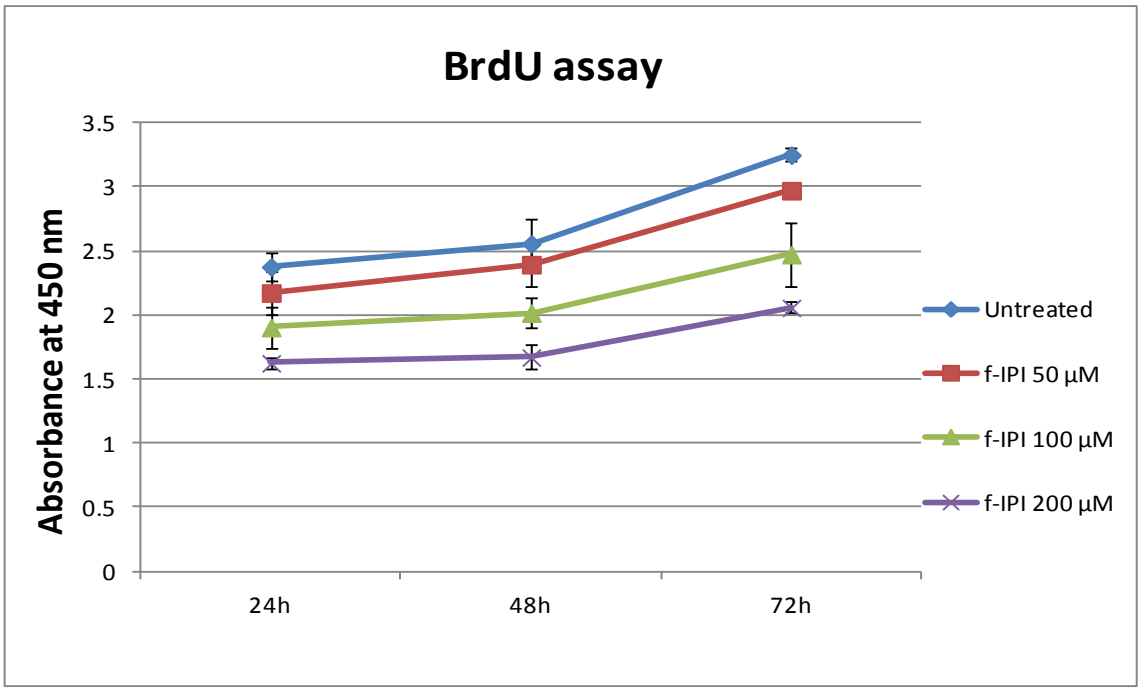

F

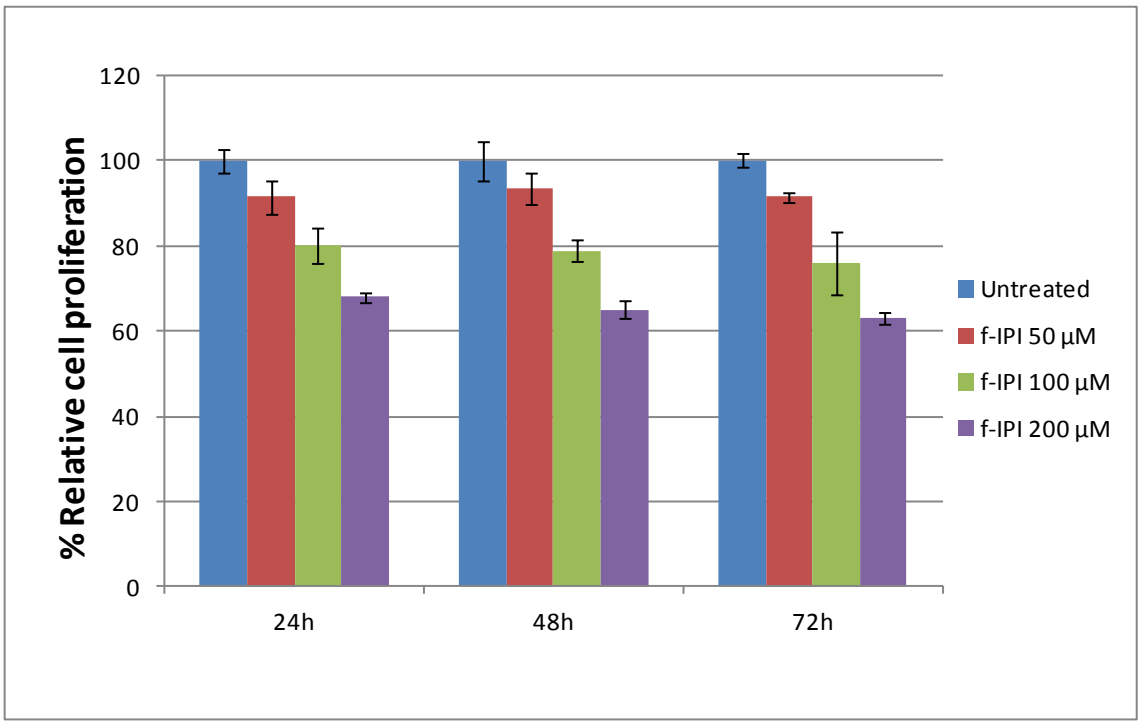

Figure 5.16 Cell survival, proliferation and apoptosis analysis of f-IPI-treated MDA-MB231 cells. **A**, Kinetics of cell survival after 50 and 100 µM f-IPI treatment of MDA-MB231 cells (CellTiter-Glo assay at 24, 48 and 72 h). **B**, Relative percentage of viable cells at 24, 48 and 72 h after f-IPI treatment. **C**, Kinetics of cell apoptosis after 50 and 100 µM f-IPI treatment of MDA-MB231 cells (Caspase-Glo 3/7 assay at 24, 48 and 72 h). **D**, Percentage of apoptotic cells at 24, 48 and 72 h after f-IPI treatment. **E**, Kinetics of cell proliferation after 50 and 100 µM f-IPI treatment of MDA-MB231 cells (BrdU incorporation assay at 24, 48 and 72 h). **F**, Relative percentage of cell proliferation at 24, 48 and 72 h after f-IPI treatment. Results are the mean of three independent experiments with error bars showing the standard deviation of the mean.

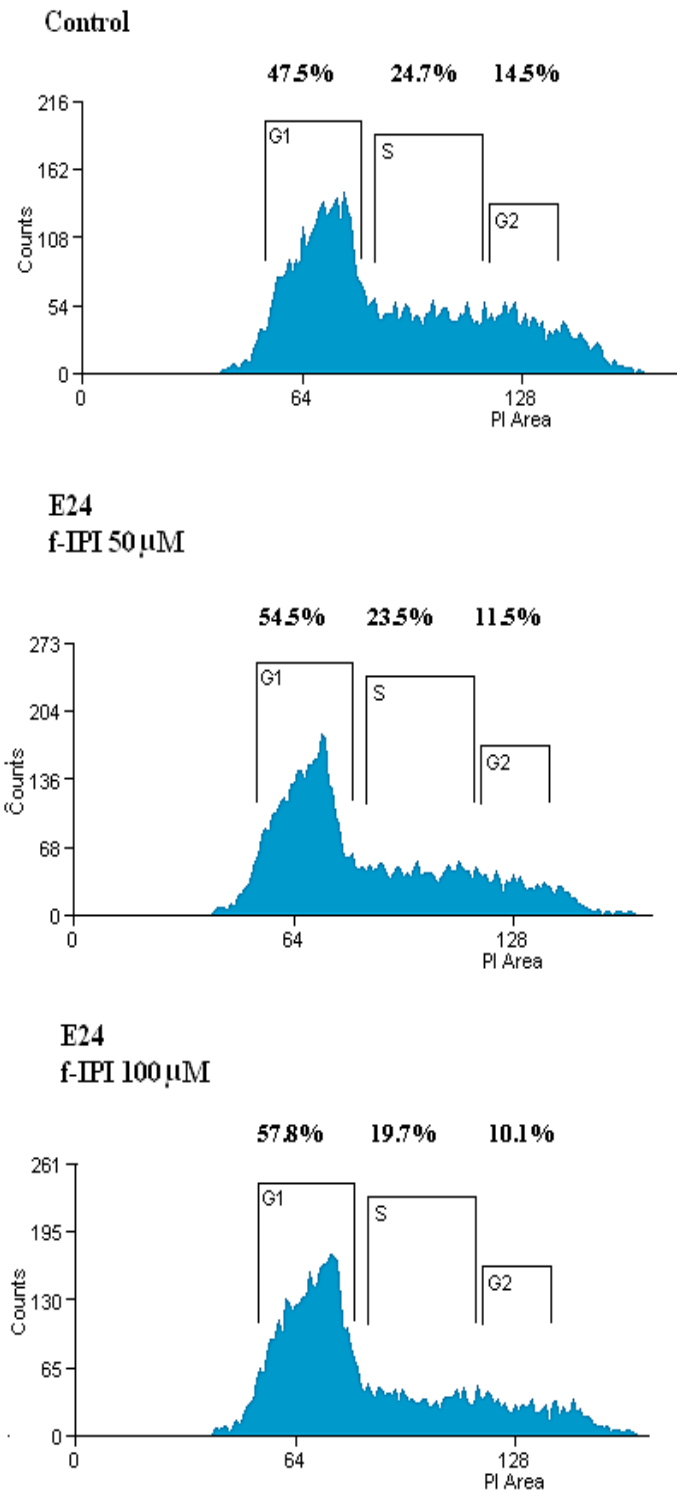

Figure 5.17 Flow cytometry analysis after f-IPI treatment. Untreated-(upper panel), 50 µM of f-IPI treated-(middle panel) and 100 µM of f-IPI treated-(lower panel) MDA-MB231 cells after 24 h respectively. Percentage of cells at different phases of the cell cycle was counted using Summit 4.3 software.

Study of the potential formation of *in situ* H-pin using the Dbf4 promoter as a model system

5.2.9 *In vitro* binding of f-IP(C_3NH_2)I, f-IP(C_3Cl)I and their combination to the Dbf4 promoter

The chemical structures and DNA binding models of f-IP(C_3NH_2)I, f-IP(C_3Cl)I and their combination have been shown in Figure 3.2A&B. These polyamides were designed to target the same binding sequence (5'-ACGCGT-3') as f-IPI, which is the core MCB sequence of the HuDbf4 promoter.

To identify the pattern of binding of f-IP(C_3NH_2)I, f-IP(C3Cl)I and their combination to the Dbf4 promoter, DNase I footprinting was carried out using the fragment shown in Figure 5.18. The autoradiogram given in Figure 5.18A shows the initial footprint by f-IP(C_3NH_2)I at 0.5 μM, having a 10-fold higher DNA-binding affinity than f-IP(C_3Cl)I (5 μM) (Figure 5.18B). When equimolar concentrations of f-IP(C_3NH_2)I and f-IP(C_3Cl)I were used, the combination binding starts to occur at 0.1 μM, thus indicating a higher DNA-binding affinity than either of f-IP(C_3NH_2)I (0.5 μM) or f-IP(C_3Cl)I (5 μM) (Figure 5.18A-C). These results suggest that the combination can form a favorable complex *in situ* at the target MCB sequence, potentially forming an H-pin structure.

A

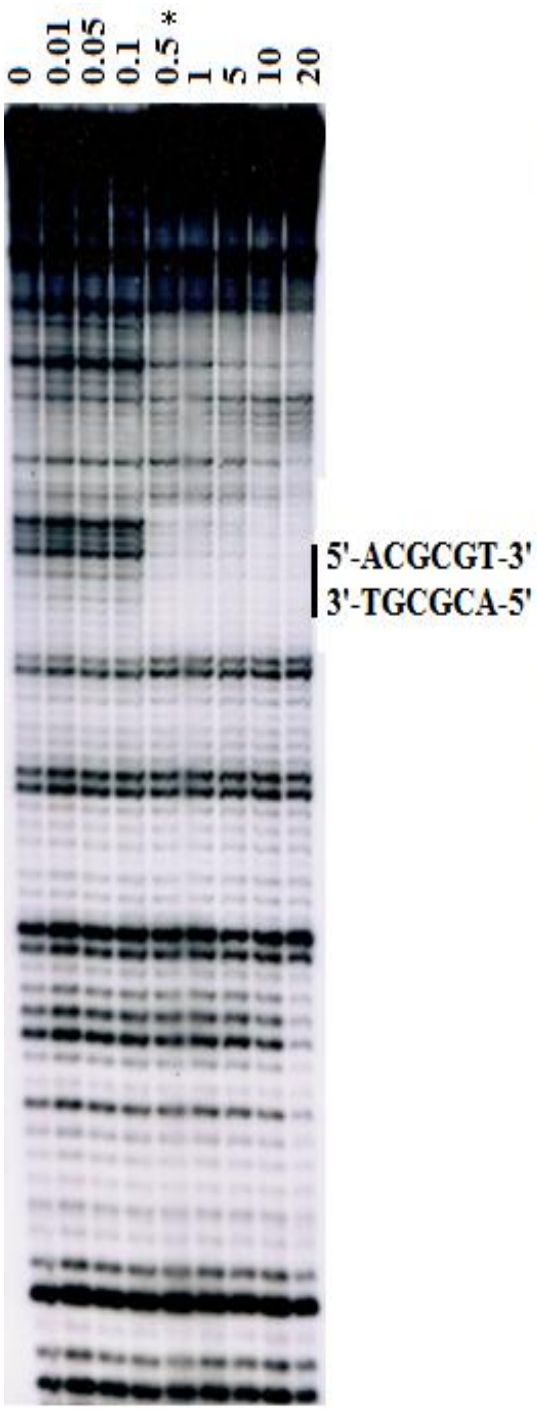
0
0.01
0.05
0.1
0.5 *
1
5
10
20
5'-ACGCGT-3'
3'-TGCGCA-5'

B

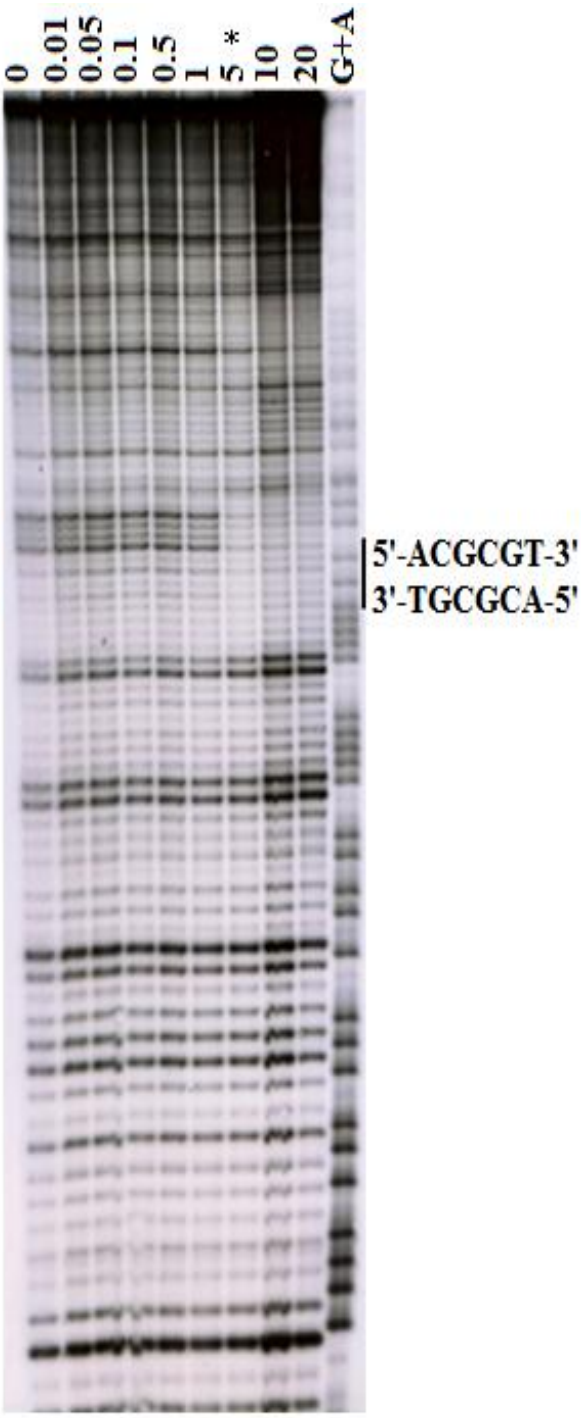
0
0.01
0.05
0.1
0.5
1
5 *
10
20
G+A
5'-ACGCGT-3'
3'-TGCGCA-5'

C

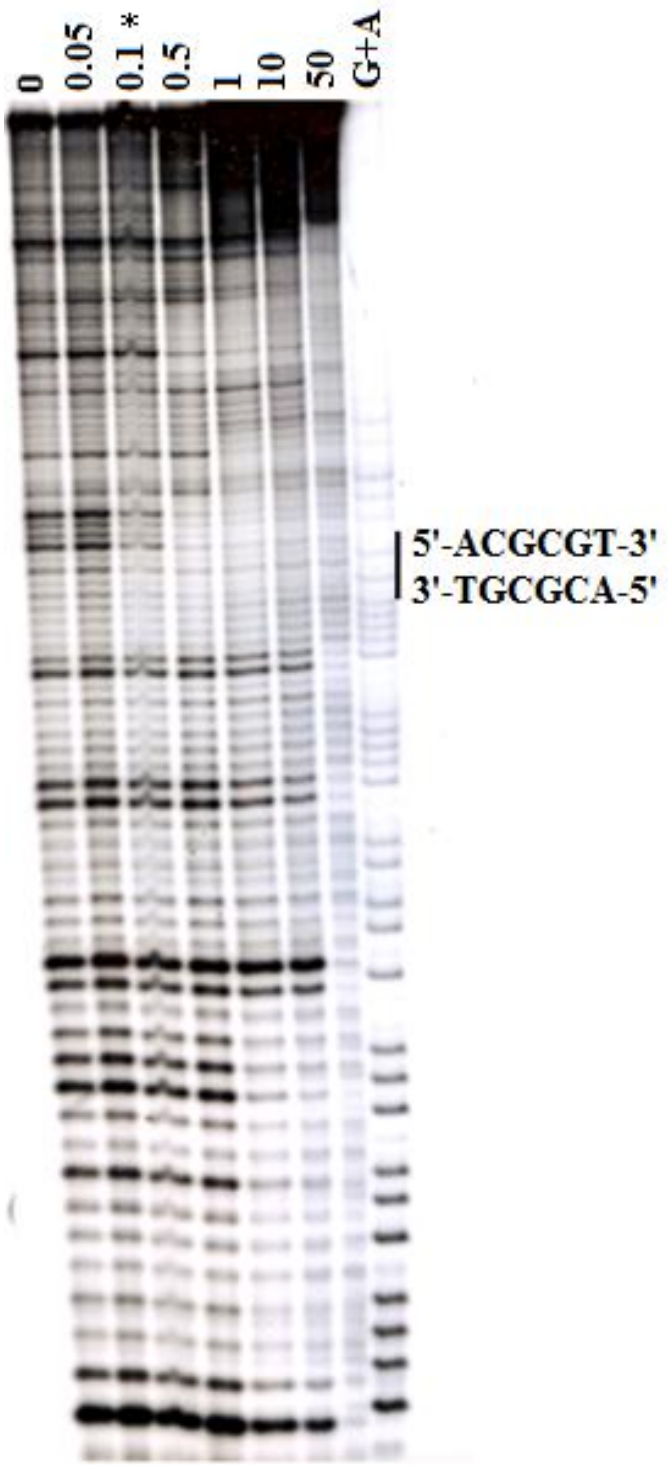

Figure 5.18 Sequence binding of compounds [**A, B** and **C**; f-IP(C_3NH_2)I, f-IP(C_3Cl)I and their combination, respectively] to their cognate, target sequence 5'-ACGCGT-3' within the Dbf4 promoter. DNase I footprinting was performed using a 131bp 5'-γ [^{32}P]-radiolabeled DNA fragment containing the Dbf4 core promoter sequence from -285 to -211. Asterisk indicates the concentration of polyamide at which protection from DNase I cleavage is initially observed. The cognate binding site is highlighted by solid bar. G+A refers to the sequencing lane.

To further demonstrate that f-IP(C_3NH_2)I, f-IP(C_3Cl)I and their combination can bind to the MCB motif, EMSA studies were carried out using radiolabelled oligonucleotides containing the MCB element, incubated with the respective compounds and nuclear extracts from confluent MDA-MB231 cells.

As shown in Figure 5.19A, pre-incubation of the radioactive oligonucleotides containing the MCB target sequence (5'-ACGCGT-3') with f-IP(C_3NH_2)I, for 1 h and subsequent addition of nuclear extracts causes the inhibition of protein binding to the MCB at 0.5 μM. In contrast, there is limited inhibition of protein binding to the MCB after the incubation with f-IP(C_3Cl)I at 10 μM (Figure 5.19B). When an equimolar concentration of f-IP(C_3NH_2)I was mixed with f-IP(C_3Cl)I, the inhibition of protein binding to the MCB by the combination occurs at 0.5 μM as was the case for f-IP(C_3NH_2)I alone (Figure 5.19C). The EMSA results are consistent with DNA footprinting analysis, also suggesting the favorable interaction *in situ* and partial formation of an H-pin structure.

A

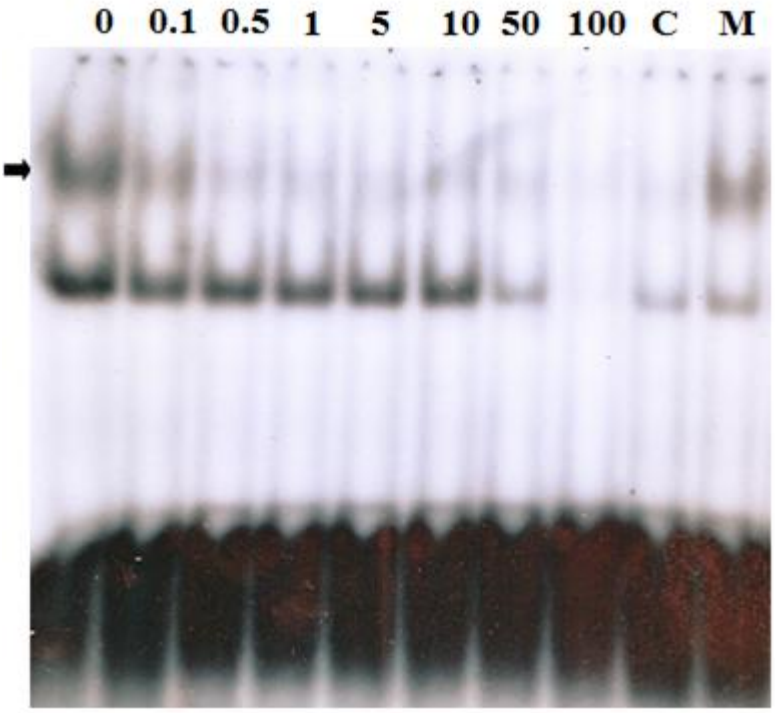

f-IP(C_3NH_2)I

B

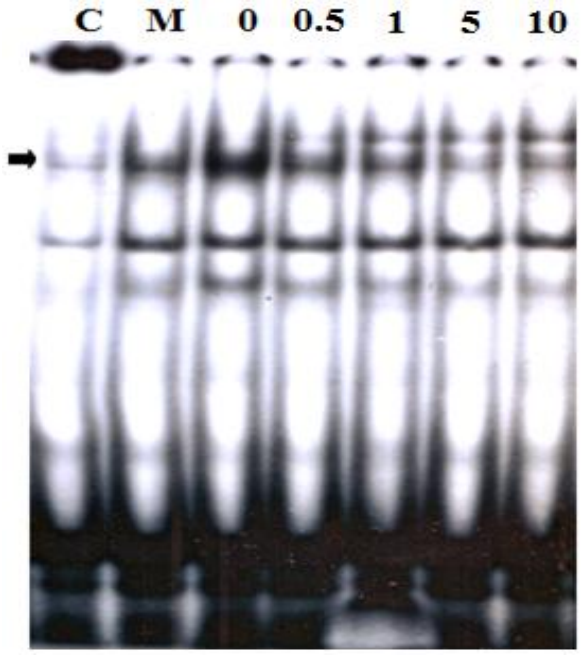

f-IP(C_3Cl)I

C

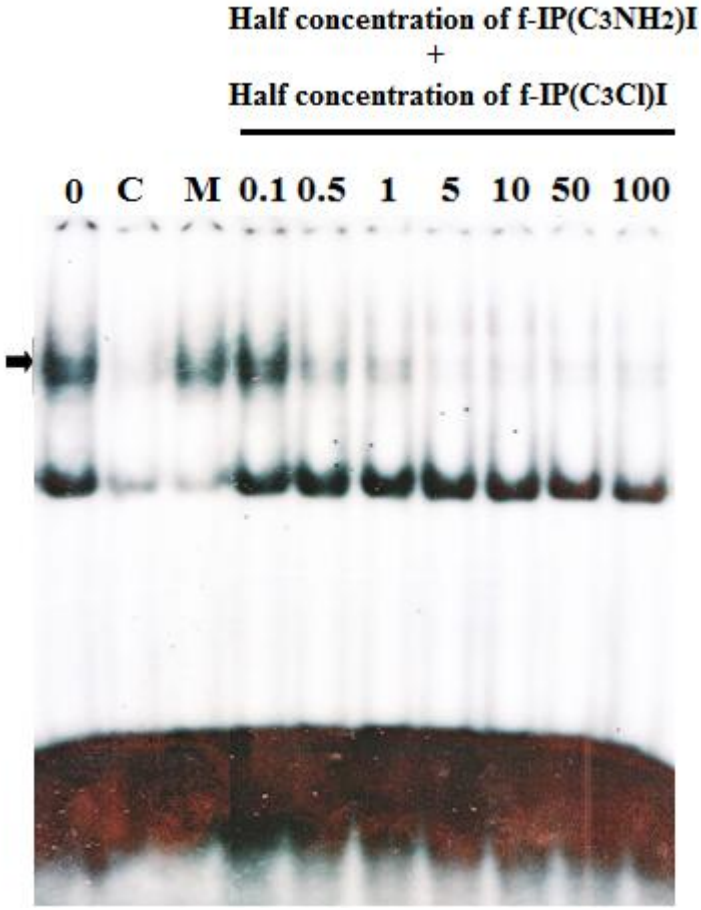

f-IP(C_3NH_2)I + f-IP(C_3Cl)I

D

MCB wild type oligo: 5'-GCGTGACGCGTTTTCAAATCTTCAACC-3'
MCB mutant oligo: 5'-GCGTGAC*TA*GTTTTCAAATCTTCAACC-3'

Figure 5.19 Interaction of compounds [f-IP(C_3NH_2)I, f-IP(C_3Cl)I and their combination] and the MCB in the promoter of human Dbf4. **A, B** and **C,** EMSA was carried out using 10 µg MDA-MB231 nuclear extracts and the radioactive DNA oligonucleotides shown in (**D**). The arrow denotes the DNA-protein complex. MCB "wild type" oligonucleotides were incubated with increasing concentration (µM) of compounds f-IP(C_3NH_2)I, f-IP(C_3Cl)I and their combination (0.1-100 µM). An equimolar concentration of f-IP(C_3NH_2)I mixed with f-IP(C_3Cl)I indicate the total concentration (**C).** Lane C and M represent reactions with unlabeled and mutated MCB oligonucleotides, respectively.

5.2.10 Effects of f-IP(C_3Cl)I, f-IP(C_3NH_2)I and their combination on the cellular levels of Dbf4: RT-PCR and Western Blot analysis

The effects of compounds f-IP(C_3Cl)I, f-IP(C_3NH_2)I and their combination on Dbf4 expression were analyzed in exponentially growing MDA-MB231 cells. Following incubation of the cells with 50 µM and 100 µM f-IP(C_3Cl)I, there is a 7% and 13% reduction in Dbf4 mRNA levels at 24 h, respectively, compared to untreated cells (Figure 5.20A). Higher reduction of Dbf4 mRNA levels (15% and 26%, respectively) by 50 µM and 100 µM f-IP(C_3NH_2)I is shown at 24 h in Figure 5.20B and C compared to that of f-IP(C_3Cl)I treatments. Furthermore, when 25 µM or 50 µM of f-IP(C_3NH_2)I were mixed with 25 µM or 50 µM of f-IP(C_3Cl)I, their combination results in the reduction of Dbf4 mRNA levels by 30% and 46%, respectively at 24 h, which represents a greater effect than either of the compounds alone (Figure 5.20B&C).

A

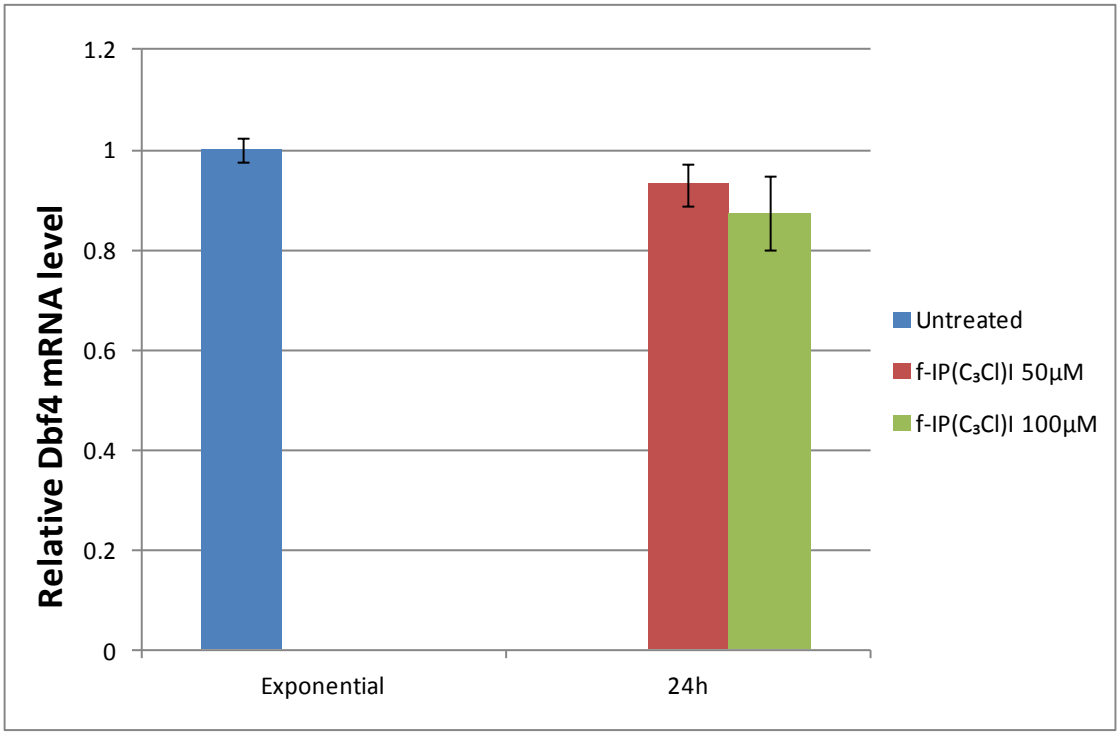

B

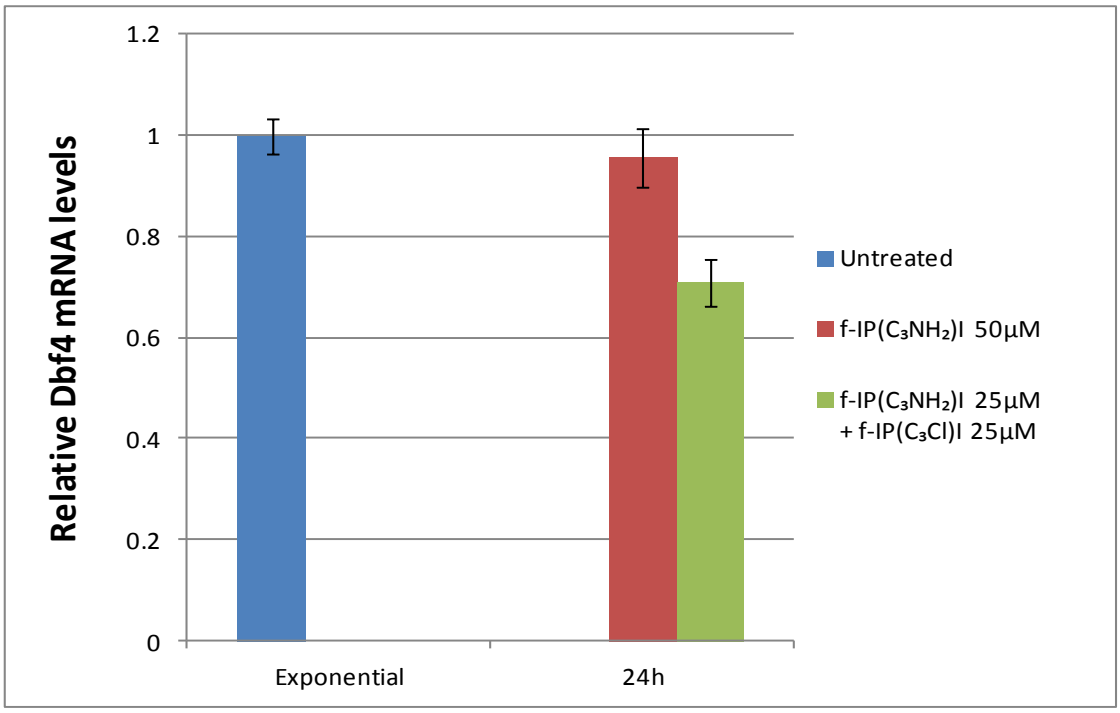

C

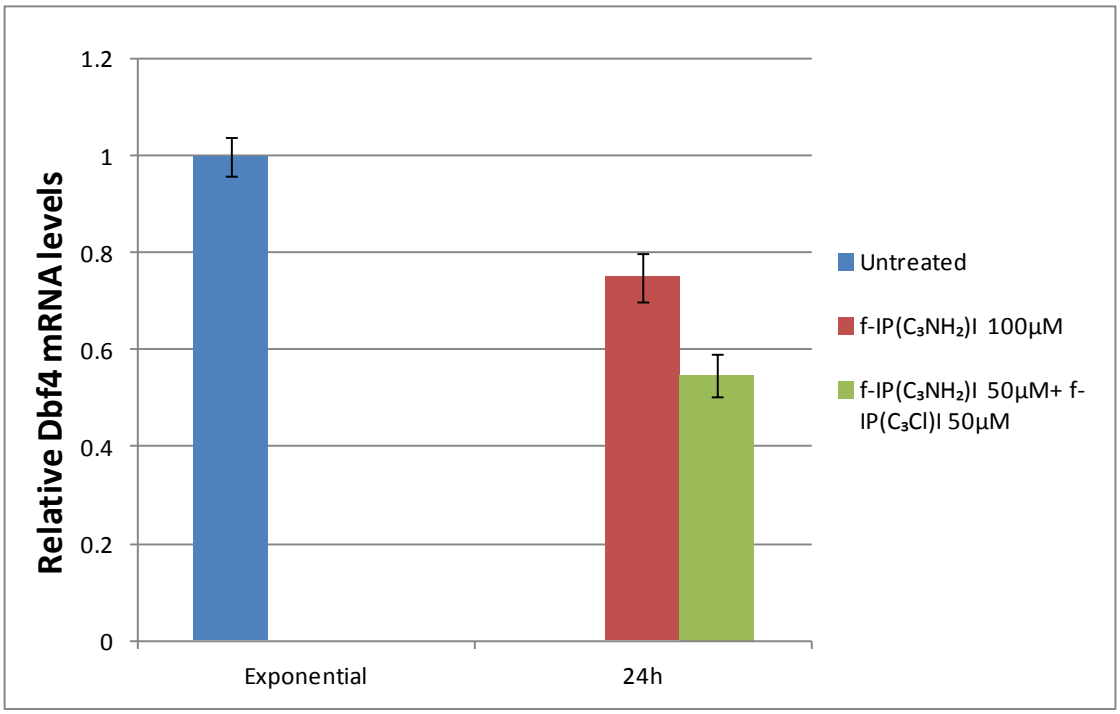

Figure 5.20 Cell survival, apoptosis and proliferation analysis after f-IP(C_3Cl)I, f-IP(C_3NH_2)I and their combination treatments. **A,** Exponentially growing MDA-MB231 cells were treated with 50 and 100 µM of f-IP(C_3Cl)I for 24 h. **B,** The cells were treated with 50 µM of f-IP(C_3NH_2)I and the combination (25 µM from each compounds) respectively for 24h. **C,** The cells were treated with 100 µM of f-IP(C_3NH_2)I and the combination (50 µM from each) respectively for 24 h. mRNA levels in the chemical compounds-treated cells were expressed relative to exponentially growing cells. Results are the mean of three independent experiments with error bars showing the standard deviation of the mean.

Exponentially growing MDA-MB231 cells were incubated with 50 µM and 100 µM of f-IP(C_3Cl)I, f-IP(C_3NH_2)I and their combination for 24 h. Western blot analysis of treated cells was performed and the results are shown in Figure 5.21A and B. The results demonstrate that f-IP(C_3Cl)I has no effect on Dbf4 protein expression after 24 h of exposure (Figure 5.21A). In contrast, f-IP(C_3NH_2)I treatments result in a reduction in the Dbf4 protein levels in a dose-dependent fashion after a 24 h incubation (Figure 5.21B). When 25 µM or 50 µM of f-IP(C_3NH_2)I were mixed with 25 µM or 50 µM of f-IP(C_3Cl)I, the combination exhibits a higher reduction of Dbf4 protein levels than either f-IP(C_3Cl)I or f-IP(C_3NH_2)I alone at 24 h at 50 µM and 100 µM, respectively (Figure 5.21B). The immunoblotting data is therefore consistent with the RT-PCR analysis, thus suggesting that f-IP(C_3Cl)I interacts *in situ* with f-IP(C_3NH_2)I to potentially form a H-pin structure in the cell.

A

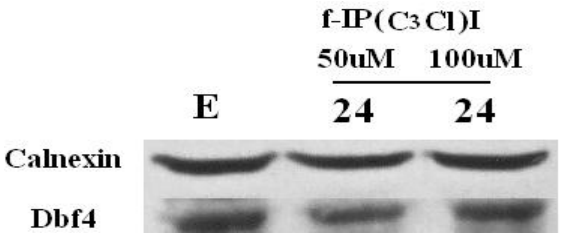

B

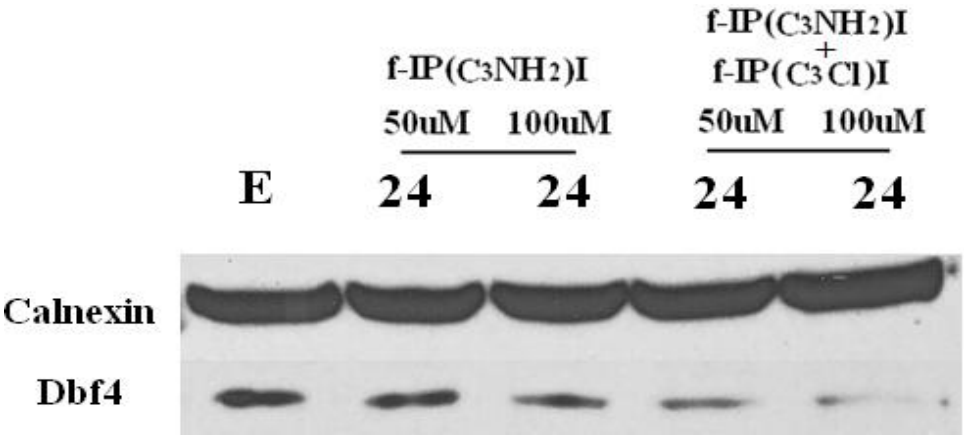

Figure 5.21 Immunoloting analysis of MDA-MB231 cell extracts following treatment with f-IP(C_3Cl)I, IP(C_3NH_2)I and their combination. **A** and **B,** Immunoblotting of cell nuclear extracts following 50 µM and 100 µM of f-IP(C_3Cl)I, IP(C_3NH_2)I and their combination treatment. An equimolar concentration of f-IP(C_3NH_2)I mixed with f-IP(C_3Cl)I indicate the total concentration (**B**). Protein and RNA samples from exponentially growing cells (*E*).

5.2.11 Effects of f-IP(C_3Cl)I, f-IP(C_3NH_2)I and their combination on the cell cycle

To further investigate the effect of Dbf4 on exponentially growing MDA-MB231 cells, cell cycle analysis of 50 μM and 100 μM of each of f-IP(C_3Cl)I and f-IP(C_3NH_2)I treated-cells and 50 μM and 100 μM of their combination treated-cells were performed after a 24 h incubation. As shown in Figure 5.22A, f-IP(C_3Cl)I has no effect on the cell cycle at 50 μM and 100 μM after a 24 h of exposure. In contrast, there is a 4.21% increase of 100 μM f-IP(C_3NH_2)I treated-cells in G_1 compared to the untreated cells (Figure 5.22A). However, when 50 μM of f-IP(C_3NH_2)I were mixed with 50 μM of f-IP(C_3Cl)I, the combination at 100 μM induces a 9.48% increase of treated-cells in G_1 at 24 h, indicating a greater effect of the combination than either f-IP(C_3NH_2)I or f-IP(C_3Cl)I treatment alone (Figure 5.22B).

5.2.12 Effects of f-IP(C_3Cl)I, f-IP(C_3NH_2)I and their combination on cell growth, apoptosis and proliferation in the MDA-MB231 cells

To investigate the effects of f-IP(C_3Cl)I, f-IP(C_3NH_2)I and their combination in MDA-MB231 cells, the same assays as in section 5.2.5 were carried out.

As shown in Figure 5.23A and B, the luminescence levels and the relative cell viability percentages of f-IP(C_3Cl)I-treated cells decrease slightly in response to increasing concentrations of f-IP(C_3Cl)I at 24 and 48 h, respectively. The luminescence levels in the cell apoptosis assay and the corresponding cell apoptosis percentages of f-IP(C_3Cl)I-treated cells increase slightly in response to increasing concentrations of f-IP(C_3Cl)I at 24 and 48 h (Figure 5.23C&D). The absorbance and the relative cell proliferation

percentages of f-IP(C_3Cl)I-treated cells exhibit the similar pattern as shown in the cell viability assay (Figure 5.23E&F).

As shown in Figure 5.24A and B, cell viability percentages of f-IP(C_3NH_2)I and the combination-treated cells decrease in a dose-dependent fashion at 24, 48 and 72 h. At 72 h, f-IP(C_3NH_2)I at either 50 μM or 100 μM shows a higher reduction of cell viability than the combination. Cell apoptosis percentages of f-IP(C_3NH_2)I and the combination-treated cells increase in response to increasing concentrations of these compounds (Figure 5.24C&D). At 72 h, f-IP(C_3NH_2)I at either 50 μM or 100 μM produces a greater level of apoptosis than the combination. The cell proliferation percentages of f-IP(C_3NH_2)I and the combination-treated cells decrease in a dose-dependent fashion at 24, 48 and 72 h (Figure 5.24 E&F). The combination at either 50 μM or 100 μM produces a higher decrease of cell proliferation than f-IP(C_3NH_2)I at 72 h. Overall, f-IP(C_3NH_2)I at 100 μM has a greater effect on cell viability and apoptosis than either f-IP(C_3Cl)I or the combination. However, the combination at 100 μM exhibits a higher reduction of cell proliferation than either f-IP(C_3NH_2)I or f-IP(C_3Cl)I alone, suggesting the potential formation of an H-pin structure.

A

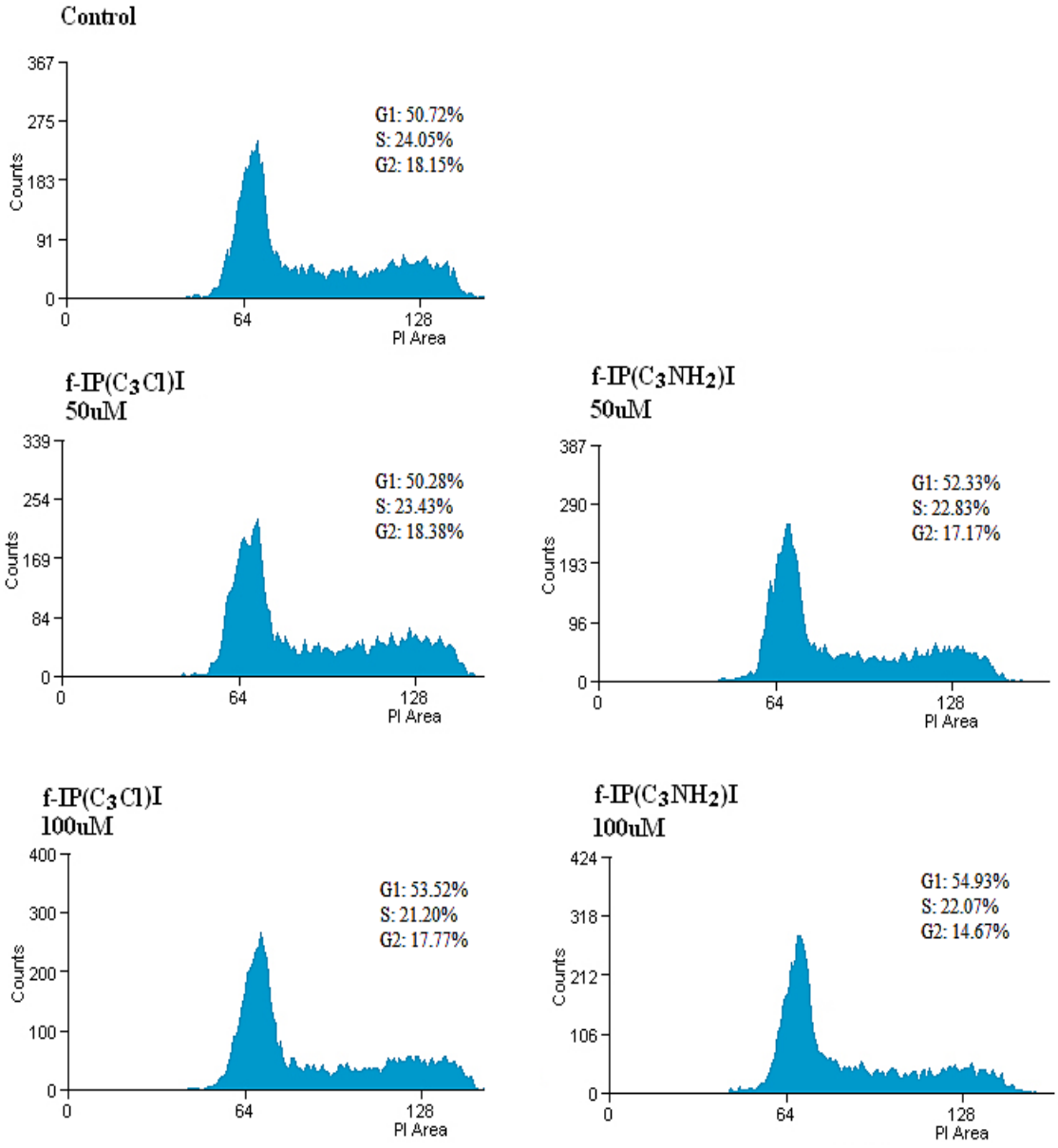
Control
G1: 50.72%
S: 24.05%
G2: 18.15%
Counts
PI Area
f-IP(C3Cl)I
50uM
G1: 50.28%
S: 23.43%
G2: 18.38%
f-IP(C3NH2)I
50uM
G1: 52.33%
S: 22.83%
G2: 17.17%
f-IP(C3Cl)I
100uM
G1: 53.52%
S: 21.20%
G2: 17.77%
f-IP(C3NH2)I
100uM
G1: 54.93%
S: 22.07%
G2: 14.67%

B

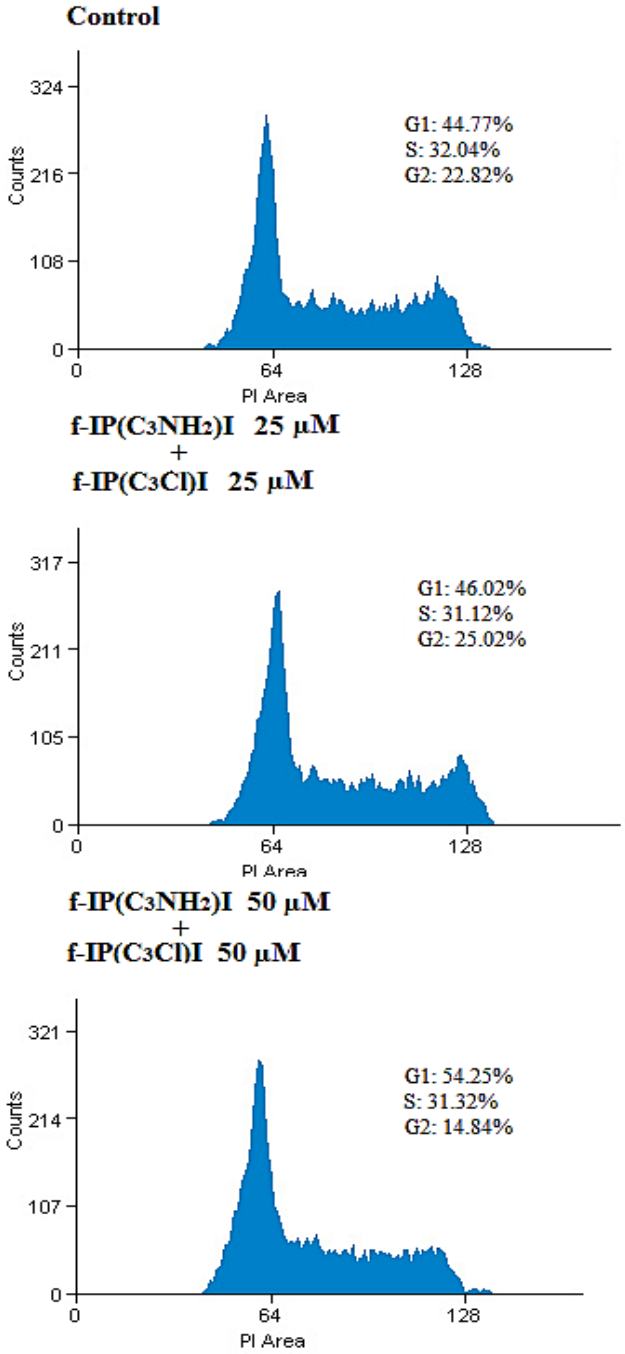

Figure 5.22. Flow cytometry analysis of f-IP(C_3Cl)I, f-IP(C_3NH_2)I and the combination-treated MDA-MB231 cells. **A**, Untreated-(upper panel), 50 µM f-IP(C_3Cl)I treated-(left middle panel) and 100 µM f-IP(C_3Cl)I treated-(left lower panel) MDA-MB231 cells after 24 h respectively. 50 µM f-IP(C_3NH_2)I treated-(right middle panel) and 100 µM f-IP(C_3NH_2)I treated-(right lower panel) MDA-MB231 cells after 24 h respectively. **B**, Untreated-(upper panel), 50 µM the combination [25 µM each of f-IP(C_3Cl)I and f-IP(C_3NH_2)I] treated-(middle panel) and 100 µM the combination [50 µM each of f-IP(C_3Cl)I and f-IP(C_3NH_2)I] treated-(lower panel) MDA-MB231 cells after 24 h respectively. Percentage of cells at different phases of the cell cycle was counted using Summit 4.3 software.

A

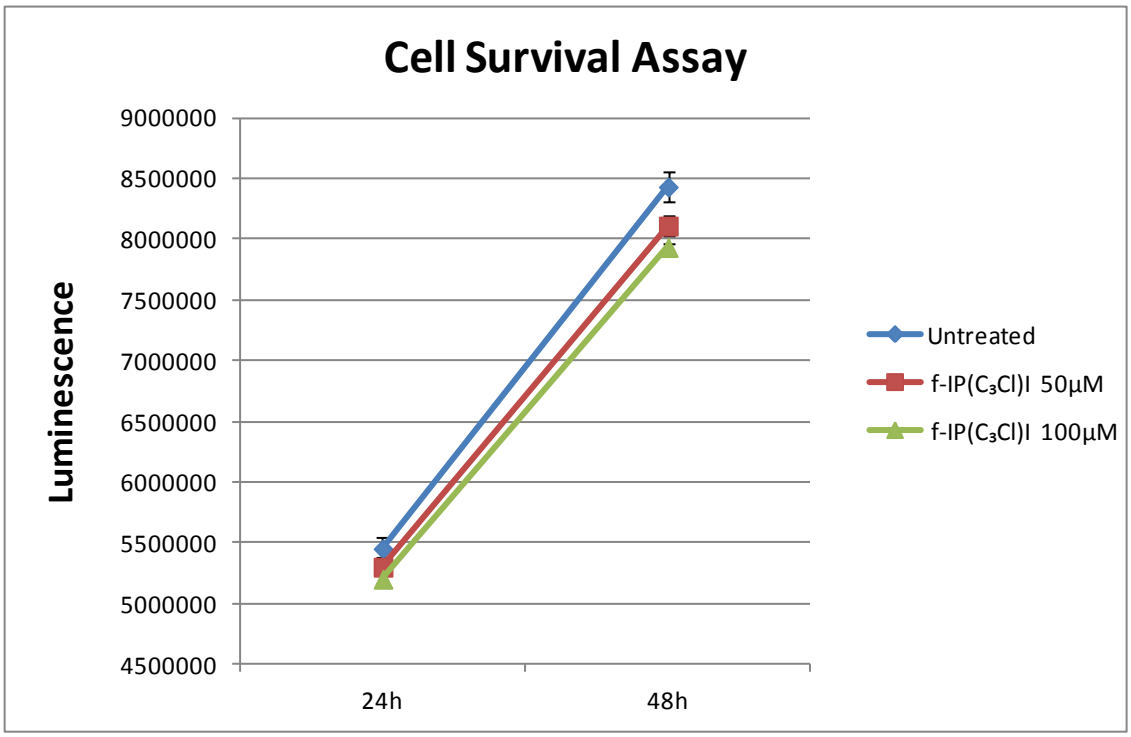
Cell Survival Assay
Luminescence
9000000
8500000
8000000
7500000
7000000
6500000
6000000
5500000
5000000
4500000
24h
48h
Untreated
f-IP(C3Cl)I 50µM
f-IP(C3Cl)I 100µM

B

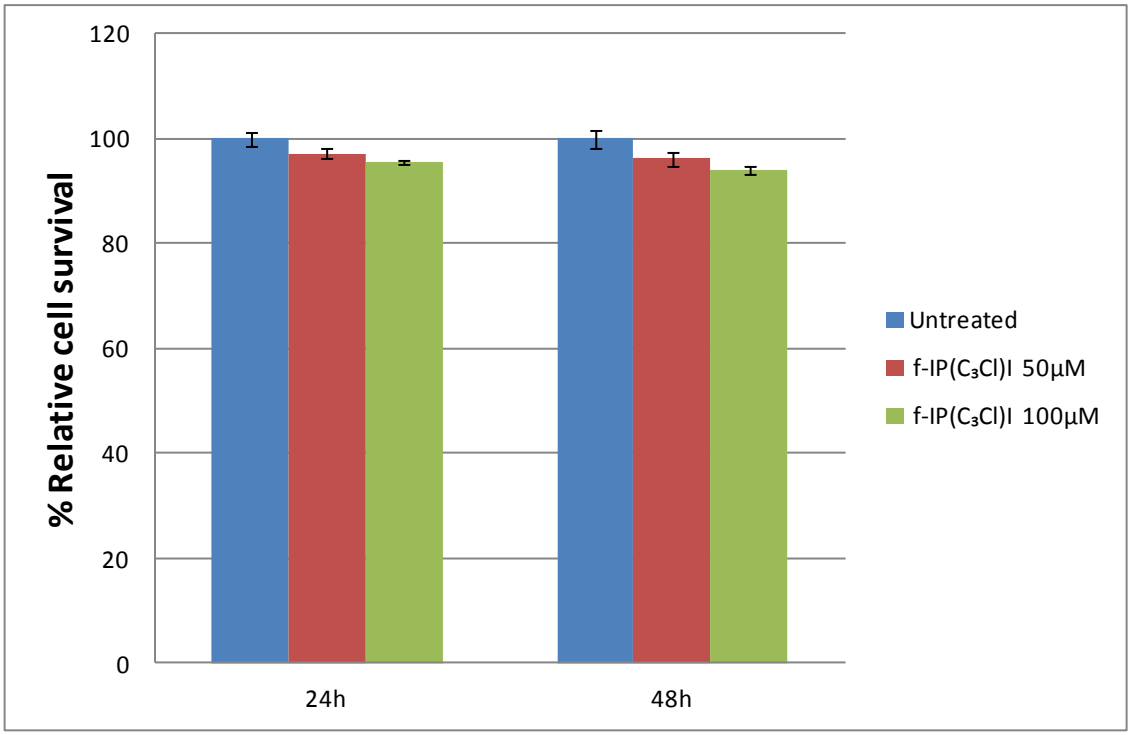
% Relative cell survival
120
100
80
60
40
20
0
24h
48h
Untreated
f-IP(C3Cl)I 50µM
f-IP(C3Cl)I 100µM

C

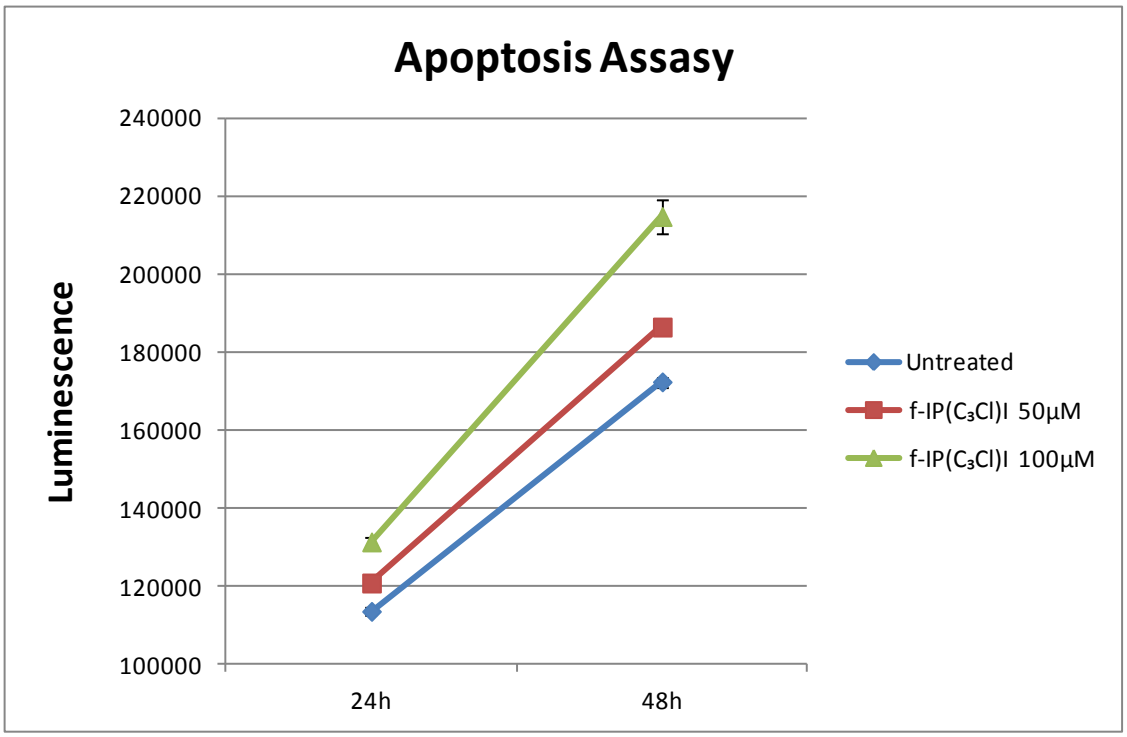
Apoptosis Assay
Luminescence
240000
220000
200000
180000
160000
140000
120000
100000
24h
48h
Untreated
f-IP(C₃Cl)I 50µM
f-IP(C₃Cl)I 100µM

D

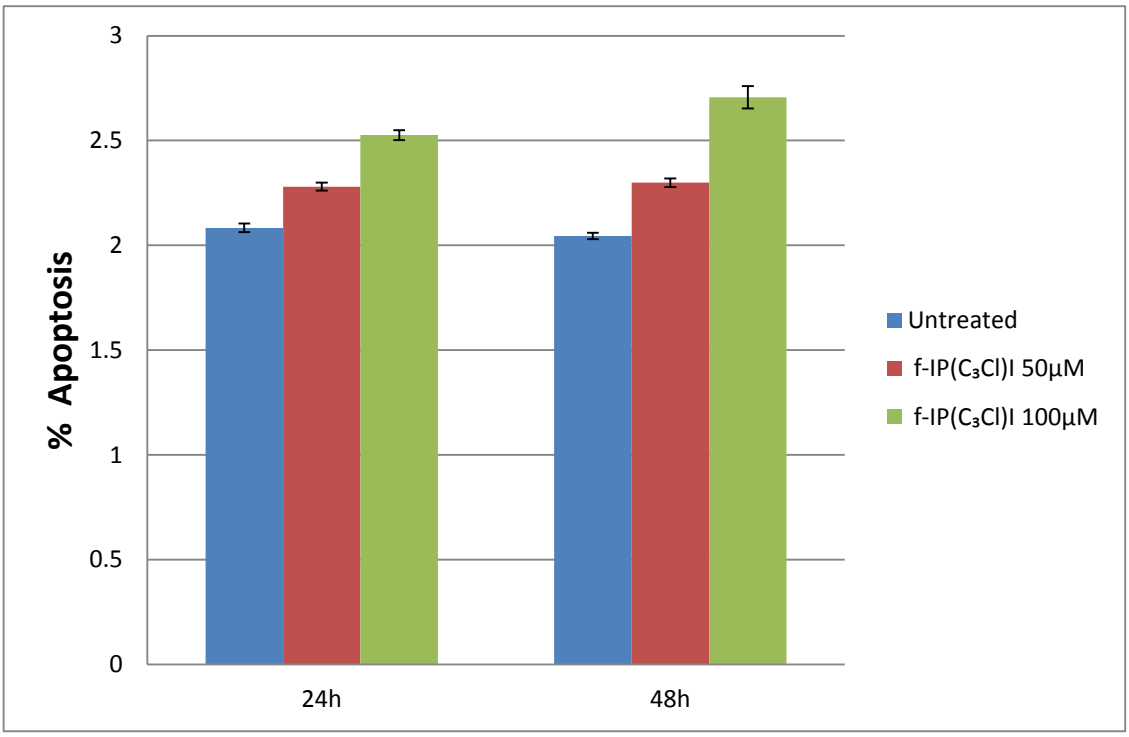
% Apoptosis
3
2.5
2
1.5
1
0.5
0
24h
48h
Untreated
f-IP(C₃Cl)I 50µM
f-IP(C₃Cl)I 100µM

E

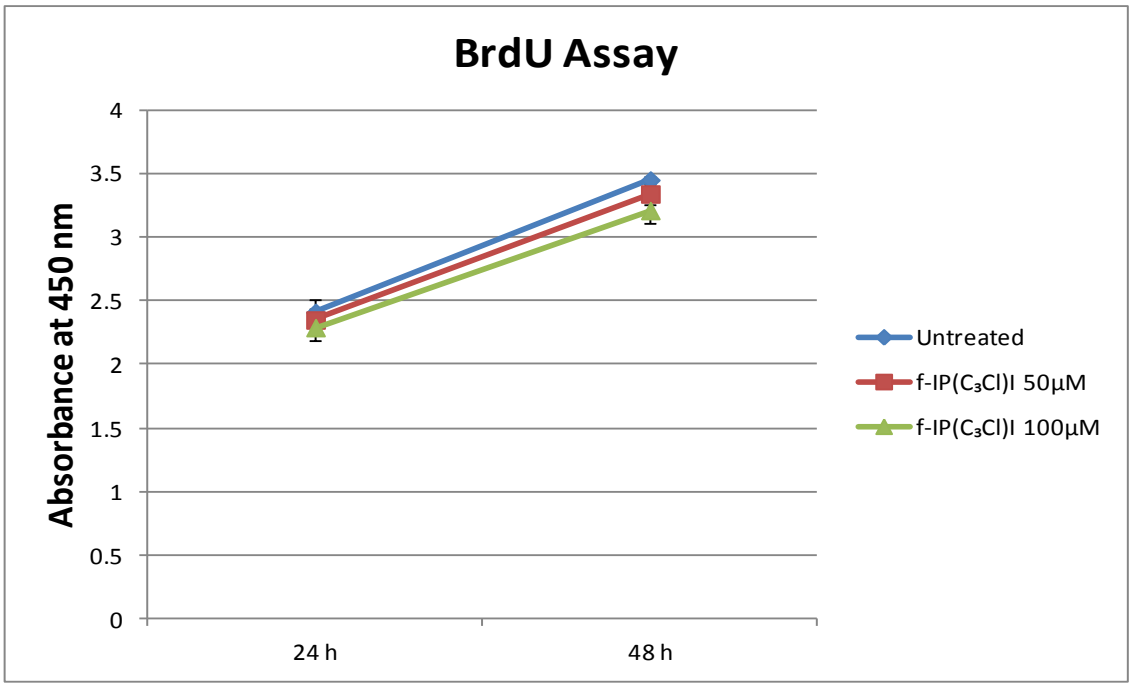

F

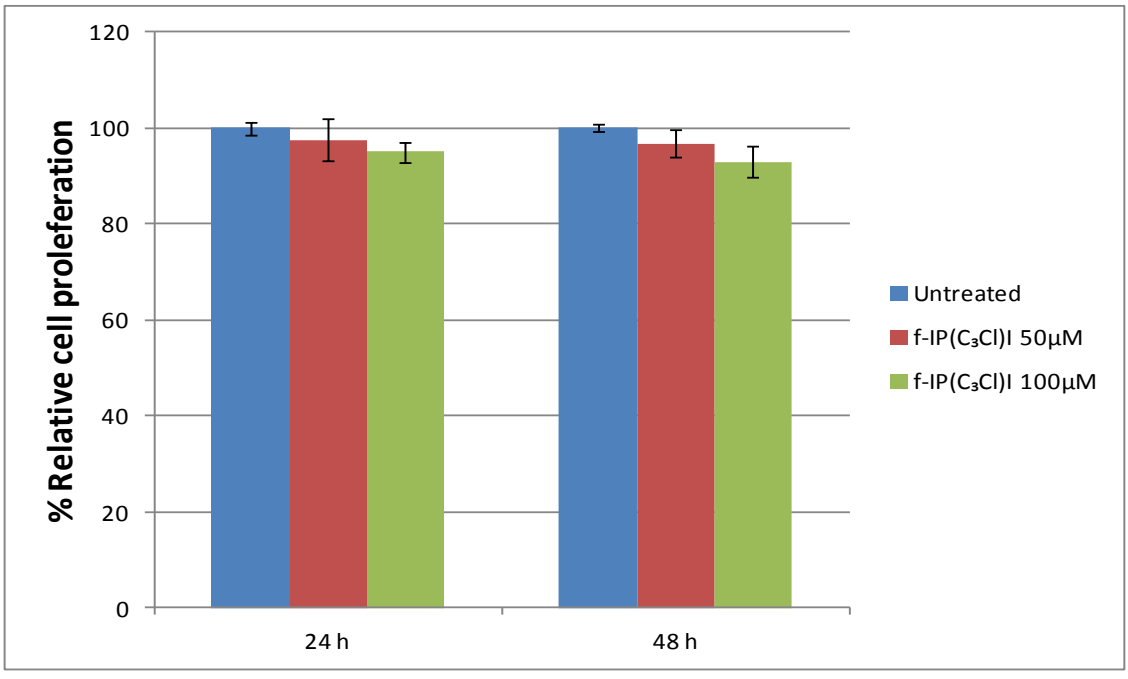

Figure 5.23 Cell survival, apoptosis and proliferation analysis of f-IP(C_3Cl)I-treated MDA-MB231 cells. **A**, Kinetics of cell viability after 50 and 100 µM f-IP(C_3Cl)I treated MDA-MB231 cells at 24 and 48 h respectively. **B**, Relative percentage of viable cells after 50 µM and 100 µM f-IP(C_3Cl)I treated MDA-MB231 cells at 24 and 48 h respectively. **C**, Kinetics of cell apoptosis after 50 µM and 100 µM f-IP(C_3Cl)I treated MDA-MB231 cells at 24 and 48 h respectively. **D**, Percentage of apoptotic cells after 50 µM and 100 µM f-IP(C_3Cl)I treated MDA-MB231 cells at 24 and 48 h respectively. **E**, Kinetics of cell proliferation after 50 µM and 100 µM f-IP(C_3Cl)I treated MDA-MB231 cells at 24 and 48 h respectively. **F**, Relative percentage of cell proliferation after 50 µM and 100 µM f-IP(C_3Cl)I treated MDA-MB231 cells at 24 and 48 h respectively. Results are the mean of three independent experiments with error bars showing the standard deviation of the mean.

A

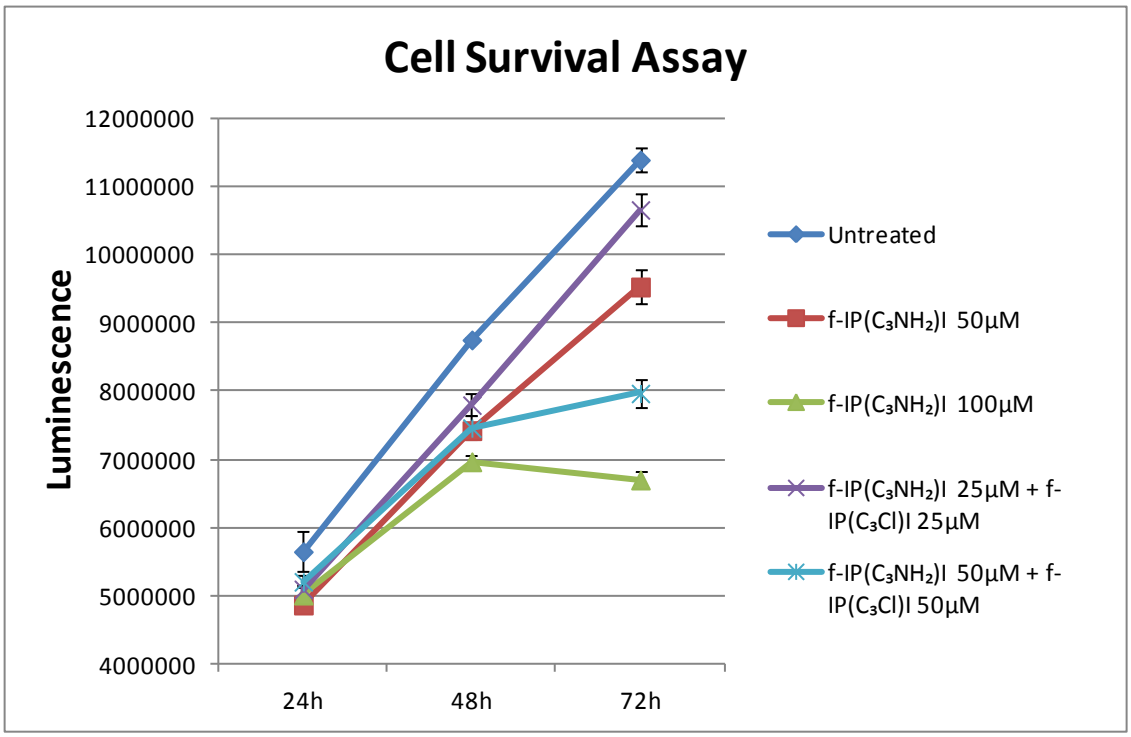
Cell Survival Assay
Luminescence
12000000
11000000
10000000
9000000
8000000
7000000
6000000
5000000
4000000
24h
48h
72h
Untreated
f-IP(C3NH2)I 50µM
f-IP(C3NH2)I 100µM
f-IP(C3NH2)I 25µM + f-IP(C3Cl)I 25µM
f-IP(C3NH2)I 50µM + f-IP(C3Cl)I 50µM

B

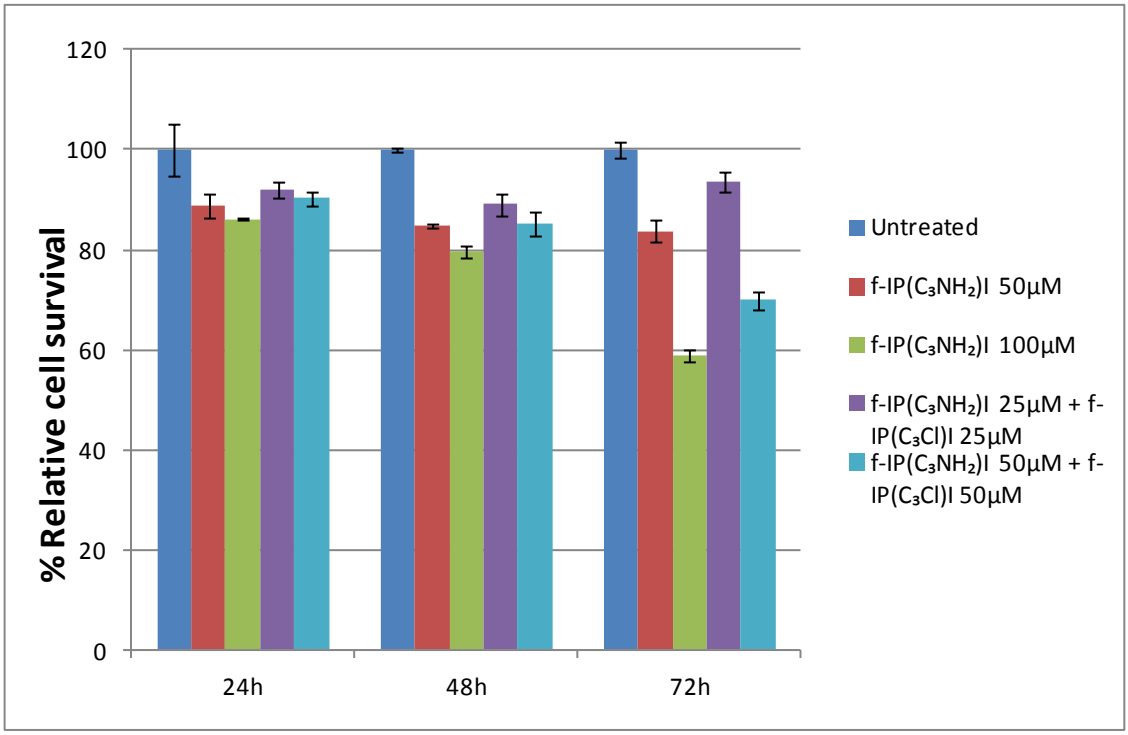
% Relative cell survival
120
100
80
60
40
20
0
24h
48h
72h
Untreated
f-IP(C3NH2)I 50µM
f-IP(C3NH2)I 100µM
f-IP(C3NH2)I 25µM + f-IP(C3Cl)I 25µM
f-IP(C3NH2)I 50µM + f-IP(C3Cl)I 50µM

C

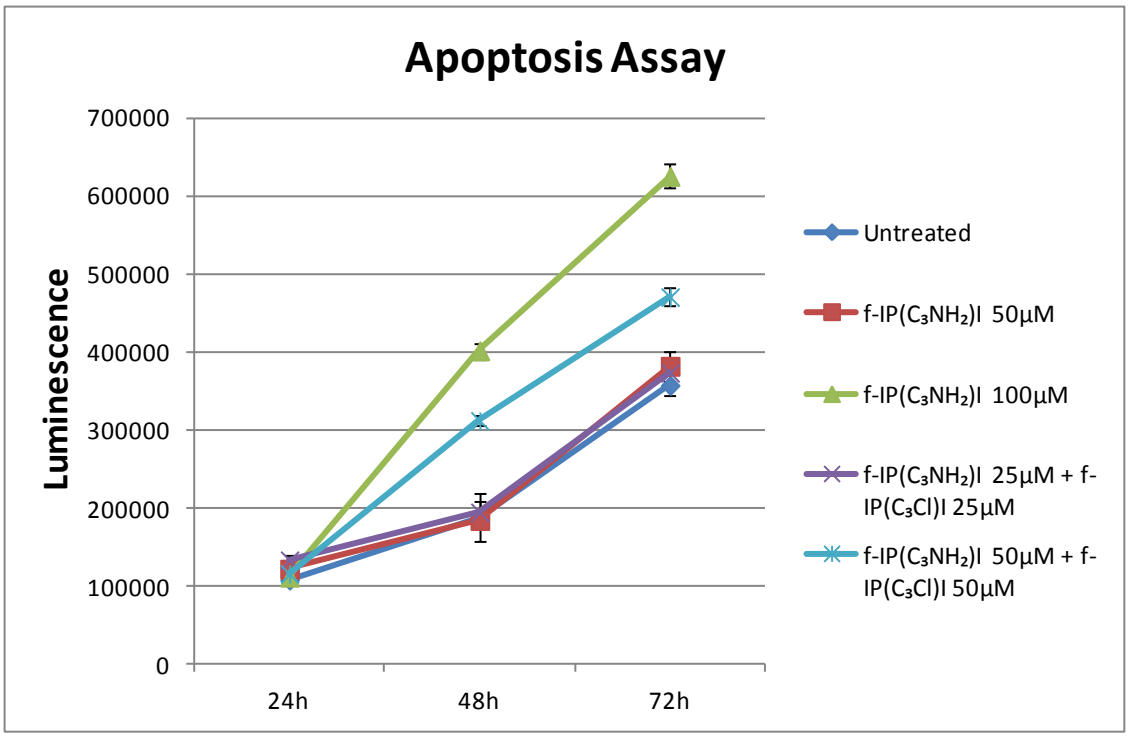
Apoptosis Assay
Luminescence
700000
600000
500000
400000
300000
200000
100000
0
24h
48h
72h
Untreated
f-IP(C3NH2)I 50µM
f-IP(C3NH2)I 100µM
f-IP(C3NH2)I 25µM + f-IP(C3Cl)I 25µM
f-IP(C3NH2)I 50µM + f-IP(C3Cl)I 50µM

D

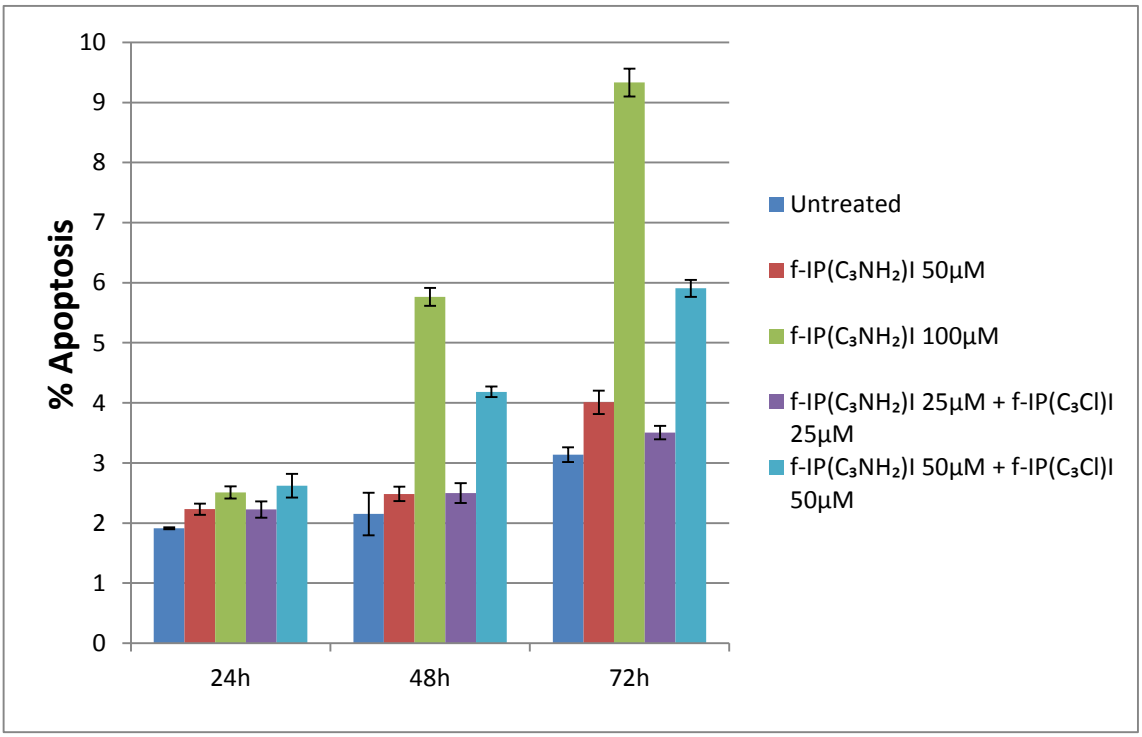
% Apoptosis
10
9
8
7
6
5
4
3
2
1
0
24h
48h
72h
Untreated
f-IP(C3NH2)I 50µM
f-IP(C3NH2)I 100µM
f-IP(C3NH2)I 25µM + f-IP(C3Cl)I 25µM
f-IP(C3NH2)I 50µM + f-IP(C3Cl)I 50µM

E

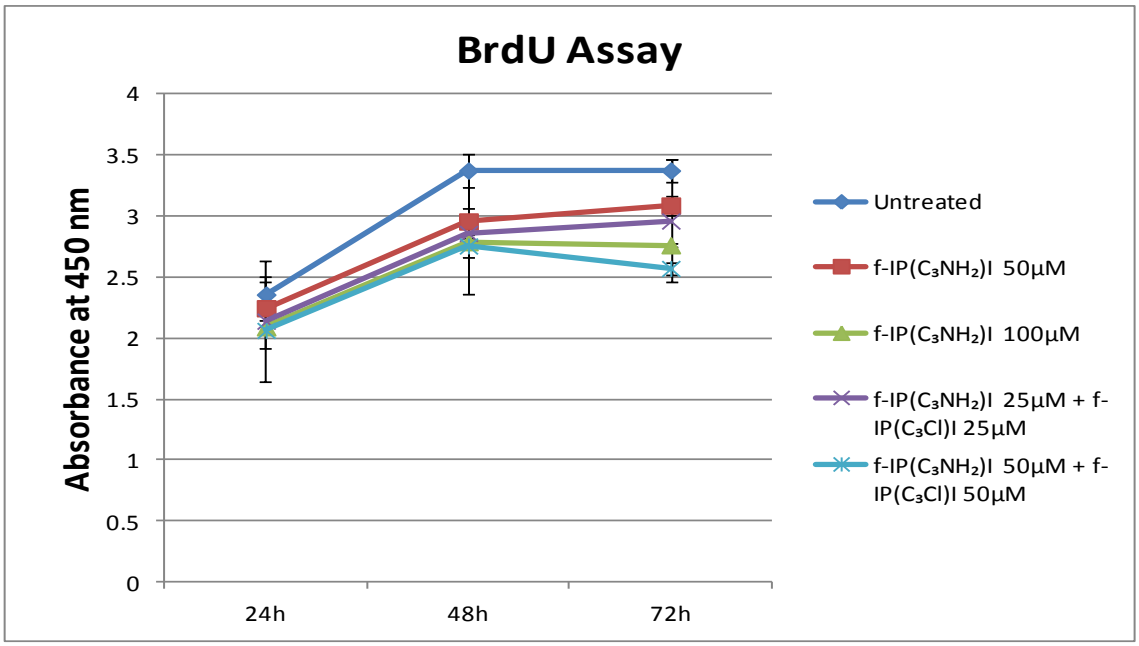

F

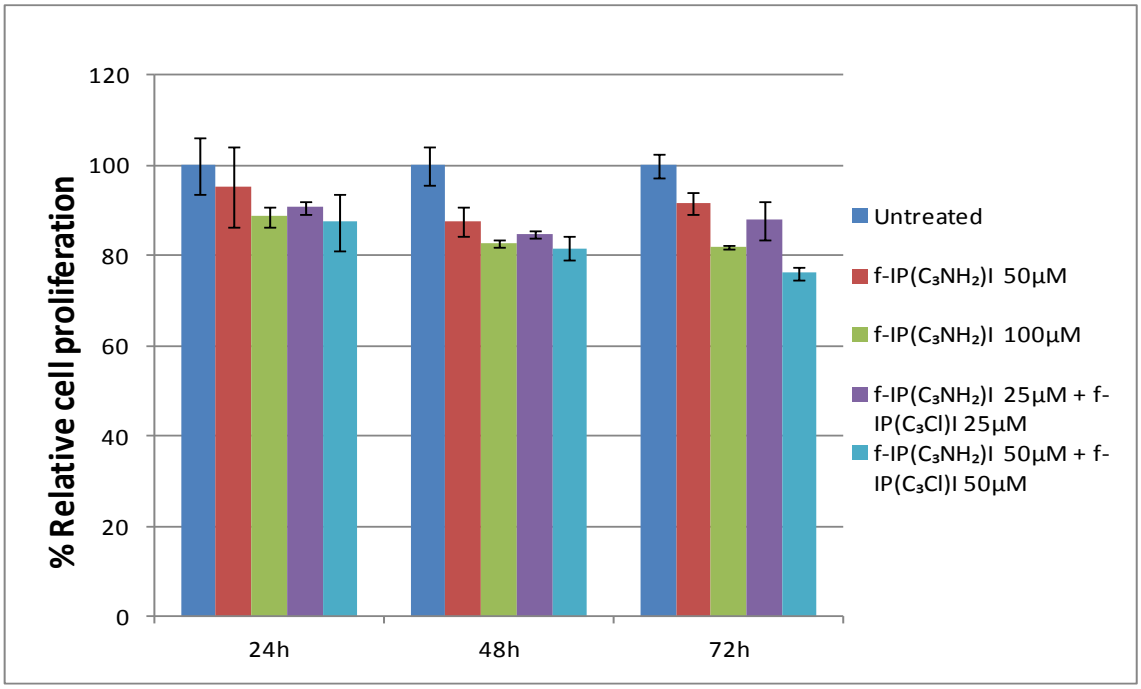

Figure 5.24 Cell survival, apoptosis and proliferation analysis of f-IP(C_3NH_2)I/the combination-treated MDA-MB231 cells. **A**, Kinetics of cell viability after 50 and 100 µM f-IP(C_3NH_2)I/the combination treated MDA-MB231 cells at 24, 48 and 72 h, respectively. **B**, Relative percentage of viable cells after 50 and 100 µM f-IP(C_3NH_2)I/the combination treated MDA-MB231 cells at 24, 48 and 72 h, respectively. **C**, Kinetics of cell apoptosis after 50 and 100 µM f-IP(C_3NH_2)I/the combination treated MDA-MB231 cells at 24, 48 and 72 h, respectively. **D**, Percentage of apoptotic cells after 50 and 100 µM f-IP(C_3NH_2)I/the combination treated MDA-MB231 cells at 24, 48 and 72 h, respectively. **E**, Kinetics of cell proliferation after 50 and 100 µM f-IP(C_3NH_2)I/the combination treated MDA-MB231 cells at 24, 48 and 72 h, respectively. **F**, Relative percentage of cell proliferation after 50 and 100 µM f-IP(C_3NH_2)I/the combination treated MDA-MB231 cells at 24, 48 and 72 h, respectively. Results are the mean of three independent experiments with error bars showing the standard deviation of the mean.

Investigation of the effects of fluorescent analogues *in vitro* and in MDA-MB231 cells

5.2.13 *In vitro* binding of Aza-Hx-PI, Aza-Hx-P(C_3NH_2)I and Aza-Hx-PI(C_3NH_2) to the Dbf4 promoter

The compounds contain a *p*-anisylbenzimidazolecarboxamido (Hx) containing an additional nitrogen as an Aza-Hx moiety attached to PI, P(C_3NH_2)I or PI(C_3NH_2) unit, giving compounds Aza-Hx-PI, Aza-Hx-P(C_3NH_2)I or Aza-Hx-PI(C_3NH_2), respectively. The chemical structures of Aza-Hx-PI, Aza-Hx-P(C_3NH_2)I and Aza-Hx-PI(C_3NH_2) are shown in Figure 5.25A. The proposed DNA sequence binding model for the tested compounds is shown in Figure 5.25B, based on the previous finding that Hx moiety can mimic pyrrole-pyrrole or formamido-pyrrole (Chavda et al., 2011). The binding of Aza-Hx-PI, Aza-Hx-P(C_3NH_2)I and Aza-Hx-PI(C_3NH_2) to the MCB (5'-ACGCGT-3') present in the 131bp radiolabeled Dbf4 promoter sequence (Figure 5.8A) was investigated by DNase I footprinting. The autoradiograms depicted in Figure 5.26A and B show that an initial footprint is observed for Aza-Hx-PI and Aza-Hx-P(C_3NH_2)I at the binding site 5'-ACGCGT-3' at 5 μM. However, Aza-Hx-PI(C_3NH_2)'s footprint occurs at 1 μM and becomes clearer at 5 μM, thus suggesting a slightly higher binding affinity than either Aza-Hx-PI or Aza-Hx-P(C_3NH_2)I (Figure 5.26C). The DNA footprinting analysis suggest that Aza-Hx behaves as a formamido-imidazole or pyrrole-imidazole unit as designed. Binding of Aza-Hx-P(C_3NH_2)I and Aza-Hx-PI(C_3NH_2) at the non-specific binding site 5'-AAACGA-3' occurs at 5 μM and 1 μM, respectively (Figure 5.26B&C). However, no binding is observed for Aza-Hx-PI, suggesting a greater specificity for this compound (Figure 5.26A).

A

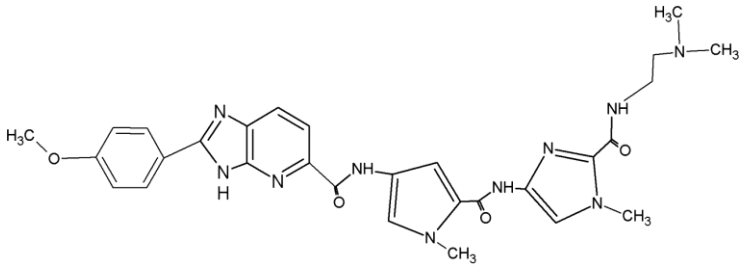

Aza-Hx-PI

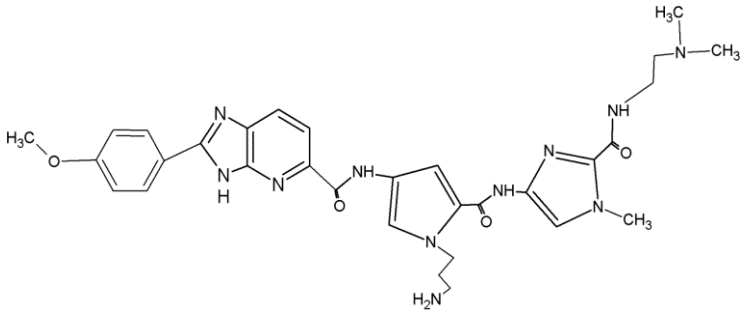

Aza-Hx-P(C_3NH_2)I

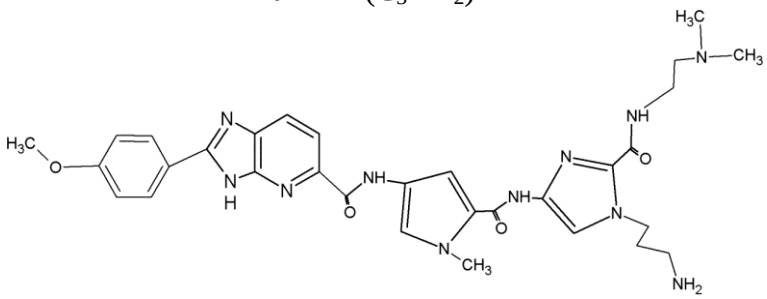

Aza-Hx-PI(C_3NH_2)

B

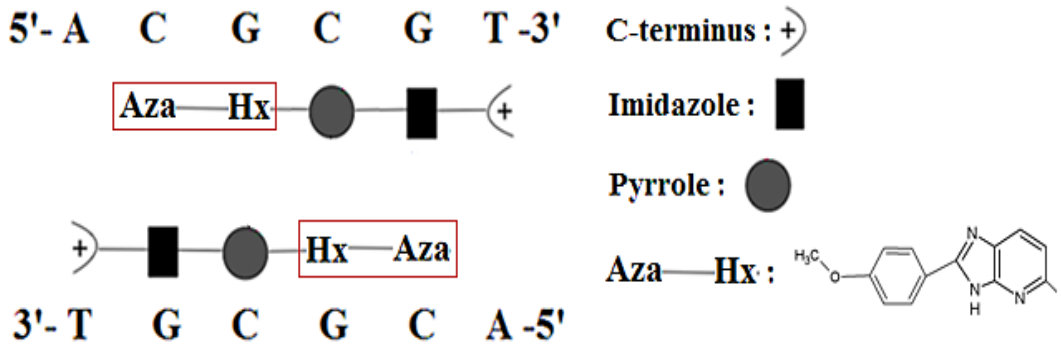

Figure 5.25 A, Chemical structures (**A)** and binding model (**B**) of Aza-Hx-PI and its analogues.

A

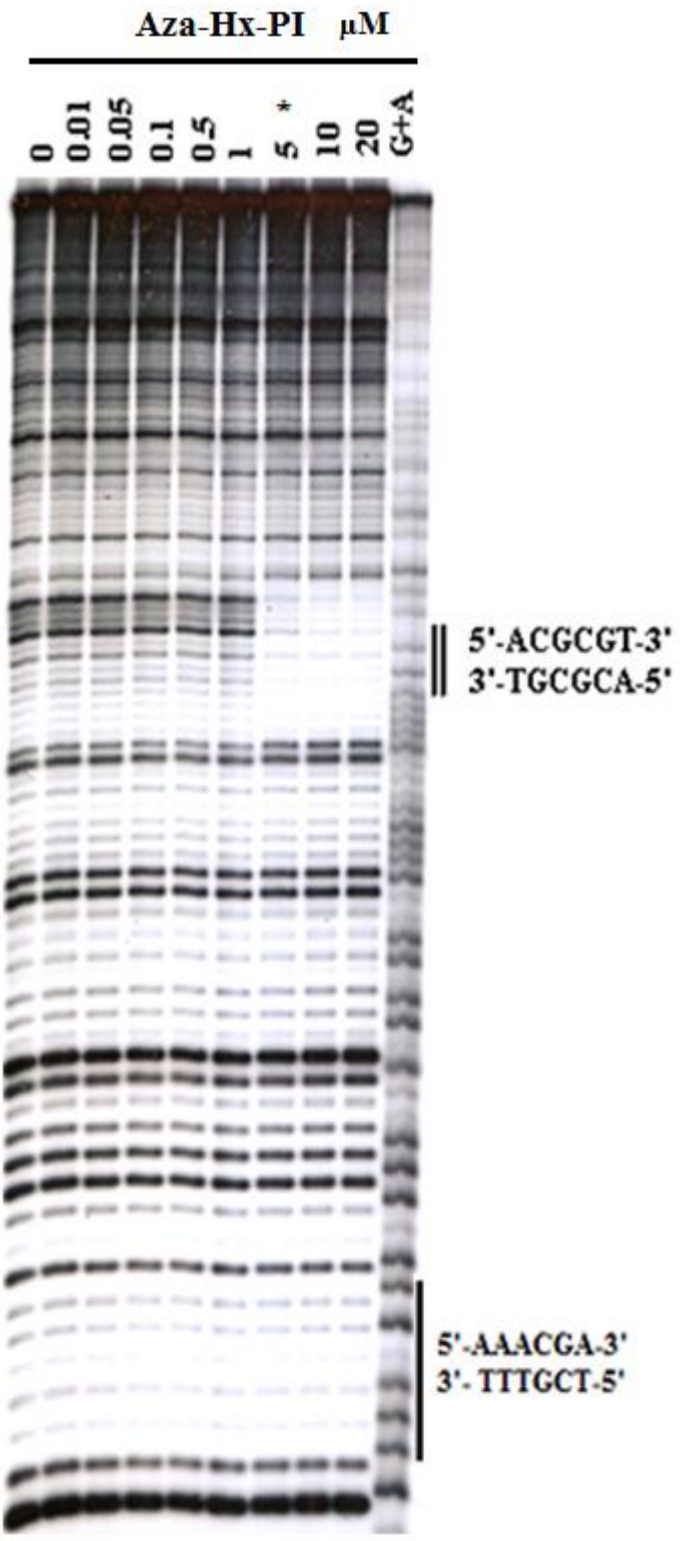
Aza-Hx-PI μM
0
0.01
0.05
0.1
0.5
1
5 *
10
20
G+A
5'-ACGCGT-3'
3'-TGCGCA-5'
5'-AAACGA-3'
3'- TTTGCT-5'

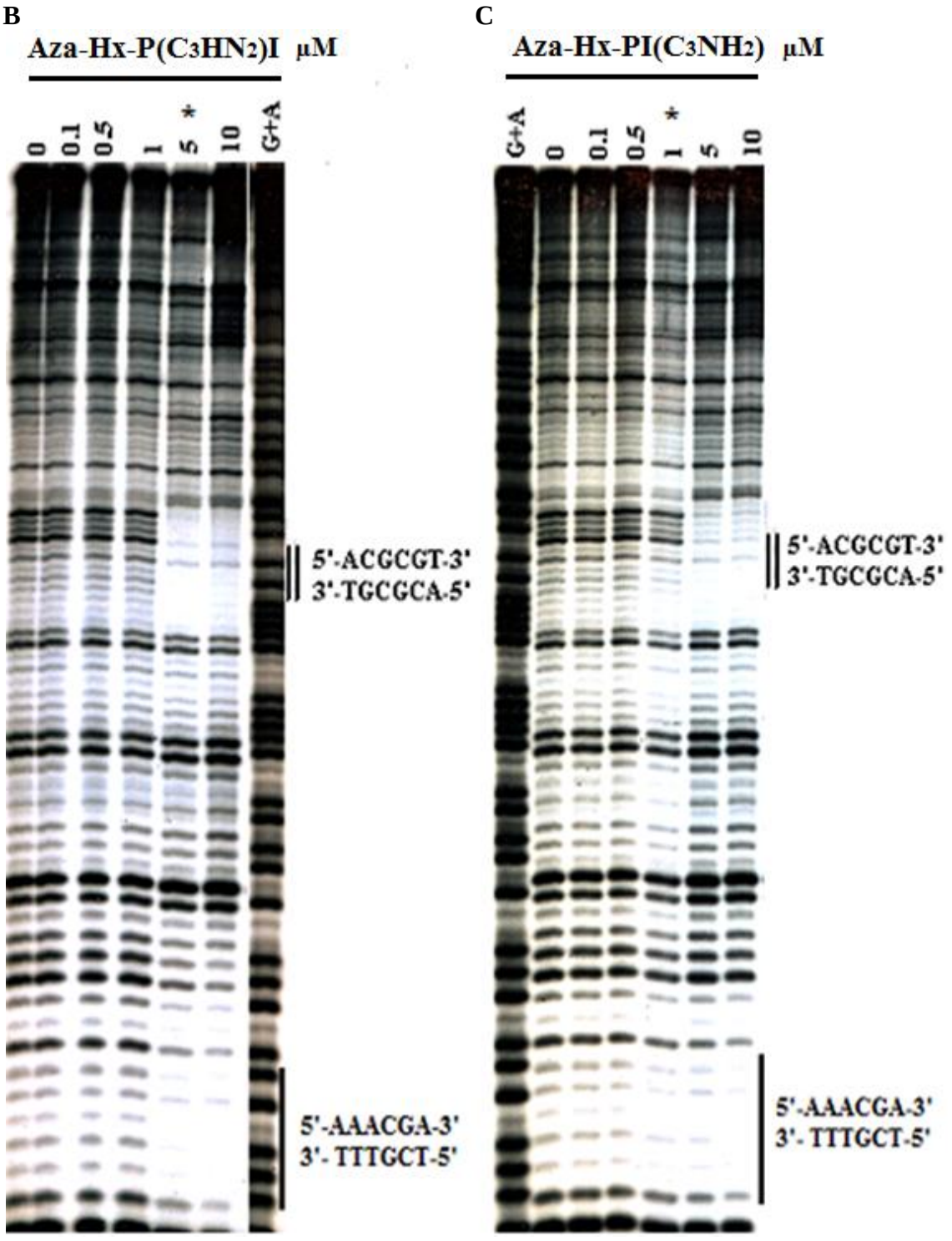

Figure 5.26 Sequence binding of compounds (**A, B** and **C**; Aza-Hx-PI, Aza-Hx-P(C_3NH_2)I and Aza-Hx-PI(C_3NH_2) respectively) to their cognate, target sequence 5'-ACGCGT-3' within the Dbf4 promoter. DNase I footprinting was performed using a 131bp 5'-γ-[^{32}P]-radiolabeled DNA fragment containing the Dbf4 promoter sequence from -285 to -211 (described in Figure 5.8A). Asterisk indicates the concentration of polyamide at which protection from DNase I cleavage is initially observed. The cognate binding site is highlighted by double solid bar. G+A refers to the sequencing lane.

To further demonstrate that Aza-Hx-PI, Aza-Hx-P(C_3NH_2)I and Aza-Hx-PI(C_3NH_2) can bind to the MCB motif and potentially affect the HuDbf4 promoter activity, EMSA studies were carried out using radiolabeled oligonucleotides containing the MCB, incubated with the respective compounds and nuclear extracts from MDA-MB231 cells. As shown in Figure 5.27A, pre-incubation of the radioactive oligonucleotides containing the MCB with Aza-Hx-PI, for 1 h and subsequent addition of nuclear extracts results in the inhibition of protein binding to the MCB at drug concentrations >0.5 μM. The inhibition of protein binding with Aza-Hx-P(C_3NH_2)I and Aza-Hx-PI(C_3NH_2) treatment is observed at the concentrations >1 μM, thus suggesting a lower binding affinity than Aza-Hx-PI (Figure 5.27B&C). The same experiments were repeated with the nuclear extracts incubated with the radioactive oligonucleotides first, for 1 h, before addition of the tested compounds. The MCB binding inhibition patterns were identical (data not shown) suggesting that the tested compounds can not only compete but also displace transcription factors bound to DNA, including the MCB.

A

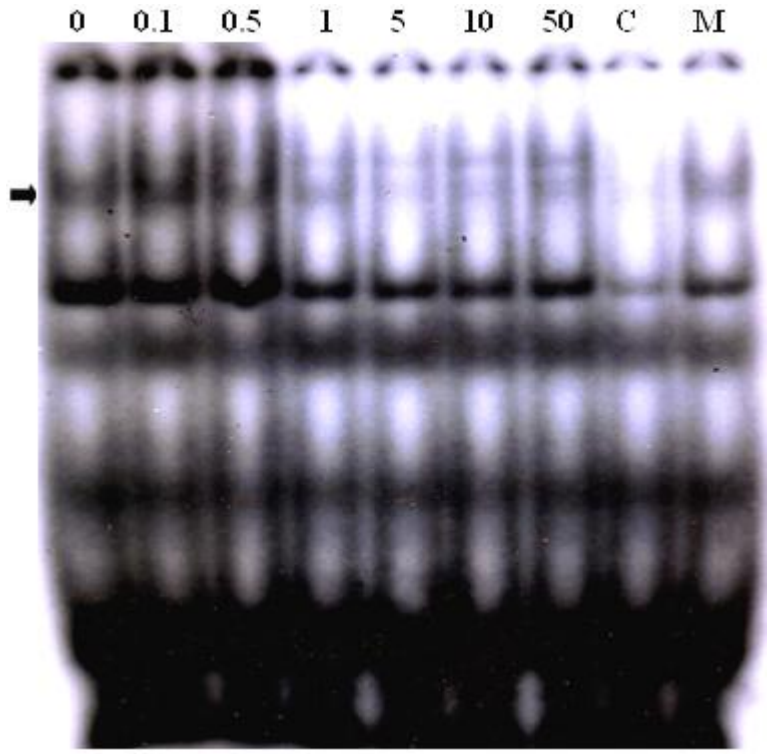

Aza-Hx-PI

B

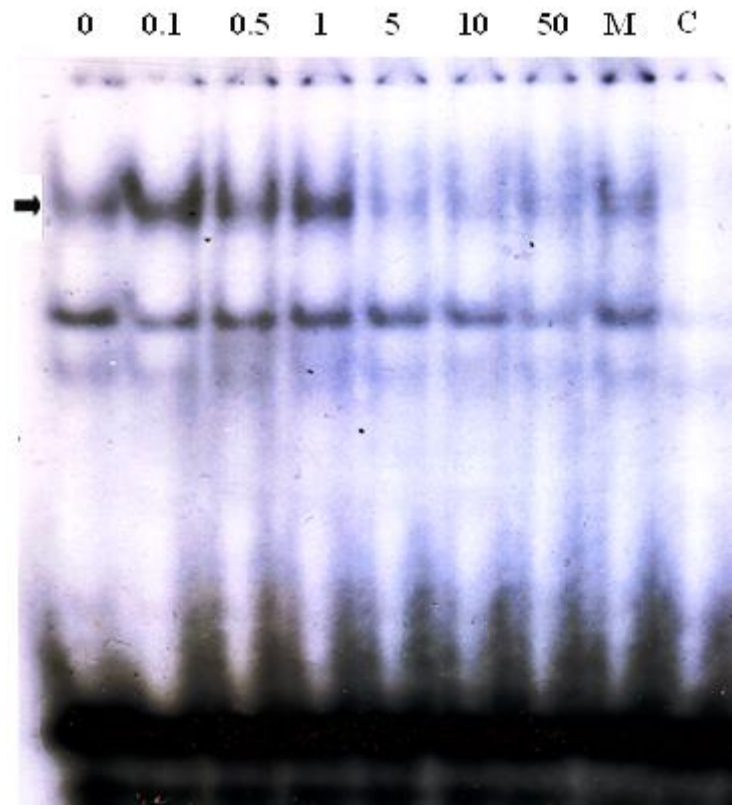

Aza-Hx-P(C_3NH_2)I

C

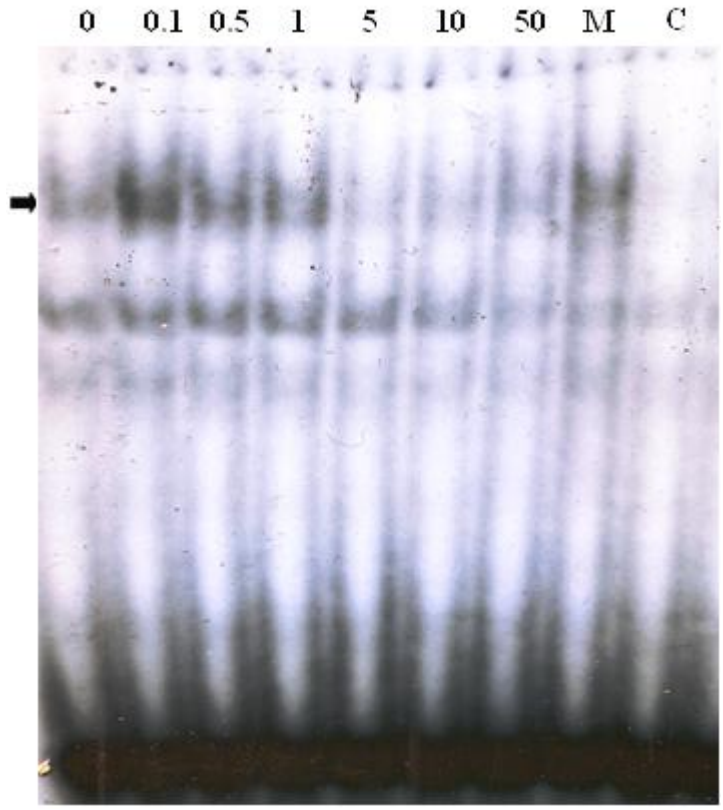

Aza-Hx-PI(C_3NH_2)

Figure 5.27 Interaction of Aza-Hx-PI, Aza-Hx-P(C_3NH_2)I and Aza-Hx-PI(C_3NH_2) with the MCB within the Dbf4 promoter. The oligonucleotide (described in Figure 5.9D) was incubated with Aza-Hx-PI (**A**), Aza-Hx-P(C_3NH_2)I (**B**) and Aza-Hx-PI(C_3NH_2) (**C**) (concentrations ranging from 0.1–50 μM) for 1 h at room temperature prior to incubation with nuclear extracts from MDA-MB231 cells. Cold (C) and mutated (M) lanes represent reactions carried out in the presence of excess unlabeled and mutated MCB oligonucleotides. The same nuclear extracts were used under the same experimental conditions in all lanes.

5.2.14 Effects of Aza-Hx-PI, Aza-Hx-P(C_3NH_2)I and Aza-Hx-PI(C_3NH_2) on the cellular levels of HuDbf4: RT-PCR and western blot analysis

The effects of Aza-Hx-PI, Aza-Hx-P(C_3NH_2)I and Aza-Hx-PI(C_3NH_2) on Dbf4 expression were analyzed in exponentially growing MDA-MB231 cells. Following 50 μM and 100 μM of Aza-Hx-PI, there is a 16.76% and 43% reduction in Dbf4 mRNA levels at 24 h, respectively, compared to untreated cells (Figure 5.28A&B). Dbf4 mRNA levels do not change noticeably when treated with 50 μM of Aza-Hx-P(C_3NH_2)I and Aza-Hx-PI(C_3NH_2) respectively at 24 h (Figure 5.28C). However, after 100 μM of Aza-Hx-P(C_3NH_2)I and Aza-Hx-PI(C_3NH_2) treatment, there is a 22% and 24% reduction in Dbf4 mRNA levels at 24 h, respectively (Figure 5.28D). At 100 μM, Aza-Hx-PI produces ~2-fold greater inhibition of mRNA levels at 24 h than either Aza-Hx-P(C_3NH_2)I or Aza-Hx-PI(C_3NH_2).

The ability of Aza-Hx-PI, Aza-Hx-P(C_3NH_2)I and Aza-Hx-PI(C_3NH_2) to affect protein expression was investigated using immunoblotting. MDA-MB231 cells were incubated with 50 μM and 100 μM Aza-Hx-PI for 24 h. Western blot analysis was performed and the results are shown in Figure 5.29.

As shown in Figure 5.29A, Aza-Hx-PI reduces the levels of Dbf4 protein after 24 h of exposure in a dose-dependent manner. In contrast, Aza-Hx-P(C_3NH_2)I has no effect on Dbf4 protein levels at even 100 μM after a 24 h incubation (Figure 5.29B). However, in Figure 5.29B, Aza-Hx-PI(C_3NH_2) shows inhibitory effects on Dbf4 protein levels at 100 μM at 24 h. As a loading control, the levels of calnexin in the cells were probed and found to be unaltered by polyamide exposure.

A

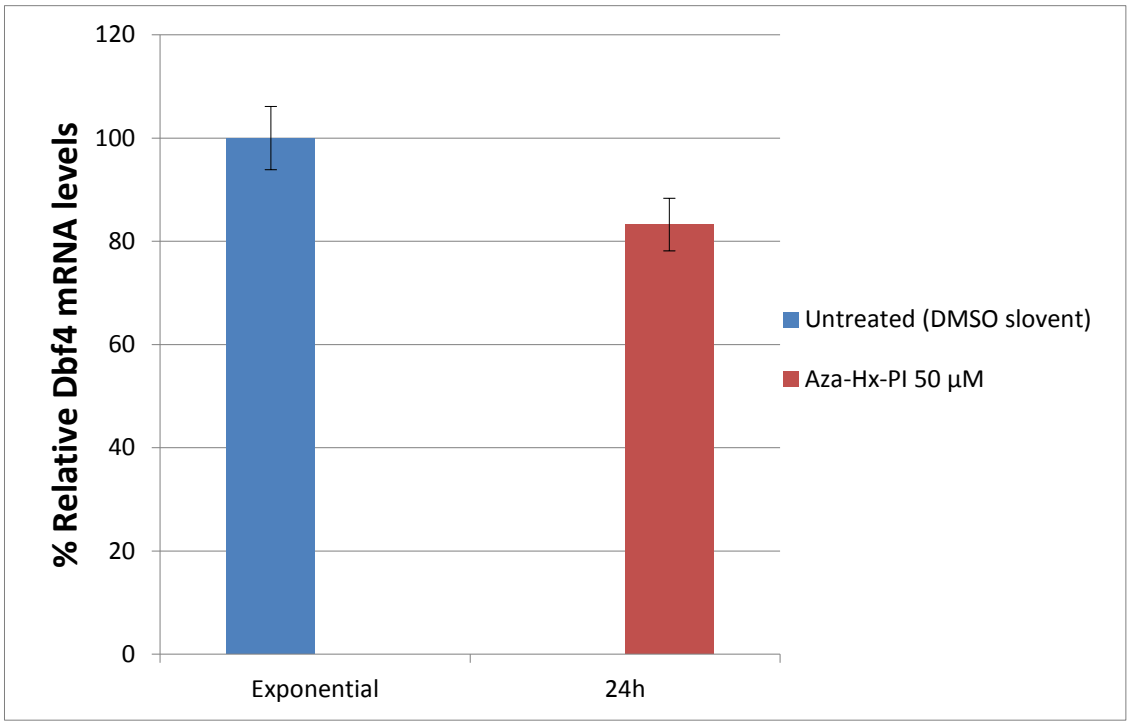
120
100
80
60
40
20
0
% Relative Dbf4 mRNA levels
Exponential
24h
Untreated (DMSO slovent)
Aza-Hx-PI 50 µM

B

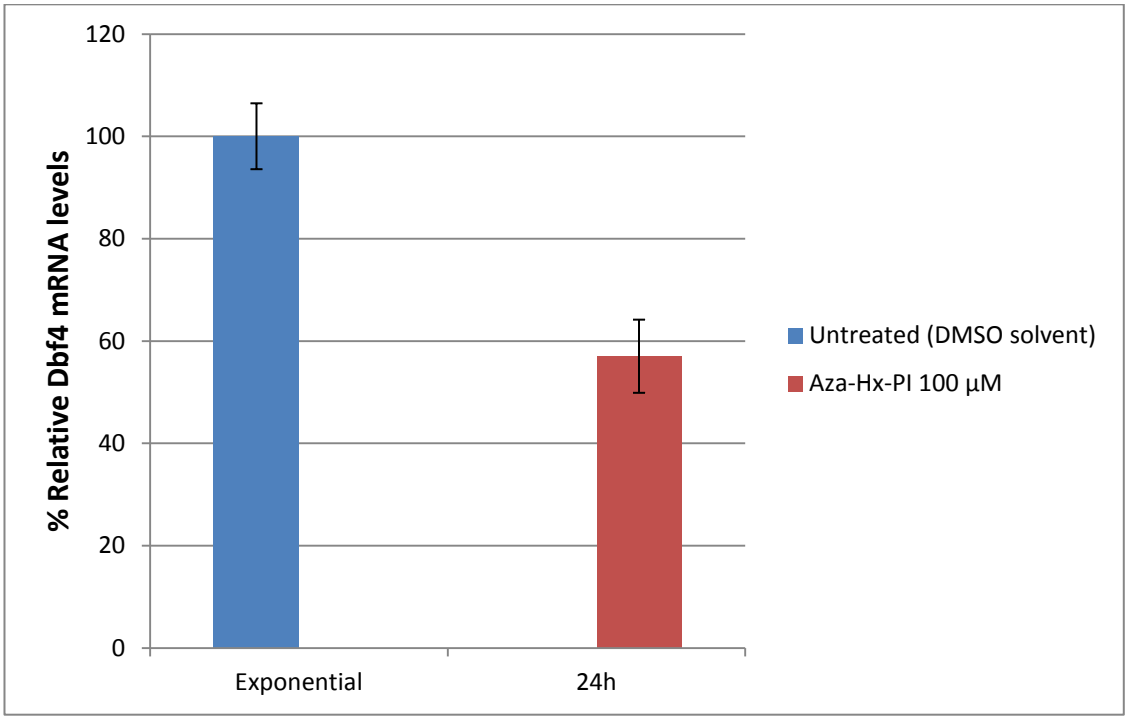
120
100
80
60
40
20
0
% Relative Dbf4 mRNA levels
Exponential
24h
Untreated (DMSO solvent)
Aza-Hx-PI 100 µM

C

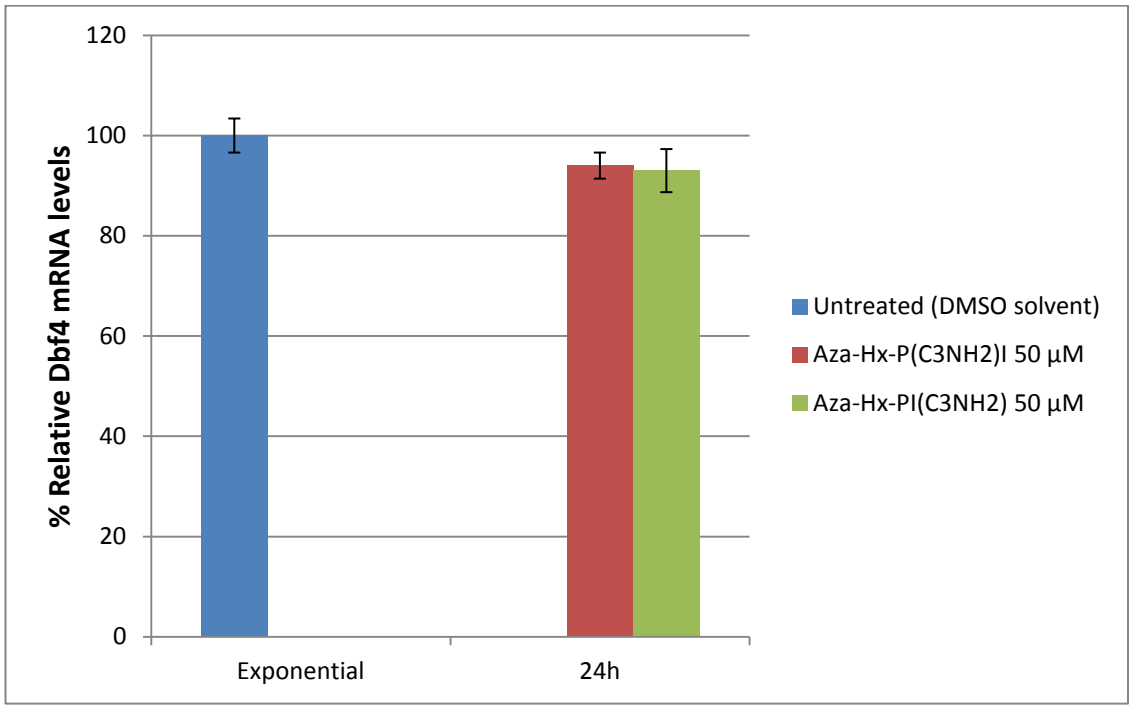

D

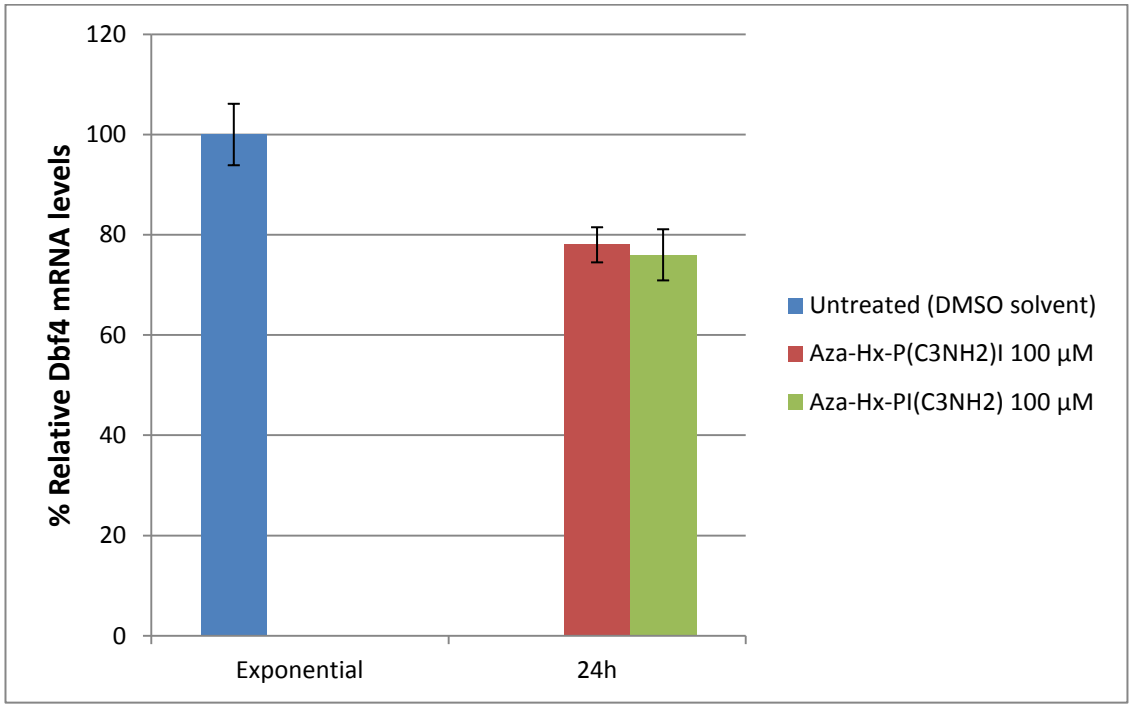

Figure 5.28 Exponentially growing MDA-MB231 cells were treated with up to 100 µM Aza-Hx-PI, Aza-Hx-P(C_3NH_2)I and Aza-Hx-PI(C_3NH_2) for 24 h. mRNA levels in Aza-Hx-PI-(**A**), Aza-Hx-P(C_3NH_2)I-(**B**) and Aza-Hx-PI(C_3NH_2)-(**C**) treated cells were expressed relative to untreated exponentially growing MDA-MB231 cells. Results are the mean of three independent experiments with error bars showing the standard deviation of the mean.

A

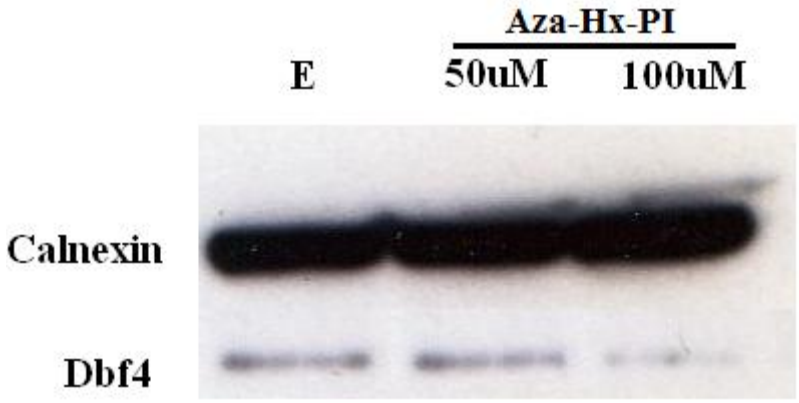

B

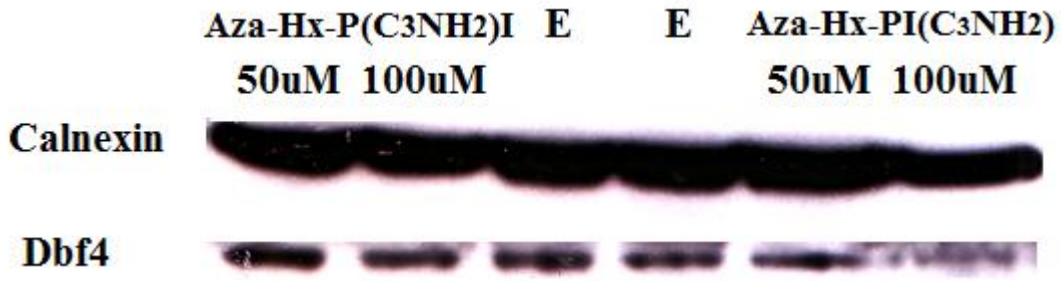

Figure 5.29 Western blot analysis of nuclear extracts following treatment with Aza-Hx-PI (**A)**, Aza-Hx-P(C_3NH_2)I and Aza-Hx-PI(C_3NH_2) (**B**). Exponential cells were treated with 50 and 100 μM Aza-Hx-PI, Aza-Hx-P(C_3NH_2)I and Aza-Hx-PI(C_3NH_2) respectively and analysis was carried out on samples collected after 24 h of drug treatment as indicated. Calnexin is shown as a loading control. Protein and RNA samples from exponentially growing cells (*E*).

5.2.15 Cellular uptake and nuclear localization of Aza-Hx-PI, Aza-Hx-P(C_3NH_2)I and Aza-Hx-PI(C_3NH_2)

MDA-MB231 breast cancer cells were used in this study of the nuclear uptake of compounds Aza-Hx-PI, Aza-Hx-P(C_3NH_2)I and Aza-Hx-PI(C_3NH_2). Figure 5.30A shows confocal microscopy images of MDA-MB231 cells exposed to Aza-Hx-PI. The cells were treated with Aza-Hx-PI at 10 μM, 30 μM and 50 μM for 2 h at 37 ℃, washed, fixed with 2.5% paraformaldehyde, and then counterstained 20 μg/μl propidium iodide (PI), which binds strongly to nucleic acids and stains principally the nucleus in red. With increasing concentrations, Aza-Hx-PI is more efficiently localized in the cell nuclei and its fluorescence (blue) colocalizes with PI (Figure 5.30A). Accumulation of the blue fluorescence in the nuclear compartment at 10 μM, 30 μM and 50 μM after 2 h exposure of Aza-Hx-PI is observed respectively while no fluorescence is detected in the untreated cells, suggesting a dose-dependent effect (Figure 5.30A). Figure 5.30B-D shows confocal images of MDA-MB231 cells exposed to Aza-Hx-PI, Aza-Hx-P(C_3NH_2)I and Aza-Hx-PI(C_3NH_2) at 50 μM for 10 min, 30 min and 2 h with the same experimental conditions described above. In all cases, the tested compounds at 50 μM are efficiently localized in the cell nuclei within minutes and their blue fluorescence signal and therefore their nuclear DNA binding increase in a time-dependent fashion (Figure 5.30B-D).

A

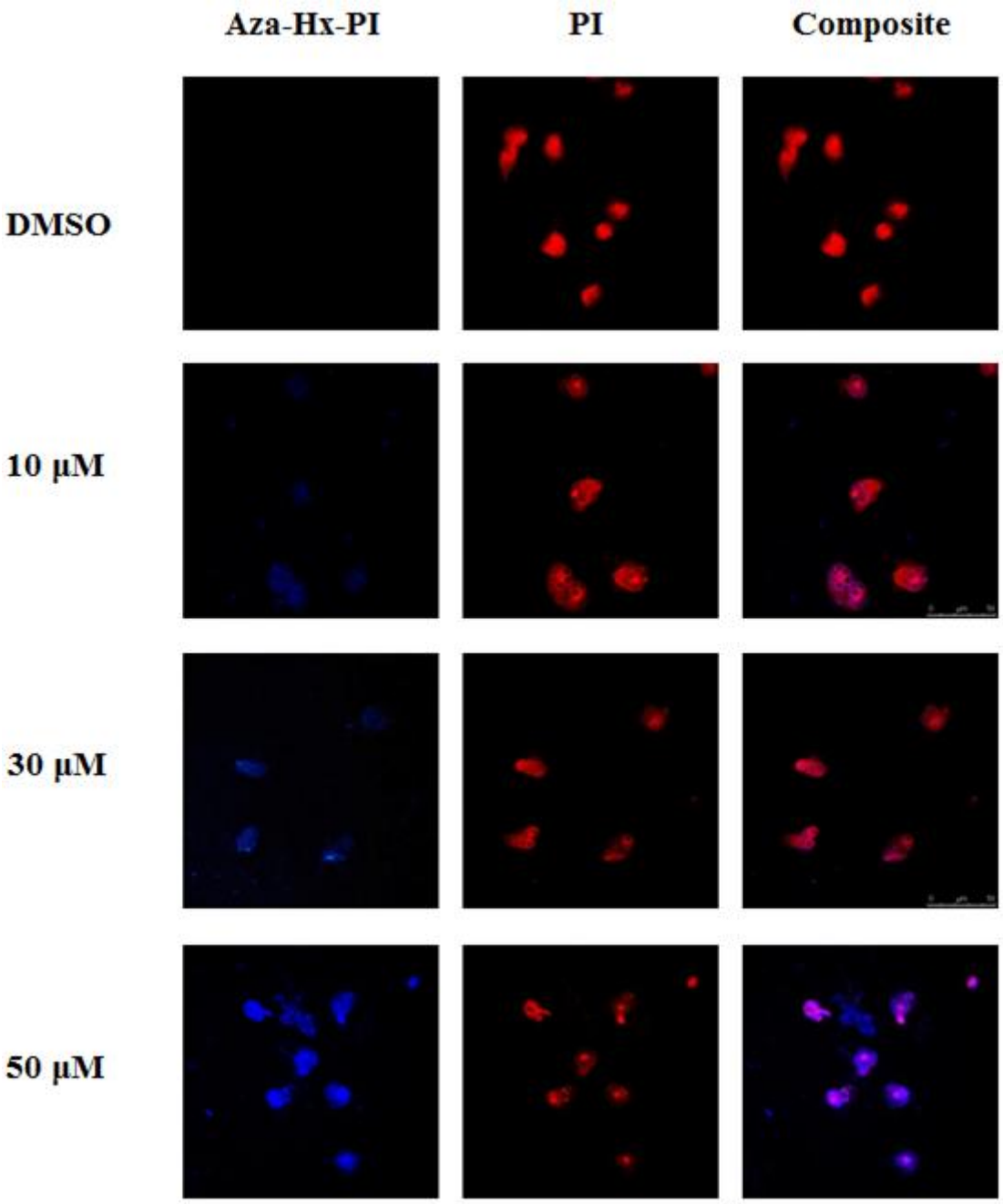

B

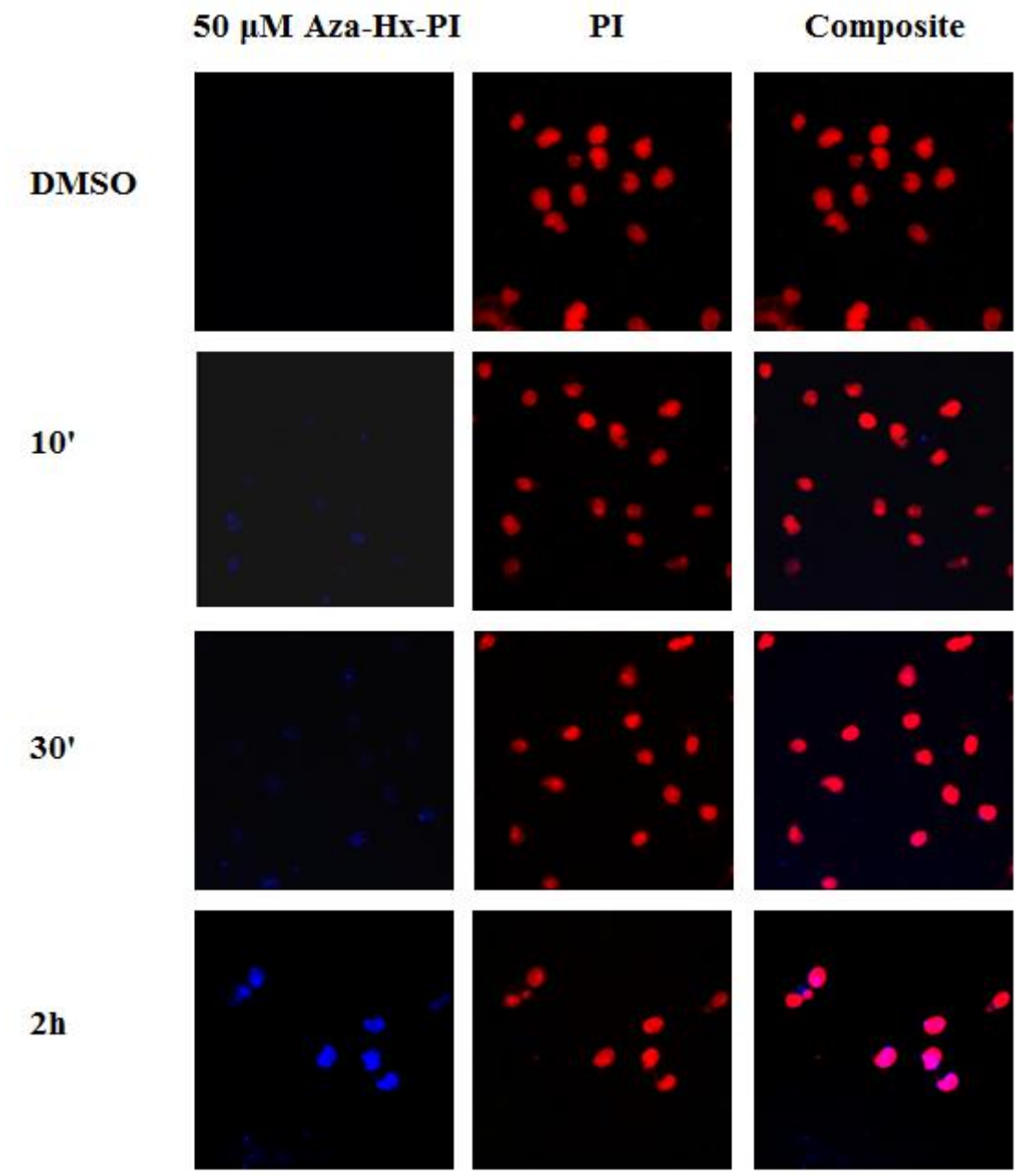

C

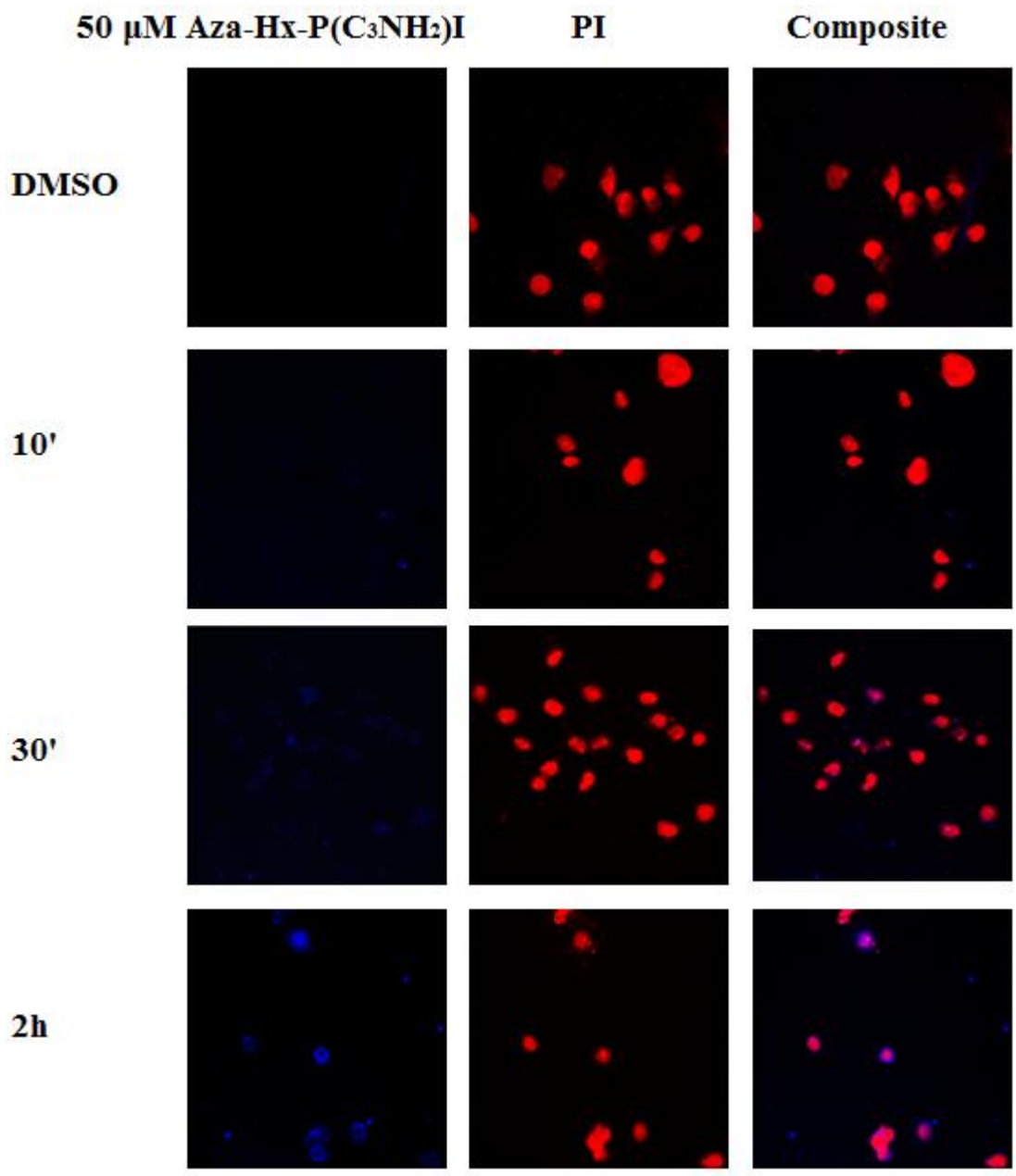

D

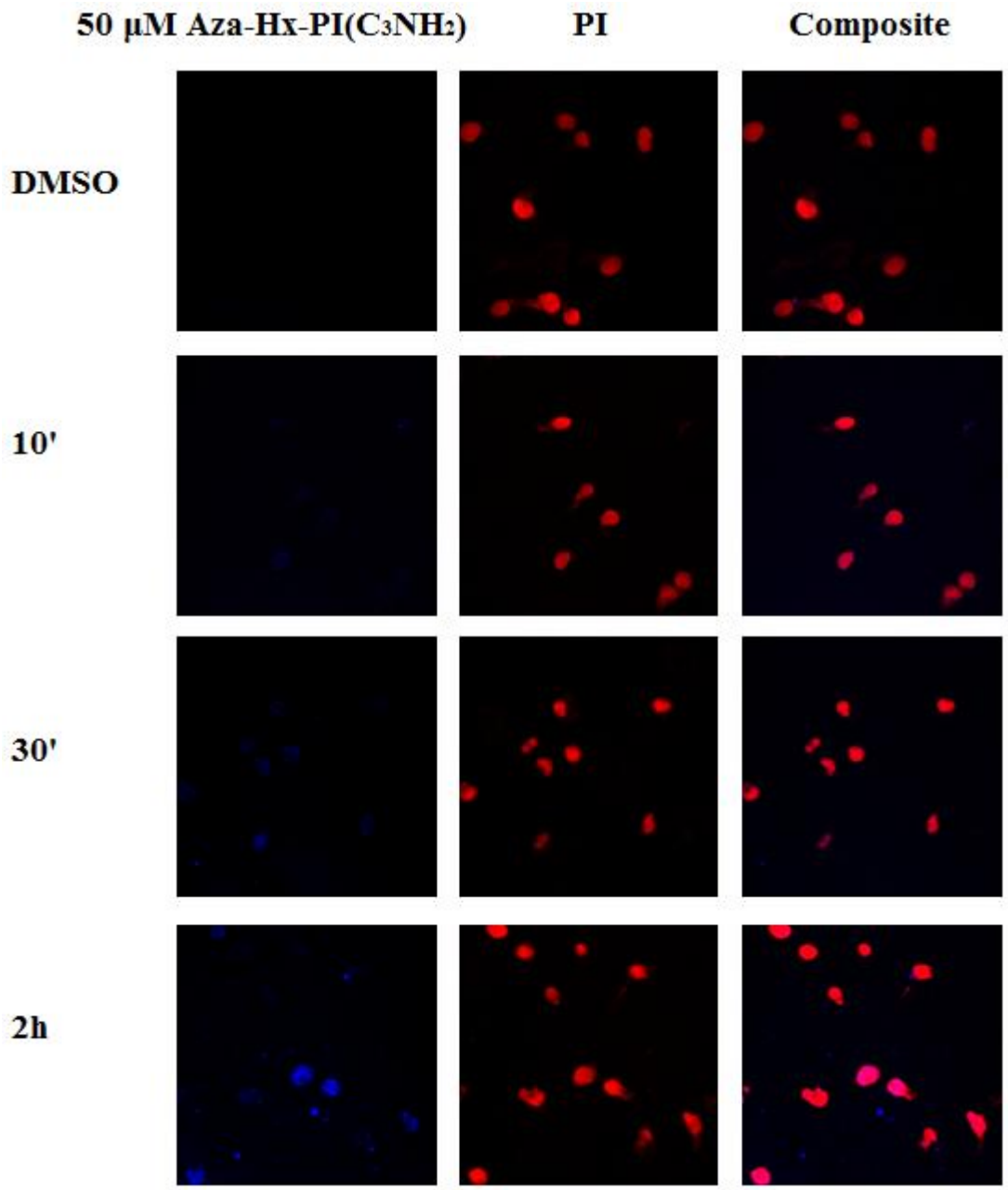

Figure 5.30 Confocal image of MDA-MB231cells stained with Aza-Hx-PI (**A,** 0, 10, 30 and 50 µM treatments for 2 h; **B,** 0 and 50 µM treatments for 10 min, 30 min and 2 h), Aza-Hx-P(C_3NH_2)I and Aza-Hx-PI(C_3NH_2) (**C** and **D,** 0 and 50 µM treatments for 10 min, 30 min and 2 h respectively), with PI (in red). The cells were incubated with the test compounds for the indicated time, washed, fixed with 2.5% paraformaldehyde, and then labelled with PI (20 µg/µl) before the microscopy observation (× 63).

5.3 Discussion

A previous study has indicated that Cdc7/Dbf4 protein levels are very low or undetectable in normal tissues (e.g., lung, breast and ovary) and cell lines (e.g., WI-38) but have increased expression in ~50% of the 62 human tumour cell lines examined (Bonte et al., 2008). The MDA-MB231 cell line has also been shown to exhibit increased Cdc7 and Dbf4 protein levels (Bonte et al., 2008).

Wu and Lee (2002) generated genomic libraries with a DNA segment containing 20kb upstream of the human Dbf4 (HuDbf4) promoter. Subsequently, the genomic libraries were pooled and transiently transfected into MDA-MB231 cells to identify the HuDbf4 DNA fragments containing promoter activity. Consequently, they found that the HuDbf4 core promoter is localized within -211 to -285 (75bp) of the translation ATG start-codon. They also showed that the MCB element present on the promoter of human Dbf4 is essential for promoter activation and a point mutation within the MCB element significantly decreases promoter activity (Wu and Lee, 2002).

The binding of polyamides to the MCB sequence in the core HuDbf4 promoter was utilized as a model system to test our rationally designed polyamide compounds, e.g. f-IPI. Many published papers have shown that f-IPI has an exceptionally high DNA-binding affinity and selectivity (e.g. Buchmueller., et al 2005, 2006). The cognate sequence 5'-ACGCGT-3'of f-IPI is a binding site of interest because it is present in the core sequence of the MCB transcriptional element found in the promoter of the human Dbf4 gene (Wu and Lee, 2002). This is an example where rationally designed

polyamides could interact with a transcriptional element and potentially control gene expression.

This study shows that sequence-specific polyamides can be used to block transcription factor/DNA interactions and therefore modulate cell-cycle progression.

The thesis investigated the potential for f-IPI, which can block MCB-targeted transcription factor/DNA interactions, to downregulate Dbf4 expression in MDA-MB231 cells. DNase I footprinting was initially employed to demonstrate that f-IPI exhibits a good binding affinity for the MCB present in the core Dbf4 promoter (Figure 5.8B). In comparison to f-IPI, its H-pin derivative showed a 2-fold improved binding affinity at the MCB (Figure 5.8C). This is consistent with the f-IPI H-pin ensuring the staggered binding motif of a 1:1 ligand/DNA complex as has been shown by our previous study (O'Hare et al., 2007). Although f-IPI prefers such a 2:1 formation, it may not always be energetically favorable. In addition, f-IPI may also bind in a mixed 2:1 and 1:1 motif, thus reducing the overall affinity. EMSA studies can provide direct evidence for the ability of small molecules to interfere with the binding of proteins to target DNA sequences. The involvement of MCB-targeted proteins in the transcriptional regulation of Dbf4 in cells was shown with EMSAs (Figure 5.9), indicating that the MCB-targeted proteins are displaced by f-IPI addition in a dose-dependent fashion (Figure 5.9A). Not surprisingly, f-IPI H-pin exhibits a greater effect on the inhibition of the MCB-targeted proteins binding compared to f-IPI (Figure 5.9C), which is consistent with the DNase I footprinting analysis.

The concept of sequence specificity achieved by polyamides is based on the pioneering work of Dervan and Lown groups (Lown et al., 1986; Swalley et al., 1996; Dervan and Edelson, 2003). The ability of these compounds to block DNA interactions in some genes at nanomolar concentrations have been shown in *vitro*, although higher concentrations need to be used in *vivo* (Best et al., 2003; Dickinson et al., 2004). However, nuclear penetration problems by these compounds have been raised as the size of the polyamide is increased as in hairpin or cyclic polyamides (Best et al., 2003; Franks et al., 2010).

The cellular effects of f-IPI and f-IPI H-pin treatments were assessed in exponentially growing MDA-MB231 cells by using RT-PCR and western blot analysis. These studies showed a reduction of Dbf4 mRNA and protein levels by f-IPI treatment in a dose-dependent fashion, suggesting a correlation between inhibition of the MCB-targeted proteins binding and down-regulation of HuDbf4 in cells (Figure 5.11 and Figure 5.12). However, in contrast to the f-IPI monomer, the H-pin analogue had no effect on the levels of HuDbf4 in cells, suggesting that the H-pin molecule does not enter the nucleus, presumably due to the large molecular size. This result is interesting in that it directly compares a monomer and an H-pin that, despite having similar binding characteristics, demonstrate such vastly different cellular properties.

The role of Dbf4 was demonstrated using a siRNA-mediated specific depletion of Dbf4 in MDA-MB231 cells. Depletion of Dbf4 at 72 h after siRNA treatment was found to be associated with a detectable reduction in cell survival (17%) and proliferation (10%) without any significant alteration in apoptosis levels (Figure 5.14). However, a previous study showed that depletion of Dbf4 in the melanoma cell line MV3, 72 h after siRNA

treatment was associated with a 40.7% and 65% decrease in cell survival and proliferation without any significant change in apoptosis (Nambiar et al., 2007). The different outcomes in the two different Dbf4 siRNA knockdown cell lines may suggest that the role of Dbf4 varies in different cell lines. This inability to produce a complete loss of cell survival and proliferation in MDA-MB231 cells and in MV3 cells may be explained by the redundancy of proliferative pathways in such cancer. Alternatively, it is also possible that in the absence of Dbf4, its homolog Drf1 may have a role in driving cell proliferation (Yoshizawa-Sugata., et al 2005). Flow cytometry analysis of untreated, scrambled-control and Dbf4 siRNA knockdown cells was performed at 24 and 48 h post transfection (Figure 5.15). Detectable G_1 arrest was observed at 48 h in siRNA-treated cells as compared to scrambled or untreated control cells.

The effects of f-IPI on cell growth, apoptosis and proliferation in MDA-MB231 cells were investigated using cell survival, apoptosis and proliferation assays. Without any significant effect on apoptosis, there was a respective 27.2% and 33.5% reduction in cell survival and proliferation after treatment with 200 μM f-IPI for 24 h (Figure 5.16). Compared to siRNA-mediated specific depletion of Dbf4, 200 μM f-IPI showed a 2-3 fold greater effect on cell survival and proliferation at 24 h. However, 200 μM f-IPI only induced a 57% depletion of Dbf4 mRNA levels at 24 h, compared to >90% depletion by Dbf4 siRNA knockdown. These results suggest that f-IPI might target other key genes (e.g., Drf1) that have a complementary role in driving cell proliferation or Dbf4 might be partially involved in the DNA replication and cell growth regulation in MDA-MB231 breast cancer cells. Subsequently, flow cytometry analysis of 50 and 100 μM f-IPI-treated MDA-MB231 cells was carried out (Figure 5.17). f-IPI induces a noticeable G_1 arrest in MDA-MB231 cells in the dose-dependent manner. This result

suggests that the alteration of the Dbf4 protein levels is associated with a role in cell cycle regulation, in addition to Dbf4 siRNA knockdown-induced G_1 arrest in MDA-MB231 cells.

The f-IPI H-pin analogue showed improved DNA binding affinity and greater inhibition of protein binding *in vitro* than its monomer f-IPI. However, it did not exhibit cellular effects, suggesting that it cannot enter the nucleus, presumably because of its large molecular size. Therefore, the subsequent study aimed to test the *in situ* reaction of two rationally designed polyamide monomers [f-IP(C_3NH_2)I and f-IP(C_3Cl)I] capable of potentially forming H-pin structure by click chemistry in the nucleus.

DNase I footprinting was employed and a footprint was produced at 0.5 μM by f-IP(C_3NH_2)I, indicating a 10-fold higher DNA-binding affinity for the MCB than f-IP(C_3Cl)I. In comparison, when 0.05 μM of f-IP(C_3NH_2)I were mixed with 0.05 μM of f-IP(C_3Cl)I, a footprint occurs, which suggest that the hybrid molecule possesses a higher DNA-binding affinity than either f-IP(C_3NH_2)I or f-IP(C_3Cl)I alone (Figure 5.18).

The EMSA studies showed that a dose-dependent inhibition of the MCB-targeted protein binding is caused by f-IP(C_3NH_2)I treatment with the inhibitory effect observed from 0.1 μM. In contrast, there is only a limited inhibition of protein binding by f-IP(C_3Cl)I at 10 μM. When 0.25 μM of f-IP(C_3NH_2)I were mixed with 0.25 μM of f-IP(C_3Cl)I, the inhibition of the MCB-targeted protein binding by the combination occurs as was the case for 0.5 μM f-IP(C_3NH_2)I alone (Figure 5.19). The question raised from these results is how f-IP(C_3Cl)I when used at half the concentration (0.25 μM) in

combination with f-IP(C_3NH_2)I, which generates a lower protein binding inhibition, produces the same results as when f-IP(C_3NH_2)I is used alone at double the concentration (0.5 μM). One possibility is that f-IP(C_3NH_2)I does react with f-IP(C_3Cl)I to form a favorable H-pin compound, which can compensate for the lower inhibitory effect of f-IP(C_3Cl)I on protein binding to the MCB in the *in situ* reaction.

The cellular effects of compounds f-IP(C_3NH_2)I, f-IP(C_3Cl)I and their combination were tested in exponentially growing MDA-MB231 cells by using RT-PCR, western blot analysis and flow cytometry analysis. f-IP(C_3NH_2)I caused a greater reduction of Dbf4 mRNA and protein levels at either 50 μM or 100 μM at 24 h than f-IP(C_3Cl)I (Figure 5.20A&B and Figure 5.21A&B). However, when 25 μM of f-IP(C_3NH_2)I were mixed with 25 μM of f-IP(C_3Cl)I, the combination produced the greatest reduction of Dbf4 mRNA and protein levels at 24 h when compared to either 50 μM of f-IP(C_3NH_2)I or 50 μM of f-IP(C_3Cl)I alone (Figure 5.20 and Figure 5.21). The effects were more pronounced at a higher concentration, when 50 μM of f-IP(C_3NH_2)I were mixed with 50 μM of f-IP(C_3Cl)I. Flow cytometry analysis showed that the combination (50 μM of each compound) induces a greater G_1 arrest at 24 h than either 100 μM of f-IP(C_3NH_2)I or 100 μM of f-IP(C_3Cl)I alone (Figure 5.22).

The effects of the tested compounds f-IP(C_3NH_2)I, f-IP(C_3Cl)I and their combination on cell growth, apoptosis and proliferation in MDA-MB231 cells were investigated using cell survival, apoptosis and proliferation assays (Figure 5.23 and Figure 5.24). The dose-dependent effects of f-IP(C_3NH_2)I on cell survival were shown and this polyamide presented a greater decrease of cell survival than either the combination or f-IP(C_3Cl)I

(Figure 5.24A&B). F-IP(C_3NH_2)I also exhibited higher apoptosis levels than either the combination or f-IP(C_3Cl)I in a dose-dependent fashion (Figure 5.24C&D). However, the combination showed a greater reduction of DNA replication in the cell proliferation assay than either f-IP(C_3NH_2)I or f-IP(C_3Cl)I in a dose-dependent fashion, suggesting a potential H-pin structure formation (Figure 5.24E&F).

Together the results suggest that f-IP(C_3NH_2)I may react with f-IP(C_3Cl)I under a nucleophilic substitution reaction, to produce *in situ* H-pin formation. The resulting H-pin molecule would be expected to have a greater DNA-binding affinity and be capable of producing inhibition of the MCB-targeted protein binding in *vitro* more efficiently. Additionally, it would be expected to elicit a higher reduction of Dbf4 mRNA and protein levels, and cause G_1 arrest at a higher level with a greater reduction in DNA replication in cells.

With the aim of incorporating a recognition element that acts as a fluorescent probe upon binding to DNA, three novel pyrrole (P) and imidazole (I)-containing polyamides were synthesized. The compounds Aza-Hx-PI, Aza-Hx-P(C_3NH_2)I and Aza-Hx-PI(C_3NH_2) were then tested.

These fluorescent analogues were designed to target the 5'-ACGCGT-3' sequence and this was therefore tested against the MCB by using DNase I footprinting and EMSAs analysis. DNA footprinting revealed a footprint for Aza-Hx-PI and Aza-Hx-P(C_3NH_2)I over the MCB site at the same concentration (Figure 5.26A&B). In comparison, Aza-Hx-PI(C_3NH_2) exhibited a slightly higher binding affinity than either Aza-Hx-PI or Aza-Hx-P(C_3NH_2)I (Figure 5.26C). However, Aza-Hx-P(C_3NH_2)I and Aza-Hx-

PI(C_3NH_2) also showed binding over the non-cognate 5'-AAACGA-3' sequence compared to Aza-Hx-PI, suggesting that Aza-Hx-P(C_3NH_2)I and Aza-Hx-PI(C_3NH_2) possessed less sequence specificity. In EMSA studies, a dose-dependent inhibition of MCB-targeted protein binding was observed after treatment with Aza-Hx-PI and the effect was shown at doses as low as 0.5 μM. Aza-Hx-PI exhibited a greater inhibition than either Aza-Hx-P(C_3NH_2)I or Aza-Hx-PI(C_3NH_2) (Figure 5.27). The DNase I footprinting and EMSAs analysis confirmed that these fluorescent hybrids mimic f-IPI or PIPI, targeting the MCB present in the Dbf4 core promoter sequences.

RT-PCR and western blot analysis were also employed in the study for investigating the cellular effects of Aza-Hx-PI, Aza-Hx-P(C_3NH_2)I and Aza-Hx-PI(C_3NH_2) in exponentially growing MDA-MB231 cells (Figure 5.28 and Figure 5.29). Aza-Hx-PI treatment of cells resulted in reduced Dbf4 mRNA and protein levels in a dose-dependent fashion at 24 h (Figure 5.29A). In contrast, Aza-Hx-P(C_3NH_2)I and Aza-Hx-PI(C_3NH_2) resulted in a much lower decrease of Dbf4 mRNA and protein levels at 24 h than Aza-Hx-PI (Figure 5.29B).

Aza-Hx-PI, Aza-Hx-P(C_3NH_2)I and Aza-Hx-PI(C_3NH_2) were found to efficiently localize in the cell nuclei by as early as 10 min at 50 μM, suggesting that these fluorescent analogues can be used as probes for monitoring cellular uptake and nuclear localization in cells, in addition to the specific modulation of gene expression.

CHAPTER 6

CONCLUSION

The limited success of many current chemotherapies requires a new generation of anticancer strategies, able to discriminate more effectively between tumour and normal tissues. In the past, it has been attempted to regulate the transcription of key disease-related genes either indirectly by targeting gene transcripts or alternatively by direct interaction with genomic DNA (Pandolfi, 2001; Darnell, 2002). Many minor groove-binding polyamides have been developed for this purpose and demonstrate the strong DNA sequence recognition that would be required for specific targeting of genomic DNA. The discovery that distamycin A can form an antiparallel dimer in the minor groove of AT-rich sequences initiated the rational design of the original DNA sequence reading polyamides (Urbach and Dervan, 2001; Dervan and Burlii, 1999). Pyrrole-imidazole containing polyamide analogues of distamycin A can bind in the minor groove of DNA at specific DNA sequences in a stacked fashion (Mitra et al., 1999; Pelton and Wemmer, 1999). After extensive research, the basic 'pairing rules' were developed for the minor groove binding of polyamides containing pyrrole and imidazole groups (Wade et al., 1992; Gottesfeld et al., 1997; Dervan et al., 1999, 2003). Such polyamides can target predetermined DNA sequences with high affinity and potentially modulate gene expression by interfering with the binding of transcription factors to DNA (Gottesfeld et al., 1997; Dickinson et al., 1999; Mapp et al., 2000; Hochhauser et al., 2007; Kotecha et al., 2008).

H-pin analogues have been previously designed and tested by our group, showing enhanced DNA binding affinity and selectivity compared to monomer polyamides

(O'Hare et al., 2007). However, their large molecular size is associated with poor cellular uptake (Franks et al., 2010). A new class of unlinked polyamide precursors containing appropriate pendant reactive and biocompatible functional groups was designed and synthesized. In this thesis, the approach of the *in situ* reaction of two rationally designed polyamide monomers capable of potentially forming either H-pin or Hairpin conjugates in the nucleus was tested. DNase I footprinting results suggest that f-IP(C_3NH_2)I has the potential of interacting with f-IP(C_3Cl)I to form a favorable H-pin compound under a nucleophilic substitution; the two monomers f-IP(C_3N_3)I and f-PP(C_3-alkyne)P can interact *in situ* to form a heterodimer H-pin molecule under an azide-alkyne Huisgen reaction; f-IP(C_3-alkyne)I can interact with f-PP(C_3N_3)P to allow *in situ* formation of a heterodimer H-pin polyamide. Although the footprinting data suggest H-pin formation, it was difficult to prove whether a stable 2:1 complex is covalently formed. Further studies and assessment by other techniques is therefore required. It is interesting to find that the different pendant reactive groups on polyamides [e.g. f-IP(C_3NH_2)I vs f-IP(C_3Cl)I] can influence binding affinity, so further evaluation of different reactive groups on the same parent polyamides is also required.

The f-IPI analogues were modified with the aim of acquiring analogues with improved sequence specificity, stronger binding affinity and high solubility in biological media. The polyamides containing a pyrrole-N1-alkyl spermine/spermidine group target A/T rich sequences and bind with high affinity because the additional cationic groups interact with the negatively charged phosphodiester groups of DNA (Satz and Bruice, 2002). The diamino f-I(C_3NH_2)PI, f-P(C_3NH_2)IP, f-IPP(C_3NH_2) and phenyl-IP(C_3NH_2)I were designed and tested, showing higher DNA binding affinity than their non-amino counterparts. Compared to the monoamino polyamides, the diamino polyamides possess

enhanced water solubility because of the ease in dissolving in media. Overall, it is evident that the incorporation of an orthogonally positioned aminopropyl side chain in the polyamide backbone can afford favorable physicochemical and DNA binding properties. In addition, positioning the pendant reactive group at different sites on the polyamides can influence binding affinity [e.g. f-IP(C_3NH_2)I vs f-I(C_3NH_2)PI], thus its position within the polyamides is important and required for a further evaluation.

The identification of novel molecular targets is essential for the development of new and efficient cancer therapies. Previous studies on the molecular basis of various diseases have revealed that kinases are one of the most common drug targets, associated with many disease states, particular cancer (Noble et al., 2004). Therefore, modulating aberrant kinase activities in cancer cells may form an effective cancer therapy, with fewer side effects than traditional cytotoxic drugs. Cell cycle progression is regulated by a number of kinases, some of which are being developed to treat cancer. Cell death is caused by acute genomic instability, induced by the combined effects of the aberrant cell cycle progression, destabilization of replication forks, impaired DNA damage responses and uncoupling of S phase with mitosis due to checkpoint defects. Cancer cells are generally associated with defects in checkpoint response pathways, and hence indicate greater sensitivity to S phase perturbation than normal cells. Thereby the critical importance of Cdc7-Dbf4 kinase in the survival of tumour cells and the tumor-specific cell death observed with Cdc7 inhibition or depletion (Kim et al., 2003) makes this a potential target for anti-cancer drug development.

Dbf4 is the regulatory subunit of Cdc7 (cyclin dependent 7) kinase, which is a conserved serine/threonine kinase essential for the initiation of DNA replication, likely

by activating the MCM DNA helicase at the G_1- to S-phase transition (Bousse and Diffley, 1998). Cdc7 kinase activity is cell-cycle dependent as it is low during G_1 and becomes activated with the initiation of the S phase, whereas its mRNA and protein levels are relatively constant throughout the cell cycle (Jiang et al., 1999; Kumagai et al., 1999; Ferreira et al., 2000). High levels of Dbf4 protein are generally associated with Cdc7 kinase activity and are critically important for its regulation (Jackson et al., 1993; Nougarede et al., 2000). Therefore, maintaining appropriate levels of Dbf4 protein is a primary control point at the initiation of DNA replication (Chapman and Johnston, 1989; Lepke et al., 1999). Cdc7 and Dbf4 proteins form a complex *in vivo* to generate an active protein kinase (Kumagai et al., 1999), which is a target of the S-phase checkpoint pathway, and plays an important role in promoting DNA damage response in multiple organisms (Takeda et al., 1999; Weinreich and Stillman, 1999). Human Cdc7-Dbf4 kinase activity is essential for cell proliferation by activating DNA replication. High levels of the human Cdc7/Dbf4 kinase activity have been implicated in a large number of aggressive solid cancers (Hess et al., 1998; Yamada et al., 2002).

An investigation into the *in vitro* binding characteristics of f-IPI to the HuDbf4 and its cellular effects in MDA-MB231 cells was carried out in Chapter 5. f-IPI has a good binding affinity for the MCB sequences present in the core Dbf4 promoter and can also inhibit protein binding to the MCB *in vitro*. However, the f-IPI H-pin derivative shows an enhanced DNA binding affinity and a higher degree of inhibition of MCB-targeted protein binding.

The cellular studies in this thesis showed a f-IPI dose-dependent reduction in the levels of Dbf4 mRNA and protein in MDA-MB231 cells, suggesting a good correlation

between inhibition of the MCB-targeted protein binding and down-regulation of Dbf4 in cells. However, in contrast to the f-IPI monomer, the f-IPI H-pin exhibits no effect on the Dbf4 protein levels in cells, suggesting that the H-pin polyamide does not enter the nucleus, presumably due to its large molecular size and cannot bind the MCB *in vivo*. Flow cytometry analysis showed that both f-IPI and Dbf4 siRNA knockdown can induce G_1 arrest in MDA-MB231 cells, confirming that Dbf4 plays an important role in regulating cell cycle.

The Dbf4 siRNA treatment in MDA-MB231 cells at 72 h results in greater reduction of Dbf4 mRNA levels compared to treatment with 200 μM f-IPI. However, f-IPI has a higher effect on cell survival and proliferation than the Dbf4 siRNA treatment, suggesting that f-IPI targets other key genes (e.g., Dbf4's homolog Drf1) that have a complementary role in driving cell proliferation or Dbf4 might only have a partial role in DNA replication and cell growth regulation in MDA-MB231 cells. Nambiar and co-workers reported that siRNA-mediated depletion of Dbf4 in the melanoma cell line MV3 at 72 h cause a greater decrease of cell survival and proliferation without any significant change in apoptosis, when compared to Dbf4 siRNA knockdown in MDA-MB231 cells (Nambiar et al., 2007). This suggests that the role of Dbf4 varies in different cancer cell lines. Further investigation of the involvement of Drf1 and the role of Dbf4 in different cancer cell lines is therefore required.

Collectively, the pyrrole-imidazole polyamides represent a class of small molecules that can be designed to recognize predetermined DNA sequence. These molecules have affinities and specificities that equal or exceed natural eukaryotic transcriptional

regulatory proteins, and are potent inhibitors of protein-DNA interactions, thus they can be potentially used as a gene control agent, especially for anti-cancer drug development. The Dbf4 promoter was utilized as a model system for f-IPI and was also employed for the study of the *in situ* formation of H-pin approach *in vitro* and in cells. The studies demonstrated that f-IP(C_3NH_2)I does react with f-IP(C_3Cl)I, forming in *situ* the H-pin structure that is capable of eliciting higher DNA-binding affinity and greater inhibition of the protein binding to the MCB in *vitro.* Moreover, the H-pin molecule downregulates Dbf4, produces G_1 arrest and prevents DNA replication at a higher level than each compound alone in MDA-MB231 cells. The data confirmed that the approach is feasible and can be used to design the next generation of polyamides that form H-pin structure in the nucleus, having greater DNA binding affinity and selectivity.

Hx-polyamide compounds bind DNA in a highly sequence selective manner (Chavda et al., 2011). The Hx moiety when incorporated into polyamides provides a direct means to measure polyamide binding in the minor groove of DNA in a test tube or in cells by fluorescence. The fluorescent hybrids, Aza-Hx-PI, Aza-Hx-P(C_3NH_2)I and Aza-Hx-PI(C_3NH_2), mimic f-IPI and target the MCB sequences present in the core Dbf4 promoter. Aza-Hx-PI, Aza-Hx-P(C_3NH_2)I and Aza-Hx-PI(C_3NH_2) were found to efficiently localize in the cell nuclei within minutes. The Hx moiety represents a significant advancement in the polyamide field, owing to its simple molecular design and ease of synthesis. Sequence targeted Hx polyamides such as those presented in this study provide a direct and simple way to monitor binding, without the incorporation of a bulky fluorescent tag. Therefore such fluorophores can be used to detect polyamides' cellular uptake and nuclear localization, in addition to their ability to target the DNA sequences as a potential gene-control agents.

In conclusion the *in vitro* study of the DNA selectivity and affinity of polyamides, the effects of structural modifications on their interactions with DNA and the incorporation of fluorophores for monitoring their nuclear localization, enable us to further improve their use for gene targeting purposes. In addition, for the prediction of the biological consequences of polyamide binding in cells to be possible, a greater understanding is required of the accessibility of sequences in genomic DNA, the dynamics of nucleosomal organization and the mechanisms of transcriptional activation. Consequently, the design of the next generation of polyamides will require a more thorough understanding of these factors to achieve realistic therapeutic utility.

REFERENCES

1. Ahmed MM. Regulation of radiation-induced apoptosis by early growth response-1 gene in solid tumors. Curr Cancer Drug Targets 2004;4:43-52.

2. Ahmed MM, Sells SF, Venkatasubbarao K, et al. Ionizing radiation-inducible apoptosis in the absence of p53 linked to transcription factor EGR-1. J Biol Chem 1997;272:33056-61.

3. Alvarez D, Chou CJ, Latella L, et al. A two-hit mechanism for pre-mitotic arrest of cancer cell proliferation by a polyamide-alkylator conjugate. Cell Cycle 2006;5:1537-48.

4. Andrews BJ, Moore LA. Interaction of the yeast Swi4 and Swi6 cell cycle regulatory proteins in vitro. Proc Natl Acad Sci U S A 1992;89:11852-6.

5. Arcamone F. Synthesis and DNA binding selectivity of pyrrole-amidine oligopeptides. Farmaco 1993;48:143-50.

6. Ayash LJ, Wright JE, Tretyakov O, et al. Cyclophosphamide pharmacokinetics: correlation with cardiac toxicity and tumor response. J Clin Oncol 1992;10:995-1000.

7. Babu B, Liu Y, Plaunt A, et al. Design, synthesis and DNA binding properties of orthogonally positioned diamino containing polyamide f-IPI. Biochem Biophys Res Commun;404:848-52.

8. Bailly C, Chaires JB. Sequence-specific DNA minor groove binders. Design and synthesis of netropsin and distamycin analogues. Bioconjug Chem 1998;9:513-38.

9. Baldwin EL, Osheroff N. Etoposide, topoisomerase II and cancer. Curr Med Chem Anticancer Agents 2005;5:363-72.

10. Ballou LM, Lin RZ. Rapamycin and mTOR kinase inhibitors. J Chem Biol 2008;1:27-36.

11. Baraldi PG, Bovero A, Fruttarolo F, et al. DNA minor groove binders as potential antitumor and antimicrobial agents. Medicinal Research Reviews 2004;24:475-528.

12. Baraldi PG, Cacciari B, Guiotto A, et al. [2,1-c][1,4]benzodiazepine (PBD)-distamycin hybrid inhibits DNA binding to transcription factor Sp1. Nucleosides Nucleotides Nucleic Acids 2000;19:1219-29.

13. Baraldi PG, Cacciari B, Romagnoli R, et al. Pyrazolo[4,3-e]1,2,4-triazolo[1,5-c]pyrimidine derivatives as highly potent and selective human A(3) adenosine receptor antagonists: influence of the chain at the N(8) pyrazole nitrogen. J Med Chem 2000;43:4768-80.

14. Baraldi PG, Preti D, Fruttarolo F, Tabrizi MA, Romagnoli R. Hybrid molecules between distamycin A and active moieties of antitumor agents. Bioorganic & Medicinal Chemistry 2007;15:17-35.

15. Barbacid M, Ortega S, Sotillo R, et al. Cell cycle and cancer: genetic analysis of the role of cyclin-dependent kinases. Cold Spring Harb Symp Quant Biol 2005;70:233-40.

16. Bardelli A, Parsons DW, Silliman N, et al. Mutational analysis of the tyrosine kinome in colorectal cancers. Science 2003;300:949.

17. Belitsky JM, Leslie SJ, Arora PS, Beerman TA, Dervan PB. Cellular uptake of N-methylpyrrole/N-methylimidazole polyamide-dye conjugates. Bioorg Med Chem 2002;10:3313-8.

18. Bell SP, Dutta A. DNA replication in eukaryotic cells. Annu Rev Biochem 2002;71:333-74.

19. Berger JM, Gamblin SJ, Harrison SC, Wang JC. Structure and mechanism of DNA topoisomerase II. Nature 1996;379:225-32.

20. Berger JM, Wang JC. Recent developments in DNA topoisomerase II structure and mechanism. Curr Opin Struct Biol 1996;6:84-90.

21. Best TP, Edelson BS, Nickols NG, Dervan PB. Nuclear localization of pyrrole-imidazole polyamide-fluorescein conjugates in cell culture. Proc Natl Acad Sci U S A 2003;100:12063-8.

22. Bodley A, Liu LF, Israel M, et al. DNA topoisomerase II-mediated interaction of doxorubicin and daunorubicin congeners with DNA. Cancer Res 1989;49:5969-78.

23. Boger DL, Johnson DS. CC-1065 and the duocarmycins: unraveling the keys to a new class of naturally derived DNA alkylating agents. Proc Natl Acad Sci U S A 1995;92:3642-9.

24. Bonte D, Lindvall C, Liu H, Dykema K, Furge K, Weinreich M. Cdc7-Dbf4 kinase overexpression in multiple cancers and tumor cell lines is correlated with p53 inactivation. Neoplasia 2008;10:920-31.

25. Bontemps J, Houssier C, Fredericq E. Physico-chemical study of the complexes of "33258 Hoechst" with DNA and nucleohistone. Nucleic Acids Res 1975;2:971-84.

26. Boulikas T, Pantos A, Bellis E, Christofis P. Designing platinum compounds in cancer: structures and mechanisms. Cancer Therapy 2007;5:537-83.

27. Boulikas T, Vougiouka M. Cisplatin and platinum drugs at the molecular level. (Review). Oncol Rep 2003;10:1663-82.

28. Boulikas T, Vougiouka M. Recent clinical trials using cisplatin, carboplatin and their combination chemotherapy drugs (review). Oncol Rep 2004;11:559-95.

29. Bousset K, Diffley JF. The Cdc7 protein kinase is required for origin firing during S phase. Genes Dev 1998;12:480-90.

30. Breeden L, Nasmyth K. Similarity between cell-cycle genes of budding yeast and fission yeast and the Notch gene of Drosophila. Nature 1987;329:651-4.

31. Breeden L, Nasmyth K. Cell cycle control of the yeast HO gene: cis- and trans-acting regulators. Cell 1987;48:389-97.

32. Bremer RE, Szewczyk JW, Baird EE, Dervan PB. Recognition of the DNA minor groove by pyrrole-imidazole polyamides: comparison of desmethyl- and N-methylpyrrole. Bioorg Med Chem 2000;8:1947-55.

33. Brown GW, Kelly TJ. Cell cycle regulation of Dfp1, an activator of the Hsk1 protein kinase. Proc Natl Acad Sci U S A 1999;96:8443-8.

34. Brown K, Luddington R, Baglin T. A common polymorphism in the tumour necrosis factor-alpha gene associated with high TNF levels is not a risk factor for venous thromboembolism. Br J Haematol 1998;101:480-2.

35. Brown T, Mackay H, Turlington M, et al. Modifying the N-terminus of polyamides: PyImPyIm has improved sequence specificity over f-ImPyIm. Bioorg Med Chem 2008;16:5266-76.

36. Buchmueller KL, Bailey SL, Matthews DA, et al. Physical and structural basis for the strong interactions of the -ImPy- central pairing motif in the polyamide f-ImPyIm. Biochemistry 2006;45:13551-65.

37. Buchmueller KL, Staples AM, Uthe PB, et al. Molecular recognition of DNA base pairs by the formamido/pyrrole and formamido/imidazole pairings in stacked polyamides. Nucleic Acids Res 2005;33:912-21.

38. Buchmueller KL, Taherbhai Z, Howard CM, et al. Design of a hairpin polyamide, ZT65B, for targeting the inverted CCAAT box (ICB) site in the multidrug resistant (MDR1) gene. Chembiochem 2005;6:2305-11.

39. Burden DA, Osheroff N. Mechanism of action of eukaryotic topoisomerase II and drugs targeted to the enzyme. Biochim Biophys Acta 1998;1400:139-54.

40. Burkhart DL, Sage J. Cellular mechanisms of tumour suppression by the retinoblastoma gene. Nat Rev Cancer 2008;8:671-82.

41. Butel JS. Viral carcinogenesis: revelation of molecular mechanisms and etiology of human disease. Carcinogenesis 2000;21:405-26.

42. Cai X, Gray PJ, Jr., Von Hoff DD. DNA minor groove binders: back in the groove. Cancer Treat Rev 2009;35:437-50.

43. Cargill C, Bachmann E, Zbinden G. Effects of daunomycin and anthramycin on electrocardiogram and mitochondrial metabolism of the rat heart. J Natl Cancer Inst 1974;53:481-6.

44. Chandra P, Zunino F, Gotz A, et al. Template specific inhibition of DNA polymerases from RNA tumor viruses by distamycin A and its structural analogues. FEBS Lett 1972;21:154-8.

45. Chapman JW, Johnston LH. The yeast gene, DBF4, essential for entry into S phase is cell cycle regulated. Exp Cell Res 1989;180:419-28.

46. Chavda S, Liu Y, Babu B, et al. Hx, a novel fluorescent, minor groove and sequence specific recognition element: design, synthesis, and DNA binding properties of p-anisylbenzimidazole-imidazole/pyrrole-containing polyamides. Biochemistry 2011;50:3127-36.

47. Chavda S, Mulder K, Brown T, et al. DNA recognition: design, synthesis and biophysical characteristics of pyrrole(H) based polyamides. Med Chem 2010;6:150-8.

48. Chen AY, Yu C, Gatto B, Liu LF. DNA minor groove-binding ligands: a different class of mammalian DNA topoisomerase I inhibitors. Proc Natl Acad Sci U S A 1993;90:8131-5.

49. Chen Y-H, Lown JW. A New DNA Minor Groove Binding Motif: Cross-Linked Lexitropsins. J AM Chem Soc 1994;116:6995-7005.

50. Cheng L, Collyer T, Hardy CF. Cell cycle regulation of DNA replication initiator factor Dbf4p. Mol Cell Biol 1999;19:4270-8.

51. Cherry M, Williams DH. Recent kinase and kinase inhibitor X-ray structures: mechanisms of inhibition and selectivity insights. Curr Med Chem 2004;11:663-73.

52. Chou CJ, Farkas ME, Tsai SM, Alvarez D, Dervan PB, Gottesfeld JM. Small molecules targeting histone H4 as potential therapeutics for chronic myelogenous leukemia. Mol Cancer Ther 2008;7:769-78.

53. Cipolla L, Araujo AC, Airoldi C, Bini D. Pyrrolo[2,1-c][1,4]benzodiazepine as a scaffold for the design and synthesis of anti-tumour drugs. Anticancer Agents Med Chem 2009;9:1-31.

54. Cohen P. Protein kinases--the major drug targets of the twenty-first century? Nat Rev Drug Discov 2002;1:309-15.

55. Cohen P, Alessi DR. Kinase Drug Discovery - What's Next in the Field? ACS Chem Biol 2013;8:96-104.

56. Collett MS, Erikson RL. Protein kinase activity associated with the avian sarcoma virus src gene product. Proc Natl Acad Sci U S A 1978;75:2021-4.

57. Costanzo V, Gautier J. Single-strand DNA gaps trigger an ATR- and Cdc7-dependent checkpoint. Cell Cycle 2003;2:17.

58. Costanzo V, Shechter D, Lupardus PJ, Cimprich KA, Gottesman M, Gautier J. An ATR- and Cdc7-dependent DNA damage checkpoint that inhibits initiation of DNA replication. Mol Cell 2003;11:203-13.

59. Cozzi P. A new class of cytotoxic DNA minor groove binders: alpha-halogenoacrylic derivatives of pyrrolecarbamoyl oligomers. Farmaco 2001;56:57-65.

60. Cozzi P, Beria I, Biasoli G, et al. Novel phenyl nitrogen mustard and half-mustard derivatives of distamycin A. Bioorg & Med Chem Lett 1997;7:2985-90.

61. Cozzi P, Beria I, Caldarelli M, et al. Phenyl sulfur mustard derivatives of distamycin A. Bioorg Med Chem Lett 2000;10:1653-6.

62. Cozzi P, Beria I, Caldarelli M, Capolongo L, Geroni C, Mongelli N. Cytotoxic halogenoacrylic derivatives of distamycin A. Bioorg Med Chem Lett 2000;10:1269-72.

63. Cristofanilli M, Bryan WJ, Miller LL, et al. Phase II study of adozelesin in untreated metastatic breast cancer. Anticancer Drugs 1998;9:779-82.

64. Cuvier O, Hirano T. A role of topoisomerase II in linking DNA replication to chromosome condensation. J Cell Biol 2003;160:645-55.

65. D'Allessio R, Geroni C, Biasoli G, Pesenti E, Grandi M, Mongelli N. Structure-activity relationship of novel distamycin a derivatives : synthesis and antitumor activity. Bioorg & Med Chem Lett 1994;4:1467-72.

66. Damsma GE, Alt A, Brueckner F, Carell T, Cramer P. Mechanism of transcriptional stalling at cisplatin-damaged DNA. Nat Struct Mol Biol 2007;14:1127-33.

67. D'Andrea AD, Grompe M. The Fanconi anaemia/BRCA pathway. Nat Rev Cancer 2003;3:23-34.

68. Darnell JE, Jr. Transcription factors as targets for cancer therapy. Nat Rev Cancer 2002;2:740-9.

69. Davies SP, Reddy H, Caivano M, Cohen P. Specificity and mechanism of action of some commonly used protein kinase inhibitors. Biochem J 2000;351:95-105.

70. Denny WA. DNA minor groove alkylating agents. Curr Med Chem 2001;8:533-44.

71. Dervan PB. Molecular recognition of DNA by small molecules. Bioorg Med Chem 2001;9:2215-35.

72. Dervan PB, Burli RW. Sequence-specific DNA recognition by polyamides. Curr Opin Chem Biol 1999;3:688-93.

73. Dervan PB, Edelson BS. Recognition of the DNA minor groove by pyrrole-imidazole polyamides. Curr Opin Struct Biol 2003;13:284-99.

74. Deshpande A, Sicinski P, Hinds PW. Cyclins and cdks in development and cancer: a perspective. Oncogene 2005;24:2909-15.

75. Dickinson LA, Burnett R, Melander C, et al. Arresting cancer proliferation by small-molecule gene regulation. Chem Biol 2004;11:1583-94.

76. Dickinson LA, Trauger JW, Baird EE, Ghazal P, Dervan PB, Gottesfeld JM. Anti-repression of RNA polymerase II transcription by pyrrole-imidazole polyamides. Biochemistry 1999;38:10801-7.

77. Dierov J, Dierova R, Carroll M. BCR/ABL translocates to the nucleus and disrupts an ATR-dependent intra-S phase checkpoint. Cancer Cell 2004;5:275-85.

78. D'Incalci M, Sessa C. DNA minor groove binding ligands: a new class of anticancer agents. Expert Opin Investig Drugs 1997;6:875-84.

79. Dowell SJ, Romanowski P, Diffley JF. Interaction of Dbf4, the Cdc7 protein kinase regulatory subunit, with yeast replication origins in vivo. Science 1994;265:1243-6.

80. Edelson BS, Best TP, Olenyuk B, et al. Influence of structural variation on nuclear localization of DNA-binding polyamide-fluorophore conjugates. Nucleic Acids Res 2004;32:2802-18.

81. Fabbro D, Parkinson D, Matter A. Protein tyrosine kinase inhibitors: new treatment modalities? Curr Opin Pharmacol 2002;2:374-81.

82. Fabbro D, Ruetz S, Buchdunger E, et al. Protein kinases as targets for anticancer agents: from inhibitors to useful drugs. Pharmacol Ther 2002;93:79-98.

83. Fechter EJ, Olenyuk B, Dervan PB. Sequence-specific fluorescence detection of DNA by polyamide-thiazole orange conjugates. J Am Chem Soc 2005;127:16685-91.

84. Ferreira MF, Santocanale C, Drury LS, Diffley JF. Dbf4p, an essential S phase-promoting factor, is targeted for degradation by the anaphase-promoting complex. Mol Cell Biol 2000;20:242-8.

85. Finlay AC, Hochstein FA, Sobin BA, Murphy FX. Netropsin, a New Antibiotic Produced by a Streptomyces. J Am Chem Soc 1951;73:341-3.

86. Fleming PJ, Rose GD. Do all backbone polar groups in proteins form hydrogen bonds? Protein Sci 2005;14:1911-7.

87. Forsburg SL. Eukaryotic MCM proteins: beyond replication initiation. Microbiol Mol Biol Rev 2004;68:109-31.

88. Fox KR, Waring MJ. DNA structural variations produced by actinomycin and distamycin as revealed by DNAase I footprinting. Nucleic Acids Res 1984;12:9271-85.

89. Franks A, Tronrud C, Kiakos K, et al. Targeting the ICB2 site of the topoisomerase IIalpha promoter with a formamido-pyrrole-imidazole-pyrrole H-pin polyamide. Bioorg Med Chem 2010;18:5553-61.

90. Garber K. Rapamycin may prevent post-transplant lymphoma. J Natl Cancer Inst 2001;93:1519.

91. Garber K. Rapamycin's resurrection: a new way to target the cancer cell cycle. J Natl Cancer Inst 2001;93:1517-9.

92. Gerber DE. Targeted therapies: a new generation of cancer treatments. Am Fam Physician 2008;77:311-9.

93. Ghielmini M, Bosshard G, Capolongo L, et al. Estimation of the haematological toxicity of minor groove alkylators using tests on human cord blood cells. Br J Cancer 1997;75:878-83.

94. Gilman A. Therapeutic applications of chemical warfare agents. Fed Proc 1946;5:285-92.

95. Gottesfeld JM, Neely L, Trauger JW, Baird EE, Dervan PB. Regulation of gene expression by small molecules. Nature 1997;387:202-5.

96. Gottesfeld JM, Turner JM, Dervan PB. Chemical approaches to control gene expression. Gene Expr 2000;9:77-91.

97. Gravatt GL, Baguley BC, Wilson WR, Denny WA. DNA-directed alkylating agents. 6. Synthesis and antitumor activity of DNA minor groove-targeted aniline mustard analogues of pibenzimol (Hoechst 33258). J Med Chem 1994;37:4338-45.

98. Greenman C, Stephens P, Smith R, et al. Patterns of somatic mutation in human cancer genomes. Nature 2007;446:153-8.

99. Hallahan DE, Dunphy E, Virudachalam S, Sukhatme VP, Kufe DW, Weichselbaum RR. C-jun and Egr-1 participate in DNA synthesis and cell survival in response to ionizing radiation exposure. J Biol Chem 1995;270:30303-9.

100. Hanahan D, Weinberg RA. Hallmarks of cancer: the next generation. Cell 2011;144:646-74.

101. Hande KR. Etoposide: four decades of development of a topoisomerase II inhibitor. Eur J Cancer 1998;34:1514-21.

102. Harshman KD, Dervan PB. Molecular recognition of B-DNA by Hoechst 33258. Nucleic Acids Res 1985;13:4825-35.

103. Hartwell LH. Genetic control of the cell division cycle in yeast. IV. Genes controlling bud emergence and cytokinesis. Exp Cell Res 1971;69:265-76.

104. Hartwell LH. Genetic control of the cell division cycle in yeast. II. Genes controlling DNA replication and its initiation. J Mol Biol 1971;59:183-94.

105. Hartwell LH, Kastan MB. Cell cycle control and cancer. Science 1994;266:1821-8.

106. Heffernan TP, Unsal-Kacmaz K, Heinloth AN, et al. Cdc7-Dbf4 and the human S checkpoint response to UVC. J Biol Chem 2007;282:9458-68.

107. Heitman J, Movva NR, Hall MN. Targets for cell cycle arrest by the immunosuppressant rapamycin in yeast. Science 1991;253:905-9.

108. Helleday T, Lo J, van Gent DC, Engelward BP. DNA double-strand break repair: from mechanistic understanding to cancer treatment. DNA Repair (Amst) 2007;6:923-35.

109. Hertzberg RP, Hecht SM, Reynolds VL, Molineux IJ, Hurley LH. DNA sequence specificity of the pyrrolo[1,4]benzodiazepine antitumor antibiotics. Methidiumpropyl-EDTA-iron(II) footprinting analysis of DNA binding sites for anthramycin and related drugs. Biochemistry 1986;25:1249-58.

110. Hess G, Herbrecht R, Romaguera J, et al. Phase III study to evaluate temsirolimus compared with investigator's choice therapy for the treatment of relapsed or refractory mantle cell lymphoma. J Clin Oncol 2009;27:3822-9.

111. Hess GF, Drong RF, Weiland KL, Slightom JL, Sclafani RA, Hollingsworth RE. A human homolog of the yeast CDC7 gene is overexpressed in some tumors and transformed cell lines. Gene 1998;211:133-40.

112. Hidaka H, Inagaki M, Kawamoto S, Sasaki Y. Isoquinolinesulfonamides, novel and potent inhibitors of cyclic nucleotide dependent protein kinase and protein kinase C. Biochemistry 1984;23:5036-41.

113. Hochhauser D, Kotecha M, O'Hare C, et al. Modulation of topoisomerase IIalpha expression by a DNA sequence-specific polyamide. Mol Cancer Ther 2007;6:346-54.

114. Hounam RF, Williams J. Levels of airborne dust in furniture making factories in the High Wycombe area. Br J Ind Med 1974;31:1-9.

115. Huang S, Bjornsti MA, Houghton PJ. Rapamycins: mechanism of action and cellular resistance. Cancer Biol Ther 2003;2:222-32.

116. Huang S, Houghton PJ. Targeting mTOR signaling for cancer therapy. Curr Opin Pharmacol 2003;3:371-7.

117. Huang S, Shu L, Dilling MB, et al. Sustained activation of the JNK cascade and rapamycin-induced apoptosis are suppressed by p53/p21(Cip1). Mol Cell 2003;11:1491-501.

118. Huentelman MJ, Stephan DA, Talboom J, et al. Peripheral delivery of a ROCK inhibitor improves learning and working memory. Behav Neurosci 2009;123:218-23.

119. Hurley LH. DNA and associated targets for drug design. J Med Chem 1989;32:2027-33.

120. Hurley LH. DNA and its associated processes as targets for cancer therapy. Nat Rev Cancer 2002;2:188-200.

121. Hurley LH, Reck T, Thurston DE, et al. Pyrrolo[1,4]benzodiazepine antitumor antibiotics: relationship of DNA alkylation and sequence specificity to the biological activity of natural and synthetic compounds. Chem Res Toxicol 1988;1:258-68.

122. Im JS, Lee JK. ATR-dependent activation of p38 MAP kinase is responsible for apoptotic cell death in cells depleted of Cdc7. J Biol Chem 2008;283:25171-7.

123. Isaacs RJ, Harris AL, Hickson ID. Regulation of the human topoisomerase IIalpha gene promoter in confluence-arrested cells. J Biol Chem 1996;271:16741-7.

124. Jackson SP. Sensing and repairing DNA double-strand breaks. Carcinogenesis 2002;23:687-96.

125. Jakupec MA, Galanski M, Keppler BK. Tumour-inhibiting platinum complexes--state of the art and future perspectives. Rev Physiol Biochem Pharmacol 2003;146:1-54.

126. Jares P, Blow JJ. Xenopus cdc7 function is dependent on licensing but not on XORC, XCdc6, or CDK activity and is required for XCdc45 loading. Genes Dev 2000;14:1528-40.

127. Jares P, Donaldson A, Blow JJ. The Cdc7/Dbf4 protein kinase: target of the S phase checkpoint? EMBO Rep 2000;1:319-22.

128. Jiang W, Hunter T. Identification and characterization of a human protein kinase related to budding yeast Cdc7p. Proc Natl Acad Sci U S A 1997;94:14320-5.

129. Jiang W, McDonald D, Hope TJ, Hunter T. Mammalian Cdc7-Dbf4 protein kinase complex is essential for initiation of DNA replication. EMBO J 1999;18:5703-13.

130. Johnston LH, Masai H, Sugino A. First the CDKs, now the DDKs. Trends Cell Biol 1999;9:249-52.

131. Judson I, Kelland LR. New developments and approaches in the platinum arena. Drugs 2000;59 Suppl 4:29-36; discussion 7-8.

132. Kelland L. The resurgence of platinum-based cancer chemotherapy. Nat Rev Cancer 2007;7:573-84.

133. Khalaf AI. Minor groove binders: Some recent research in drug development. Curr Trend Med Chem 2009;6:53-63.

134. Kielkopf CL, Baird EE, Dervan PB, Rees DC. Structural basis for G.C recognition in the DNA minor groove. Nat Struct Biol 1998;5:104-9.

135. Kielkopf CL, Bremer RE, White S, et al. Structural effects of DNA sequence on T.A recognition by hydroxypyrrole/pyrrole pairs in the minor groove. J Mol Biol 2000;295:557-67.

136. Kielkopf CL, White S, Szewczyk JW, et al. A structural basis for recognition of A.T and T.A base pairs in the minor groove of B-DNA. Science 1998;282:111-5.

137. Kiess M, Gill RM, Hamel PA. Expression and activity of the retinoblastoma protein (pRB)-family proteins, p107 and p130, during L6 myoblast differentiation. Cell Growth Differ 1995;6:1287-98.

138. Kim JM, Kakusho N, Yamada M, Kanoh Y, Takemoto N, Masai H. Cdc7 kinase mediates Claspin phosphorylation in DNA replication checkpoint. Oncogene 2008;27:3475-82.

139. Kim JM, Nakao K, Nakamura K, et al. Inactivation of Cdc7 kinase in mouse ES cells results in S-phase arrest and p53-dependent cell death. EMBO J 2002;21:2168-79.

140. Kim JM, Sato N, Yamada M, Arai K, Masai H. Growth regulation of the expression of mouse cDNA and gene encoding a serine/threonine kinase related to Saccharomyces cerevisiae CDC7 essential for G1/S transition. Structure, chromosomal localization, and expression of mouse gene for s. cerevisiae Cdc7-related kinase. J Biol Chem 1998;273:23248-57.

141. Kim JM, Yamada M, Masai H. Functions of mammalian Cdc7 kinase in initiation/monitoring of DNA replication and development. Mutat Res 2003;532:29-40.

142. Koch C, Moll T, Neuberg M, Ahorn H, Nasmyth K. A role for the transcription factors Mbp1 and Swi4 in progression from G1 to S phase. Science 1993;261:1551-7.

143. Koch C, Nasmyth K. Cell cycle regulated transcription in yeast. Curr Opin Cell Biol 1994;6:451-9.

144. Kohn KW. Beyond DNA cross-linking: history and prospects of DNA-targeted cancer treatment--fifteenth Bruce F. Cain Memorial Award Lecture. Cancer Res 1996;56:5533-46.

145. Kopka ML, Goodsell DS, Baikalov I, Grzeskowiak K, Cascio D, Dickerson RE. Crystal structure of a covalent DNA-drug adduct: anthramycin bound to C-C-A-A-C-G-T-T-G-G and a molecular explanation of specificity. Biochemistry 1994;33:13593-610.

146. Kopka ML, Goodsell DS, Han GW, Chiu TK, Lown JW, Dickerson RE. Defining GC-specificity in the minor groove: side-by-side binding of the di-imidazole lexitropsin to C-A-T-G-G-C-C-A-T-G. Structure 1997;5:1033-46.

147. Kopka ML, Yoon C, Goodsell D, Pjura P, Dickerson RE. The molecular origin of DNA-drug specificity in netropsin and distamycin. Proc Natl Acad Sci U S A 1985;82:1376-80.

148. Korman S, Tendler MD. Clinical investigation of cancer chemotherapeutic agents for neoplastic disease. J New Drugs 1965;5:275-85.

149. Kotecha M, Kluza J, Wells G, et al. Inhibition of DNA binding of the NF-Y transcription factor by the pyrrolobenzodiazepine-polyamide conjugate GWL-78. Mol Cancer Ther 2008;7:1319-28.

150. Krautschick AW. Metabolic evaluation and medical therapy for stone formation. Curr Opin Urol 1999;9:335-8.

151. Krueger WC, Hatzenbuhler NT, Prairie MD, Shea MH. DNA sequence recognition by the antitumor antibiotic CC-1065 and analogs of CC-1065. Chem Biol Interact 1991;79:265-86.

152. Krueger WC, Prairie MD. The origin of the DNA induced circular dichroism of CC-1065 and analogs. Chem Biol Interact 1991;79:137-49.

153. Krystof V, Chamrad I, Jorda R, Kohoutek J. Pharmacological targeting of CDK9 in cardiac hypertrophy. Med Res Rev 2010;30:646-66.

154. Krystof V, Uldrijan S. Cyclin-dependent kinase inhibitors as anticancer drugs. Curr Drug Targets 2010;11:291-302.

155. Kumagai H, Sato N, Yamada M, et al. A novel growth- and cell cycle-regulated protein, ASK, activates human Cdc7-related kinase and is essential for G1/S transition in mammalian cells. Mol Cell Biol 1999;19:5083-95.

156. Lacy ER, Cox KK, Wilson WD, Lee M. Recognition of T*G mismatched base pairs in DNA by stacked imidazole-containing polyamides: surface plasmon resonance and circular dichroism studies. Nucleic Acids Res 2002;30:1834-41.

157. Lacy ER, Le NM, Price CA, Lee M, Wilson WD. Influence of a terminal formamido group on the sequence recognition of DNA by polyamides. J Am Chem Soc 2002;124:2153-63.

158. Lane MJ, Dabrowiak JC, Vournakis JN. Sequence specificity of actinomycin D and Netropsin binding to pBR322 DNA analyzed by protection from DNase I. Proc Natl Acad Sci U S A 1983;80:3260-4.

159. Larner JM, Lee H, Little RD, Dijkwel PA, Schildkraut CL, Hamlin JL. Radiation down-regulates replication origin activity throughout the S phase in mammalian cells. Nucleic Acids Res 1999;27:803-9.

160. Larsen TA, Goodsell DS, Cascio D, Grzeskowiak K, Dickerson RE. The structure of DAPI bound to DNA. J Biomol Struct Dyn 1989;7:477-91.

161. Le NM, Sielaff AM, Cooper AJ, et al. Binding of f-PIP, a pyrrole- and imidazole-containing triamide, to the inverted CCAAT box-2 of the topoisomerase IIalpha promoter and modulation of gene expression in cells. Bioorg Med Chem Lett 2006;16:6161-4.

162. Leahy M, Ray-Coquard I, Verweij J, et al. Brostallicin, an agent with potential activity in metastatic soft tissue sarcoma: a phase II study from the European Organisation for Research and Treatment of Cancer Soft Tissue and Bone Sarcoma Group. Eur J Cancer 2007;43:308-15.

163. Lee AY, Chiba T, Truong LN, et al. Dbf4 is direct downstream target of ataxia telangiectasia mutated (ATM) and ataxia telangiectasia and Rad3-related (ATR) protein to regulate intra-S-phase checkpoint. J Biol Chem 2012;287:2531-43.

164. Lee CH, Hu WP, Hong CH, et al. Pyrrolo[2,1-c][1,4]benzodiazepine and indole conjugate (IN6CPBD) has better efficacy and superior safety than the mother compound DC-81 in suppressing the growth of established melanoma in vivo. Chem Biol Interact 2009;180:360-7.

165. Lee H, Larner JM, Hamlin JL. A p53-independent damage-sensing mechanism that functions as a checkpoint at the G1/S transition in Chinese hamster ovary cells. Proc Natl Acad Sci U S A 1997;94:526-31.

166. Lee M, Rhodes AL, Wyatt MD, Forrow S, Hartley JA. Design, synthesis, and biological evaluation of DNA sequence and minor groove selective alkylating agents. Anticancer Drug Des 1993;8:173-92.

167. Lei M, Kawasaki Y, Young MR, Kihara M, Sugino A, Tye BK. Mcm2 is a target of regulation by Cdc7-Dbf4 during the initiation of DNA synthesis. Genes Dev 1997;11:3365-74.

168. Lepke M, Putter V, Staib C, et al. Identification, characterization and chromosomal localization of the cognate human and murine DBF4 genes. Mol Gen Genet 1999;262:220-9.

169. Levitzki A. Protein kinase inhibitors as a therapeutic modality. Acc Chem Res 2003;36:462-9.

170. Li TK, Liu LF. Tumor cell death induced by topoisomerase-targeting drugs. Annu Rev Pharmacol Toxicol 2001;41:53-77.

171. Little JB. Failla Memorial Lecture. Changing views of cellular radiosensitivity. Radiat Res 1994;140:299-311.

172. Liu Y, Wilson WD. Quantitative analysis of small molecule-nucleic acid interactions with a biosensor surface and surface plasmon resonance detection. Methods Mol Biol 2010;613:1-23.

173. Loontiens FG, Regenfuss P, Zechel A, Dumortier L, Clegg RM. Binding characteristics of Hoechst 33258 with calf thymus DNA, poly[d(A-T)], and d(CCGGAATTCCGG): multiple stoichiometries and determination of tight binding with a wide spectrum of site affinities. Biochemistry 1990;29:9029-39.

174. Lorusso D, Zanaboni F, etc. Phase II exploratory study of brostallicin in patients with ovarian cancer resistant/refractory to platinum-based chemotherapy. J Clin Oncol 2008;26.

175. Lown JW. Design of sequence-specific agents:lexitropsins. Molecular aspects of anticaner Drug-DNA interactions 1993;1:322-55.

176. Lown JW, Krowicki K, Bhat UG, Skorobogaty A, Ward B, Dabrowiak JC. Molecular recognition between oligopeptides and nucleic acids: novel imidazole-containing oligopeptides related to netropsin that exhibit altered DNA sequence specificity. Biochemistry 1986;25:7408-16.

177. Maher LJ, 3rd. DNA triple-helix formation: an approach to artificial gene repressors? Bioessays 1992;14:807-15.

178. Maher LJ, 3rd, Wold B, Dervan PB. Inhibition of DNA binding proteins by oligonucleotide-directed triple helix formation. Science 1989;245:725-30.

179. Maity A, McKenna WG, Muschel RJ. The molecular basis for cell cycle delays following ionizing radiation: a review. Radiother Oncol 1994;31:1-13.

180. Malumbres M. Revisiting the "Cdk-centric" view of the mammalian cell cycle. Cell Cycle 2005;4:206-10.

181. Malumbres M, Barbacid M. To cycle or not to cycle: a critical decision in cancer. Nat Rev Cancer 2001;1:222-31.

182. Malumbres M, Barbacid M. Mammalian cyclin-dependent kinases. Trends Biochem Sci 2005;30:630-41.

183. Malumbres M, Barbacid M. Cell cycle, CDKs and cancer: a changing paradigm. Nat Rev Cancer 2009;9:153-66.

184. Malumbres M, Pevarello P, Barbacid M, Bischoff JR. CDK inhibitors in cancer therapy: what is next? Trends Pharmacol Sci 2008;29:16-21.

185. Mapp AK, Ansari AZ, Ptashne M, Dervan PB. Activation of gene expression by small molecule transcription factors. Proc Natl Acad Sci U S A 2000;97:3930-5.

186. Marchini S, Broggini M, Sessa C, D'Incalci M. Development of distamycin-related DNA binding anticancer drugs. Expert Opin Investig Drugs 2001;10:1703-14.

187. Marchini S, Ciro M, Gallinari F, et al. Alpha-bromoacryloyl derivative of distamycin A (PNU 151807): a new non-covalent minor groove DNA binder with antineoplastic activity. Br J Cancer 1999;80:991-7.

188. Marchini S, Damia G, Broggini M, et al. 4-Demethoxy-3'-deamino-3'-aziridinyl-4'-methylsulphonyl-daunorubicin (PNU-159548), a novel anticancer agent active against tumor cell lines with different resistance mechanisms. Cancer Res 2001;61:1991-5.

189. Markovic SN, Suman VJ, Vukov AM, et al. Phase II trial of KW2189 in patients with advanced malignant melanoma. Am J Clin Oncol 2002;25:308-12.

190. Marques MA, Doss RM, Urbach AR, Dervan PB. Toward an Understanding of the Chemical Etiology for DNA Minor-Groove Recognition by Polyamides. Helv Chim Acta 2002;85:4485-517.

191. Masai H, Arai K. Dbf4 motifs: conserved motifs in activation subunits for Cdc7 kinases essential for S-phase. Biochem Biophys Res Commun 2000;275:228-32.

192. Masai H, Arai K. Cdc7 kinase complex: a key regulator in the initiation of DNA replication. J Cell Physiol 2002;190:287-96.

193. Masai H, Matsui E, You Z, Ishimi Y, Tamai K, Arai K. Human Cdc7-related kinase complex. In vitro phosphorylation of MCM by concerted actions of Cdks and Cdc7 and that of a criticial threonine residue of Cdc7 bY Cdks. J Biol Chem 2000;275:29042-52.

194. Masai H, Miyake T, Arai K. hsk1+, a Schizosaccharomyces pombe gene related to Saccharomyces cerevisiae CDC7, is required for chromosomal replication. EMBO J 1995;14:3094-104.

195. Masai H, Sato N, Takeda T, Arai K. CDC7 kinase complex as a molecular switch for DNA replication. Front Biosci 1999;4:D834-40.

196. Masai H, Taniyama C, Ogino K, et al. Phosphorylation of MCM4 by Cdc7 kinase facilitates its interaction with Cdc45 on the chromatin. J Biol Chem 2006;281:39249-61.

197. Matsuda H, Fukuda N, Ueno T, et al. Transcriptional inhibition of progressive renal disease by gene silencing pyrrole-imidazole polyamide targeting of the transforming growth factor-beta1 promoter. Kidney Int 2011;79:46-56.

198. Matsuoka M, Tani K, Asano S. Interferon-alpha-induced G1 phase arrest through up-regulated expression of CDK inhibitors, p19Ink4D and p21Cip1 in mouse macrophages. Oncogene 1998;16:2075-86.

199. McCune JS, Slattery JT. Pharmacological considerations of primary alkylators. Cancer Treat Res 2002;112:323-45.

200. McHugh PJ, Spanswick VJ, Hartley JA. Repair of DNA interstrand crosslinks: molecular mechanisms and clinical relevance. Lancet Oncol 2001;2:483-90.

201. Mendez J, Stillman B. Perpetuating the double helix: molecular machines at eukaryotic DNA replication origins. Bioessays 2003;25:1158-67.

202. Metting NF, Little JB. Transient failure to dephosphorylate the cdc2-cyclin B1 complex accompanies radiation-induced G2-phase arrest in HeLa cells. Radiat Res 1995;143:286-92.

203. Michelson RJ, Weinert T. Closing the gaps among a web of DNA repair disorders. Bioessays 2000;22:966-9.

204. Mimura S, Takisawa H. Xenopus Cdc45-dependent loading of DNA polymerase alpha onto chromatin under the control of S-phase Cdk. EMBO J 1998;17:5699-707.

205. Minoshima M, Chou JC, Lefebvre S, et al. Potent activity against K562 cells by polyamide-seco-CBI conjugates targeting histone H4 genes. Bioorg Med Chem 2010;18:168-74.

206. Mitchison TJ. The proliferation rate paradox in antimitotic chemotherapy. Mol Biol Cell 2012;23:1-6.

207. Mitra SN, Wahl MC, Sundaralingam M. Structure of the side-by-side binding of distamycin to d(GTATATAC)2. Acta Crystallogr D Biol Crystallogr 1999;55:602-9.

208. Montagnoli A, Tenca P, Sola F, et al. Cdc7 inhibition reveals a p53-dependent replication checkpoint that is defective in cancer cells. Cancer Res 2004;64:7110-6.

209. Montagnoli A, Valsasina B, Brotherton D, et al. Identification of Mcm2 phosphorylation sites by S-phase-regulating kinases. J Biol Chem 2006;281:10281-90.

210. Moore MJ. Clinical pharmacokinetics of cyclophosphamide. Clin Pharmacokinet 1991;20:194-208.

211. Moore MJ, Kaizer L, Erlichman C, et al. A clinical and pharmacological study of 5-fluorouracil, leucovorin and interferon alfa in advanced colorectal cancer. Cancer Chemother Pharmacol 1995;37:86-90.

212. Moser HE, Dervan PB. Sequence-specific cleavage of double helical DNA by triple helix formation. Science 1987;238:645-50.

213. Motzer RJ, Escudier B, Oudard S, et al. Efficacy of everolimus in advanced renal cell carcinoma: a double-blind, randomised, placebo-controlled phase III trial. Lancet 2008;372:449-56.

214. Mrksich M, Dervan PB. Enhanced sequence specific recognition in the minor groove of DNA by covalent peptide dimers: bis(pyridine-2-carboxamidonetropsin)(CH2)3-6. J Am Chem Soc 1993;115:9892-9.

215. Mrksich M, Dervan PB. Design of peptides for sequence-specific recognition of the minor groove of DNA. J Am Chem Soc 1994;116:3663-4.

216. Mrksich M, Wade WS, Dwyer TJ, Geierstanger BH, Wemmer DE, Dervan PB. Antiparallel side-by-side dimeric motif for sequence-specific recognition in the minor groove of DNA by the designed peptide 1-methylimidazole-2-carboxamide netropsin. Proc Natl Acad Sci U S A 1992;89:7586-90.

217. Muzikar KA, Nickols NG, Dervan PB. Repression of DNA-binding dependent glucocorticoid receptor-mediated gene expression. Proc Natl Acad Sci U S A 2009;106:16598-603.

218. Nakanishi M, Shimada M, Niida H. Genetic instability in cancer cells by impaired cell cycle checkpoints. Cancer Sci 2006;97:984-9.

219. Nambiar S, Mirmohammadsadegh A, Hassan M, et al. Identification and functional characterization of ASK/Dbf4, a novel cell survival gene in cutaneous melanoma with prognostic relevance. Carcinogenesis 2007;28:2501-10.

220. Nasmyth K, Dirick L. The role of SWI4 and SWI6 in the activity of G1 cyclins in yeast. Cell 1991;66:995-1013.

221. Neal AJ, Hoskin PJ. Clinical Oncology: Basic Principles and Practice. 2009.

222. Neshat MS, Mellinghoff IK, Tran C, et al. Enhanced sensitivity of PTEN-deficient tumors to inhibition of FRAP/mTOR. Proc Natl Acad Sci U S A 2001;98:10314-9.

223. Newton BA. Berenil, a trypanocide with selective activity against extranuclear DNA. Antibiotics 1975;3:34-47.

224. Nguyen B, Lee MP, Hamelberg D, et al. Strong binding in the DNA minor groove by an aromatic diamidine with a shape that does not match the curvature of the groove. J Am Chem Soc 2002;124:13680-1.

225. Nickols NG, Dervan PB. Suppression of androgen receptor-mediated gene expression by a sequence-specific DNA-binding polyamide. Proc Natl Acad Sci U S A 2007;104:10418-23.

226. Niida H, Nakanishi M. DNA damage checkpoints in mammals. Mutagenesis 2006;21:3-9.

227. Noble ME, Endicott JA, Johnson LN. Protein kinase inhibitors: insights into drug design from structure. Science 2004;303:1800-5.

228. Nougarede R, Della Seta F, Zarzov P, Schwob E. Hierarchy of S-phase-promoting factors: yeast Dbf4-Cdc7 kinase requires prior S-phase cyclin-dependent kinase activation. Mol Cell Biol 2000;20:3795-806.

229. O'Hare CC, Mack D, Tandon M, et al. DNA sequence recognition in the minor groove by crosslinked polyamides: The effect of N-terminal head group and linker length on binding affinity and specificity. Proc Natl Acad Sci U S A 2002;99:72-7.

230. O'Hare CC, Uthe P, Mackay H, et al. Sequence recognition in the minor groove of DNA by covalently linked formamido imidazole-pyrrole-imidazole polyamides: effect of H-pin linkage and linker length on selectivity and affinity. Biochemistry 2007;46:11661-70.

231. Ohtani H, Strauss HW, Southern JF, et al. Intercellular adhesion molecule-1 induction: a sensitive and quantitative marker for cardiac allograft rejection. J Am Coll Cardiol 1995;26:793-9.

232. Oshiro G, Owens JC, Shellman Y, Sclafani RA, Li JJ. Cell cycle control of Cdc7p kinase activity through regulation of Dbf4p stability. Mol Cell Biol 1999;19:4888-96.

233. Owens JC, Detweiler CS, Li JJ. CDC45 is required in conjunction with CDC7/DBF4 to trigger the initiation of DNA replication. Proc Natl Acad Sci U S A 1997;94:12521-6.

234. Paggi MG, Baldi A, Bonetto F, Giordano A. Retinoblastoma protein family in cell cycle and cancer: a review. J Cell Biochem 1996;62:418-30.

235. Panasik N, Jr., Fleming PJ, Rose GD. Hydrogen-bonded turns in proteins: the case for a recount. Protein Sci 2005;14:2910-4.

236. Pandolfi PP. Transcription therapy for cancer. Oncogene 2001;20:3116-27.

237. Pasero P, Duncker BP, Schwob E, Gasser SM. A role for the Cdc7 kinase regulatory subunit Dbf4p in the formation of initiation-competent origins of replication. Genes Dev 1999;13:2159-76.

238. Patterson M, Sclafani RA, Fangman WL, Rosamond J. Molecular characterization of cell cycle gene CDC7 from Saccharomyces cerevisiae. Mol Cell Biol 1986;6:1590-8.

239. Paulovich AG, Hartwell LH. A checkpoint regulates the rate of progression through S phase in S. cerevisiae in response to DNA damage. Cell 1995;82:841-7.

240. Pelton JG, Wemmer DE. Structural characterization of a 2:1 distamycin A.d(CGCAAATTGGC) complex by two-dimensional NMR. Proc Natl Acad Sci U S A 1989;86:5723-7.

241. Pelton JG, Wemmer DE. Structure and dynamics of distamycin A with d(CGCAAATTGGC):d(GCCAATTTGCG) at low drug:DNA ratios. J Biomol Struct Dyn 1990;8:81-97.

242. Pezzoni G, Grandi M, Biasoli G, et al. Biological profile of FCE 24517, a novel benzoyl mustard analogue of distamycin A. Br J Cancer 1991;64:1047-50.

243. Pfaffl MW. A new mathematical model for relative quantification in real-time RT-PCR. Nucleic Acids Res 2001;29:e45.

244. Pizzorno GH, R.E; Cheng, Y.C. Chapter 47 Pyrimidine and Purine Antimetabolites. Holland-Frei Cancer Medicine 5th edition 2000.

245. Podsypanina K, Lee RT, Politis C, et al. An inhibitor of mTOR reduces neoplasia and normalizes p70/S6 kinase activity in Pten+/- mice. Proc Natl Acad Sci U S A 2001;98:10320-5.

246. Pulido D, Sánchez A, Robles J, Pedroso E, Grandas A. Guanine-Containing DNA Minor-Groove Binders. Eur J of Org Chem 2009:1398-406.

247. Radford IR, Murphy TK. Radiation response of mouse lymphoid and myeloid cell lines. Part III. Different signals can lead to apoptosis and may influence sensitivity to killing by DNA double-strand breakage. Int J Radiat Biol 1994;65:229-39.

248. Raskatov JA, Meier JL, Puckett JW, Yang F, Ramakrishnan P, Dervan PB. Modulation of NF-kappaB-dependent gene transcription using programmable DNA minor groove binders. Proc Natl Acad Sci U S A 2012;109:1023-8.

249. Raskatov JA, Nickols NG, Hargrove AE, Marinov GK, Wold B, Dervan PB. Gene expression changes in a tumor xenograft by a pyrrole-imidazole polyamide. Proc Natl Acad Sci U S A 2012;109:16041-5.

250. Rehm KE, Connor RF, Jones GJ, Yimbu K, Mannie MD, Roper RL. Vaccinia virus decreases major histocompatibility complex (MHC) class II antigen presentation, T-cell priming, and peptide association with MHC class II. Immunology 2009;128:381-92.

251. Rewari BB, Gupta G, Agarwal AK. Supportive Care in Oncology. clinical medicine 2004;5(1):38-46. http://medind.nic.in/jac/t04/i1/jact04i1p38.pdf.

252. Rizzieri DA, Feldman E, Dipersio JF, et al. A phase 2 clinical trial of deforolimus (AP23573, MK-8669), a novel mammalian target of rapamycin inhibitor, in patients with relapsed or refractory hematologic malignancies. Clin Cancer Res 2008;14:2756-62.

253. Roberts BT, Ying CY, Gautier J, Maller JL. DNA replication in vertebrates requires a homolog of the Cdc7 protein kinase. Proc Natl Acad Sci U S A 1999;96:2800-4.

254. Ronchi A, Bellorini M, Mongelli N, Mantovani R. CCAAT-box binding protein NF-Y (CBF, CP1) recognizes the minor groove and distorts DNA. Nucleic Acids Res 1995;23:4565-72.

255. Rosenberg B. Noble metal complexes in cancer chemotherapy. Adv Exp Med Biol 1977;91:129-50.

256. Rothenberg ML. Topoisomerase I inhibitors: review and update. Ann Oncol 1997;8:837-55.

257. Royou A, McCusker D, Kellogg DR, Sullivan W. Grapes(Chk1) prevents nuclear CDK1 activation by delaying cyclin B nuclear accumulation. J Cell Biol 2008;183:63-75.

258. Ruiz van Haperen VW, Peters GJ. New targets for pyrimidine antimetabolites for the treatment of solid tumours. 2: Deoxycytidine kinase. Pharm World Sci 1994;16:104-12.

259. Saenger W. Principles of nucleic acid structure. Springer-Verlag, New York 1984:556.

260. Sarkaria JN, Bristow RG. Overview of cancer molecular radiobiology. Cancer Treat Res 2008;139:117-33.

261. Satam V, Babu B, Chavda S, et al. Novel diamino imidazole and pyrrole-containing polyamides: Synthesis and DNA binding studies of mono- and diamino-phenyl-ImPy*Im polyamides designed to target 5'-ACGCGT-3'. Bioorg Med Chem;20:693-701.

262. Satam V, Babu B, Porte A, et al. Synthesis and DNA binding properties of 1-(3-aminopropyl)-imidazole-containing triamide f-Im*PyIm: a novel diamino polyamide designed to target 5'-ACGCGT-3'. Bioorg Med Chem Lett;22:5898-902.

263. Sato N, Arai K, Masai H. Human and Xenopus cDNAs encoding budding yeast Cdc7-related kinases: in vitro phosphorylation of MCM subunits by a putative human homologue of Cdc7. EMBO J 1997;16:4340-51.

264. Satyanarayana A, Kaldis P. Mammalian cell-cycle regulation: several Cdks, numerous cyclins and diverse compensatory mechanisms. Oncogene 2009;28:2925-39.

265. Satz AL, Bruice TC. Recognition in the minor groove of double-stranded DNA by microgonotropens. Acc Chem Res 2002;35:86-95.

266. Satz AL, Bruice TC. Recognition of nine base pair sequences in the minor groove of DNA at subpicomolar concentrations by a novel microgonotropen. Bioorg Med Chem 2002;10:241-52.

267. Sawa M, Masai H. Drug design with Cdc7 kinase: a potential novel cancer therapy target. Drug Des Devel Ther 2009;2:255-64.

268. Schmitt E, Paquet C, Beauchemin M, Bertrand R. DNA-damage response network at the crossroads of cell-cycle checkpoints, cellular senescence and apoptosis. J Zhejiang Univ Sci B 2007;8:377-97.

269. Sclafani RA. Cdc7p-Dbf4p becomes famous in the cell cycle. J Cell Sci 2000;113 (Pt 12):2111-7.

270. Shapiro GI. Cyclin-dependent kinase pathways as targets for cancer treatment. J Clin Oncol 2006;24:1770-83.

271. Sharma SK, Billaud JN, Tandon M, et al. Inhibition of feline immunodeficiency virus (FIV) replication by DNA binding polyamides. Bioorg Med Chem Lett 2002;12:2007-10.

272. Shibuya M, Suzuki Y, Sugita K, et al. Effect of AT877 on cerebral vasospasm after aneurysmal subarachnoid hemorrhage. Results of a prospective placebo-controlled double-blind trial. J Neurosurg 1992;76:571-7.

273. Small EJ, Figlin R, Petrylak D, et al. A phase II pilot study of KW-2189 in patients with advanced renal cell carcinoma. Invest New Drugs 2000;18:193-7.

274. Smeets MF, Mooren EH, Begg AC. The effect of radiation on G2 blocks, cyclin B expression and cdc2 expression in human squamous carcinoma cell lines with different radiosensitivities. Radiother Oncol 1994;33:217-27.

275. Soderlind KJ, Gorodetsky B, Singh AK, Bachur NR, Miller GG, Lown JW. Bis-benzimidazole anticancer agents: targeting human tumour helicases. Anticancer Drug Des 1999;14:19-36.

276. Sonoda E, Sasaki MS, Buerstedde JM, et al. Rad51-deficient vertebrate cells accumulate chromosomal breaks prior to cell death. EMBO J 1998;17:598-608.

277. Spence RaJ, P Chapter 3 Cancer treatment. Oncology 4 th Edition 2001:88.

278. Suzuki-Takahashi I, Kitagawa M, Saijo M, et al. The interactions of E2F with pRB and with p107 are regulated via the phosphorylation of pRB and p107 by a cyclin-dependent kinase. Oncogene 1995;10:1691-8.

279. Swalley SE, Baird EE, Dervan PB. Recognition of a 5‘-(A,T)GGG(A,T)2-3‘ Sequence in the Minor Groove of DNA by an Eight-Ring Hairpin Polyamide. J AM Chem Soc 1996;118:8198-206.

280. Swords R, Mahalingam D, O'Dwyer M, et al. Cdc7 kinase - a new target for drug development. Eur J Cancer 2010;46:33-40.

281. Takeda T, Ogino K, Matsui E, et al. A fission yeast gene, him1(+)/dfp1(+), encoding a regulatory subunit for Hsk1 kinase, plays essential roles in S-phase initiation as well as in S-phase checkpoint control and recovery from DNA damage. Mol Cell Biol 1999;19:5535-47.

282. Takimoto CC, E. Principles of Oncologic Pharmacotherapy. in Pazdur R, Wagman LD, Camphausen KA, Hoskins WJ (Eds) Cancer Management: A Multidisciplinary Approach 11 ed 2008. http://www.cancernetwork.com/cancer-management-11/.

283. Tannock l, Hill R, Bristow R, Harrington L. The Basic Science of Oncology. New York, 4 ed 2005.

284. Tenca P, Brotherton D, Montagnoli A, Rainoldi S, Albanese C, Santocanale C. Cdc7 is an active kinase in human cancer cells undergoing replication stress. J Biol Chem 2007;282:208-15.

285. Tercero JA, Labib K, Diffley JF. DNA synthesis at individual replication forks requires the essential initiation factor Cdc45p. EMBO J 2000;19:2082-93.

286. Tietze LF, Bell HP, Chandrasekhar S. Natural product hybrids as new leads for drug discovery. Angew Chem Int Ed Engl 2003;42:3996-4028.

287. Timur M, Akbas SH, Ozben T. The effect of Topotecan on oxidative stress in MCF-7 human breast cancer cell line. Acta Biochim Pol 2005;52:897-902.

288. Tolner B, Hartley JA, Hochhauser D. Transcriptional regulation of topoisomerase II alpha at confluence and pharmacological modulation of expression by bis-benzimidazole drugs. Mol Pharmacol 2001;59:699-706.

289. Trauger JW, Baird EE, Dervan PB. Extended hairpin polyamide motif for sequence-specific recognition in the minor groove of DNA. Chem Biol 1996;3:369-77.

290. Tsai SM, Farkas ME, Chou CJ, Gottesfeld JM, Dervan PB. Unanticipated differences between alpha- and gamma-diaminobutyric acid-linked hairpin polyamide-alkylator conjugates. Nucleic Acids Res 2007;35:307-16.

291. Tsugaya M, Washida H, Hirao N, Hachisuka Y, Sakagami H, Iwase Y. The treatment of bladder cancer by neothramycin. Hinyokika Kiyo 1986;32:1443-8.

292. Tsuji T, Ficarro SB, Jiang W. Essential role of phosphorylation of MCM2 by Cdc7/Dbf4 in the initiation of DNA replication in mammalian cells. Mol Biol Cell 2006;17:4459-72.

293. Urbach AR, Dervan PB. Toward rules for 1:1 polyamide:DNA recognition. Proc Natl Acad Sci U S A 2001;98:4343-8.

294. Valkov NI, Sullivan DM. Tumor p53 status and response to topoisomerase II inhibitors. Drug Resist Updat 2003;6:27-39.

295. Verheij M, Bose R, Lin XH, et al. Requirement for ceramide-initiated SAPK/JNK signalling in stress-induced apoptosis. Nature 1996;380:75-9.

296. Vieth M, Higgs RE, Robertson DH, Shapiro M, Gragg EA, Hemmerle H. Kinomics-structural biology and chemogenomics of kinase inhibitors and targets. Biochim Biophys Acta 2004;1697:243-57.

297. Wade WS, Mrksich M, Dervan PB. Design of peptides that bind in the minor groove of DNA at 5'-(A,T)G(A,T)C(A,T)-3' sequences by a dimeric side-by-side motif. J AM Chem Soc 1992;114:8783-94.

298. Wang JC. DNA topoisomerases: why so many? J Biol Chem 1991;266:6659-62.

299. Wang LG, Liu XM, Ji XJ. Determination of DNA topoisomerase II activity from L1210 cells--a target for screening antitumor agents. Zhongguo Yao Li Xue Bao 1991;12:108-14.

300. Wartell RM, Larson JE, Wells RD. Netropsin. A specific probe for A-T regions of duplex deoxyribonucleic acid. J Biol Chem 1974;249:6719-31.

301. Watson JD, Crick FH. Molecular structure of nucleic acids; a structure for deoxyribose nucleic acid. Nature 1953;171:737-8.

302. Weinreich M, Stillman B. Cdc7p-Dbf4p kinase binds to chromatin during S phase and is regulated by both the APC and the RAD53 checkpoint pathway. EMBO J 1999;18:5334-46.

303. Wells G, Martin CR, Howard PW, et al. Design, synthesis, and biophysical and biological evaluation of a series of pyrrolobenzodiazepine-poly(N-methylpyrrole) conjugates. J Med Chem 2006;49:5442-61.

304. Wemmer DE. Designed sequence-specific minor groove ligands. Annu Rev Biophys Biomol Struct 2000;29:439-61.

305. White S, Baird EE, Dervan PB. On the pairing rules for recognition in the minor groove of DNA by pyrrole-imidazole polyamides. Chem Biol 1997;4:569-78.

306. White S, Szewczyk JW, Turner JM, Baird EE, Dervan PB. Recognition of the four Watson-Crick base pairs in the DNA minor groove by synthetic ligands. Nature 1998;391:468-71.

307. Wong ET, Berkenblit A. The role of topotecan in the treatment of brain metastases. Oncologist 2004;9:68-79.

308. Woynarowski JM, Krugliak M, Ginsburg H. Pharmacogenomic analyses of targeting the AT-rich malaria parasite genome with AT-specific alkylating drugs. Mol Biochem Parasitol 2007;154:70-81.

309. Wu X, Lee H. Human Dbf4/ASK promoter is activated through the Sp1 and MluI cell-cycle box (MCB) transcription elements. Oncogene 2002;21:7786-96.

310. Xiao Z, Hao Y, Liu B, Qian L. Indirubin and meisoindigo in the treatment of chronic myelogenous leukemia in China. Leuk Lymphoma 2002;43:1763-8.

311. Yamada M, Sato N, Taniyama C, Ohtani K, Arai K, Masai H. A 63-base pair DNA segment containing an Sp1 site but not a canonical E2F site can confer growth-dependent and E2F-mediated transcriptional stimulation of the human ASK gene encoding the regulatory subunit for human Cdc7-related kinase. J Biol Chem 2002;277:27668-81.

312. Yang YH, Wang QH, Nie H, Chen H, Cheng MS. Synthesis, biological evaluation, and modeling of dimeric PPI analogues as novel DNA minor groove binders. Molecules 2008;13:1179-88.

313. Yasuzawa T, Iida T, Muroi K, Ichimura M, Takahashi K, Sano H. Structures of duocarmycins, novel antitumor antibiotics produced by Streptomyces sp. Chem Pharm Bull (Tokyo) 1988;36:3728-31.

314. Yoon HJ, Loo S, Campbell JL. Regulation of Saccharomyces cerevisiae CDC7 function during the cell cycle. Mol Biol Cell 1993;4:195-208.

315. Yoshida M, Banville DL, Shafer RH. Structural analysis of d(GCAATTGC)2 and its complex with berenil by nuclear magnetic resonance spectroscopy. Biochemistry 1990;29:6585-92.

316. Yoshizawa-Sugata N, Ishii A, Taniyama C, Matsui E, Arai K, Masai H. A second human Dbf4/ASK-related protein, Drf1/ASKL1, is required for efficient progression of S and M phases. J Biol Chem 2005;280:13062-70.

317. Zhang J, Yang PL, Gray NS. Targeting cancer with small molecule kinase inhibitors. Nat Rev Cancer 2009;9:28-39.

318. Zhang Y, Sicot G, Cui X, et al. Targeting a DNA binding motif of the EVI1 protein by a pyrrole-imidazole polyamide. Biochemistry 2011;50:10431-41.

319. Zimmer C, Puschendorf B, Grunicke H, Chandra P, Venner H. Influence of netropsin and distamycin A on the secondary structure and template activity of DNA. Eur J Biochem 1971;21:269-78.

320. Zou L, Stillman B. Formation of a preinitiation complex by S-phase cyclin CDK-dependent loading of Cdc45p onto chromatin. Science 1998;280:593-6.

321. Zou L, Stillman B. Assembly of a complex containing Cdc45p, replication protein A, and Mcm2p at replication origins controlled by S-phase cyclin-dependent kinases and Cdc7p-Dbf4p kinase. Mol Cell Biol 2000;20:3086-96.

PUBLICATIONS FROM THIS THESIS

1. Babu B, Liu Y, Plaunt A, et al. Design, synthesis and DNA binding properties of orthogonally positioned diamino containing polyamide f-IPI. Biochem Biophys Res Commun 2011;404:848-52.

2. Chavda S, Liu Y, Babu B, et al. Hx, a novel fluorescent, minor groove and sequence specific recognition element: design, synthesis, and DNA binding properties of p-anisylbenzimidazole-imidazole/pyrrole-containing polyamides. Biochemistry 2011; 50:3127-36.

3. Chavda S, Mulder K, Brown T, et al. DNA recognition: design, synthesis and biophysical characteristics of pyrrole(H) based polyamides. Med Chem 2010;6:150-8.

4. Satam V, Babu B, Chavda S, et al. Novel diamino imidazole and pyrrole-containing polyamides: Synthesis and DNA binding studies of mono- and diamino-phenyl-ImPy*Im polyamides designed to target 5'-ACGCGT-3'. Bioorg Med Chem 2012;20:693-701.

5. Satam V, Babu B, Porte A, et al. Synthesis and DNA binding properties of 1-(3-aminopropyl)-imidazole-containing triamide f-Im*PyIm: a novel diamino polyamide designed to target 5'-ACGCGT-3'. Bioorg Med Chem Lett 2012;22:5898-902.